NIAC PHASE II FINAL REPORT

Mach Effects for In-Space Propulsion: Interstellar Mission

Date of Report: August 20, 2020
Period under review: April 2018 – August 2020
Grant (18-18NIACPro2-0003)

Space Studies Institute Principal Investigator James F. Woodward,
Institutional-PI, H. Fearn,
Physics Department,
California State University Fullerton
SSI Program Manager Gary C. Hudson
Co-PI's José Rodal, Paul March, Marshall Eubanks & Jonathan Woodland

Additional scientific associations with Daniel Kennifick, Michelle Broyles, Chip Akins and John Brandenburg

FINAL REPORT – NIAC PHASE II

Mach Effects for In-Space Propulsion: Interstellar Mission

Period under review: April 2018 - August 2020
Grant (18-18NIACPro2-0003) submitted to the 2018 NASA Innovative Advanced Concepts (NIAC) Phase II Solicitation (80HQTR18NOA01-18NIAC_A2)

Space Studies Institute Principal Investigator James F. Woodward,
Institutional-PI, H. Fearn, Physics Department, California State University Fullerton
SSI Program Manager Gary C. Hudson
Co-PI's José Rodal, Paul March, Marshall Eubanks & Jonathan Woodland

Additional scientific associations with Daniel Kennifick, Michelle Broyles, Chip Akins and John Brandenburg
Cover rendering by Tom Brosz, SSI

Table of Contents

Addendum

1. Executive Summary

At the beginning for the Phase 2 grant period, we employed devices made of Steiner Martins SM-111 material, (lead zirconium titanate) PZT, eight discs 2mm thick glued together with a brass mass and an aluminum mass, using rubber pads between the brass and the static L mount bracket. These devices produced on the order of 1μN of force. These early devices are discussed in the introduction, Section 2. The balance beam and its dynamics are treated in Sections 3 and 4. We found doming the brass and aluminum ballast masses prevented the PZT stacks from cracking around the edges, and determined the optimum dome height, see Section 5. We decided that to reduce high frequency vibration transmitted to the Faraday cage and hence the balance arm, a sledge arrangement might be superior to the static L bracket. See Figure 1.1.

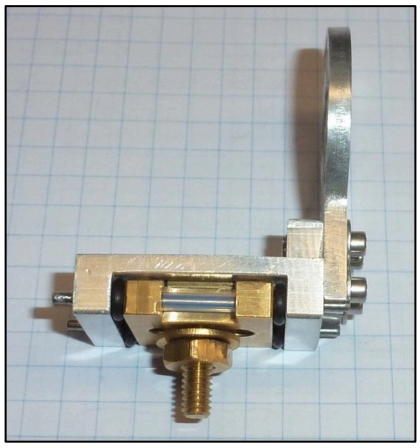

Figure 1.1 Sledge design Number 1. This design permits the aluminum frame to move on steel rails over the static brass bolted to the Faraday cage.

We then performed a number of tests to determine which design was better for force generation, the L bracket or new sledge, see Sections 6 & 7. Also, how much vibration was transmitted to the Faraday cage, see Section 8. We also tried different materials for the washers (instead of the rubber pad) with the static L bracket and sledge configuration, see Section 9, and different numbers of washers. At this stage we were seeing forces of order 10's of microNewtons. Stacks glued to the masses seemed to work well and improved the force. Then came the second sledge design, see Figure 1.2, rather late – only a couple of months before the end of Phase 2. We are still in the process of testing this arrangement but have made several improvements. With this free-free motion of the device, a true in-space configuration, we are regularly seeing 100 μN or so. See Section 10. We address center of mass (CoM) shifts in Section 11.

We may not yet have a space-ready device, but we are close to one.

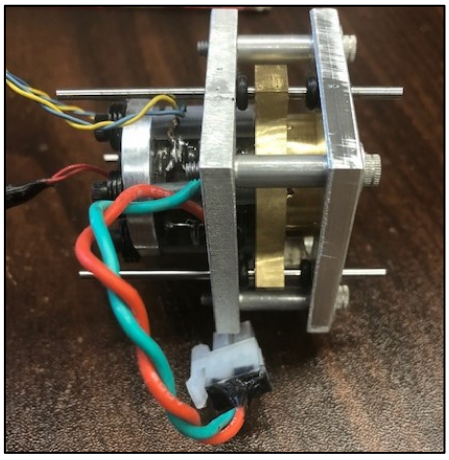

Figure 1.2 New sledge design. The steel rods run on linear ball bearings mounted inside the 3 "ears" of the brass mass. We also installed springs, made of guitar wire, of different thicknesses, to prevent the device from collisions with the O-rings causing random oscillations.

2. Introduction

The goal of the activities funded by both NIAC phase 1 and 2 grants is captured in the title. The goal is demonstration of a propulsion system that, when scaled, is capable of supporting missions to the stars with travel times that are some reasonable fraction of a human lifetime. We have not yet produced devices that can be used as propulsors of a starship. We have, however, produced demonstration devices, suitable for deployment in space if desired, that will show the proof-of-concept beyond any doubt by perceptibly changing the motion of the vehicle carrying it. As detailed below, significant progress toward that goal has been made in the past year, and our goal of a flight ready system in a few years remains achievable.

Mach Effects And How They Are Generated

Mach effects are fluctuations in the rest masses of objects being "properly" accelerated while their internal energies are changing. (Proper accelerations are ones that involve changing motion with respect to local inertial frames, and consequently, the production of inertial forces. Accelerations that appear as the result of observer acceleration are not proper accelerations.) These conditions are producible in stacks of lead zirconium titanate (PZT) crystals by applying ultrasound frequency, alternating electrical voltages to electrodes embedded in the stacks. Normally, these stacks are run at an auspicious electrical resonance of the power circuit where the base frequency of the driving signal produces the expected mass fluctuations, and the second harmonic (double frequency) of the driving signal is excited and has the correct phase with respect to the base signal to "rectify" the force that the second harmonic signal produces acting on the mass fluctuations that also take place at the second harmonic frequency.

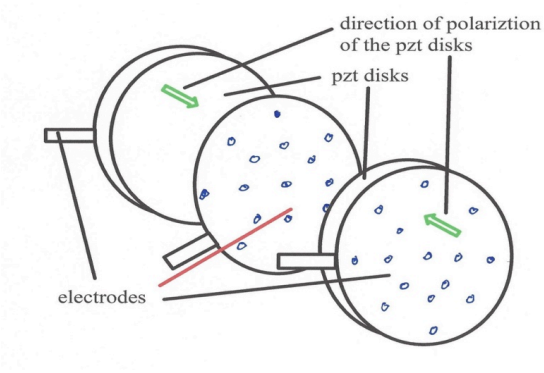

Figure 2.1. A "cell" consisting of two PZT disks, oriented with like polarities facing each other, and electrodes used to energize the cell. The outer electrodes are kept at ground potential while the electrode between the disks is excited by positive or negative voltages, causing the cell to either expand or contract in the direction through the disks. A "stack", for this project, consists of four cells stacked together.

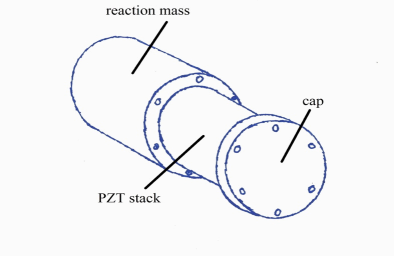

Figure 2.2. A schematic diagram of the basic device used in this project. An aluminum cap (C) holds a stack (S) of 8 PZT disks onto a brass reaction mass (RM) with 6 machine screws. When an oscillating voltage of the correct frequency and amplitude is applied to the stack, the stack expands and contracts along the longitudinal symmetry axis of this CSRM assembly, and the oscillation of the stack against the reaction mass causes the end of the stack near the cap to undergo periodic accelerations due to its motions of a few hundred nanometers. This produces a Mach effect mass fluctuation with a frequency twice that of the exiting voltage. If a second mechanical oscillation is created in the stack at the frequency of the mass fluctuation with the correct phase, a steady force will be generated in the CSRM, causing it to accelerate – without the ejection of propellant.

Over the past several years, in no small part by trial and error, devices based on a stack of 8 PZT disks 19 mm in diameter by 2 mm thick (polarized through the thickness) have been developed that a year ago produced thrusts below the micro-Newton level. While these devices can be produced in arrays to increase the thrust available for a given purpose, we hoped to engineer each of them to produce more thrust, reducing the number of discrete devices needed for a particular application.

This has been the focus of our activities throughout this Phase 2 grant. It will continue to be a central consideration in our post-grant activities.

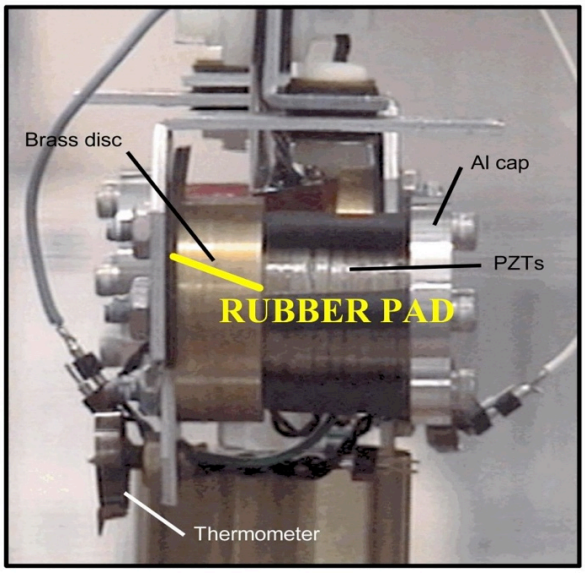

Figure 2.3. A late 1990s vintage thruster suspended with a rubber strap from the beam of a torsion balance. Note the thin rubber pad between the brass reaction mass and the aluminum "L" bracket. Without this pad, the device does not produce detectable thrust.

Collaborations

One of the chief concerns of the NIAC administrative staff, from the outset of both grants has been collaboration with others to avoid running afoul of issues arising from wishful thinking and self- deception. To that end, we were encouraged to collaborate with Martin Tajmar and his students at the Technical University of Dresden. During the Phase 1 grant, this consisted of sending Tajmar and his students a demonstration device (see Figure 2.4) and some ancillary equipment needed to operate it correctly. They ignored the ancillary equipment, used it as they saw fit, and reported a negative result from their activities. During the Phase 2 grant, we tried again. This time, H. Fearn (CSUF Institutional PI for this grant) took the devices to be tested along with all the equipment needed to run them to Dresden and oversaw to installation and preliminary testing to head off a repeat of the first attempt at collaboration. Shortly after she left, Tajmar's students removed a crucial part of the ancillary apparatus (a vibration suppression yoke) and

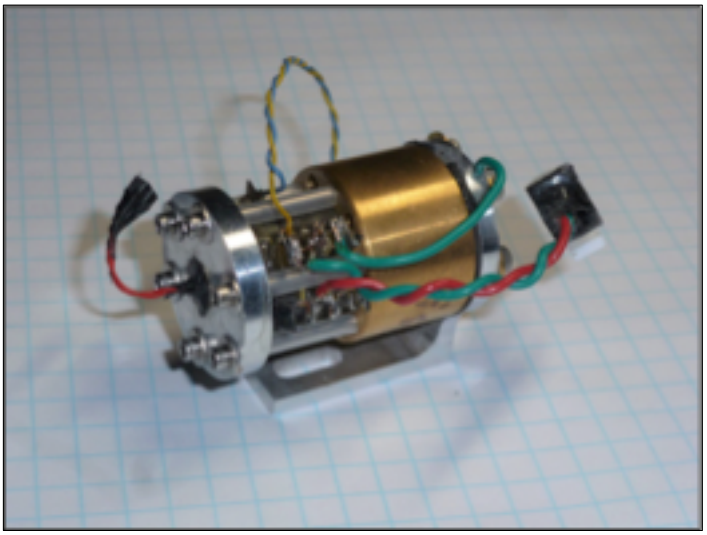

Figure 2.4. A post-2010 Mach effect thruster/MEGA drive/impulse engine. The reaction mass is longer and the L bracket is heavier than in the 1999 version. And the PZT stack is made with Steiner-Martins material SM-111, a low dissipation, high mechanical Q material, rather than Edo Corp. material EC-65, a very high dielectric constant material with a higher dissipation factor. These devices produce sub-microNewton level thrusts when operated near their mechanical resonance frequency of roughly 30 kHz.

repeated the behavior of the first collaboration attempt, producing the same result. Perhaps because of the problems with Dresden, the NIAC staff arranged to have Mike McDonald at NRL do a replicatory investigation of our work. This will be an independent effort on his part, but with devices supplied by us with necessary ancillary equipment and our assistance when needed. That was to have commenced this past spring, but the corona virus pandemic has disrupted that, and it now looks as though he will not start work on this project until after our grant is completed. This past spring, in a conversation with the Chief Scientist of a NASA center, the possibility of another person to do a "replication" came up. He suggested that George Hathaway, of Hathaway Research in Canada, perform a replication because of his long experience in this sort of work. That has been arranged through the Space Studies Institute, the sponsoring institution for our grant. We are already in contact with McDonald and Hathaway.

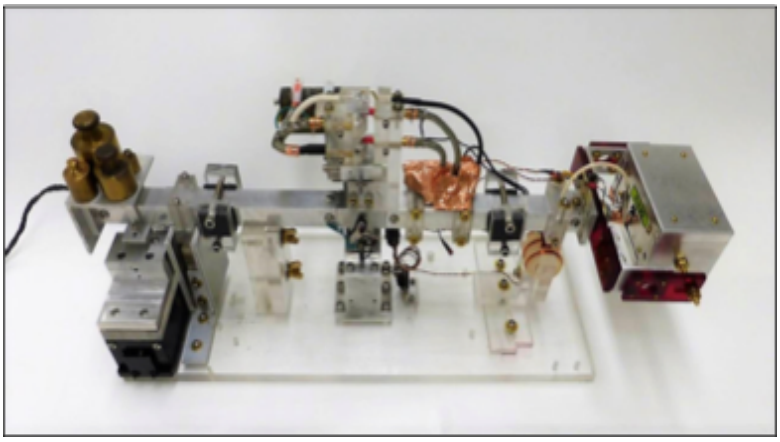

Figure 2.5. The CSUF torsion balance as built by Tom Mahood and JFW around 2010. Among the important features of this balance are the sensitivity made possible by the C-Flex flexural bearings that support the beam and the liquid metal (Galinstan) contacts (see Figure 2.6) used in the power circuit to suppress force that might be transferred to the balance beam during operation. Another crucial part of this balance is the vibration suppression yoke (see Figure 2.7), the red plastic on the right that carries the Faraday cage (a mu metal lined aluminum box) in which the test device is located. Without this yoke, the test devices, which vibrate strongly during operation, would cause the balance to vibrate, making the production of false positive results probable.

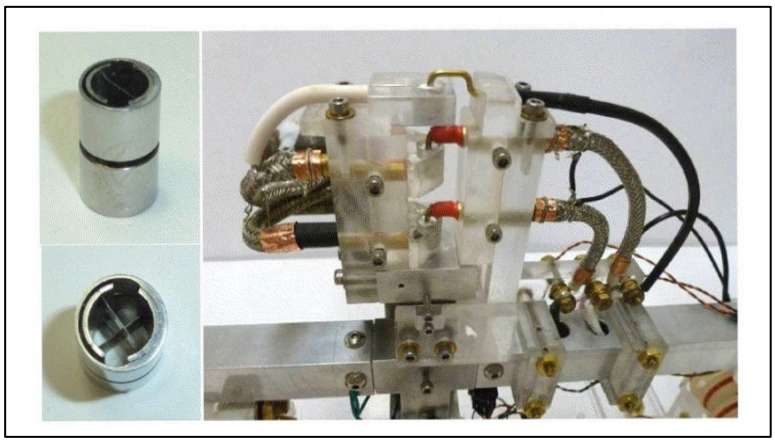

(Above) Figure 2.6. Two views of a flexural bearing on the left. They are mounted in aluminum column immediately below the Galinstan contacts shown on the right. The balance has been modified and up- graded since it was first built. But these features remain unchanged.

(Center Right) Figure 2.7. The vibration suppression yoke as first built. The red plastic parts are held together with pieces of aluminum channel and 4-40 brass machine screws. Vibration suppression is achieved with the washers and O-rings on the screws. The yoke is mounted on the end of the beam with a stud with a nut that passes through the hole in the center plastic piece. This makes reversal of the direction of the test device a simple matter of loosening the nut and rotating the yoke. Direction reversal is a critical test for false positive thrust signals.

We expect these replication efforts to commence in the near future.

Activities of Grant Team Members and Consultants:

Activities of those affiliated with this grant fall into five general categories. They are:

1. Mission architecture: how the evolving design and capabilities of the Mach effect thrusters impact the design of the starship developed in the Phase 1 grant. Primary responsibility for this activity fell to Gary Hudson and Marshall Eubanks. Work on this aspect of the grants was completed in Phase 1.

2. Improvement of existing thrusters to maximize their thrust to power behavior. All team members contributed to this activity. Execution fell to Jon Woodland (who made the parts for the demonstration systems), H. Fearn (who, especially during the corona virus when laboratory access was limited, did most of the experimental work), and Jim Woodward (PI, and originator of the thrust method that is the basis of the proposed propulsor, who built most of the apparatus and test devices). Formal, data based studies have been chiefly carried out by José Rodal.

3. Modeling of existing and proposed devices. This was done to understand how the devices and other parts of the system behave during operation. And to virtually test new designs for possible thrusters. Those chiefly responsible for modeling were José Rodal, and H. Fearn and John Brandenburg. While these efforts have led to the exploration of a variety of modifications of the devices used, ultimately the design of the core device – the stack of PZT crystals preloaded with an aluminum cap attached to a brass "reaction mass" by machine screws – has survived unchanged. What has changed, as explained below, is the way in which this assembly is configured and mounted.

4. Power and electronics. These thrusters depend strongly on as variety of operating parameters, especially PZT stack pre-load, temperature and operating frequency. In their recent realizations, they are very high "Q" devices in several regards. This makes them very sensitive to the values of several operating parameters. To optimize thruster operation, several properties of the devices must be monitored, and the monitored signals used in feedback control circuits. Those with special expertise in power electronics are Paul March and Chip Akins, with kibitzing from David Jenkins. Mr. Akins is building power amplifiers designed to work with the thrusters being developed, a project nearing completion at the time of the writing of this report.

5. Theory. The effect that can be turned into a practical propulsion system that does not require propellant that is irreversibly expelled depends on Einstein's interpretation of his general relativity theory being correct. In particular, that inertia and inertial effects are actually gravitational effects that arise from the action of cosmic "matter" on local systems. At this time, this is not the view of most mainstream general relativists. A theory group tasked with dealing with this issue came together a year ago. Members include H. Fearn, Daniel Kennefick, José Rodal, and Jim Woodward. Recently, Nathan Inan joined because of his expertise in gravitoelectromagnetism.

Institutional support for the grant has been provided by the Space Studies Institute, especially its President, Gary Hudson and its Executive Director, Robin Snelson. Their help has been superb. Toward the end of Phase 2, others have been or have become affiliated with this project. For several months this past spring, Max Comess, now of Aerospace Corporation, helped with writing code for specialized signal generation to be used to power the thrusters in development. And a few months ago, Michelle Broyles, an aerospace engineer of considerable talent and experience joined the team, making important contributions in the area of demonstration systems.

Summary of Grant Activities

This grant was funded at the end of May in 2018. For the first roughly year and a third of the grant, our attention was distracted by issues not directly related to the goals of improving the thrust to power ratio of "Mach effect thrusters" and clarifying their underlying theory. (In the course of the grant, H. Fearn hit upon a new name for these thrusters: Mach Effect Gravity Assist (MEGA) Drives.) Almost exactly coincident with the inception of the grant, Tajmar and his students reported their negative findings using the demonstration device loaned to them for investigation. The reason for their failure to see the effect routinely generated with this device at CSUF was their failure to include a special transformer (supplied to them with the tested device) in the power circuit that determines the optimal operating frequency of the system (roughly 36 kHz), not the simple mechanical resonance frequency of the device (roughly 30 kHz). The transformer is a 4 to 1 step-up transformer, and since their power amplifier was capable of driving the device at the working voltage amplitude without the transformer, they dispensed with the transformer. Working at the mechanical resonance frequency with single frequency excitation, they saw nothing. Getting across the importance of the transformer and how it affects the driving circuit proved challenging, for its influence is not obvious from simple inspection.

In September of 2018, H. Fearn organized the second of the "Estes Park Advanced Propulsion Workshops" (sponsored by the Space Studies Institute). She had been encouraged to invite an amateur enthusiast, Jamie Ciomperlik, to give a presentation of a "simulation" he had done that purported to show that "Mach effects" do not exist. That the behavior of Mach effect thrusters was nothing more than "vibrational Newtonian artifacts", and consequently that Mach effect thrusters do not work as claimed. The presentation was done with polish, and many were swayed by the argument. Some were unimpressed by the counterargument that the proposed mechanism of the displacement of the thrust balance violated momentum conservation. Upon her return to CSUF from Colorado, H. Fearn undertook some experimental tests designed to show that vibrational artifacts do not account for the thrust signals seen in tests of Mach effect thrusters. JFW remained in Colorado until the Boston NIAC Symposium a few weeks later, the first of two Symposia at which presentations of work under this Phase 2 grant were given. Thrust improvement became a secondary concern to answering our critics. Indeed, shortly after the Boston Symposium, at the suggestion of Michele Schirru, Polytech Corporation was contacted about their commercial vibrometers to explore the behavior of our system to answer the vibration issue. In the demonstration of one of their vibrometers it was demonstrated that the vibrations needed to produce a false positive in our system simply did not exist. Using Space Studies Institute non-grant funds, a "bare-bones last-year's model" vibrometer was procured

from Polytech. It has proved a very useful and versatile instrument.

Several months after the Boston NIAC Symposium, in January of 2019, H. Fearn took Mach effect thrusters and ancillary equipment to Dresden to be tested in the laboratory of M. Tajmar by his students. She remained long enough to make sure that the thrusters were properly installed and producing thrust signals like those seen with the devices at CSUF. A discrepancy was noted in this process. The signals were the same. But their magnitude was measured as much smaller on the Dresden apparatus than those measured at CSUF. After Fearn left Dresden, Tajmar's students removed the vibration suppression yoke supplied with the thrusters, an essential part of the apparatus that stops vibration from contaminating the thrust balance with false positives. Without the yoke, the thrusters were bolted directly onto the balance, and not surprisingly, they generated false positives. These they took to be evidence that Mach effects do not exist. We learned of the Dresden results in August of 2019 during a visit by Tajmar to our lab. We promptly took out our Polytech vibrometer and demonstrated for Tajmar that vibrational effects are NOT responsible for the thrusts produced by Mach effect thrusters. Tajmar declined to accept the evidence we presented.

More important than the Newtonian controversy was the discrepancy in the measured thrust between Dresden and CSUF, an issue raised at the mid-term review in May of 2019. Because the CSUF calibration system, designed and built by JFW a decade ago, does not depend on off the shelf commercial parts, it was considered suspect. The obvious way to deal with this issue was to have the CSUF calibration system itself calibrated to determine if it was working correctly. George Hathaway was recruited to do this calibration of our calibrator. It was determined that the calibrator works as claimed. However, in the course of this investigation it was also determined that an error of a factor of four had been made in the calculation of the force produced by the calibrator, reducing all of the thrust measurements with the CSUF balance to one fourth of their previously assumed values. This did not eliminate entirely the discrepancy with the Dresden claims. But it made the assumed micro-newton level thrusts measured at CSUF to be a few hundreds of nano-newtons – making thrust improvement all the more important. And making the promise of thrusts of a few tens of micro-newtons by the end of the grant a year later, made at the mid-term review in the spring, a lot more challenging.

In the early summer of 2019, José Rodal successfully published in *General Relativity and Gravitation* an article which was critical of the theoretical work on Mach effects. The core of his argument against Mach effects was that, contrary to the claim of JFW, inertia in general relativity is not an inductive gravitational effect, so, lowest order inertial forces – those that arise in Newton's third law situations – are not gravitational forces caused by chiefly cosmic matter as assumed in the "relativistic Newtonian approximation" derivation of Mach effects of JFW. (HF does not agree with this statement.)

It is important to understand that Rodal's position on the role of inertia in general relativity is that of the mainstream in the community of general relativists. This position has been that of the mainstream for many years now. The rejection of the gravitational action of matter at cosmic distances by the mainstream community of relativists is a consequence of Carl Brans' "spectator" (that is, nearby) matter argument he devised in the late 1950s when tasked by Robert Dicke, his doctoral supervisor at Princeton, to examine the physics of "Mach's

principle" – the claim that inertia arises as an inductive gravitational effect in general relativity. This had been Einstein's belief since before he created general relativity. He called it "the relativity of inertia", to which he adhered even after abandoning "Mach's principle" as a consequence of the work of Willem deSitter shortly after he enunciated Mach's principle. (See Einstein's 1924 paper "On the Aether" available on-line.) On reading Einstein's comments on Machian inertia in a lecture he gave at Princeton in 1921 (published in *The Meaning of Relativity*) where he calculated that piling up spectator matter in the vicinity of a unit mass test particle should change the test particle's rest mass owing to the gravitational potential energy conferred on the test particle by the spectator matter, Brans saw that this is a mistake, for were it correct, it would be a violation of the Equivalence Principle – Einstein's cornerstone of general relativity.

Brans' spectator matter argument notes that if spectator matter changes the rest masses of test particles (and other stuff), then it is possible to determine whether you are in a lab on the surface of the Earth, or in a rocket ship accelerating at one "gee" in deep outer space simply by checking the charge to mass ratios of elementary particles in your lab. If they have standard values – determined in the absence of spectator matter – you are in outer space. If they do not, you are in a gravitational field. No need to go look out a window at your surroundings to determine which is the case as required by the Equivalence Principle. This argument is correct. The obvious question is how do you eliminate gravitational potential energy as a source of rest mass in test particles in general relativity so that the Equivalence Principle is preserved as required? Normally, one might conjecture that invoking a gauge principle might do the trick. But gauge arguments are not applicable in general relativity, for the theory is *not* a gauge theory. Brans and Dicke, in discussions with other Princeton physicists, came up with a "coordinate condition" argument, the closest thing to a gauge argument in general relativity. In 1977 Brans published "Absence of Inertial Induction in General Relativity" (in *Phyical Review Letters* **39**, 856-7). Invoking the coordinate condition that he and Dicke had created years earlier, he remarked that, "Einstein ought to have normalized his local space-time measurements to inertial frames, in which the metric has been transformed approximately to the standard Minkowski values, and for which distant-matter contributions are not present." The Minkowski metric, assumed valid in sufficiently small regions of spacetime in the construction of general relativity, is crucial, for being a pre-general relativity Newtonian artifact, it assumes inertia as a magical (without explanation) property of space in the complete absence of gravity. Brans' normalization procedure thus not only eliminates the inductive gravitational action of distant matter, it eliminates the inductive gravitational action of *all* matter as required to avoid the consequence of his spectator matter argument. This is why it is believed that Machian inertia is not contained in general relativity.

Rodal used an exact formulation of general relativity developed by Landau and Lifschitz constructed in Minkowski spacetime. He found, in a perturbation expansion at third post Minkowskian order, a term that looks exactly like the Mach effect prediction – an E/c^2 mass fluctuation multiplied by the "local" gravitational potential. But according to Rodal, the "local" gravitational potential is due only to "local" sources, so it only produces useful propulsion in the vicinity of black holes where gravitational fields as large as those present in Machian inertia are encountered. (In Machian inertia the total Newtonian potential is a locally measured invariant equal to the square of the vacuum speed of light, which is roughly the event horizon condition

for a black hole.) This follows from the assumption of the Minkowski metric far from local concentrations of matter where inertia without gravity is assumed. JFW, of course, wrote a reply, eventually published in *General Relativity and Gravitation* in December of 2019. In it, he noted that the spectator matter argument does not require that the effective Newtonian potential of gravity be zero as Brans and Dicke concluded. It only requires that the total Newtonian potential be a locally measured invariant. This leaves open the possibility that inertia really is an inductive gravitational effect as Einstein believed.

The issue of whether inertia is a gravitational effect in general relativity is one of non-negligible contention. Chiefly for this reason, as mentioned above, a theoretical part of the grant team was created to address this issue. Original membership was H. Fearn, Daniel Kennefick (an eminent general relativist at the University of Arkansas) and JFW. Since formation, José Rodal was added, and recently Nathan Inan (a recent PhD student of Raymond Chiao at UC Merced) was invited to join because of his expertise in gravitoelectromagnetic representations of general relativity. The goal of this group is to produce an article, written at the level of the *American Journal of Physics*, that explains inertia in Einstein's terms and what implications this understanding of inertia entails for physics more broadly. It looks to be a work in progress for at least several more months. Perhaps more. It should be noted here, however, that the Mach effect impulse engine project funded by this grant makes possible an experimental test of the question whether inertia is an inductive gravitational effect or not. If the engines work as expected, inertia is an inductive gravitational effect. Mach effect impulse engines, however, do *not* violate the Equivalence Principle. Even with your impulse engine running, you still have to go look out a window to tell where you are.

The presentation for the grant at the Huntsville NIAC Symposium in September of 2019 was chiefly occupied by the calibration and Newtonian vibration issues. But thrust improvement was still the chief goal of the project. Thrust in these devices depends on several parameters, each and all of which might be adjusted. But the key to thrust improvement has been understood since the thruster was first created in the fall of 1999. That was when a rubber pad was inserted between the cap-stack-reaction mass [CSRM] system and an aluminum bracket (a so-called "L" bracket) screwed to the end of the reaction mass to suspend it from the beam of a torsion balance. (See Figures 2.3 and 2.4 above.) Most who have looked at this system have assumed that the purpose of the rubber pad was to damp the vibration generated in the device to keep it from getting to the balance where it might produce false positives. But the original intent was not to damp the vibration. It was to *decouple* the high frequency vibration in the device from the mounting hardware to *increase* the amplitude of the vibration in the device, and thus the thrust. Vibration that makes it to the L bracket and rest of the balance just sinks energy that would otherwise enhance the thrust effect. Vibration damping, for the torsion balance in use in 1999, was not an issue. The rubber pad was the crucial step in the development of the thruster, for before the rubber pad they hardly worked at all.

Experimentation with replacements for the rubber pad started at the time of the Boston Symposium and continued desultorily through the Huntsville Symposium, in the background to what seemed more pressing concerns at the time. Implicit in this experimentation was the decision to try to make the working thruster before us better, rather than try to develop a new design. After Huntsville, this path was increasingly aggressively pursued. Nylon washers were

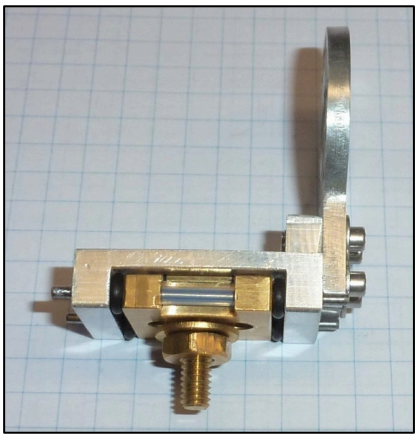

(Left) Figure 2.8. A "sledge" of the type first tested in early 2020 designed to as nearly as possible decouple high frequency vibration from the test device in operation from the enclosing Faraday cage. The sledge replaces the L bracket normally screwed to the back of the reaction mass.

first used as a substitute for the rubber pad. They increased the thrust, but eventually turned to mush in the harsh mechanical environment they had to exist. Washers were placed on both sides of the L bracket, yielding another improvement. An increasingly exotic variety of dielectric washers were tested with equivocal results. The problem with all of them was that while they worked nicely in many cases in the first run of each day, they all degraded in runs thereafter because they generated a lot of heat, and the heat degraded their elasticity, rendering them non-functional. The heating problem led to the investigation of the use of steel Belleville washers. They solved the heating problem. But no Belleville washers of the correct properties were commercially available. They had to be glued together from imperfect washers available. These investigations are presented in a series of detailed reports by H. Fearn who did the experiments as the only person allowed in the lab at the time due to the presence of the virus.

Just before the virus led to the closing of the campus, pursuing the decoupling idea that motivated the rubber pads of earlier years, a new element was added to the mounting system. The L bracket, instead of being bolted directly to the enclosing Faraday cage used with the present torsion balance (see Figures 2.5 and 2.6 above), was attached to a piece of aluminum – a "sledge" – that rode on two small steel dowels mounted in a piece of brass that was bolted to the Faraday cage. (See Figure 2.8.) The sledge was free to vibrate on the steel dowels, but very low frequency and steady forces would be transferred to the Faraday cage (and balance).

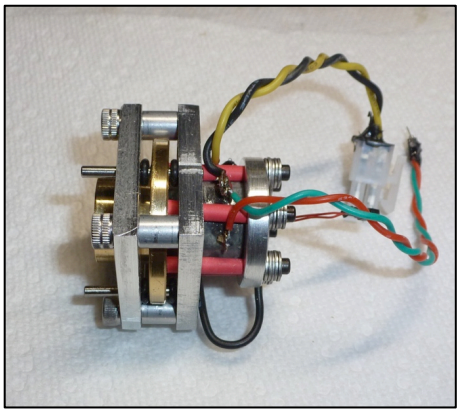

(Above) Figure 2.9. The proof of concept "sledge mount" device. Steel rods in a two piece aluminum frame pass through Teflon lined holes in a flange machined on the reaction mass to support the CSRM system. A fraction of a millimeter on either side of the flange is left for free travel. Several tedious adjustments had to be made to correct design mistakes to get the device operational.

Measurements with the Polytech vibrometer revealed that the sledges did exactly what they were supposed to do – decouple vibrations with frequencies above a few hundred Hertz from the Faraday cage that enclosed the test device (see Figure 2.5 above). But the potential of the sledges was not fully appreciated because they did not dramatically improve the first runs of the day, and in later runs the heating effect in the washers kept the high frequency vibrations from getting to the sledges, much less the Faraday cage. Eventually, it was realized that the real problem was bolting the bracket to the end of the reaction mass, and this had to be eliminated in any solution to the thrust enhancement problem. This meant that the sledge configuration would have to be applied directly to the

CSRM system directly. And the obvious place to do this would be as near to the center of mass [COM] of the CSRM system as possible, which should also be the principal node of a now "free-free" vibrating CSRM system (as the ends of the CSRM system are not attached to anything). That is, the mounting point should be in a flange at the junction between the stack and reaction mass. A proof of concept device was designed and built with a flange with Teflon lined holes and an aluminum frame that carried the steel dowels that passed through the holes in the flange. (See Figure 2.9.)

It worked. The experiment-demonstration team went to work on the new design.

The team quickly focused on two issues. The first issue was the friction of the Teflon liners on the steel rods in the mounting system. Several members of the team had previous experience with linear motion ball bushings, and they were identified as the best friction reduction method. These bushings, especially in an environment with serious vibration, are essentially frictionless. Absent the vibration, stiction is a problem. But vibration renders stiction inoperative because the bearings are constantly in (small amplitude) periodic motion. When C. Akins identified a source of suitable miniature versions of these bushings, they were immediately ordered. The second issue was how to convey any quasi- stationary force generated in the CSRM system to the frame carrying the support dowels and ultimately to the thrust balance. JFW's solution to this problem was to place rubber O-rings on the supporting dowels between the "ears" of the flange and the aluminum frame (see Figure 2.9) without compressing the O-rings. Uncompressed, the O-rings would not sink much energy from the high frequency vibrations of the CSRM system. This was deemed inelegant by the team. Chip Akins wanted "leaf" springs. Eventually, Michelle Broyles, drawing on previous experience, suggested using fine steel wires connecting the CSRM system to the aluminum frame as shown in Figure 2.10.

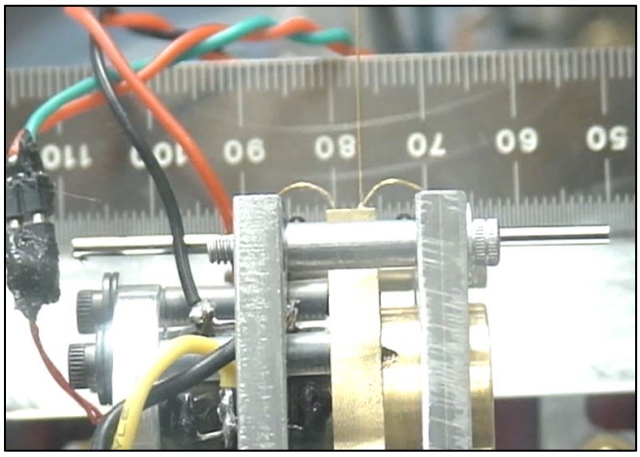

Figure 2.10. Note the two semi-circular steel wires (gold plated) that center the CSRM assembly on the dowels between the two aluminum frame plates that keep the CSRM assembly from "walking" around on the dowels during operation. Note too, the straight steel wire (at the 77 mm mark on the scale in the background affixed to the beam). H. Fearn glued this to the "ear" of the CSRM assembly to act as a crude vibrometer. Indeed, the part of this wire at the top of the photograph is blurred because this picture was taken from a movie of a run in progress.

José's comment on this system was that, because of the frictionless support system, it is the next best thing to an "in space" demonstration of the thrust effect. Duplicates of the system have been fabricated for use by the project replicators and others. A typical recording of a run of the system – a sweep of the frequencies between 45 and 25 kHz in 20 seconds – is shown in Figure 2.11. It is taken from the run movie used for Figure 2.14. This run was part of a test of the Newtonian artifact proposal. H. Fearn had found that with very soft centering springs (made of

0.008 inch diameter wire). The CSRM assembly would move 0.5mm=500 micrometers on the scale affixed to the beam (seen in Figure 2.11, upper right-hand corner) at times of large thrust. Fearn calculated that this displacement would produce a thrust signal of 6 volts, or 60 microNewtons – as observed.

HF was tempted to think that the bulk of the large thrust signals being seen – tens of microNewtons and more – was due to a Newtonian artifact of the balance re-zeroing. This notwithstanding that the artifact conjecture violates momentum conservation and the distortion of the CSRM assembly required by the conjecture, easily detected in the run movie, was clearly not present in the assembly. JFW decided to take a new device not yet tested and adjust the spacing of the aluminum frame plates so that the O-ring stops on the dowels were lightly compressed (between 5 and 10 percent) on the ears of the reaction mass flange – completely stopping any motion of the CSRM assembly of more than a few tens of nanometers due to forces in excess of several hundred microNewtons.

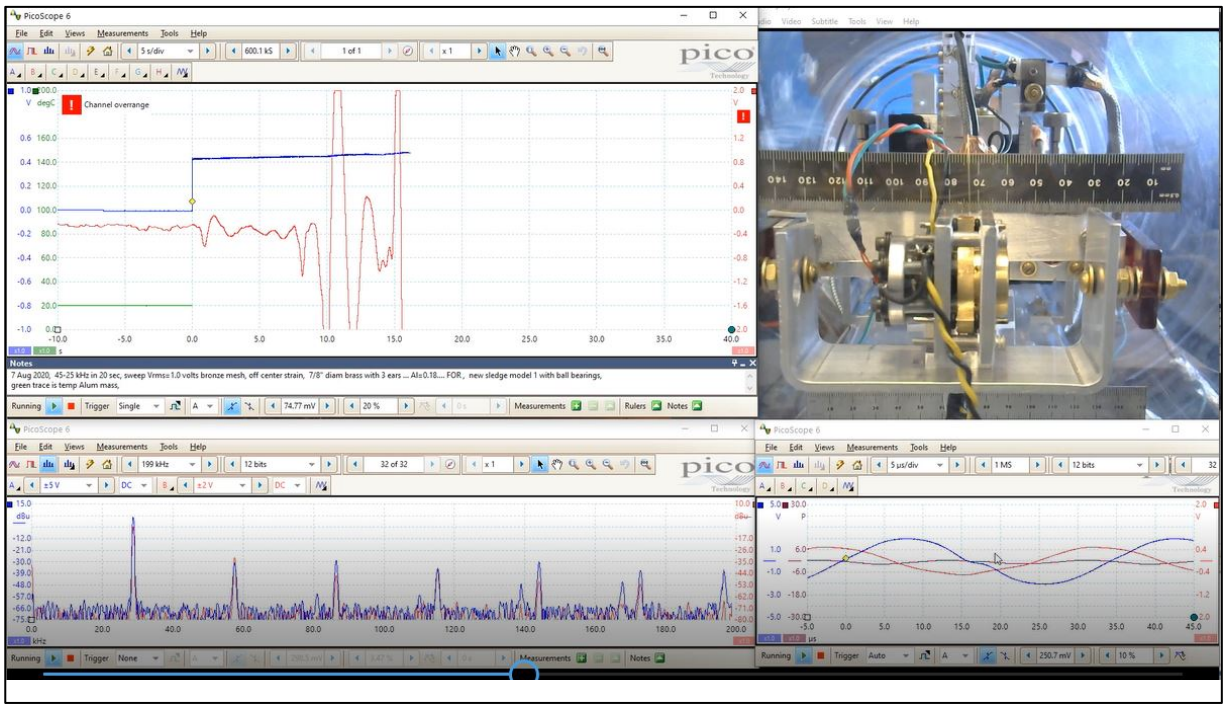

Figure 2.11. Picture of a movie of a run in progress. In the upper left-hand corner is a "strip chart" display of the voltage (blue) and thrust (red). The thrust scale is 100 mV per microNewton, that is 40 microNewtons full scale. The green trace is the temperature of the aluminum cap, computed and displayed at the termination of acquisition. In the upper right-hand corner is a webcam movie of the device in operation, made possible by the clear plastic vacuum chamber. In the lower right hand corner is the "scope" view of the voltage (blue) and strain gauge (red) waveforms of these quantities. In the lower left-hand corner, the real time FFT power spectra of the voltage (blue) and strain gauge (red) are displayed. Recording movies of this sort makes correlation of instrument readings to thrust events in the strip chart recording easy. And the frequency at which events occur is easily determined from the sweep parameters: 45 to 25 kHz, that is, 20 kHz in 20 seconds, or 1 kHz per second.

(Right) Figure 2.12. The new device tested on 7 August. The plates of the aluminum frame are separated by a "spacer" and one thin aluminum washer between the spacer and the right hand plate. This separation produces light compression of the O-rings on the dowels, stopping any significant motion along the dowels by the CSRM assembly during operation. The addition of another thin washer between the spacer and left hand plate produces a separation that decompresses the O-rings, but limits the motion of the CSRM assembly to less than 100 nanometers along the dowels.

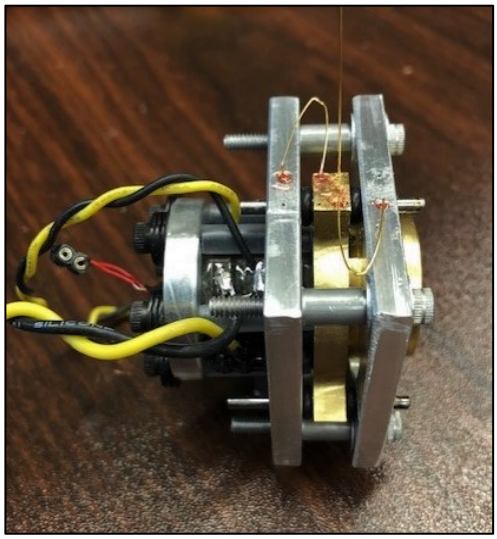

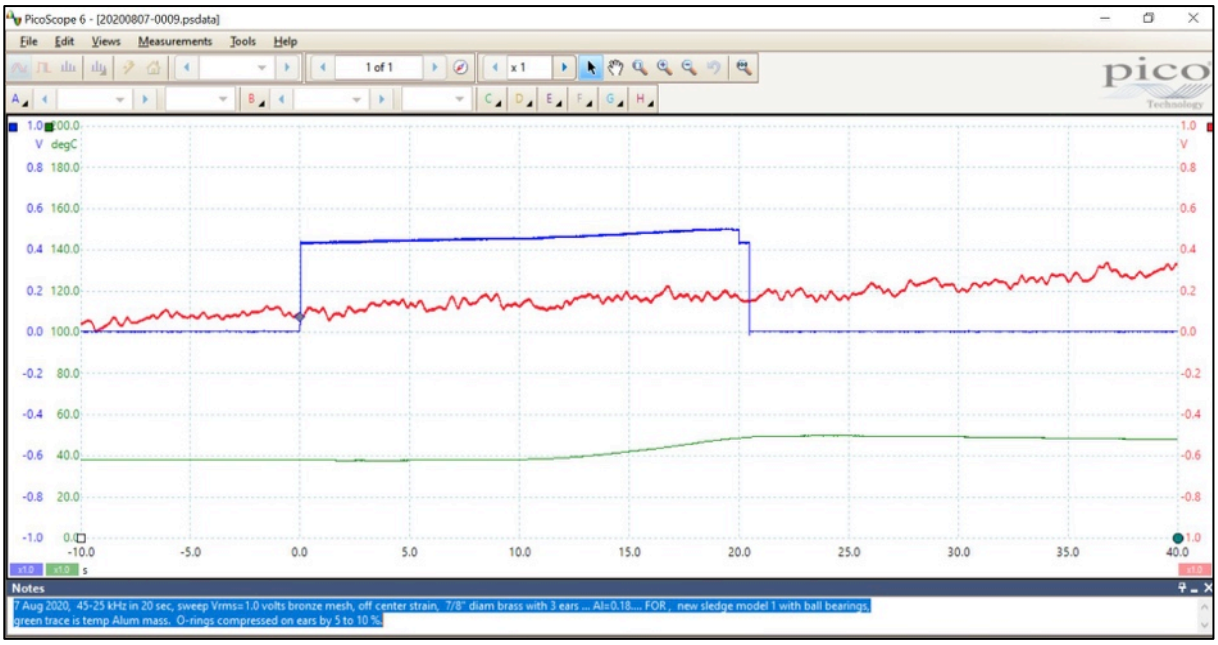

Figure 2.13. The strip chart recording for a run of the device put into operation on 7 August with light compression of the O-rings on the ears of the flange on the reaction mass. Aside from some small thermal drift of the thrust trace (red), there is no evidence of any thrust of the sort sought.

The thrust trace in Figure 2.13 came as a shock. We expected to see some thrust activity. The FFT power spectra, though, heralded this result as the second and higher harmonics in especially the strain gauge trace were strongly suppressed throughout the run. We suspected a bad stack. It was replaced with a stack known to work. The same result: no thrust. The obvious conclusion was that the light pressure of the O-rings on the flange ears was sufficient to kill the higher harmonics required to produce thrust – something hard to believe. We added a second washer to each of the four screws holding the plates together. This eliminated the compression

of the O-rings, but left less than 100 nanometers of free travel for the device on the dowels – and 0.5mm=500 micrometers was required to mimic the behavior that had been the source of Fearn's concern. Figure 2.14 shows the strip chart recording of the first run done after the second washers were added.

H. Fearn confirmed the correctness of this result later that day by putting springs ten times stiffer than those that allowed the 0.5 mm displacement that caused all of the concern into another identical device and running it. As expected, it did not produce displacements of 0.5 mm on the dowels. Indeed, hardly any displacement at all was observed. But the roughly 60 microNewton thrusts were seen in the thrust balance. Evidently, real net force is present in these devices. That is, the principles of real impulse engines are found in these devices. Mach effect thrusts are real and can be scaled, with care, to practical levels. It is worth noting that the thrusts now being generated in the tens to hundreds of microNewtons are produced with *less* power than the sub-microNewton thrusts of earlier devices. This would seem to augur well for impulse engines in the future.

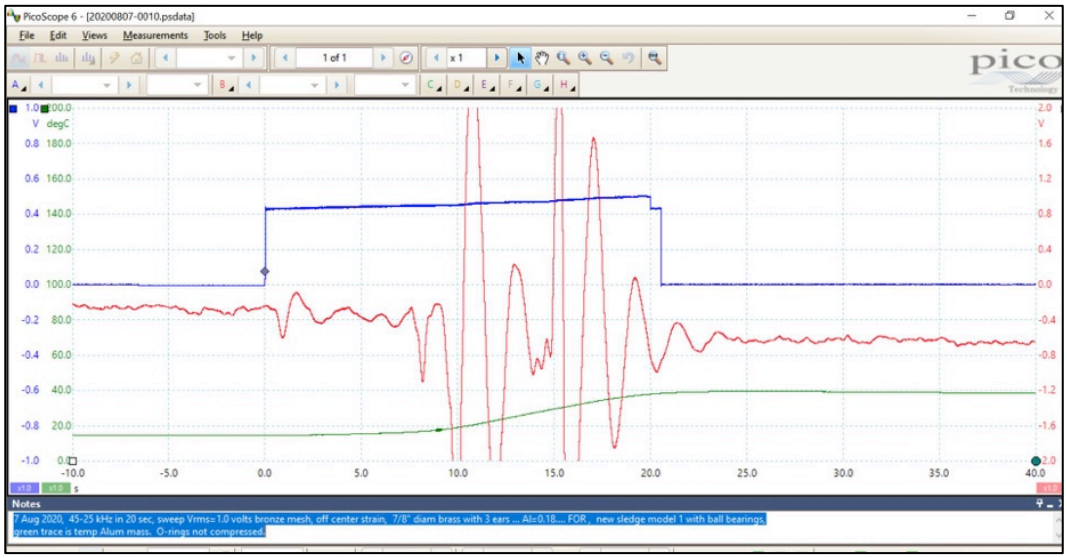

Figure 2.14: Strip chart recording of the run done after the spacing of the frame plates was increased so as to decompress the O-rings on the ears of the reaction mass flange. Note the large thrusts (greater than the 40 microNewtons full scale) generated at the usual frequencies.

Future Outlook

A year ago last spring, we had hoped that we would be able to increase the thrust produced by these Mach effect devices into the 10 to 20 microNewton range, and putting them in arrays of 4, be able to produce thrusts of 40 to 80 microNewtons per array. Two or more arrays would then be deployed in equipment suitable for a small sat mission for an in space demonstration of the reality that Mach effect thrusters actually work by altering the motion of the satellite. We had hoped to have the small spacecraft mission defined and hardware needed assembled ready for

testing by the end of the grant. Events have conspired to make these hopes even less realistic than most of the members of the mid-term review team took them to be. First, there were the calibration and artifact diversions. Then there was the virus. But through a series of coincidences – as Einstein would have them, God's way of remaining anonymous – those events that blocked any chance of reaching the hoped-for goal of a small sat mission ready set of hardware made possible the finding of way to make each device produce as much thrust as the hoped for arrays – by improving the thrust per device by more than two orders of magnitude. And, ironically, this was done by creating the next best thing to an in-space demonstration as a way of mounting the devices.

The next logical step is already provided for: careful replication by McDonald and Hathaway to make sure that we have not "fooled ourselves" in Feynman's words. But there is nothing exceptional about our apparatus that might lead them to get different results. And the physics involved, though characterized as "fringe physics" executed by those who are "the good kind of crazy" in a *Scientific American* article by Sara Scoles a year ago, is straight-forward. Successful replication looks likely.

So, looking beyond the replication efforts of McDonald and Hathaway, the question seems to be how to address the well-known TRL 3-4 valley of death. The crystal ball is cloudy on that one.

3. Calibration of balance, force and displacement

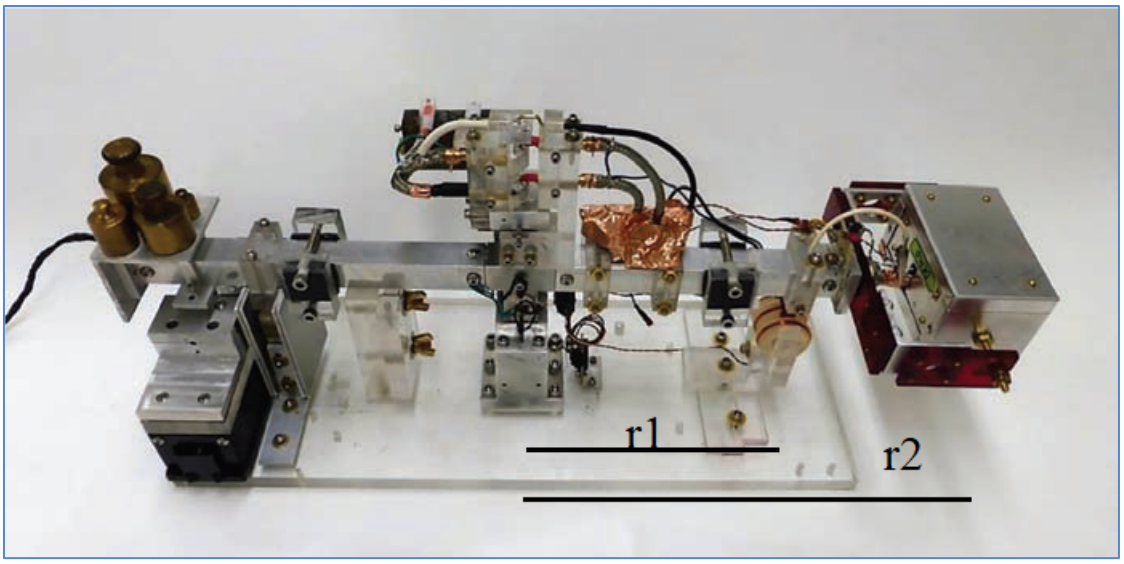

Figure 3.1. The Fullerton force balance. Weights on the left compensate for the mass of the Faraday cage with the device inside it, on the right. There is a magnetic damper visible on the left. The central column has Galinstan contacts for the power lines. The coils are for calibration purposes and are usually not powered during the operation of the device. Distance r1=15cm and distance r2=24cm.

The balance is calibrated by using a known force from the coils [1]. The force verses the voltage from the optical Philtec D63 sensor [2] is plotted and then fitted to a linear scale. Once the force in microNewtons can be given as a voltage in millivolts from the sensor, (eg. 125 mV gives 1 μN) we can adjust for the calibration of the force from the device inside the Faraday cage, by using the known distances r_1 and r_2 . The torque ($\tau = r \times F$) from the force (F) about the pivot (in the central column) must be the same for the coils as it is for the device, so we use $r_1 F_{coil} = r_2 F_{device}$. This allows us to calculate the force from the device as follows:

$$F_{device} = (r_1 / r_2) F_{coil} = F_{coil} / 1.6$$

In order to accurately measure the millivolts from the sensor (for a given force) we take an average of 10 runs. We take 5 forward (F) runs and 5 reverse (R) runs and then the averages of these and then the difference (F-R)/2 , to determine the exact maximum voltage from the sensor.

We can vary the current to the coils, which will vary the force produced.

For example we took 6 data sets with the following current through the coils: 30.5mA, 40.1 mA, 50.1mA, 60.3mA, 70.4mA and 80.7mA. We compared two difference force results; one using elliptic integrals [3] and another very simple approach generalizing a result from two parallel wires [4,5].

For ~30 mA through the coils we gathered the sample data below from the Philtec sensor using a picoscope. The current was supplied to the coils for about 15 seconds as shown in the figures below.

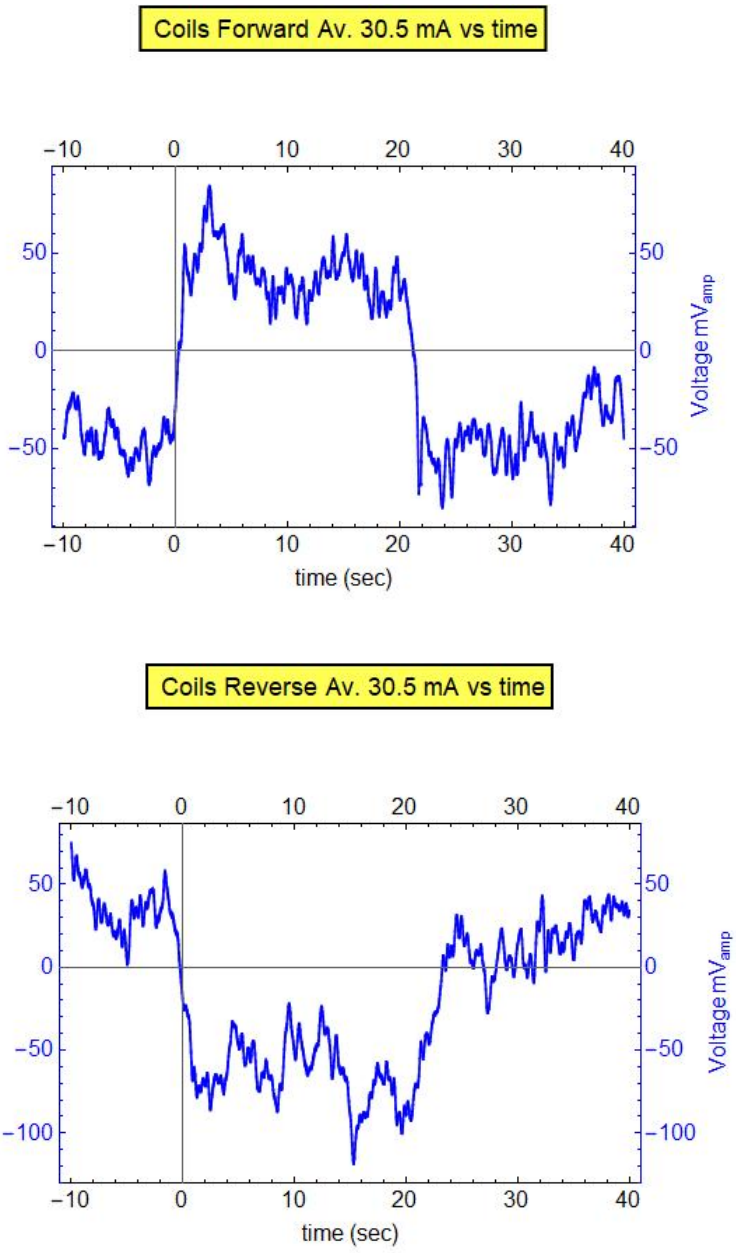

Figure 3.2 Five averaged forward runs (top) and 5 averaged reverse runs (lower).

Then we took forward-reverse runs and averaged those.

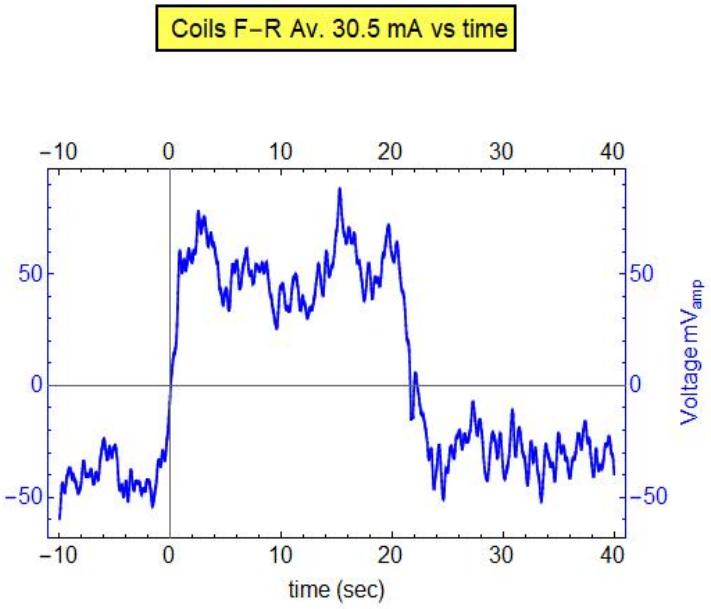

Figure 3.3. Averaged forward minus reversed runs, showing 80 mVolts.

From the last plot, we read the maximum scale for the voltage from the sensor and take the value to be 90mV. Similar plots were done for current runs of 40-80 mA.

The force equations compared here are given below [6]:

$$F_{simple} = \frac{2i^2\, n^2\, R\, \mu_0}{z}$$

$$F_{Maxwell} = \frac{i^2\, n^2\, k\, z\, \mu_0}{2\, R}\left[\frac{(2-k^2)}{(1-k^2)}E(k) \;-\; 2\,K(k)\right]$$

$$\text{where } k^2 = \frac{4R^2}{4R^2+z^2}$$

For our coils we had, the number of turns on each coil n =10, the radius of each coil R=1.5cm and the separation of each set of two coils z=1.15cm. We find k=0.933746. We multiply the known results by 2 since we have 2 sets of 2 coils giving a force, one attracting and the other repelling. The equations above already reflect this multiplication by 2.

The simple force formula above is derived from taking the force F = BIL (from a straight line current I = n i) taking the length L=2 π R and using the basic magnetic field from a wire a distance z away, $B = \frac{\mu_0\, I}{2\,\pi\, z}$. This would be the force between 2 coils, you then multiply by 2 to

get the F_{simple} given above. The elliptic integral formula was first found in a text by Maxwell in vol. 2 of *The treatise on electromagnetism* [6].

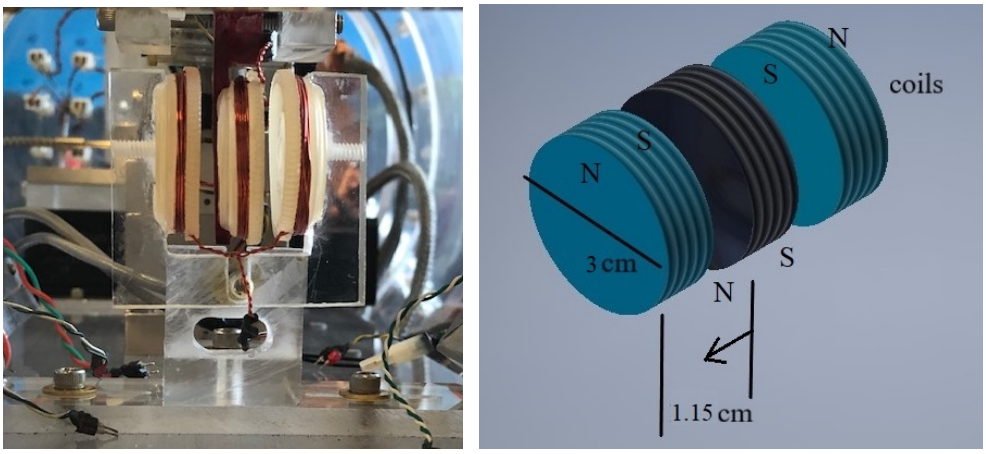

Figure 3.4. Photo left, diagram of coils right. The coil is 10 turns of 28 gauge magnetic wire wound on a lid from a 35mm camera film tube. Middle coil moves with the balance, 2 outside coils are fixed. The current in the outside coils, runs in opposite directions. This allows the left coil to attract and the right coil to repel the central coil.

See Table 3.1 below for the forces for a given current through the coils.

Current through Coils mA	Force Slobodan et al. m=k=25 cells=51	Force (Maxwell) μN	Force (simple) μN	Average sensor Volts in mV
30.5	0.210291	0.209188	0.304953	80
40.1	0.363504	0.361597	0.527135	140
50.1	0.567409	0.564432	0.822827	230
60.3	0.821969	0.817656	1.19198	320
70.4	1.120382	1.1145	1.62472	440
80.7	1.472204	1.46448	2.13491	550

Table 3.1. Table of coil current, forces and sensor voltage. (Thanks to Matthias Kößling, Technische Universität Dresden for pointing out an error in my elliptic integral *Mathematica* code. Thanks to José Rodal for calculating the small corrections due to axial misalignment of the coils, from Slobodan et al paper [3].)

If you plot voltage from the sensor in millivolts verse force in microNewtons you can fit the data to a straight line plot. For the elliptic integral case the plot is shown in Figure 3.5 below.

We may plot the current in milliAmps verse the force for the Maxwell expression as follows:

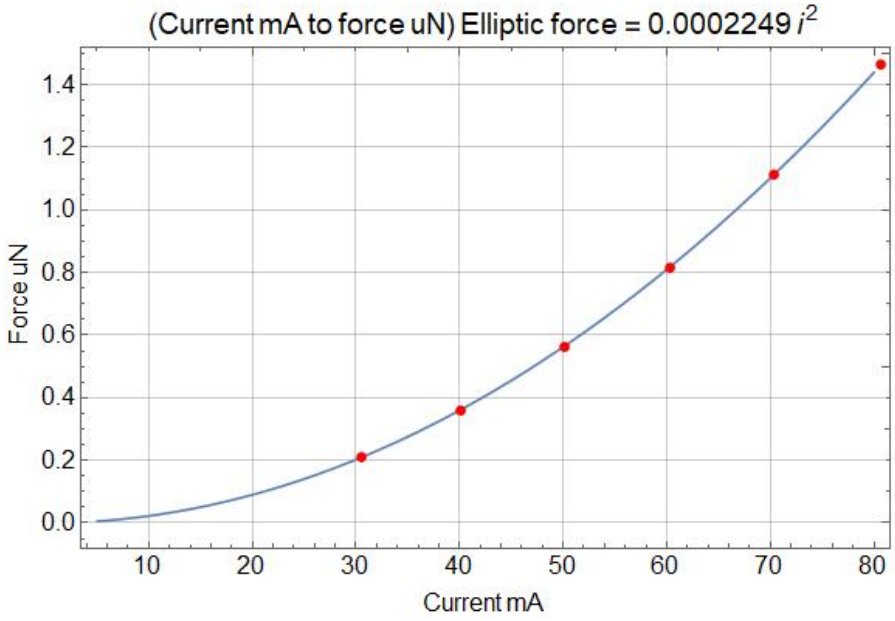

Figure 3.5a. Current applied to coils verse force (Maxwell) calculated. Approximately 67 mA would give 1 µN of force . This appears to agree very well with a weight calibration of the coils (measured on a scale) performed independently by George Hathaway.

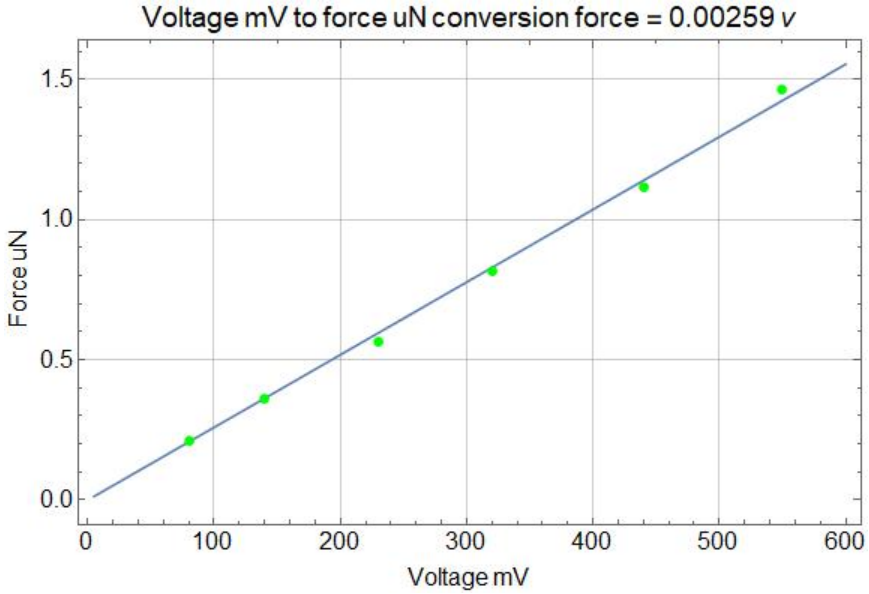

Figure 3.5b. Voltage from sensor plotted against force (Maxwell) from the coils using the elliptic integral equation. The force in µN is 0.00259 times the volts in mV.

We could plot the same thing again but this time using the simplified force equation. See Figure 3.6.

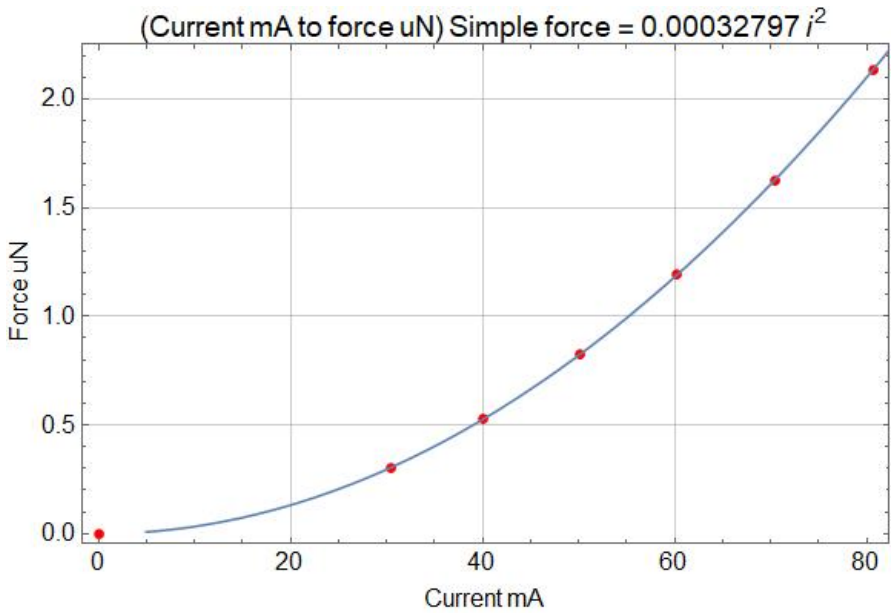

Figure 3.6a. Current applied to coils verse force (simple) calculated. This is not accurate since the simple equation only applies to large diameter coils which are very close together. The formula is derived from 2 line currents which we do not expect to be very accurate.

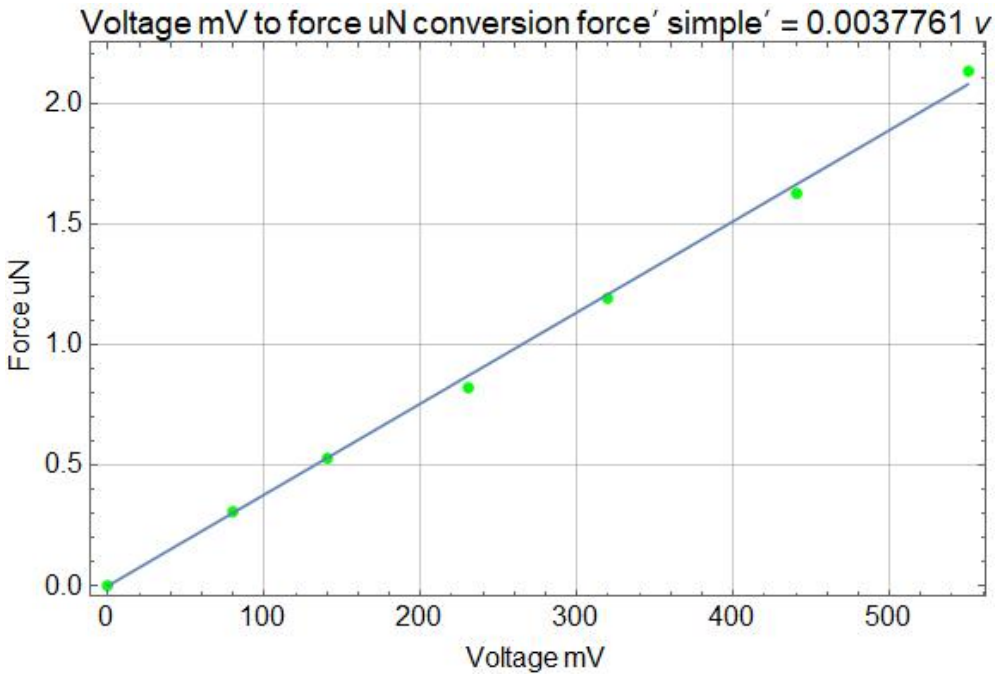

Figure 3.6b. Voltage from sensor plotted against force (simple) from the coils using the Simplified force equation. The force in μN is 0.0037761 times the volts in mV.

Using the elliptic equation by Maxwell for the force the fitted data results show that:

$$F_{coils} = 0.00259 \ (mV)$$

where the voltage would be input in mV to give a force in μN. To convert to the force from the device, which is further away from the pivot than the coils we need to divide by 1.6. Hence, the force in microNewtons is given by,

$$F_{device} = 0.00161875 \ (mV)$$

which is the same as saying that a sensor voltage of (1/0.00161875) , 617.8mV= 1μN .

Using the simple force equation, the fitted data results show that:

$$F_{coils} = 0.00377614 \ (mV)$$

where the voltage would be input in mV to give a force in μN. As before we convert to the force from the device by dividing by 1.6. Hence, the simple force in micro Newtons is given by,

$$F_{device} = 0.00236009 \ (mV)$$

which is the same as saying that a sensor voltage of (1/0.00236009), 424mV= 1 μN .

We have previously used 162 mV per 1 μN microNewton which is an overestimate by a factor of

618/162=3.8 ~4. So previously 4 μN was actually only 1 μN. The elliptic equation can be enhanced slightly by including the misalignment in the axes of the coils, thickness of the wires and layers of windings. We have tried this and it will only change the formula by a small amount.

Displacement Measurements

A rough estimate of the sensitivity of the balance can be calculated from the known force result.

Figure 3.7. C-Flex bearing single sided.

Using the torque per degree as specified by C-flex for their single side bearing E-10 we have

Single End Bearing

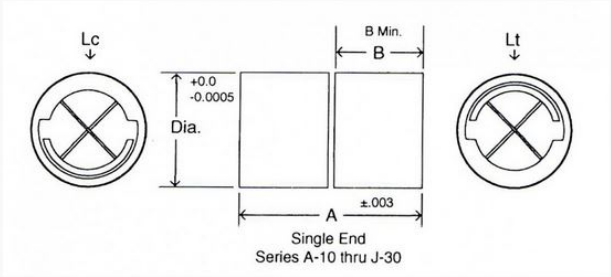

Part No. For Single End A-10 thru J-30	Diameter	Torsional Spring Rate (1)	Load Capacity (2) Lc	Load Capacity (2) Lt	+0 -.0005 Diameter	±.003 A	±.003 B
E-10	5/16	.0037	5.70	22.80	.3125	.500	.232
E-20	5/16	.0296	55.00	78.60	.3125	.500	.232
E-30	5/16	.2367	157.10	157.10	.3125	.500	.232

Figure 3.8. C-flex bearing properties. We are using the E-10 bearing above.[4]

Let us assume a deflection of 2 microns. Then we can find the force required to give a 2 micron deflection and convert from the known force to a voltage from the Philtec D63 sensor. Hence, find the voltage required for a known displacement for the Philtec sensor approximately.

The torque per degree for one bearing is $(\tau_b/\theta) = 0.0037$ pound-inch/degree. This is converted to 0.000418 Nm/deg. The torque from 2 bearings is then twice this amount.

$$\tau_{2b} = 2\,(\tau_b/\theta)\times\theta$$

For a displacement of 2microns and a radius arm length of 25cm the angular deflection would be $\theta = 4.58366\times10^{-4}$ deg. Using displacement s = r $\theta \times(180/\pi)$. Hence:

$$\tau_{2b} = 0.000418 \times 2 \times 4.58366 \times 10^{-4} = 3.832 \times 10^{-7}\ Nm$$

Now if we take $\tau_{2b} = r\,F$, where r is the arm length 0.25m then F = $\tau_{2b}/0.25 = 1.53278 \times 10^{-6}\ N$.

Let us assume this to be F = 1.533 μN which gives a deflection of 2μm.

Using our new calibration of 618 mV per 1 μN. For 1.533 μN, that would imply we have 947 mV for 2 μm.

Hence we see that we get 473.5 mV per μm sensitivity calculated. This is approximate and an underestimate since we did not take the magnetic damping into account.

We must find the exact answer for sensitivity via experiment. We measure the output voltage for known displacements. Then the sensitivity is the number of mV per μm. A jig was made up to hold the optical sensor from the Philtec device, see Figure 3.9. The Phitec optical probe was mounted onto a linear stage with a Vernier scale. The linear stage was bolted down to a plastic base. The reflective surface, from the balance, was attached to a mount and also bolted to the same base as the linear stage. The reflective surface was fixed and the bottom of the stage was also fixed. The Vernier scale could be used to move the optical probe away from the reflective surface. We measured the voltage from the Philtec probe and the distance from the probe to the reflective surface, these numbers were tabulated in Table 3.1, below.

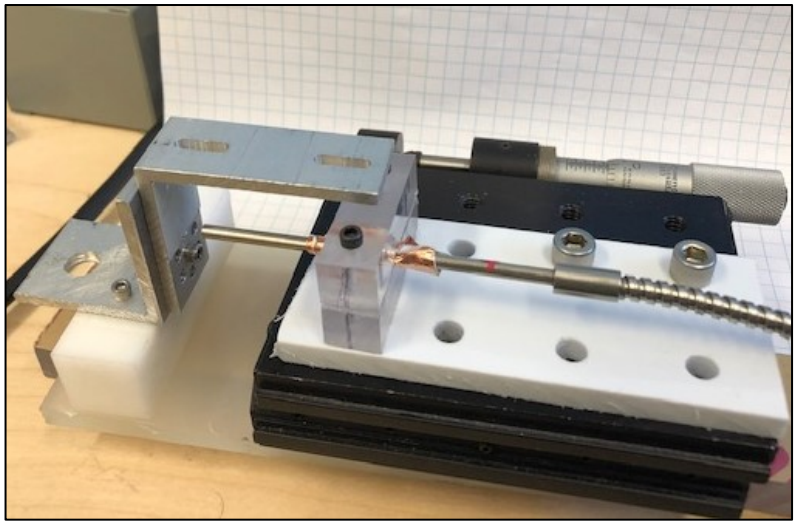

Figure 3.9. Philtec sensor calibration jig. Note that the linear stage is bolted to the same plastic base as the mount bracket for the reflective surface.

The data from Table 3.1 was plotted, and the resulting graph of Philtec voltage (V) verse displacement (μm) is shown below in Figure 3.10.

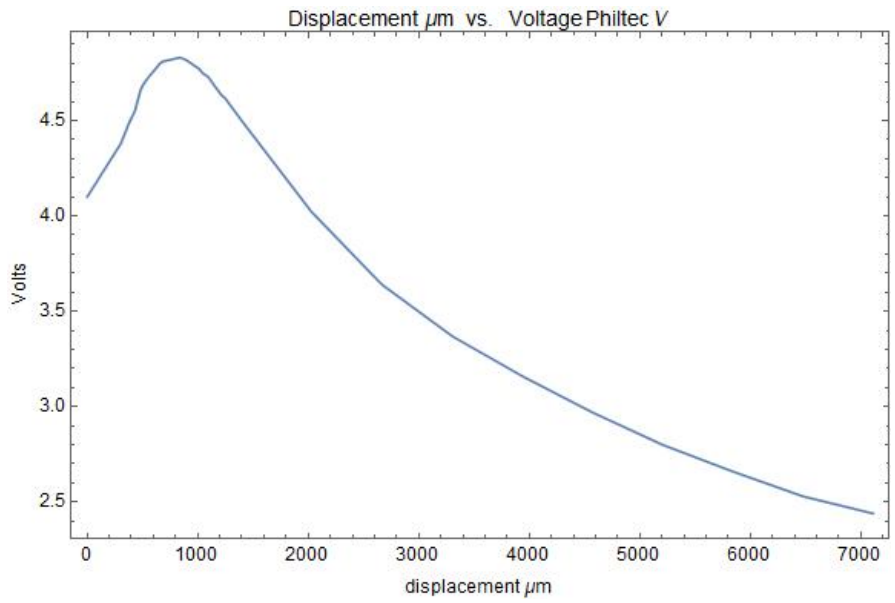

Figure 3.10. Plot of Philtec 63D probe voltage (V) vs. displacement (µm). To the left of the maximum voltage is the near side. To the right of the maximum voltage is the far side. We operate the Philtec on the far side, on the linear slope near the top of the curve.

The linear slope near the top of the curve, shown in Figure 3.10, is plotted for convenience below in Figure 3.11.

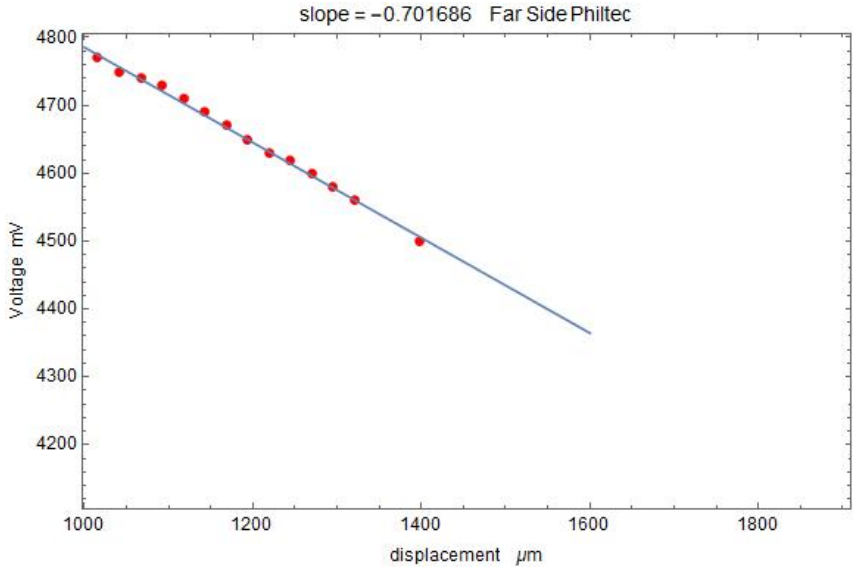

Figure 3.11. Slope of the curve far side. 0.7 mV/µm.

There is also an amplification factor to be considered. The Philtec electronics has a pre-amplifier followed by a main amplifier. The pre-amplifier is a 2-pole Butterworth filter with a gain of k=1.586. The main amplifier in the philtec circuit system was found experimentally to have a gain of 679, see Table 2 below. The slope must therefore be multiplied by these

amplification factors. The slope multiplied by the main amplifier gives 475 mV/μm. This is very close to the calculated value above. However we have not yet taken into account the 2-pole Butterworth low pass filter. The filter requires us to multiply this result by a further value k=1.586, [7]. Then 475 mV/μm * 1.586= 753 mV/μm. As a general rule we will take 750 mV/μm.

Table 3.1 Philtec sensor voltage vs displacement calibration, zero position d=0.170 inches.

Raw Philtec Voltage (V)	Displacement (inches)	Displacement-d	Micron displacement -d
4.10	0.170	0	0
4.38	0.182	0.012	304.8μm
4.49	0.185	0.015	381.0
4.55	0.187	0.017	431.8
4.66	0.189	0.019	482.6
4.69	0.190	0.020	508.0
4.73	0.192	0.022	558.8
4.78	0.195	0.025	635.0
4.80	0.196	0.026	660.4
4.81	0.197	0.027	685.8
4.82	0.200	0.030	762.0
4.83	0.203	0.033	838.2
4.82	0.205	0.035	889.0
4.81	0.206	0.036	914.4
4.80	0.207	0.037	939.8
4.79	0.208	0.038	965.2
4.78	0.209	0.039	990.6
4.77	0.210	0.040	1016.0
4.75	0.211	0.041	1041.4
4.74	0.212	0.042	1066.8
4.73	0.213	0.043	1092.2
4.71	0.214	0.044	1117.6
4.69	0.215	0.045	1143.0
4.67	0.216	0.046	1168.4
4.65	0.217	0.047	1193.8
4.63	0.218	0.048	1219.2
4.62	0.219	0.049	1244.6
4.60	0.220	0.050	1270.0
4.58	0.221	0.051	1295.4
4.56	0.222	0.052	1320.8
4.50	0.225	0.055	1397.0
4.02	0.250	0.080	2032.0
3.64	0.275	0.105	2667.0
3.37	0.300	0.130	3302.0
3.16	0.325	0.155	3937.0
2.97	0.350	0.180	4572.0
2.80	0.375	0.205	5207.0
2.66	0.400	0.230	5842.0

Table 3.2 Direct difference reading across the amplifier in the Philtec circuit.

X=Difference reading (mV)	Y=Meter reading (V)	Scale factor =Y/X
5.7	3.95	693.00
5.6	3.93	701.80
4.9	3.35	683.70
4.8	3.33	693.75
3.9	2.66	682.05
3.8	2.62	689.47
2.6	1.75	673.08
2.5	1.69	676.00
2.4	1.63	679.00
2.0	1.31	655.00
1.7	1.14	670.00
1.4	0.91	650.00
	Average	**678.9 ~ 679**

Conclusions

The Philtec sensor was found to have a scaling of 0.75volts/μm. The method of calibration of the balance remains as stated here. However after the addition of aluminum fins to the balance arm, a second calibration gave the force to be given be 0.1 volts per 1μN. The balance became heavier and required a re-calibration. The damping remained the same.

References

[1] H. Fearn & J. F. Woodward, "Experimental null test of a Mach effect thruster", J. of Space Exploration, Vol. **2**. No. 2, pp98-105, (2013).

[2] Optical Philtec D63 sensor manual online at: http://www.philtec.com/downloadssupport/documentlibrary/documents/datasheets/analog_only /D63.pdf

[3] Slobodan I. Babic & Cevdet Akyel, "Magnetic Force Calculation between thin coaxial circular coils in air", IEEE Trans. On Magnetics Vol. **44**, No. 4., pp445-452 (2008).

[4] C-flex bearings https://c-flex.com/pivot-bearings/bearings-size-performance-properties/

[4] Knight, Randall , *Physics for Scientists and Engineers, "*Magnetic forces on current carrying wires", 2nd Ed. California: Pearson, Addison-Wesley 2008. pp 1024-1026.

[5] Simple force expression see also: http://ocw.mit.edu/courses/physics/8-02t-electricity-and-magnetism-spring-2005/labs/exp08.pdf

[6] Maxwell, J., *A Treatise on Electricity and Magnetism*, Volume 2, 3rd edition 1892 (edited by J. J. Thomson), Dover Publications, Jun 1, 1954

[7] P. Horowitz and W. Hill, *The Art of Electronics,* 2nd ed. P274, Table 5.2 2 pole low pass filter gain for Butterworth filter k=1.586.

4. Balance beam dynamics

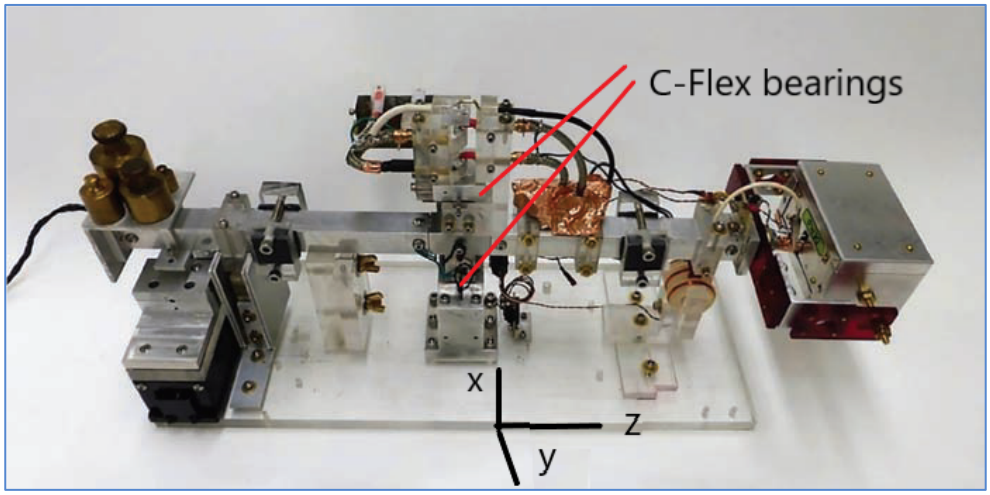

Figure 4.1. The torsional pendulum at CSU Fullerton.

The force balance is a torsional pendulum that swings in the horizontal plane. There are two bearings; these are C-Flex flexural bearings model E-10. [1].

The C-flex bearing is a so-called "frictionless" bearing which looks like the Figure 4.2 below.

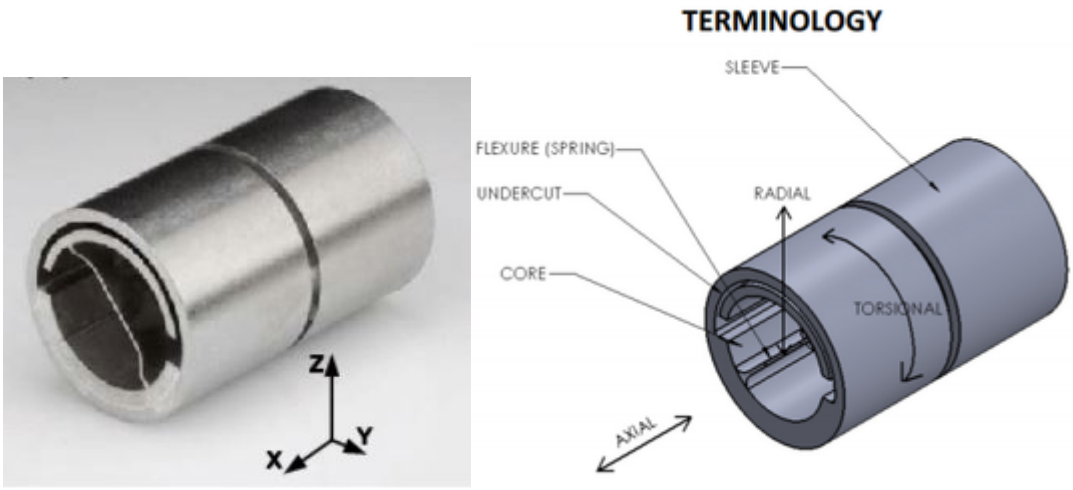

Figure 4.2. C-flex bearing and diagram labeling directions and terminology.

Hysteresis and life expectancy charts are available for the C-flex bearing company website, [1]. Two of these bearings are located in the central column one above and one below the level of the balance arms.

The operation of the balance is based on the forces damped harmonic oscillator, the theory of which is well known [2]. The pendulum torque dynamics can be understood using the following equation,

$$F(t)\,L \;=\; I\,\ddot{\theta} \;+\; C\,\dot{\theta} \;+\; k\,\theta \qquad (1)$$

where torque $\tau(t) \;=\; F(t)L$, and θ is angular position of the balance arm. I is the moment of inertia of the balance arm, with the Faraday cage on one side and the weights on the other (the weights are such as to balance the Faraday cage for no tipping motion). C is the damping constant and k is the spring constant. We may easily rearrange the equation as follows,

$$\ddot{\theta} \;+\; 2\,\gamma\omega\dot{\theta} \;+\; \omega^2\,\theta \;+\; F(t)\,L/I \qquad (2)$$

where $\omega^2 \;=\; k/I \;\; so\; that \;\; \omega = (\,k/I)^{1/2}$. Also, $2\,\gamma\omega \;=\; C/I$ and so the damping coefficient becomes,

$$\gamma \;=\; C/(2\,I\,\omega) \;=\; 0.5\,C\,/(Ik)^{1/2}$$

We assume that the force starts at time t=0 and is a steady force F_0, when t < 0 the force is taken to be zero. For the angle at steady state $\theta \;=\; \theta_{ss}$, the time derivatives of θ are zero and we get,

$$\theta_{ss} \;=\; F_0\,L/(\,\omega^2\,I) \;=\; F_0\,L/k \qquad (3)$$

We can then normalize the equation with respect to the steady state θ_{ss}. Allow

$\theta_1(t) \;=\; \theta(t)/\theta_{ss}$, then the equation of motion becomes,

$$\ddot{\theta_1} \;+\; 2\,\gamma\omega\,\dot{\theta} \;+\; \omega^2\theta_1 \;=\; \omega^2 \;. \qquad (4)$$

This can be solved by standard methods (or Laplace transform) to find the auxiliary equation to be $m \;=\; -\,\omega\gamma \;\pm\; \omega\,(\gamma^2 - 1)^{1/2}$ which takes on different values depending on the size of the damping coefficient γ. There are three specific cases, $\gamma \;> 1,\; \gamma = 1 \;and\; \gamma < 1$.

<u>Critical-Damping $\gamma = 1$</u>

The solution takes the form;

$$\frac{\theta(t)}{\theta_{ss}} = \theta_1\,(t) \;=\; e^{-\omega t}(\,A\,t \;+\; B) \;+\; const. \qquad (5)$$

since the values of the auxiliary equation are real and the same. This can now be solved by assuming that $\dot{\theta}(0) \;= 0$. We normalize the starting position to $\theta_1(0) \;=\; 1$, so that for steady state $\theta(t = 0) \;=\; \theta_{ss}$ as before. Setting $\dot{\theta_1}(0) \;= 0$, we find $A \;=\; \omega B$ which is solved when $A \;=\; -\omega \;\; and \;\; B \;=\; -1$. This gives the result,

$$\theta_1(t) \;=\; 1 \;-\; e^{-\omega t}\,(\,1 \;-\; \omega t) \qquad (6)$$

The constant can also be resolved by substituting trial Eq. (5) into the original Eq. (4), which makes clear that the constant is unity. This agrees with [2].

Using a similar method we can easily show that for damping $\gamma > 1 \ and \ \gamma < 1$ we obtain the following results.

Over-Damping $\gamma > 1$

$$\theta_1(t) = \alpha e^{-\gamma\omega t}(A\, e^{\omega t(\gamma^2-1)^{1/2}} + B e^{-\omega t(\gamma^2-1)^{1/2}}) + const. \quad (7)$$

By substituting this trial solution into the original Eq. (4) we show that the constant must be 1.

Then by setting $\dot{\theta_1}(0) = 0$ we find that the constants become,

$$A = -1/[\gamma - (\gamma^2 - 1)^{1/2}]$$

$$B = 1/[\gamma + (\gamma^2 - 1)^{1/2}]. \quad (8)$$

Requiring that $\theta_1(0) = 1$, we get the value for the constant $\alpha = 1/[2(\gamma^2 - 1)^{1/2}]$ giving,

$$\theta_1(t) = 1 - \frac{e^{-\omega\gamma t}}{2(\gamma^2-1)^{1/2}} \left[\frac{e^{\omega t(\gamma^2-1)^{1/2}}}{\gamma-(\gamma^2-1)^{1/2}} - \frac{e^{-\omega t(\gamma^2-1)^{1/2}}}{\gamma+(\gamma^2-1)^{1/2}}\right] \quad (9)$$

which we will not be using further, but corrects the minus sign typo in [2].

Under-Damping $\gamma < 1$

The damping of interest to our experiment is this one where the auxiliary equation becomes,

$$m = -\omega\gamma \pm i\,\omega\,(1-\gamma^2)^{1/2} \quad (10)$$

and leads to solutions of the form,

$$\theta_1(t) = 1 + e^{-\omega\gamma t}(A\, cos[\,\omega(1-\gamma^2)^{1/2}t] + B\, sin[\,\omega(1-\gamma^2)^{1/2}t] \quad (11)$$

where using $\dot{\theta_1}(0) = 0$ it can be shown coefficients A and B take on values,

$$A = -1\,, \quad B = \frac{-\gamma}{(1-\gamma^2)^{1/2}} \quad . \quad (12)$$

Giving

$$\theta_1(t) = 1 - e^{-\omega\gamma t}(cos[\,\omega(1-\gamma^2)^{1/2}t] + \frac{\gamma}{(1-\gamma^2)^{1/2}} sin[\,\omega(1-\gamma^2)^{1/2}t]) \quad (13)$$

which also agrees with Ref [2].

To compare the three cases, we have made up a plot using critically damped, overdamped and underdamped motions, see Figure 4.3 below.

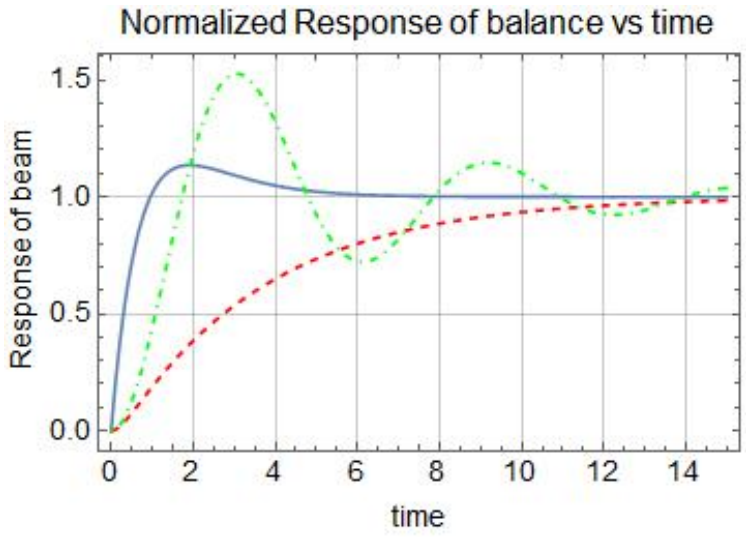

Figure 4.3. A *Mathematica* plot showing all three types of motion. Overdamped $\gamma = 2$ is dotted in red. Critically damped $\gamma = 1$ is a solid line in blue and underdamped $\gamma = 0.2$ is the dot dashed line in green.

To see how well these results agree with the real motion of the torsional pendulum, we conducted tests using a known force from a set of current carrying coils. Two of the coils are fixed on the base of the pendulum a third coil is fixed to the balance arm and moves with the arm. We supplied current (80 mA) to the three coils and watched the deflection of the balance arm on a Picoscope. Taking 5 runs forward and 5 runs reverse HF was able to get averages of the runs in both the forward and reverse directions. we could also take the difference between forward and reverse (which should cancel the non-reversing force) and the sum that shows the amount of noise in the system. The plots are shown below:

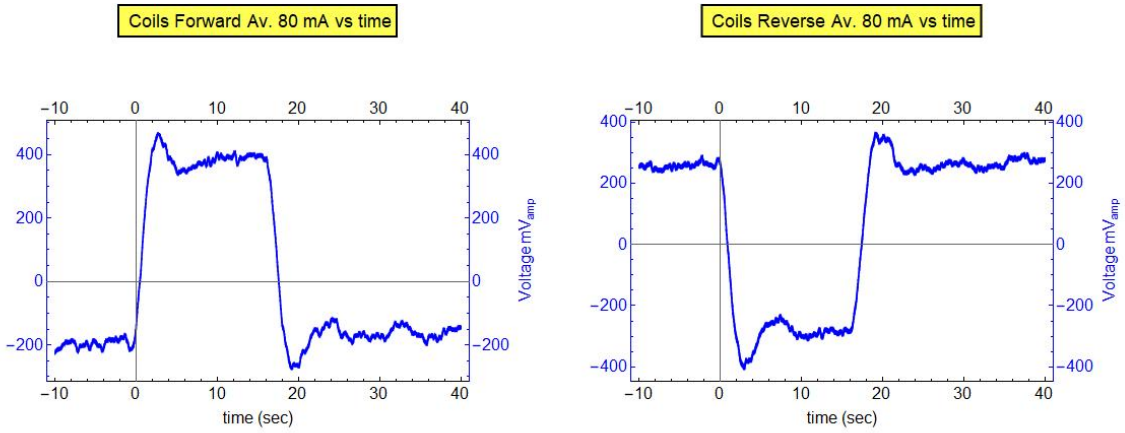

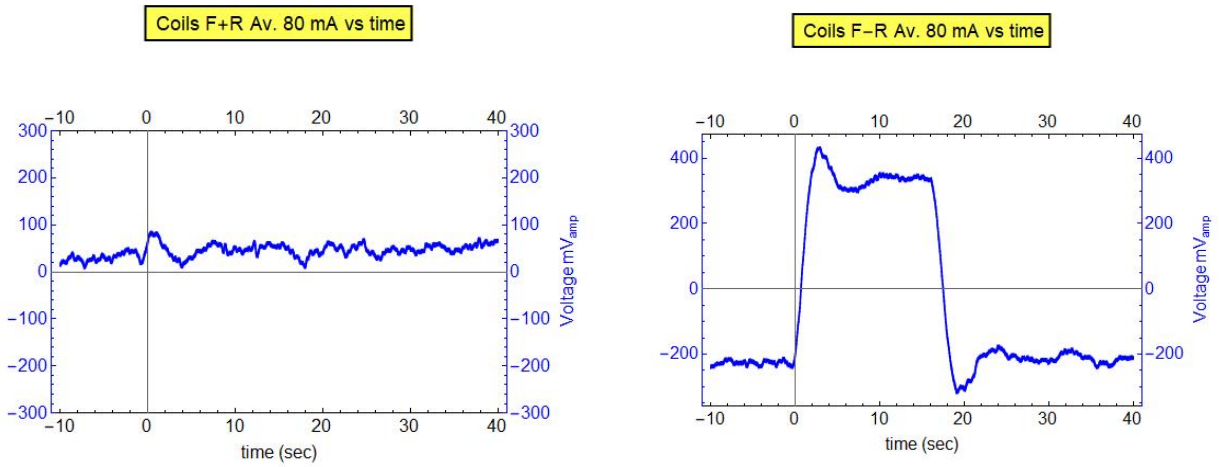

Figure 4.4. Plots of the force from the coils at 80mA. Forward, reverse the difference and sum.

In order to find the damping we took the forward minus reverse averaged data (F-R) in fig 4.5. lower left and examined the turn off, at about 16 seconds and the resulting swing back of the balance beam. In order to fit the equations above it would be necessary to invert this region, from 16 seconds to 40 seconds, of the plot, since the equations assume to start from zero and swing up and get to a steady state around unity. Normalization would also be necessary.

The plots were done using *Mathematica*. The data manipulation was also done using *Mathematica* and eventually FindFit would be used to fit the curve to the force damped harmonic oscillator equation and the coefficients for damping can then be read off.

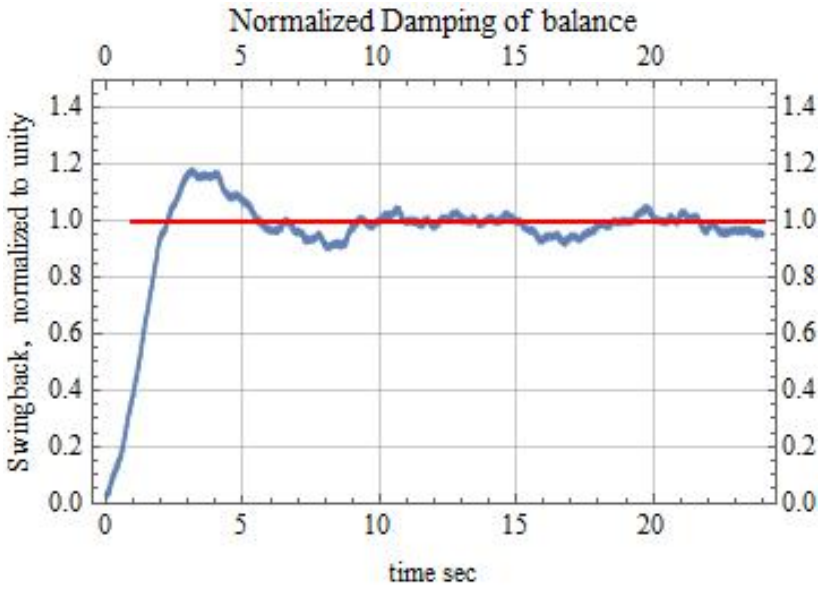

Figure 4.5. The result of taking the F-R averaged data, and subtracting off the noise from F+R. The data has been normalized using a factor of 1/340 and the time scale now reads 0-24 rather than 16-40 seconds. This data was then used to curve fit to a damped harmonic oscillator equation of the type Eq. (10) above.

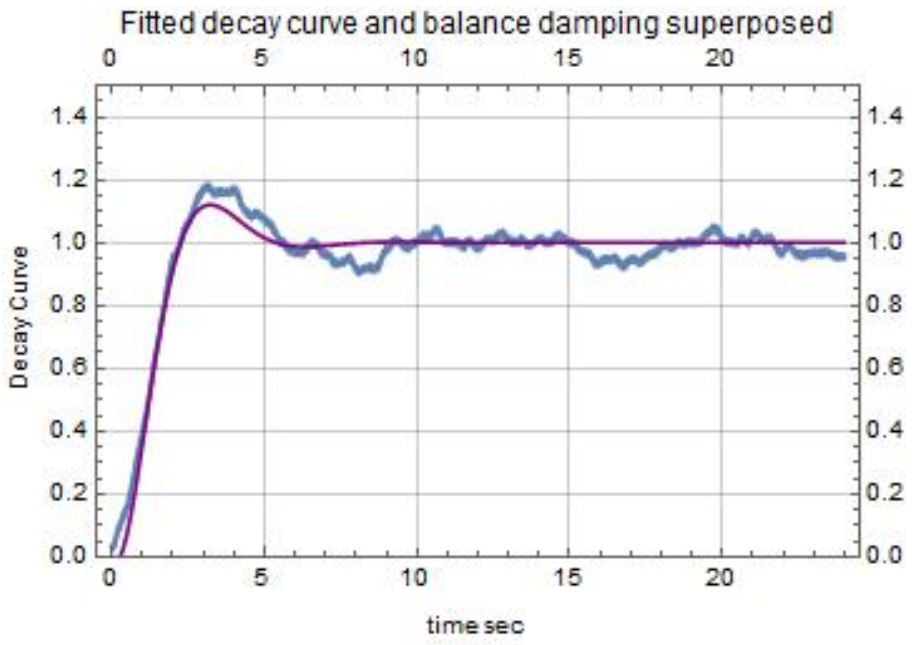

Figure 4.6. The fitted curve is seen in purple superimposed upon the data in blue.

The natural oscillation of the beam is approximately 6 seconds. This can be seen in Figures 4.5 and 4.6.

The *Mathematica* curve used for the FindFit expression was

$$y(t) = 1 - e^{-wgt}(\cos(wbt) + 0.9\sin(wbt)] \qquad (14)$$

where the fit we used parameters, w= 1.047= 2 π/6 , g=0.66~0.7 and b=0.97 . Note that the theoretical value of the coefficient of sine would be 0.879 not 0.9 exactly but we thought that was close enough due to the noise in the data. The coefficient inside the cos/sin terms should be b=0.75, so the b here is a little large, probably due to noisy data. It is a reasonable fit to the data, see Figure 4.6.

We take this to mean that the damping coefficient γ=0.66 in our balance beam. The period is about 6 seconds.

Moments of Inertia: Derivation of damping and spring constant, C and k respectively

Taking the distance from the pivot (in the central column) to the end of the balance arm (where the yoke for the Faraday cage attaches) to be of length r_1=18cm and to the middle of the faraday cage to be r_2=24cm. The mass of the square aluminum tubing for the 18 cm arm is m_{arm} ~100g and the mass of the Faraday cage with yoke is m_{cage} ~ 400g. The moment of inertia of one entire arm plus Faraday cage is $I_1 = I_{arm} + I_{cage} = \frac{1}{3} m_{arm} r_1^2 + m_{cage} r_2^2 = 0.02414$ kg m^2

. This is only for one side of the balance beam however, so for the full arm we take the moment to be,

$$I = 2\, I_1 = 0.04824 \text{ kg m}^2. \quad (15)$$

The response time of the balance is given by,

$$t = 4/(\gamma\, \omega) = 5.789 \text{ sec.} \sim 6 \text{ sec.} \quad (16)$$

The spring constant is given as [2] ,

$$k = I\, \omega^2 = 0.0529. \quad (17)$$

We also have that the damping coefficient γ is related to the damping constant C via,

$$C = 2\, \gamma \sqrt{(I\, k)} = 0.0667 \quad (18)$$

where the characteristics of the balance will be complete by specifying L=24cm. Now Eq. (1) should be a fairly good description of the balance beam.

(The aluminum square tube of 18cm is about ~50 g. There is a coil and wires inside it and a plastic and rubber damper on the beam arm they have a total mass of another ~50g hence the 100g estimate for the beam arm. This could still be an overestimate, but the results do not change that much. For comparison, if the beam arm has instead a mass of 150g, I = 0.04932 kg m^2 , k= 0.054 and C = 0.068.)

References:

[1] C-Flex Bearing Co. (See E-10 flexural bearing specifications.)
https://c-flex.com/pivot-bearings/bearings-size-performance-properties/

[2] James E.Polk et al. "Recommended Practices in thrust Measurements", IEPC-2013-440, in the 33rd International Electric Propulsion Conference, Washington DC 2013.

Appendix A. C-Flex bearing data sheets – https://c-flex.com/

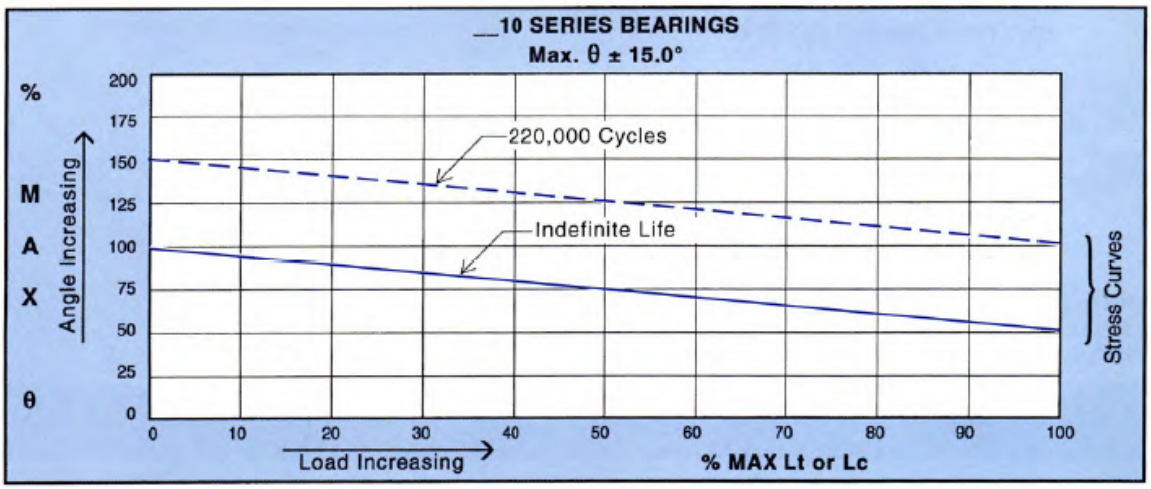

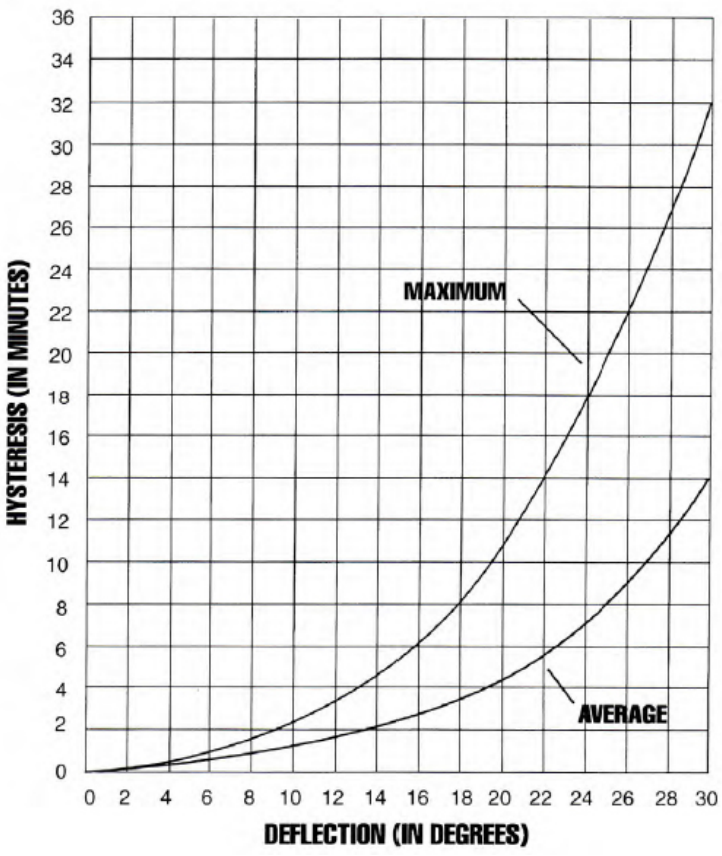

CAD simulation here: https://c-flex.com/wp-content/uploads/2016/10/Bearing-Simulation-Procedure-Customer-Version.pdf?x18635

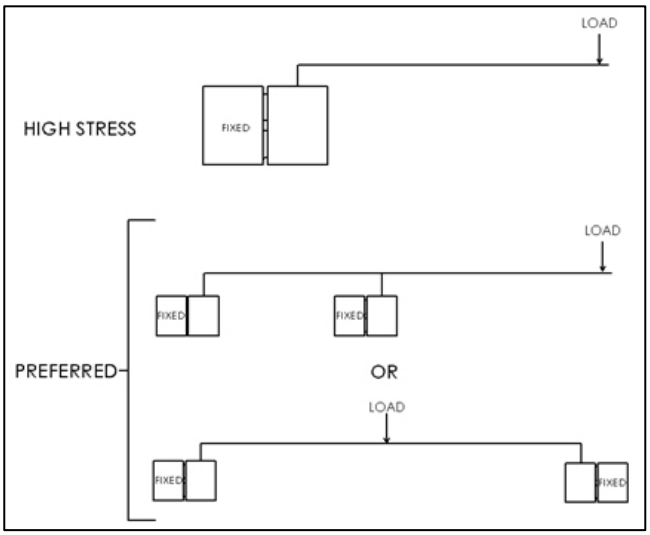

The balance beam uses the lower loading method. The c-flex bearings are above and below the arms in the central column. The arms would be the load. Imagine the lower diagram vertical.

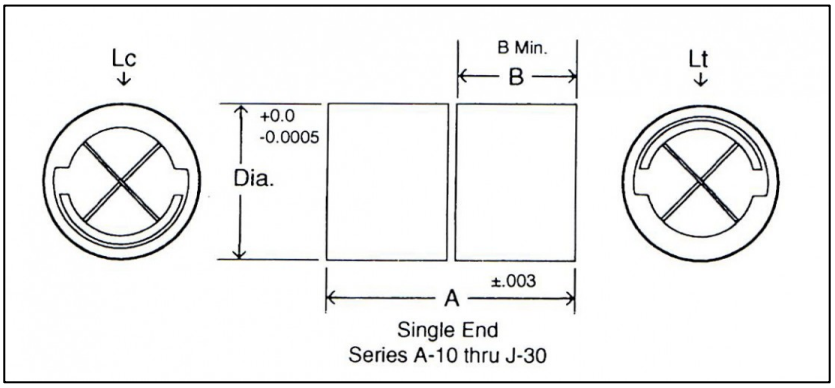

For the E-10 single end bearing: (A= 0.5 inch, B = 0.232 inch.)

*Stiffness of bearing is related to inches of deflection per pound load.

Diameter = 5/16 inch = 0.3125 inch

Torsional spring rate = 0.0037

Load capacity (load in compression) Lc = 5.70 lb

Load capacity (tension) Lt = 22.80

The total stiffness of a pair of tandem mounted cantilevered bearings connected very stiffly in a mechanical system may be determined by dividing the above values by **three.*

Appendix B. Philtec optical sensor for displacement measurements.

http://www.philtec.com/

Fiberoptic Sensor - *Reflectance Dependent*

Model D63

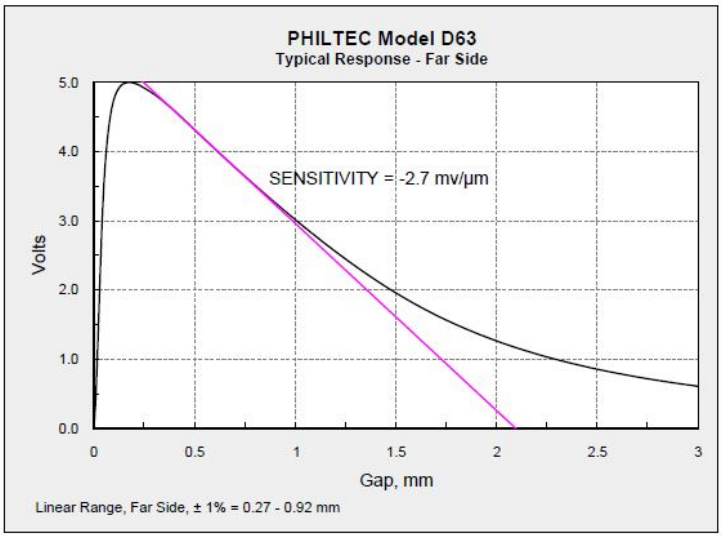

Conversions

1 µm = 39.37 µinch
1 mm = 39.37 mils

1 mil = 0.001 inch
1 mil = 25.4 µm
1 mil = 0.0254 mm

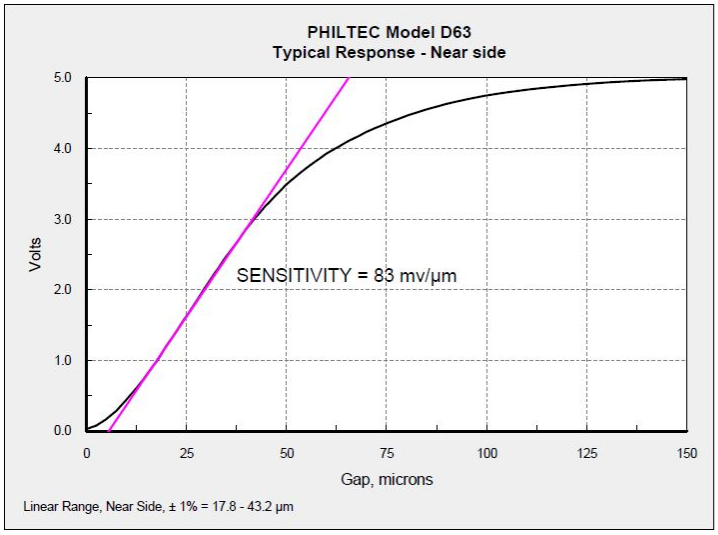

Conversions

1 µm = 39.37 µinch
1 mm = 39.37 mils

1 mil = 0.001 inch
1 mil = 25.4 µm
1 mil = 0.0254 mm

5. Doming Of The Brass And Aluminum Masses

The MEGA drive, depicted below inside a half Faraday cage shows the number 4. This stands for 0.0004" dome height on both the brass and aluminum end masses.

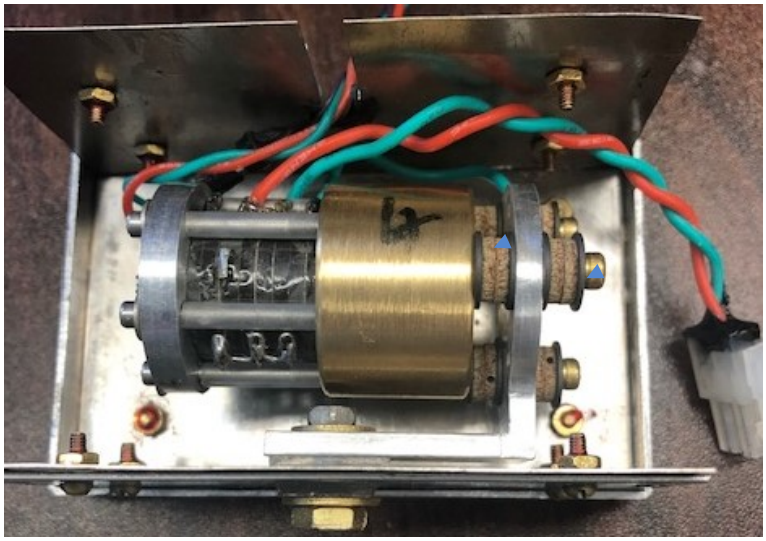

Phenolic washers for 4:40 screws and

Titanium washers.

Figure 5.1. MEGA drive with phenolic washers and titanium flat washers.

We systematically tested domes of heights 0.0004", 0.0005", 0.0006" and 0.0008 inches to discover which gave the most even transfer of pressure over a greatest area of the PZT stacks.

We also were testing for force, and under the same circumstances that provided the best force profile. We ran each dome on a separate pristine device (never before used). All of the new stacks were made of 2mm thick SM-111 crystal, 8 crystals long with an embedded accelerometer (strain gauge) 2 discs into the stack. This strain gauge is always located toward the aluminum end mass, as opposed to the brass end. We ran the devices at amplifier level 12 using a DCM2000 audio amplifier. The test was a 20 second sweep from 45 kHz down to 25 kHz.

Using a signal from a Rigol DG1032Z signal generator with V_{RMS} =1.2 volts input signal.

All the devices were run in the forward direction.

Results of these tests, by dome height, are presented following. We show the pattern of compression visible on the bronze mesh of the stack (aluminum end) and a typical sweep run showing voltage, strain gauge, temperature change and force.

Dome height 0.0008 inches: our standard height (in use for ~1 year)

The bronze mesh electrode, located at the end of the stack, reveals an impression of where it touched the dome of either the aluminum mass or the brass mass. We found that the marks from the aluminum mass were easier to see. Below is a picture of the bronze mesh after 20 or more runs of the device for 20 seconds.

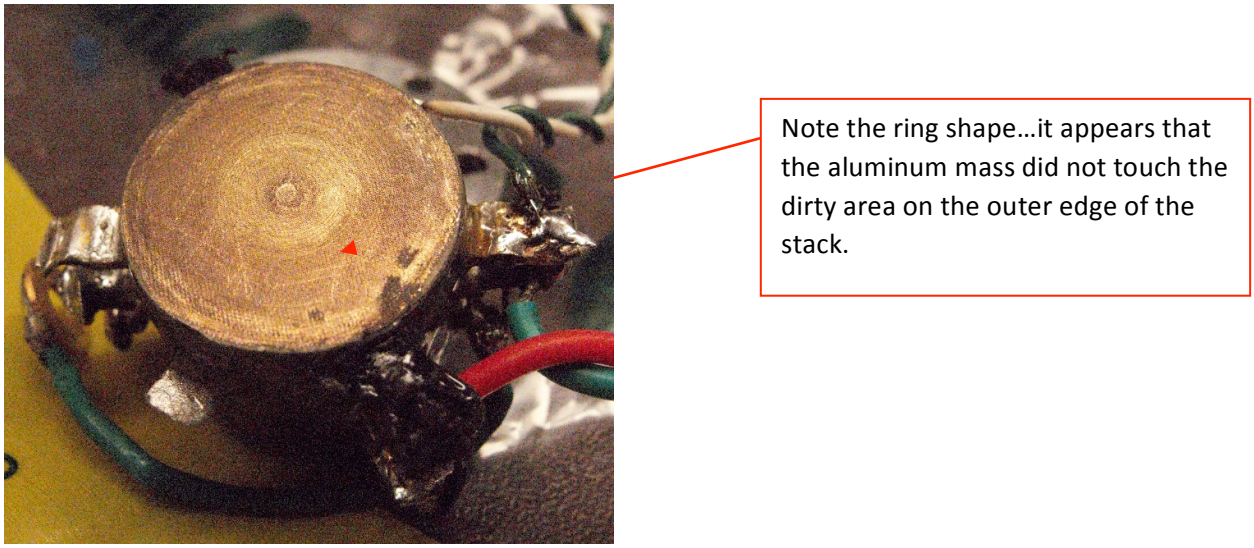

Figure 5.2. Bronze mesh, aluminum end using 0.0008" dome height.

It is clear that the 0.0008" dome height is too tall, and only the center of the mesh appears to have been touching the aluminum mass. We need to lower the dome height. The sample run was taken by JFW in January 2020.

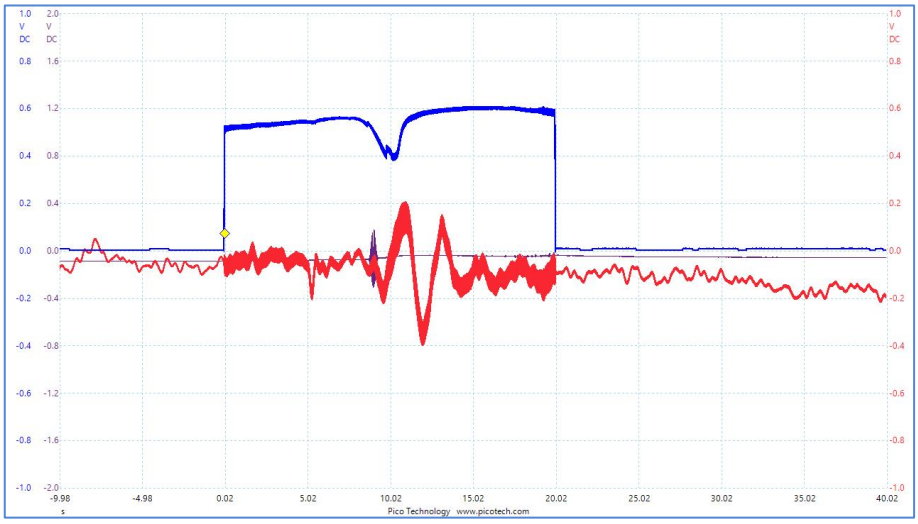

Figure 5.3. Run of NS5, using 0.0008" domes. Sweep 45-25kHz in 20 sec. Blue line is input voltage, Red line is the force, measured in volts here, and the purple line is a measure of temperature.

Dome height 0.0006 inches

Below is a picture of the bronze mesh after 20 runs of a pristine stack device for 20 seconds. The image shows a ring now much further out from the center of the stack, which means there is a better pressure distribution on the PZT crystals from compression of the stack with the bolts holding it.

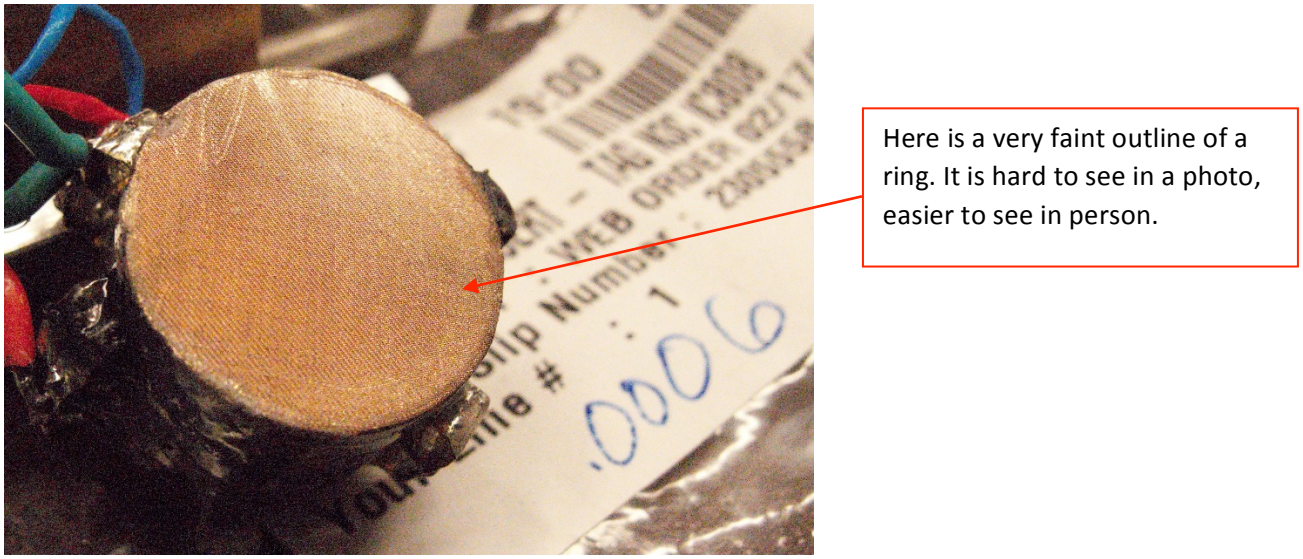

Figure 5.4. Dome height of 0.0006 inches, after 20 runs. Bronze mesh facing the Aluminum end mass. Using pristine stack 1.

A sample run of a sweep 45-25kHz for 20 seconds follows.

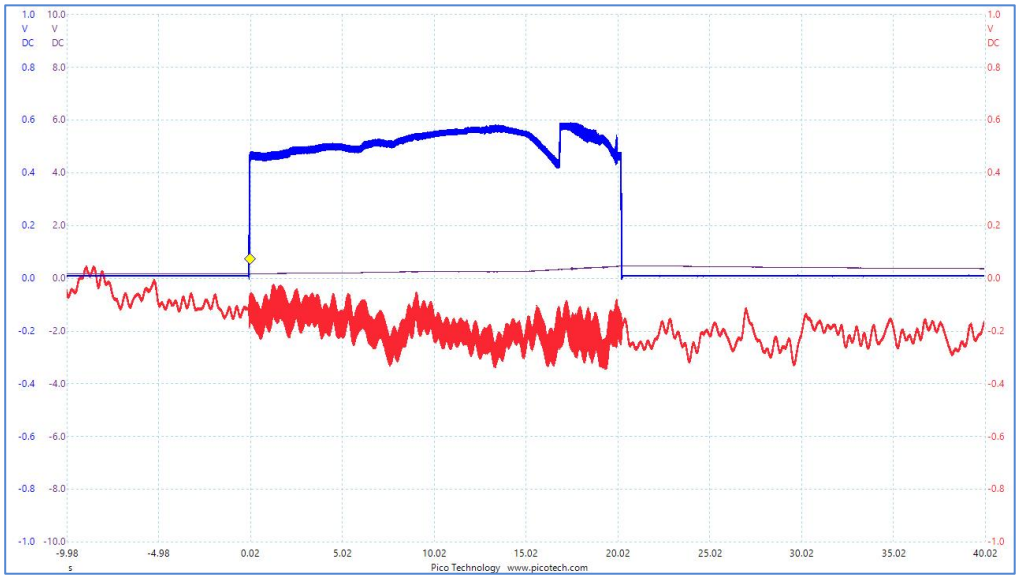

Figure 5.5. Standard sweep 45-25 kHz in 20 seconds, using pristine stack 1. Not much going on here, most likely the #1 stack is no good. Blue line is input voltage, Red line is the force, measured in volts here, and the purple line is a measure of temperature.

Dome height 0.0005 inches

Below is the image of the bronze mesh at the end of the stack using 0.0005” dome heights. The image shows several rings but the outermost ring is closest (so far) to the outside of the stack diameter. The inner rings are probably the marks of the machining process.

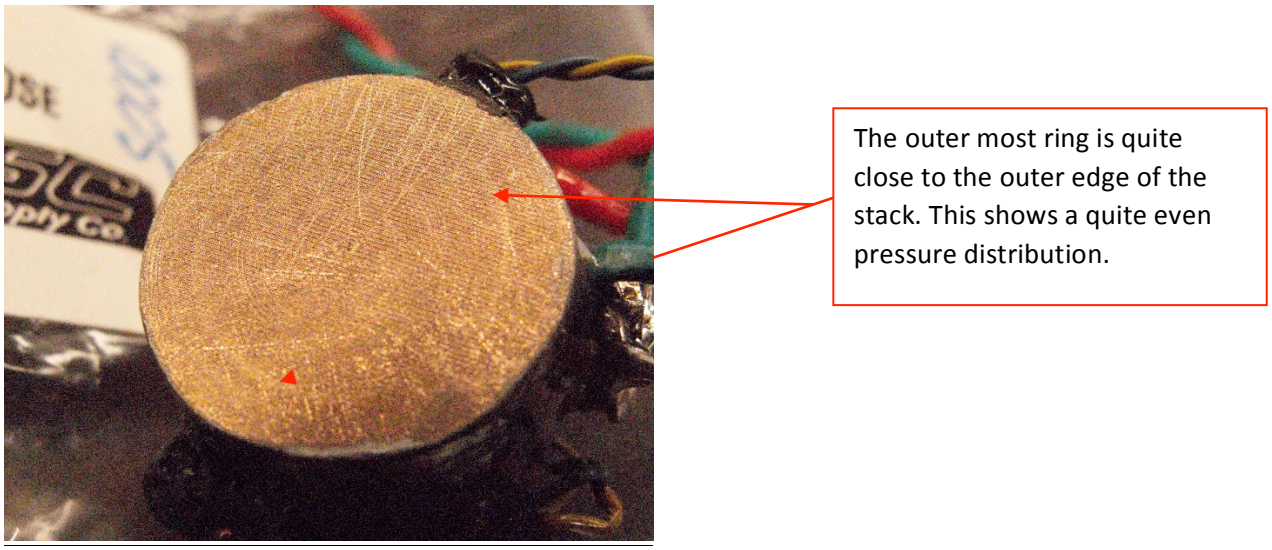

Figure 5.6. Rings on bronze mesh from Dome height 0.0005 inches.

A sample run using this pristine stack 2 with the 0.0005” dome heights for the brass and aluminum masses can be seen below.

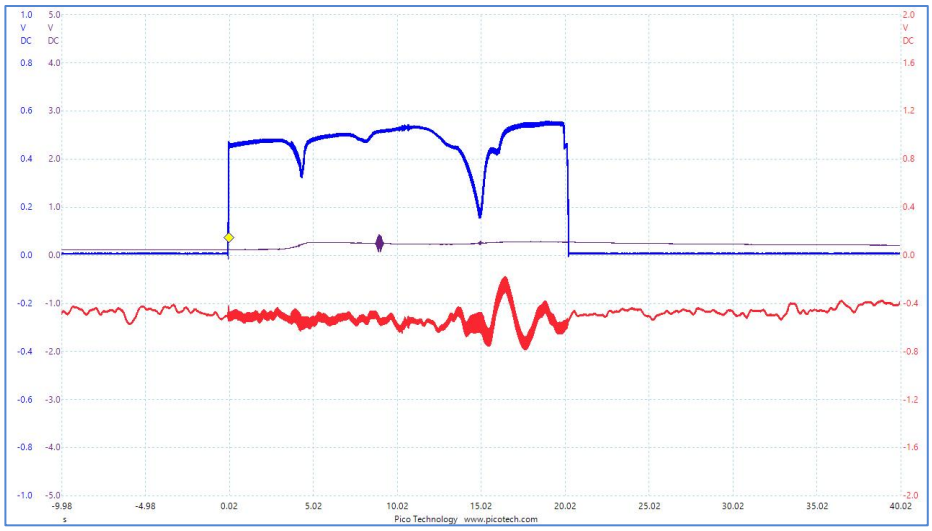

Figure 5.7. Sample run with dome height 0.0005”. Pristine stack 2. Blue line is input voltage, Red line is the force, measured in volts here, and the purple line is a measure of temperature.

Dome height 0.0004 inches

With this dome height, it was very difficult to makes out the rings on the bronze mesh. By looking at a glancing angle you can barely see a slight difference in coloration. There is a probability now that the edges are under more pressure (risk of cracking) because the dome height is too small. This was pristine stack 3.

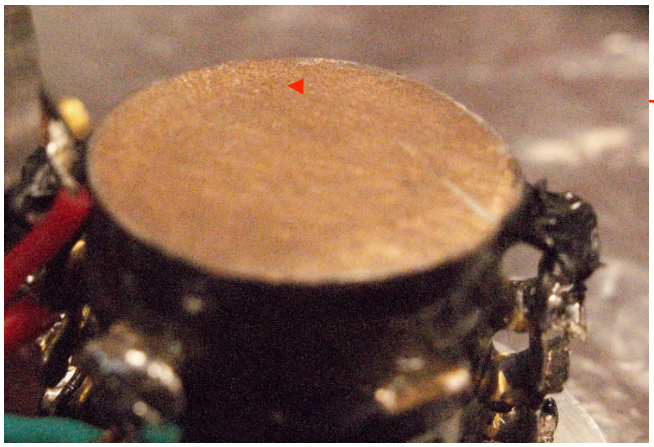

Difficult to make out, but there is a ring near the edge. Parts of the edge appear shiny. The dome maybe too flat. There could be a risk of cracking the edge of the crystals.

Figure 5.8. Bronze mesh with dome height 0.0004 ". Hard to see here but the edge looks shiny so we believe the dome is too flat now.

We took 20 sample standard sweep runs, one of them is displayed below.

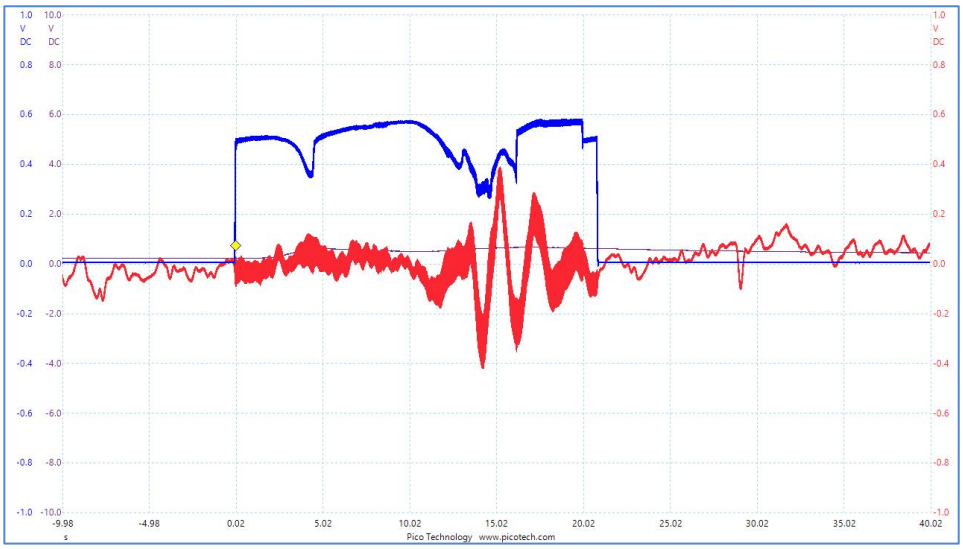

Figure 5.9. Sample run with pristine stack 3, and dome height 0.0004 inches. Stack 3, looks like a good stack. Blue line is input voltage, Red line is the force, measured in volts here, and the purple line is a measure of temperature.

Conclusions

We decided that the best dome height to use was 0.0005 inches for both the aluminum and the brass masses. The dome height 0.0004 inches also showed good results, but we ran the risk of damaging the outer edge of the PZT crystals with cracking.

6. Use Of Glued Stacks And Design #1 Sledge

The lead zirconium titanate (PZT) stacks are usually just held in between the brass and aluminum end masses by six 2-56 stainless steel screws. In this test we tried gluing the stack directly to the masses and then also applied the 4 in-lbs. torque to the screws. The same epoxy that holds the discs in the stack was used to glue the stack to the brass and aluminum. The stack was heated in a lab oven (Jeio tech OF-02G) for 1 hour at 140°F to cure the epoxy.

The stack in question was new stack #4. It use eight Steiner Martins PZT SM-111 discs that are 2mm thick and 19mm in diameter.

The brass masses to be tested are listed in table 6.1 below.

Table 6.1. List of brass masses under consideration. Highlighted masses were also glued to a stack.

Brass length	0.375"	0.4375"	0.5"	0.55"	0.618"	0.68"	0.75"
Brass mass	44.5g	52g	61g	68.5g	76g	84g	91g

We used the same testing protocol as before. A Rigol signal generator DG1032Z with V_{RMS} =1.2 volts input was used to produce a signal to a Carvin DCM2000 amplifier, at level 12. The signal used was a sweep from 45 kHz down to 25 kHz over 20 seconds. We measure the output voltage to the device, the force produced by the device and several other parameters like the strain, FFT and temperature during the run. All the data is collected by Picoscopes and a movie is recorded. Using the 0.618 inch brass mass glued stack we tested both the L bracket and the sledge. Both systems (L bracket and sledge) were using the 3 double phenolic washer mounting method and titanium flat washers.

L Bracket Mount

The 0.618" mass is slightly lighter than the standard 0.75" mass so an extra 15g is placed on the beam arm. (Even with the 0.75" mass we use a 10g mass on the beam arm near the Faraday cage.) In the first test all the weight was on the arm near the Faraday cage. In the second test a 20 g mass was placed on top of the Faraday cage, to see is the placement of the masses would make a significant difference to the force measured. Both runs were made in the forward direction.

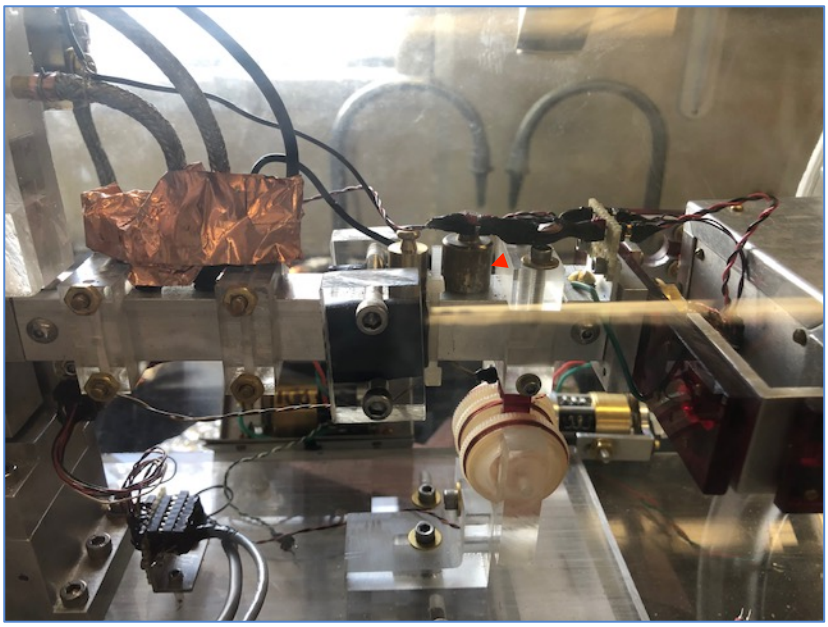

Counterpoise masses are placed here on the balance arm. 20g and a 5g mass.

A

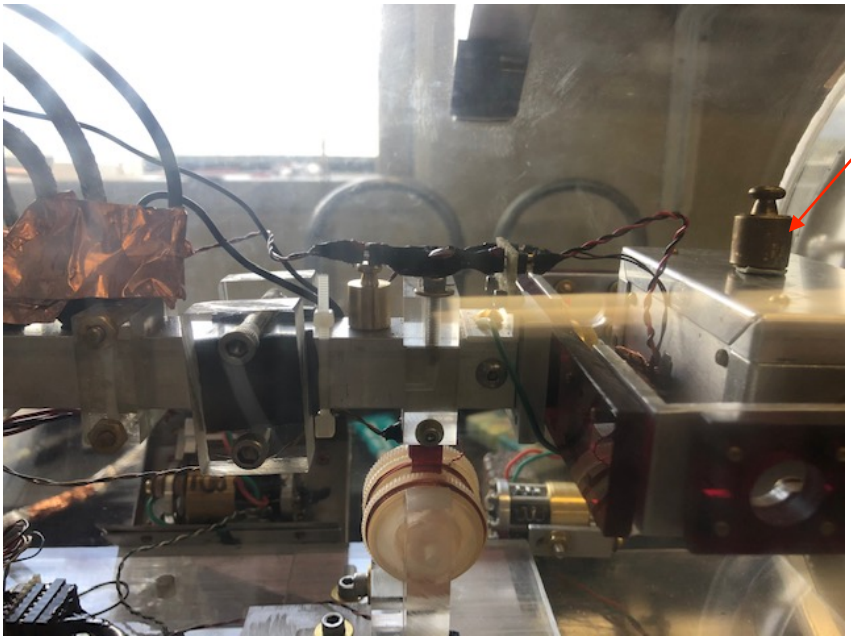

The counterpoise 20 g mass was moved onto the top of the Faraday cage- to see if there was any difference in the force signature. The 5g mass remained on the beam arm.

B

Figure 6.1. Counterpoise mass positioning on the balance arm. Does the location of the masses make a big difference to the force signature? Answer is NO – the force signature remained very nearly the same for both these configurations. In fig 1A, the masses 5g and 20g are on the balance arm. In fig 1B the 20g mass is on the Faraday cage and the 5g mass remains on the balance arm.

A note on the different mounting brackets

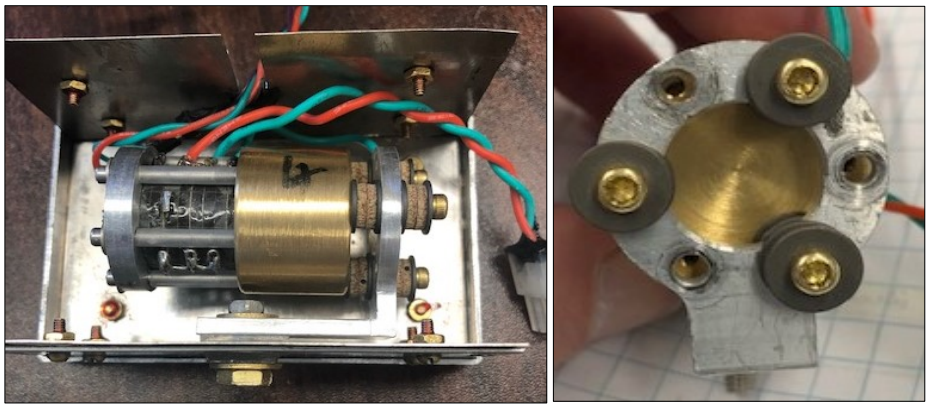

Figure 6.2. Shows the L bracket mounting. In use are 3 brass screws and double phenolic washers with titanium flat washers. The standard L bracket has 6 equally spaced screw holes, no extra holes were drilled. The screw arrangement here is not symmetrical from left to right

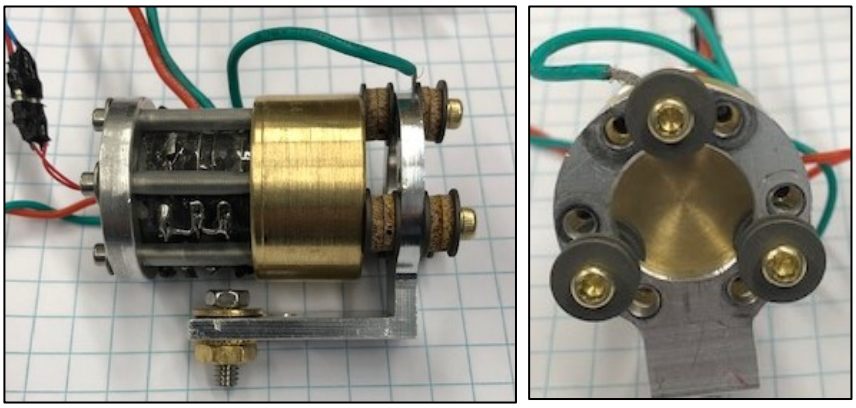

Figure 6.3. Shows the L mounting bracket using the 0.618 inch brass glued stack. The 3 screws used to hold the brass have been placed into holes which were drilled in addition to the 6 regular holes. There is one top screw and two lower screws on either side in a equilateral triangle arrangement. This is a symmetric pattern.

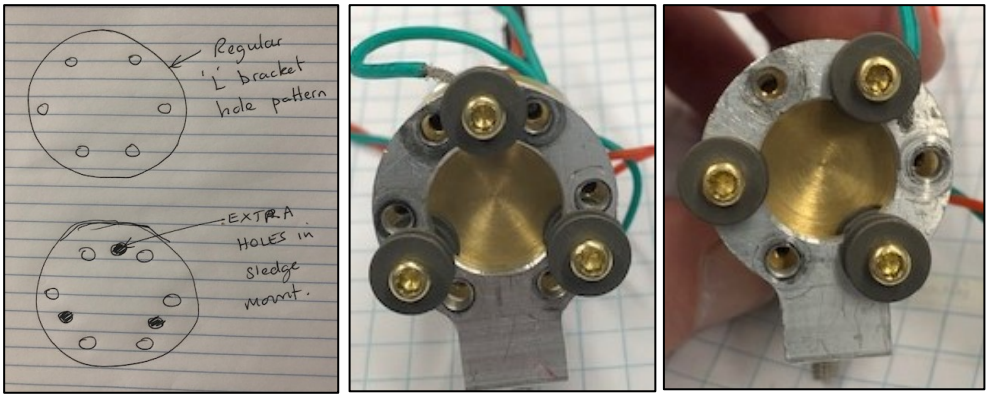

Figure 6.3a. The asymmetry in the L bracket mount and the symmetry in the Sledge mount explained. Rough sketch of the Hole pattern in the standard L bracket and the sledges.

Results using the 0.618 inch brass glued stack

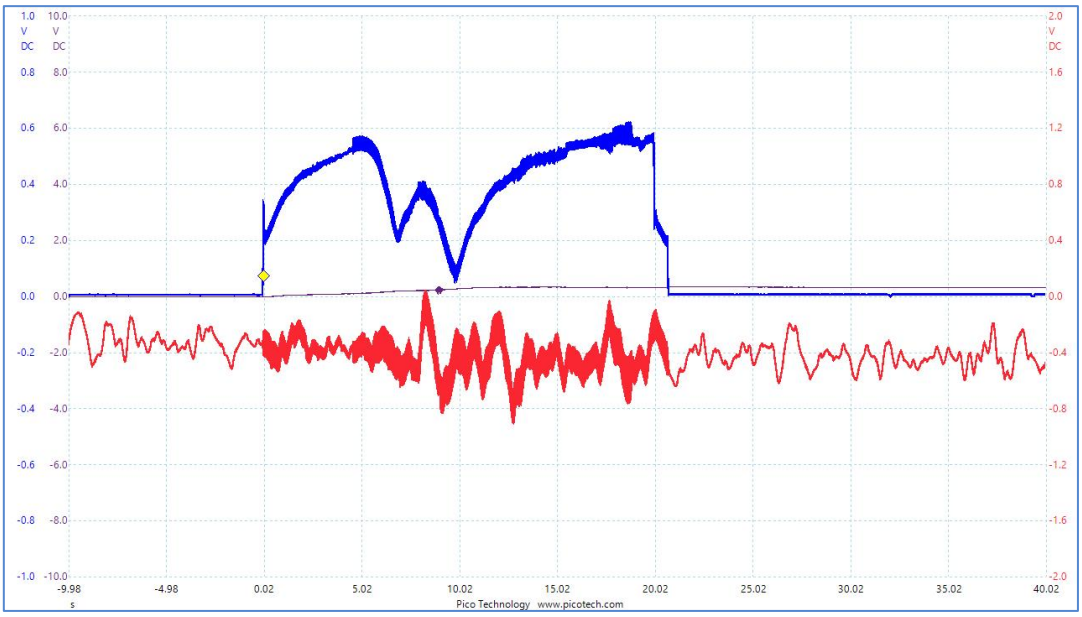

Figure 6.4. Results for 0.618" brass glued stack. Using L bracket with asymmetric screws. The blue trace is the rectified voltage (max 225 volts), the red trace is the force measured in volts here. 110 mV is equivalent to 1µN. The run shows a sweep from 45-25 kHz over 20 seconds. The 1 kHz per second linear downward sweep starts at 45kHz. There appears to be a signal at about 38 kHz. The force is about 4.5µN, zero to peak. The background noise seems to be higher than normal, due to a local earthquake.

For a photo of the L bracket mount see Figure 6.2 above. For a standard 0.75g mass we have a 10g mass on the balance arm. A counterpoise of 15 g extra was added to the balance arm to offset the lesser mass of the 0.618 inch brass. For the experimental results above, there was 25g on the balance arm, either on or near the Faraday cage.

The first run was with the 5g mass on the balance arm and the 20g mass also on the arm. The L bracket used had asymmetric screw arrangement, since no new screw holes had been added.

We ran the same setup again, but this time we changed the position of the counterpoise masses on the beam. The 20g mass was moved from the beam arm to the top of the Faraday cage, see Figure 6.2B. The results are shows below for the same conditions, same sweep.

In comparison, we also took the same sweep run 45-25 kHz in 20 seconds using the sledge mount. This has a symmetric screw pattern arrangement. The 20g mass was left on top of the Faraday cage for this run, since it didn't seem to make much difference where it was placed, as shown above.
The results for the sledge mount are shown in Figure 6.6.

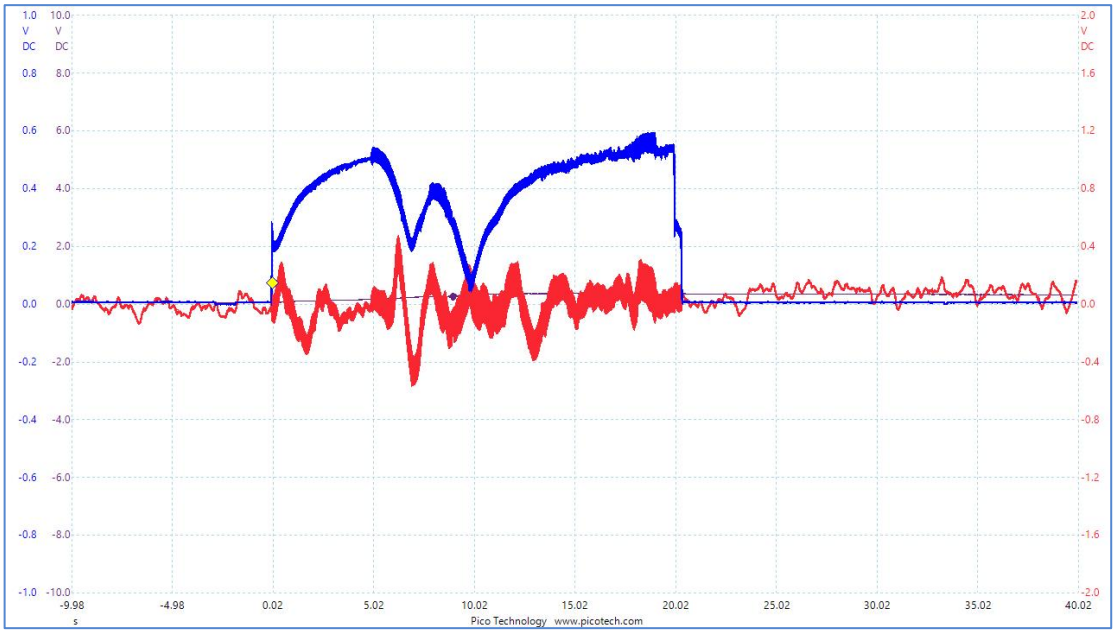

Figure 6.5. Results for 0.618 inch brass glued stack. Using L bracket with asymmetric screws. The blue trace is the rectified voltage (max 225 volts) , the red trace is the force measured in volts here. 110 mV is equivalent to 1µN. The run shows a sweep from 45-25 kHz over 20 seconds. The 20g mass is on top of the Faraday cage. There appears to be a signal at about 38 kHz. The force is about 4.5 – 5 µN, zero to peak, very similar to the previous force above. The background noise here is reduced, the local earthquake has died down. We had to open the vacuum chamber, reset the mass and then wait for a low vacuum, before taking this measurement.

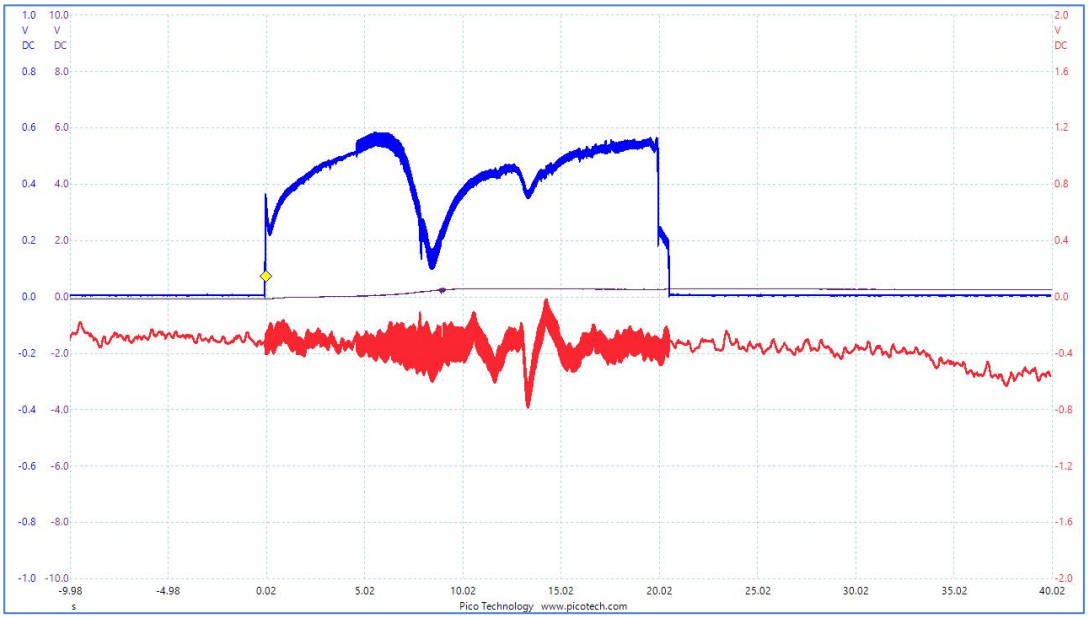

Figure 6.6. Results for 0.618 inch brass glued stack. Standard sweep run 45-25 kHz, in 20 seconds. This is using a sledge with the counterpoise 20g mass on the Faraday cage. Note that the resonance frequency has decreased, but the amplitude of the force signal is still about the same, here it is 4.5-5 µN. The resonance is now around 32-33 kHz. The sledge mass is slightly heavier than the standard L bracket by ~15g.

New L brackets with symmetric screw pattern arrangement were obtained from the machinist and the 0.618 inch brass glued stack run again. The results were as shown below.

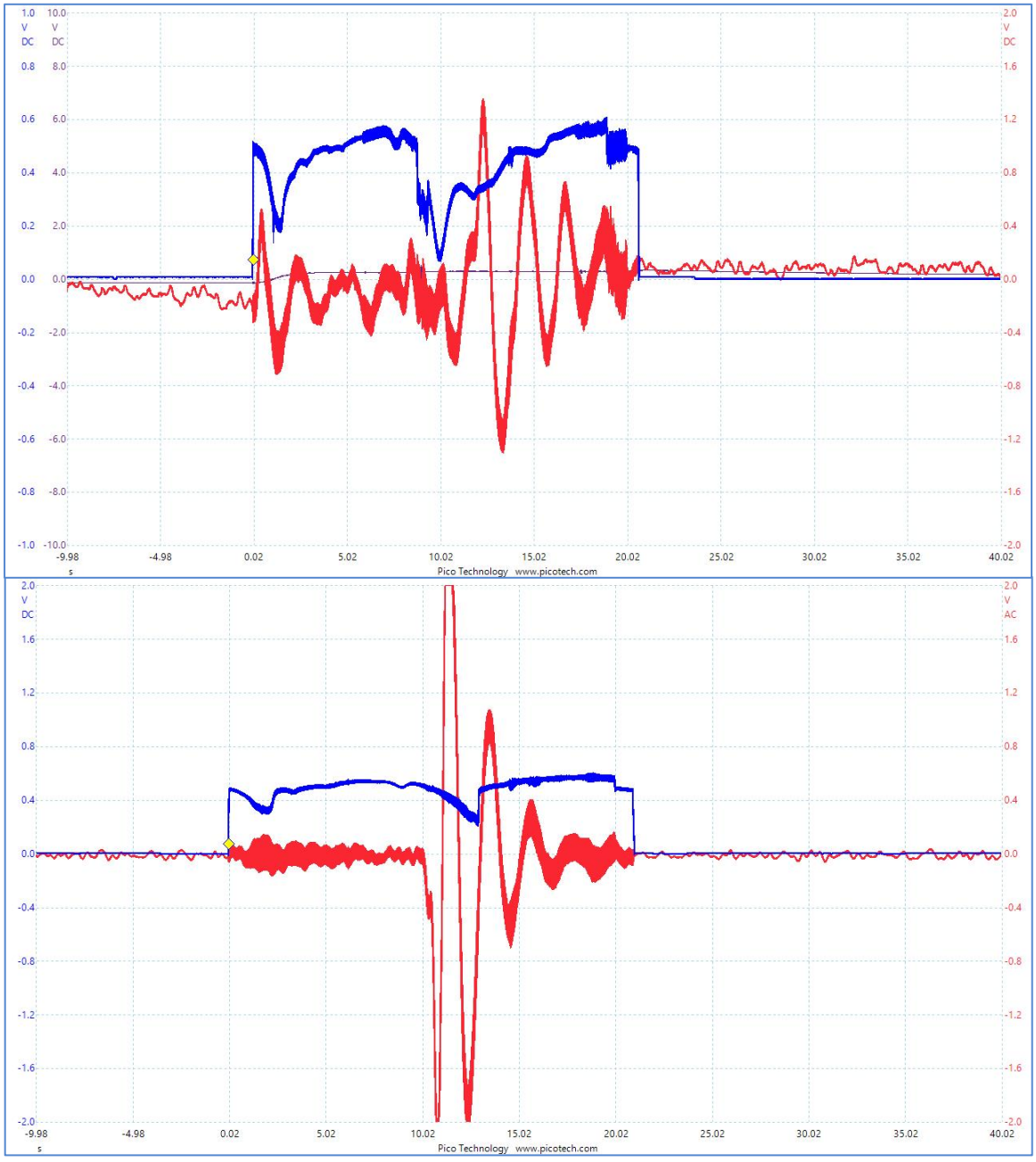

Figure 6.7. Top: Results for 0.618 inch brass glued stack. Using L bracket with a symmetric screw arrangement. Standard sweep run 45-25 kHz, in 20 seconds. This is using a symmetrically holed L bracket with the counterpoise 20g mass on the beam arm. Note that the resonance frequency is about 32-33kHz, and the amplitude of the force signal is about 10µN. Forward direction. (April 5th 2020) Bottom: Results for 0.618 inch brass glued stack. Using L bracket with a symmetric screw arrangement reverse run. (April 11th 2020). Note that the pattern reverses from the forward run. The resonant freq. is about the same. Forward force is nearly double 18 µN.

Results using the 0.5 inch brass glued stack

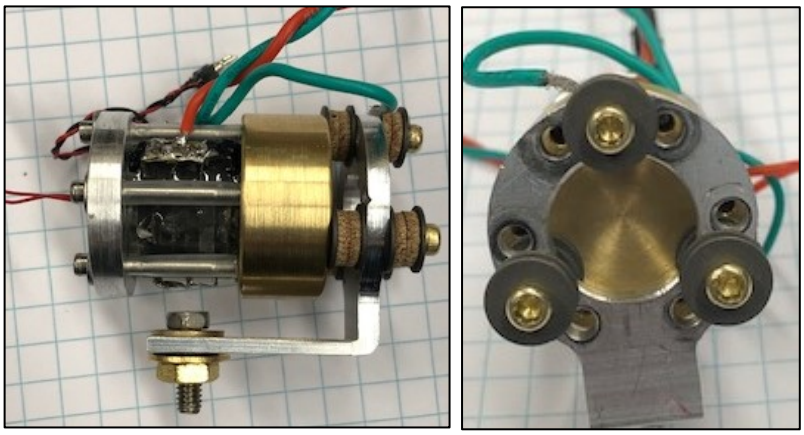

Figure 6.8. The 0.5inch brass glued stack, mounted on an L bracket. The screw arrangement is symmetric.

Shown in fig 6.8 is the 0.5 inch brass mass glued stack mounted on a standard L bracket. This stack was only used with symmetrically mounted screws for the L bracket and **both** sledges. At this point we introduced a second sledge, with Teflon sleeves on the rails.

The resulting force signature with the L bracket is shown below.

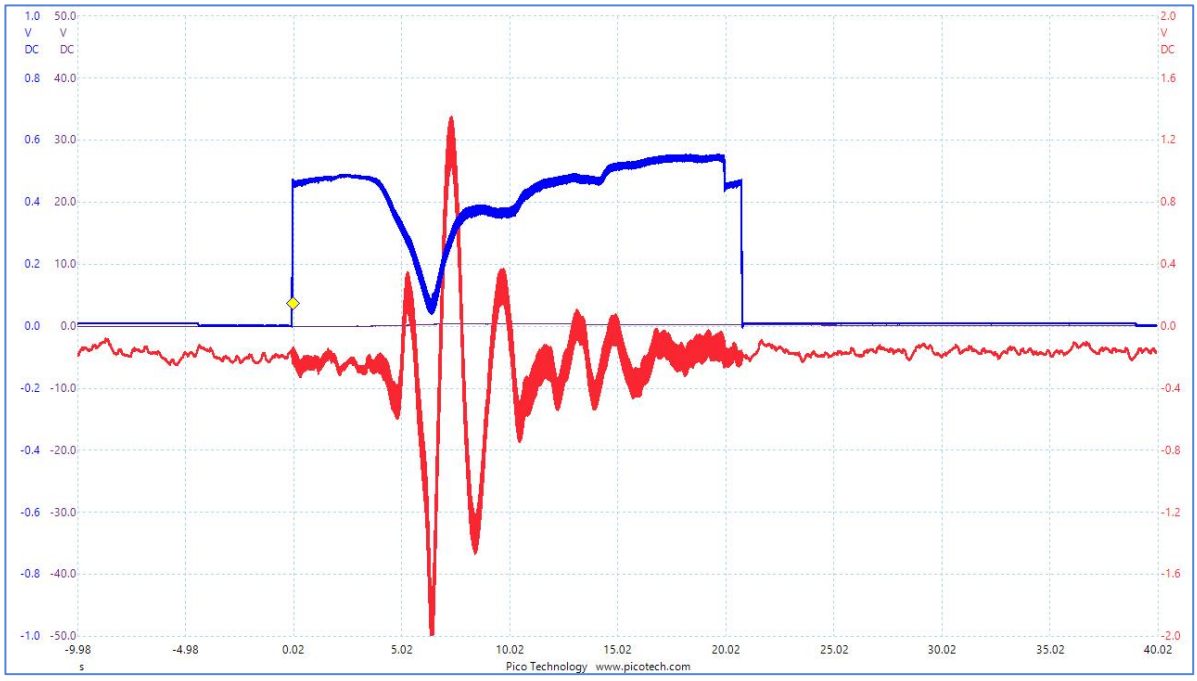

Figure 6.9. Results for the 0.5inch brass glued stack, mounted on a L bracket with symmetric screw mounting. The large deflection shows about 21 μN at roughly 38 kHz.

After the L bracket the 0.5 inch brass glued stack was mounted on the standard sledge and the device re-run.

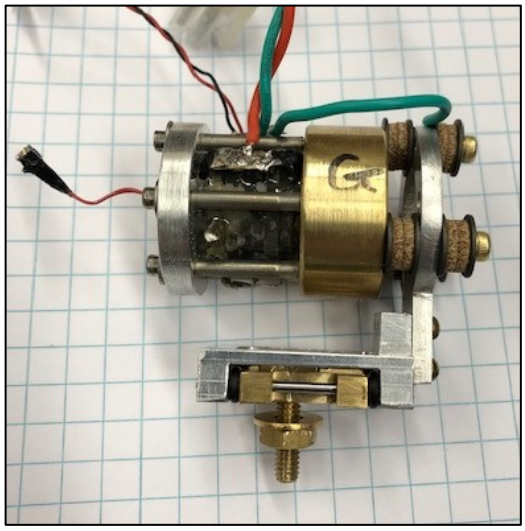

Figure 6.10. Photograph of the 0.5 inch brass glued stack mounted on a regular sledge.

Typical single low temperature results for the 0.5 inch brass glued stack and the standard sledge follows.

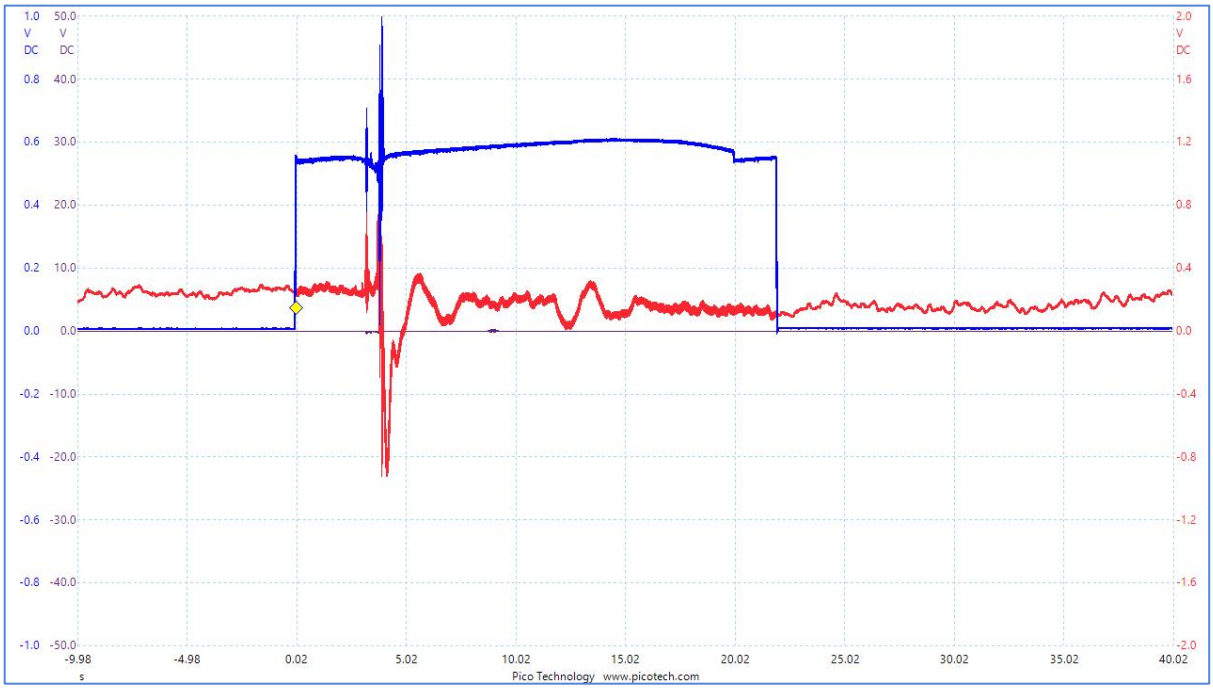

Figure 6.11. Results for the 0.5inch brass glued stack, mounted on a standard sledge with symmetric screw mounting. The large deflection shows about 4 μN at roughly 42 kHz.

Finally the 0.5 inch brass mass was mounted on a new sledge with a Teflon sleeved rail. A photo is shown below in fig 6.12.

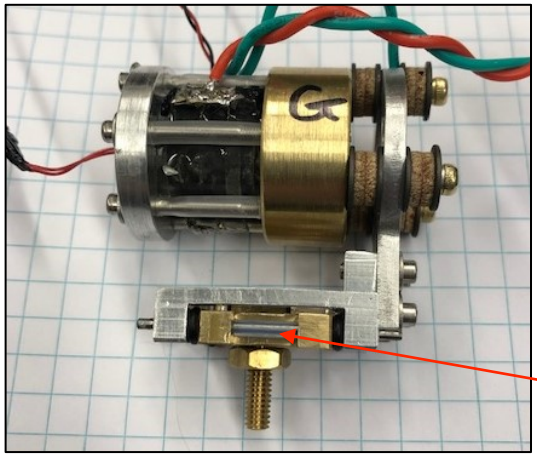

Figure 6.12. Photo of the 0.5 inch brass glued stack mounted on a sledge with Teflon on the rails.

Typical low temperature results for a Teflon sleeved sledge with the 0.5 inch brass glued stack are shown below.

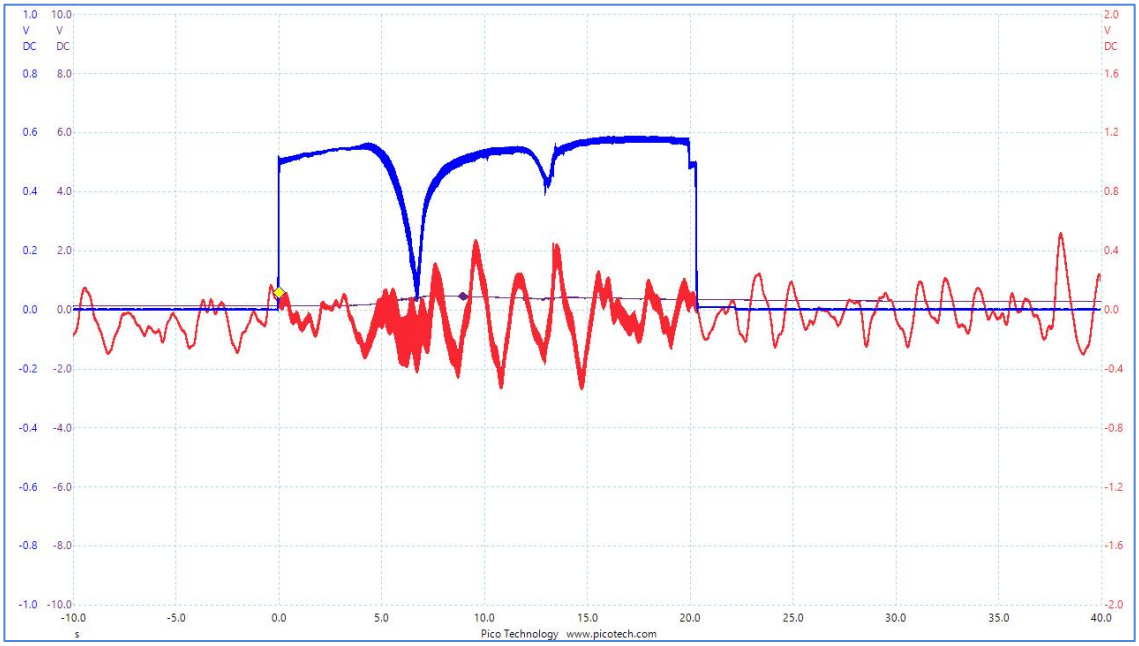

Figure 6.13a. Results for the 0.5inch brass glued stack, mounted on a Teflon sledge with symmetric screw mounting. There are several deflections shown. On average the signal size is about 4 µN. The run represents a standard sweep from 45 kHz to 25 kHz over an interval of 20 seconds.

An earthquake in the Philippines gave a noisy background for this run. The power in these runs never exceeds 12 Watts. This was recorded in the movies of the Picoscope traces.

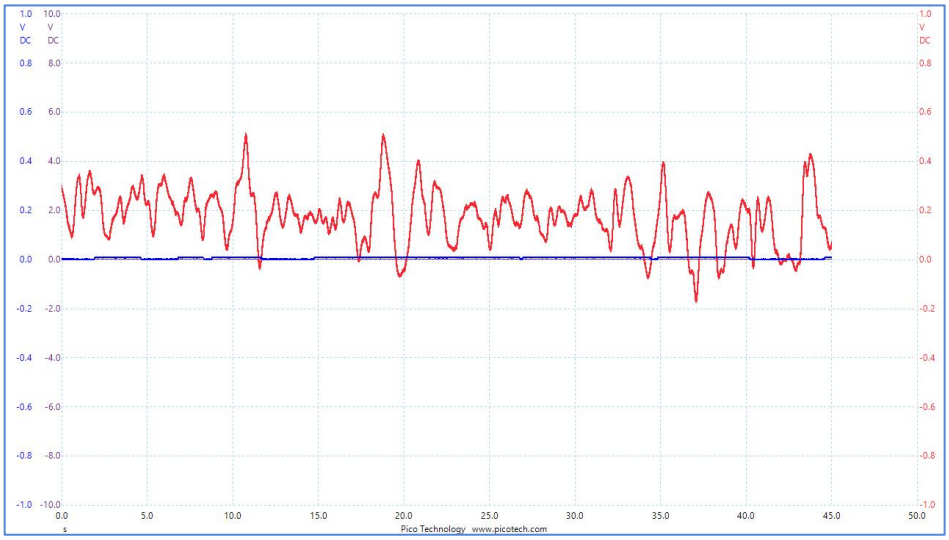

Figure 6.13b. Earthquake background noise, March 26th 2020.

Results using the 0.618 inch brass glued stack and Fiberglass washers

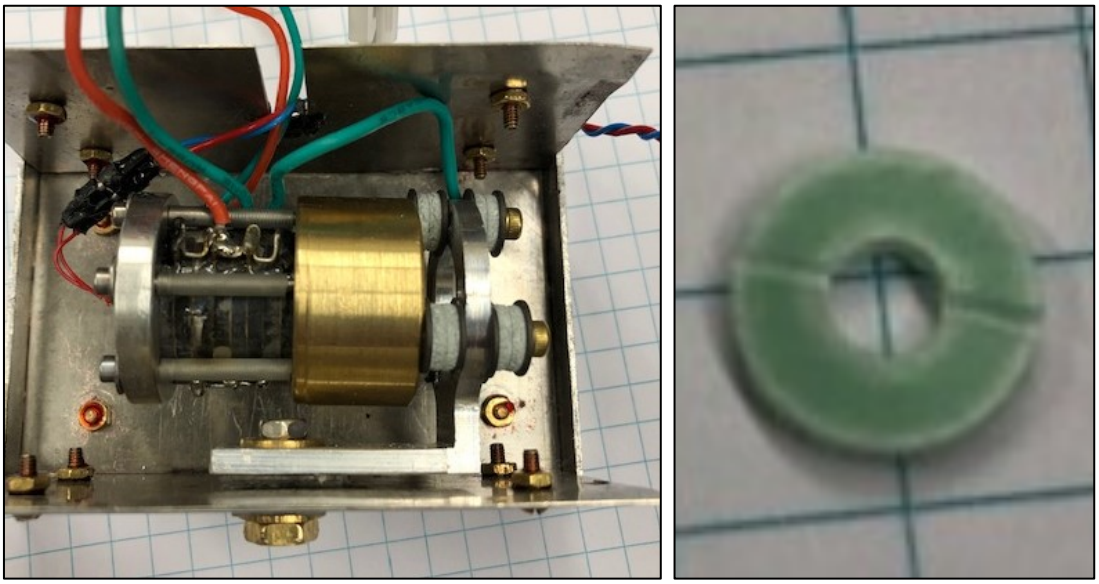

Figure 6.14. The 0.618inch brass mass glued stack on an L bracket. The photo on the right shows the scoring of the fiberglass washer to allow air to escape from the threads of the screws holding the aluminum mount bracket onto the brass mass.

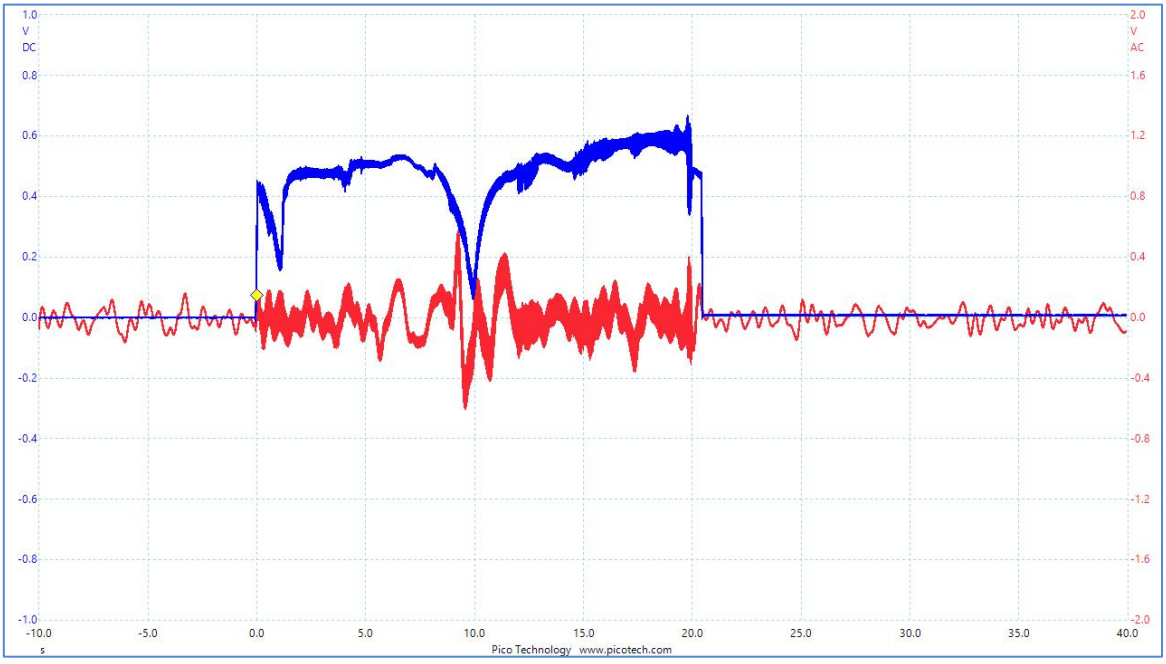

Figure 6.15. Standard sweep from 45 kHz down to 25 kHz in 20 seconds. The 0.618 inch brass mass glued stack on an L bracket with 3 symmetric screws. Fiberglass washers used. Forward direction force in red shows about 5.5 µN. The resonant frequency appears to be around 36 kHz.

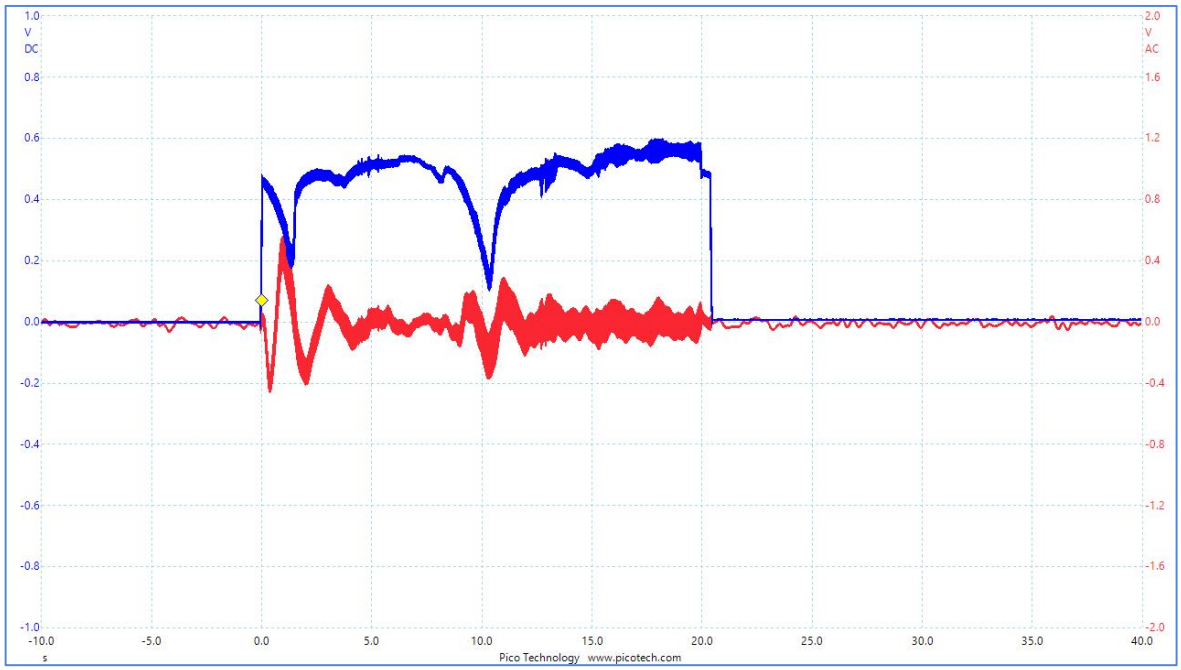

Figure 6.16. Standard sweep from 45 kHz down to 25 kHz in 20 seconds. The 0.618 inch brass mass glued stack on an L bracket with 3 symmetric screws. Fiberglass washers used. Reverse direction force in red shows about 3.6 µN at the previous resonant freq. around 36 kHz. However at the higher freq. of about 45 kHz the force is about 4.5 µN.

Conclusions

The results for the 0.5 inch brass mass were somewhat inconsistent. We decided, based on the tests here, that the optimum mass was the 0.618 inch brass with a symmetric screw arrangement. See figure 6.7 above. The L bracket seemed to give better force results than the sledge.

7. Design #1 Sledge – Where to Loctite Rails? What Ballast Mass to Use?

Two key questions emerged during the prior experimentation. The first was: at what location to Loctite the rails to the sledge? The second: what is the most effective brass mass length for force generation?

Where to glue the sledge rails?

Testing to determine the best location to red Loctite the rails to the sledge, so the pins do not come loose.

We have two options:

1. Use red Loctite on the brass part of the sledge and glue the steel rails (pins).
2. Use red Loctite on the end of the sledge and glue at the aluminum end of bracket.

We shall refer to the first option as sledge 1 and option two as sledge 2. See Figure 7.1.

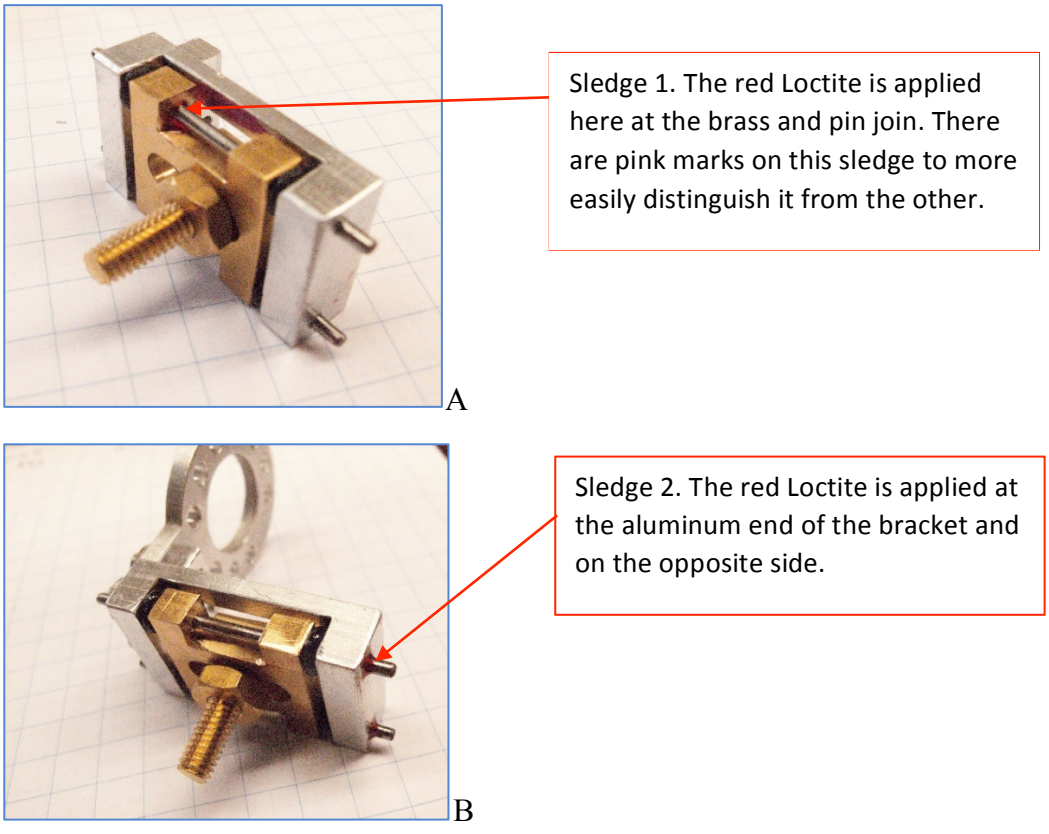

Figure 7.1 A and B are two sledges. Fig 7.1A is sledge 1 and Fig 7.1B is sledge 2.

The device (new stack #3) was mounted on sledge #1 and securely bolted to the Faraday cage, see Fig 7.2. The domes on both the brass mass and the aluminum end mass were 0.0005". The brass mass to be used for both sledge 1 and 2 was chosen to be the standard 0.75" length. The test consisted of running the Carvin DCM2000 amplifier at level 12, using a signal from the Rigol DG1032Z of a sweep from 45 – 25 kHz in 20 seconds. The input voltage for the Rigol signal generator was
V_{RMS} =1.2 volts.

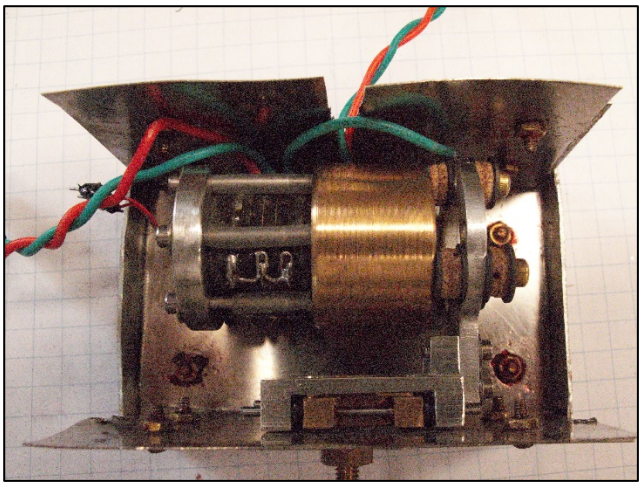

Figure 7.2. The Faraday cage with a device for testing mounted on sledge 1. Note the use of 3 screws to hold the brass mass onto the sledge and the use of double phenolic washers and titanium washers.

A typical run for the sledge 1, using the standard sweep run mentioned above, looked like Figure 7.3 below.

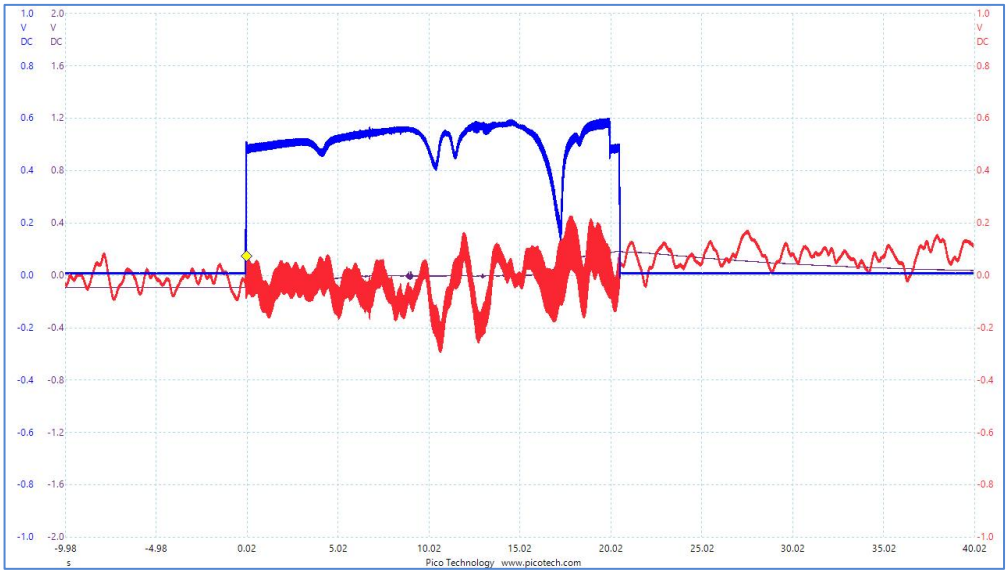

Figure 7.3. Voltage through the device is in blue, the force is shown in red and the purple line is temperature. This run was a sweep from 45 – 25 kHz in 20 seconds for sledge 1.

Using the sledge 2, we found the following data curves, see fig. 7.4 below. This data run was for the sweep of 45-25 kHz over 20 seconds. The input V_{RMS} =1.2 volts as before. The same stack #3 was used for this run. It appears that the force produced using sledge #2 is almost twice that produced by sledge #1.

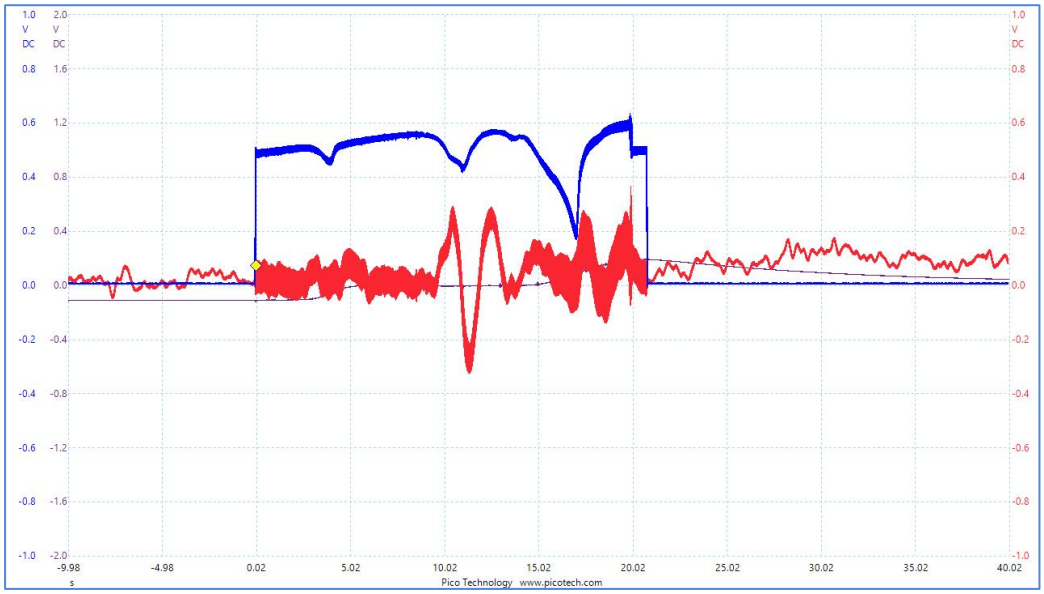

Figure 7.4. Voltage through the device is in blue, the force is shown in red and the purple line is temperature. This run was a sweep from 45 – 25 kHz in 20 seconds for sledge 2. The transient force in the center of the plot is almost twice as large as it was using the previous sledge #1. It appears sledge #2 is more appropriate.

What is the most effective brass mass length for force generation?

Once we had determined the best method of gluing the rails to the sledge , we started testing the brass mass lengths to determine which would optimize the force for a particular stack. The stack in question was new stack #3. It employs eight Steiner Martins PZT SM-111 discs that are 2mm thick and 19mm in diameter.

The brass masses to be tested are shown in Figure 7.5 and listed in Table 7.1 below.

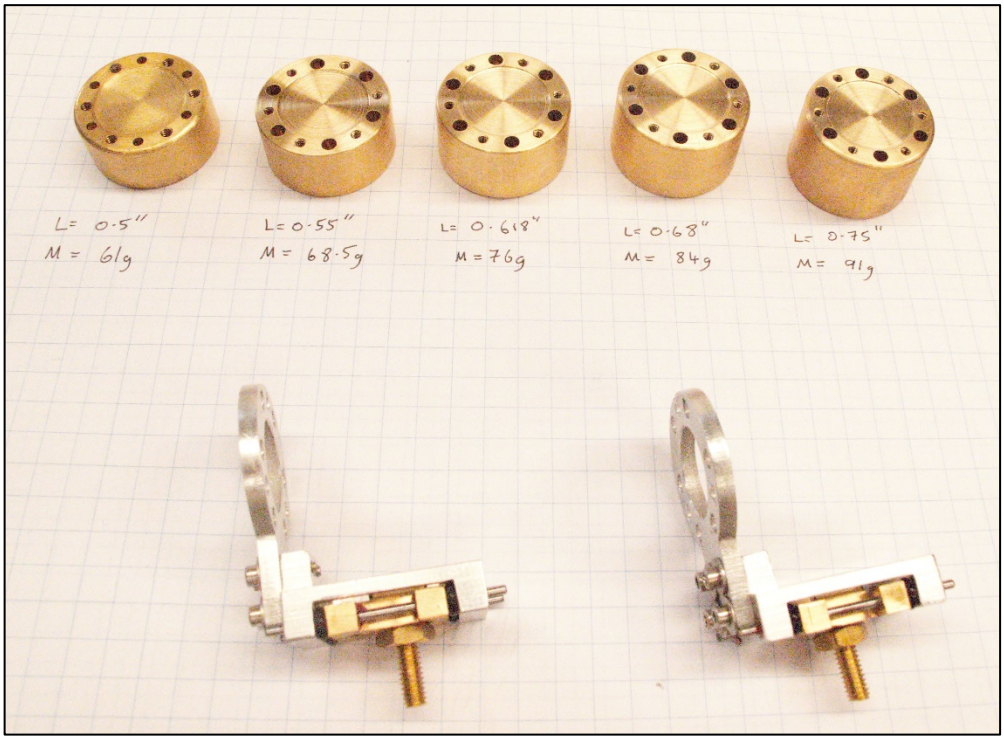

Figure 7.5. The masses and the sledges to be tested. Only 5 larger masses are shown.

Table 7.1. List of brass masses under consideration.

Brass length	0.375”	0.4375”	0.5”	0.55”	0.618”	0.68”	0.75”
Brass mass	44.5g		61g	68.5g	76g	84g	91g

After several more runs using the best sledge #2 we found that the highest force was produced using the optimum mass of 76g of length 0.618 inches. We used the same testing protocol as before. A Rigol signal generator DG1032Z with V_{RMS} =1.2 volts input was used to produce a signal to a Carvin DCM2000 amplifier, at level 12. The signal used was a sweep from 45 kHz down to 25 kHz over 20 seconds. We measure the output voltage to the device, the force produced by the device and several other parameters like the strain, FFT and temperature during the run. All the data is collected by Picoscopes and a movie is made using the screen-capture program Movavi. Using the 0.75 inch brass mass we obtained the following result, see Figure 7.6.

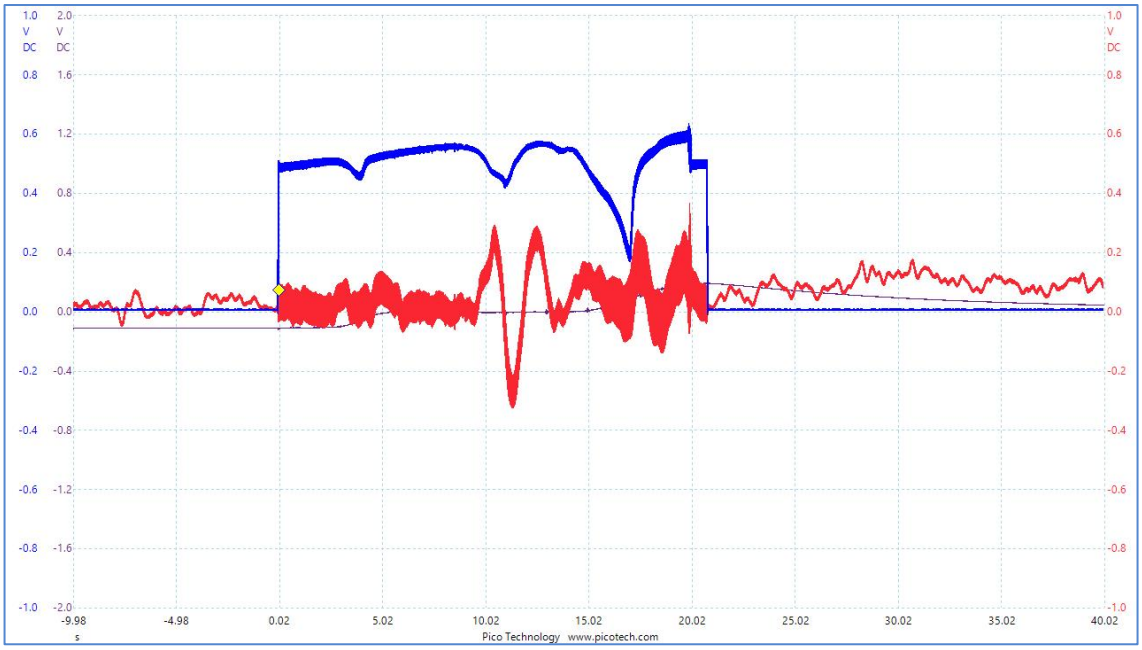

Figure 7.6. Using 0.75" brass mass with sledge and standard sweep run 45kHz to 25 kHz in 20 seconds.

We then sequentially ran the other brass masses in descending order of size. The results are shown following.

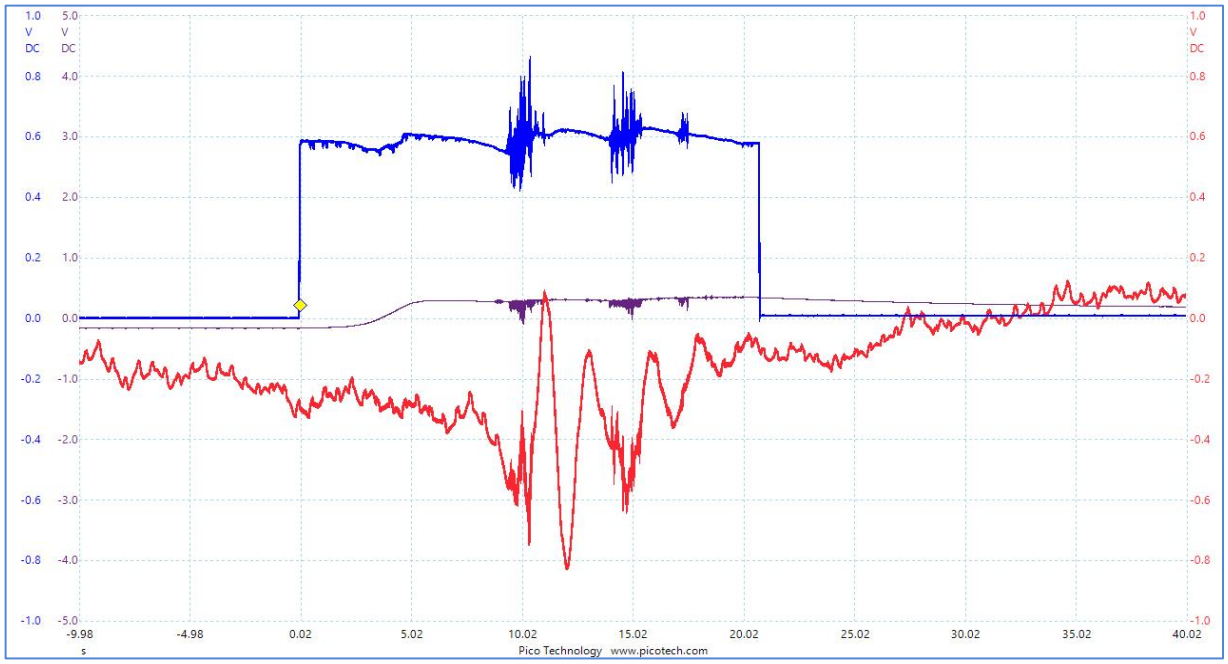

Figure 7.7. Using 0.68" brass mass with sledge and standard sweep run 45kHz to 25 kHz in 20 seconds.

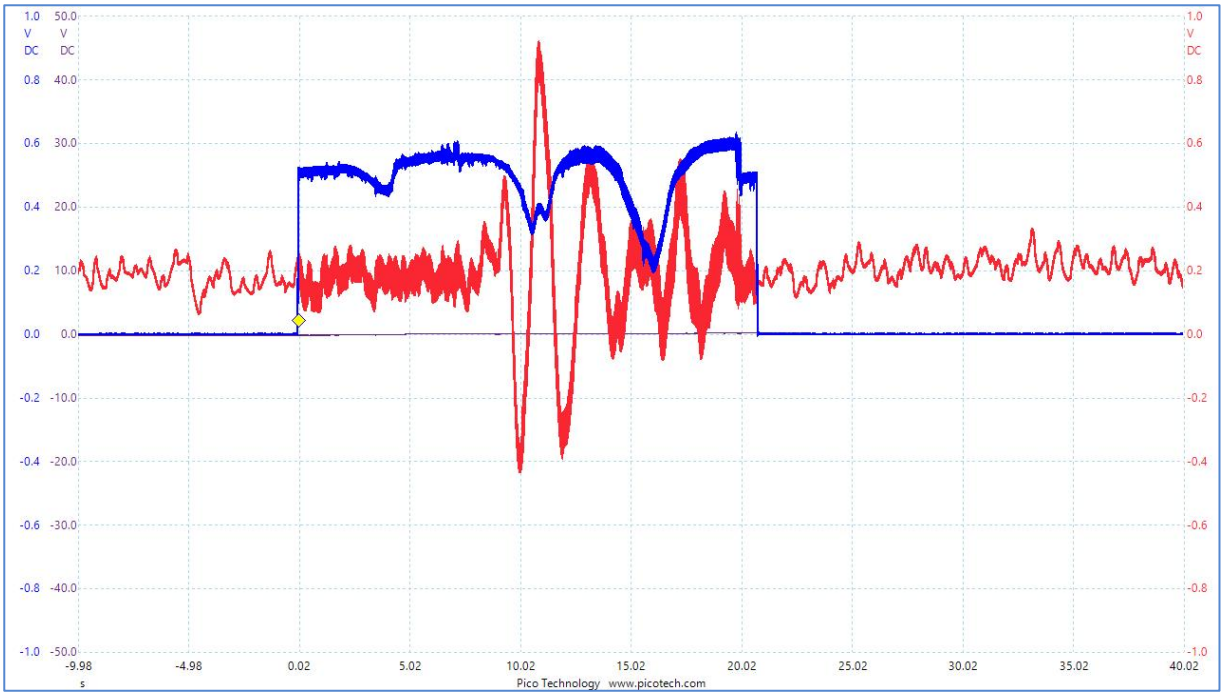

Figure 7.8. Using 0.618" brass mass with sledge and standard sweep run 45kHz to 25 kHz in 20 seconds. This was the best result seen.

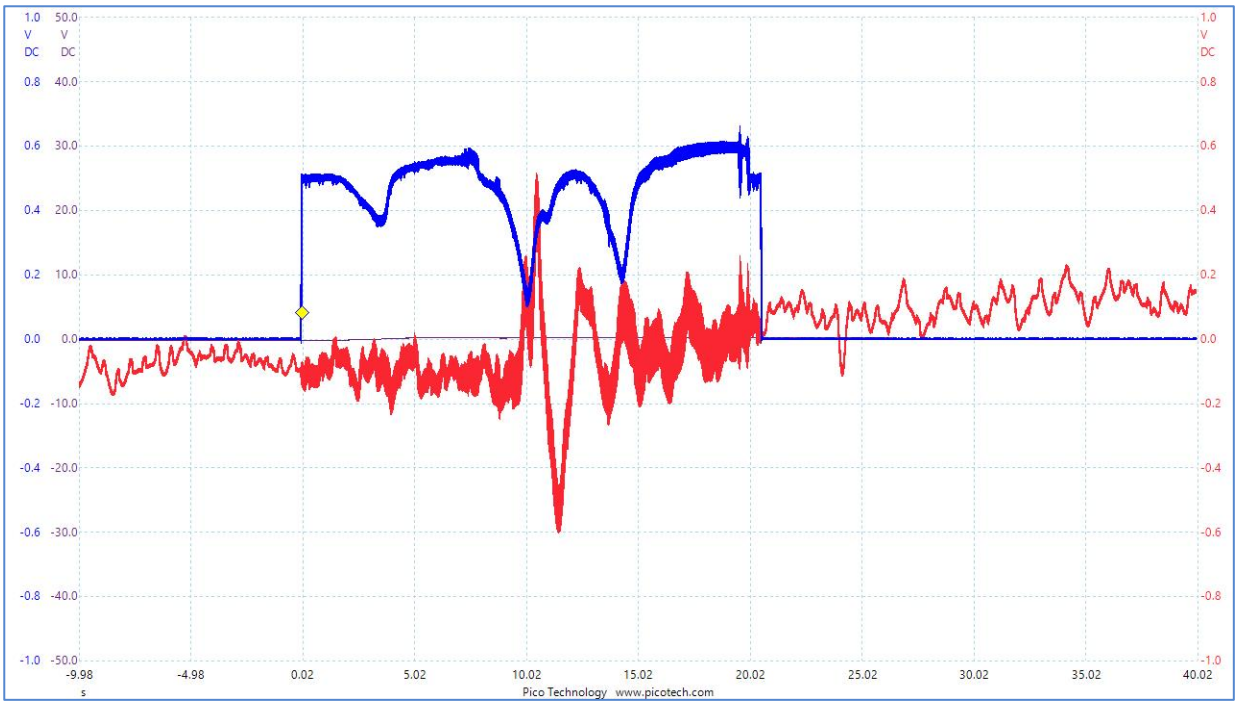

Figure 7.9. Using 0.55" brass mass with sledge and standard sweep run 45kHz to 25 kHz in 20 seconds. Forgot to reset the counter poise, or add mass to the Faraday cage side of the balance.

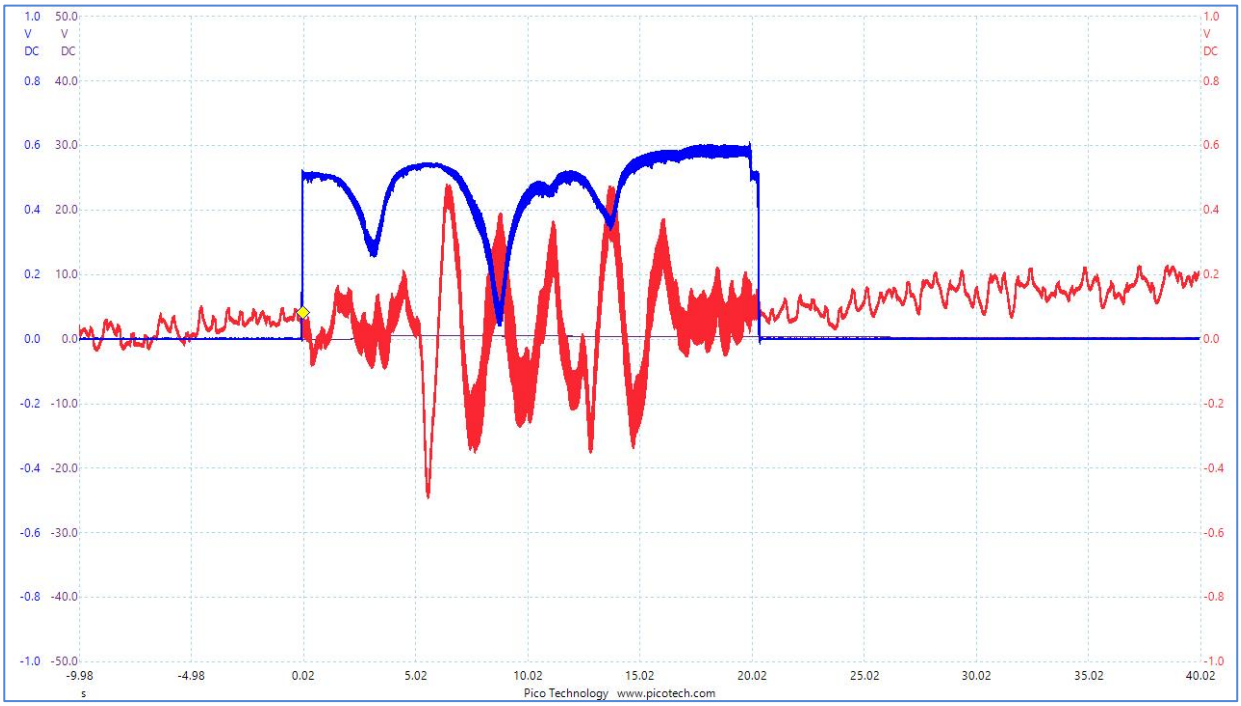

Figure 7.10. Using 0.5" brass mass with sledge and standard sweep run 45kHz to 25 kHz in 20 seconds. Adding 20g to the Faraday cage side of the balance arm.

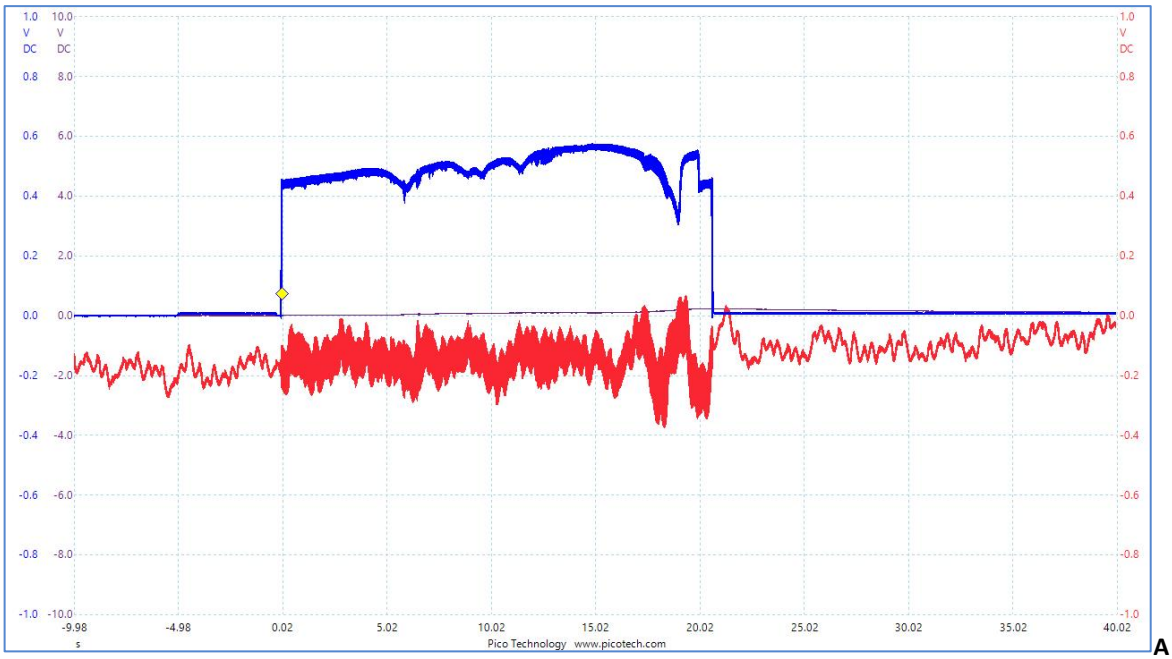

A

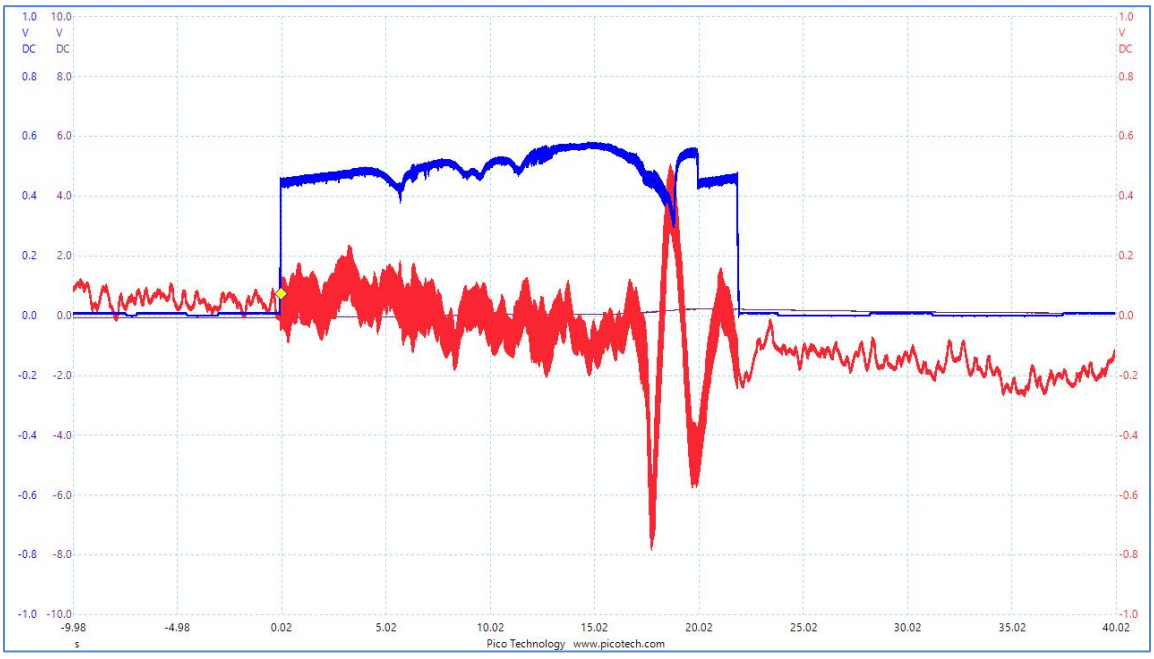

B

Figure 7.11. Top fig A is the 0.4375" brass mass run on a sledge with stack #4. This is another standard sweep of 45kHz to 25 kHz in 20 seconds. The difference between plots A and B was that in plot B a 5 g mass was added to the balance arm near the Faraday cage. These results are clearly very sensitive to masses being used for the counterpoise of the balance arm. The total mass difference between that used for the 0.75" brass and the 0.4375" brass was 42g. Both plots A and B are using the red scale $\pm$ 1 volt.

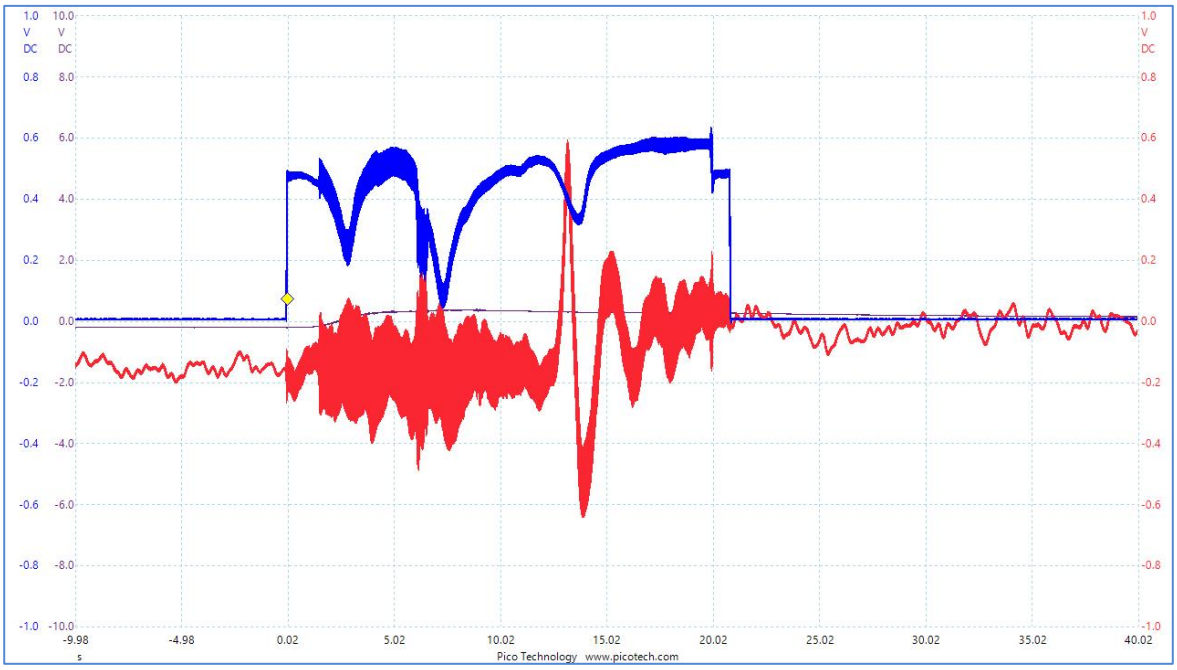

Figure 7.12. Using 0.375" brass mass with sledge and standard sweep run 45kHz to 25 kHz in 20 seconds. Adding 42g to the Faraday cage side of the balance arm.

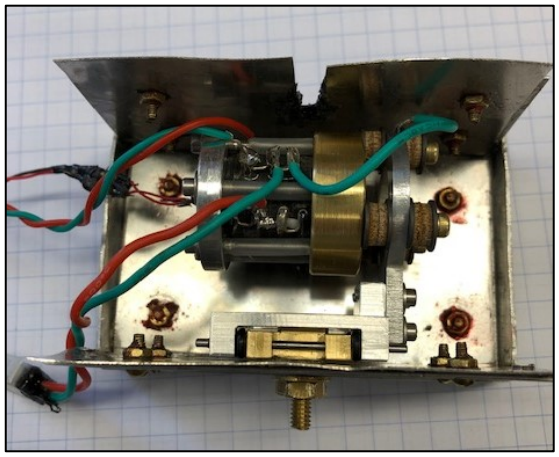

Figure 7.13. Photo of the 3/8" brass mass on the sledge.

For comparison with no sledge we ran the 0.618" brass mass with a standard "L" bracket, using the same double phenolic washer arrangement, just no sledge.

In the forward direction we found a huge signal, see Figure 7.14.

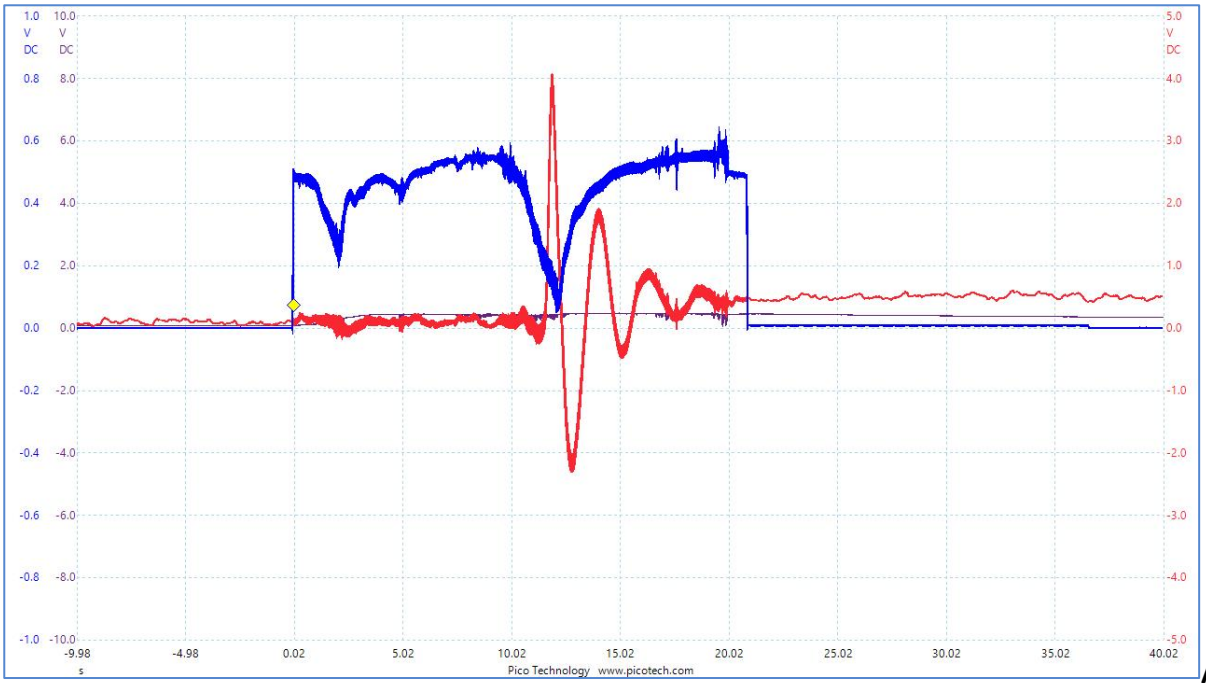

A

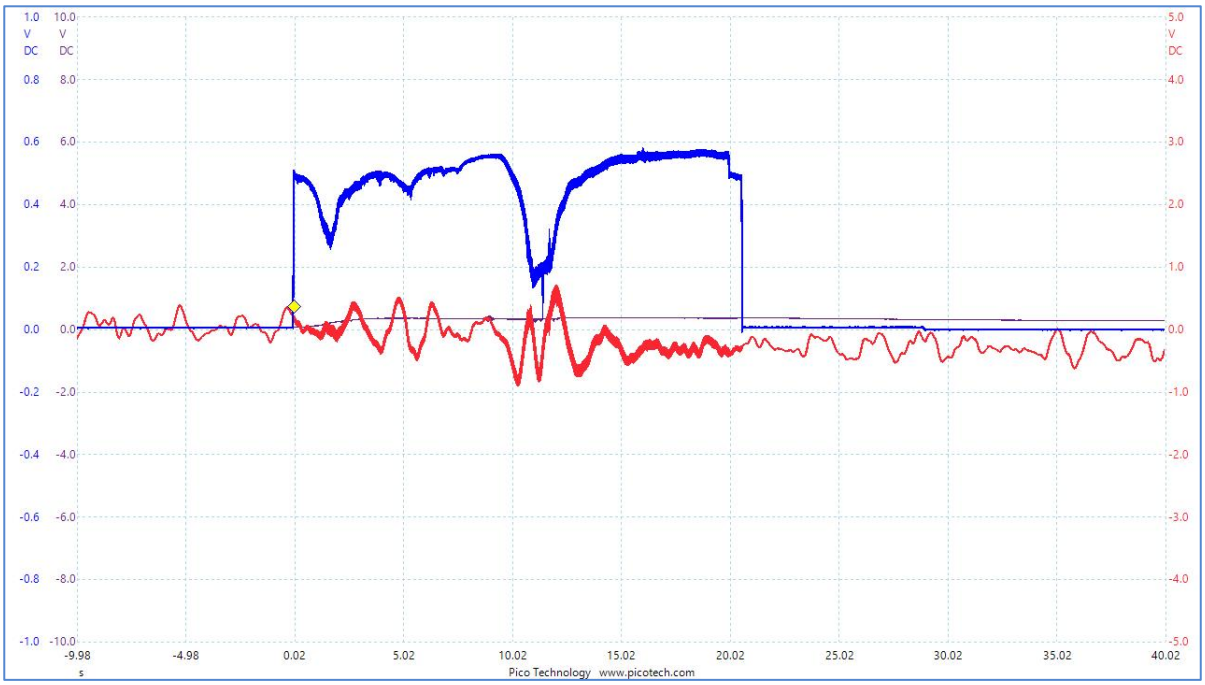

B

Figure 7.14. This is stack #3, run with no sledge just a standard solid L bracket mount. Additional 42g on the balance arm near the Faraday cage to compensate for the less massive brass (less than the 0.75" brass mass). Note the red scale here is $\pm$5 volts. Plot A was in the forward direction and plot B was in the reverse direction. Notice the signal does reverse but not with equal amplitude. During the recording of plot B there was a minor earthquake, so the background noise is a little higher than in plot A.

Conclusion

We found that mass 76g of length 0.618 inches was the optimum brass mass to use for force generation. The idea behind the sledge was to decouple the vibrations of the device from the Faraday cage. We tested this idea with the vibrometer in a later report. It also allows the device to move freely, as it would in space, with ends that are "free-free" rather than "bound-free" with the L bracket. The L bracket arrangement forces the brass end to be "fixed" or bound. A CAD drawing was made of all parts for sledge #1, see figure 7.15 below.

At this point there was a modification of the sledge design. We did not continue with testing this model of sledge.

Future tests will be performed on design #1 sledge:

- We need to rerun some previous masses being careful to adjust the counterpoise mass for the smaller masses.
- We need to try higher frequency sweep range for the smaller masses.

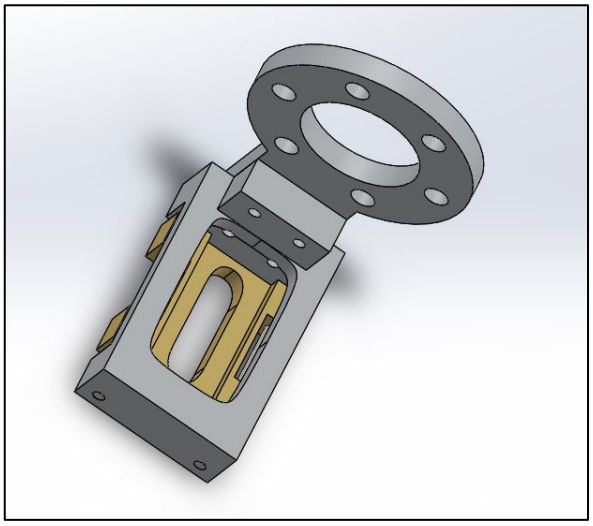

Figure 7.15. Solidworks CAD drawing of sledge design #1.
CAD drawings care of Jon Woodland and David Matalon (grad student)

8. Use Of Glued 0.618 Inch Brass Stack-Testing Vibration Transmitted To Faraday Cage

The PZT stacks are usually just held in between the brass and aluminum end masses by the 6, 2-56 stainless steel screws. In this test we used a glued stack, glued directly to the masses and then also applied the 4 in-lbs. torque to the screws. The glued stack uses eight Steiner Martins PZT SM-111 discs that are 2mm thick and 19mm in diameter.

Off Resonance Test Using Signal At 45 Khz

The vibrometer testing proceeded as follows. The L brackets with two thicknesses 1/8 inch and 1/16 inch were tested against the sledges with a mount bracket of 1/8 inch and 1/16 inch to see what kind of vibration isolation is provided by these mount brackets and what frequencies would be transmitted to the Faraday cage from the device. The same device was used for all the tests. This was the 0.618 inch brass mass glued stack. Also the same holes were used to attach the brass mass to all of the mounting brackets. The holes were marked to ensure this.

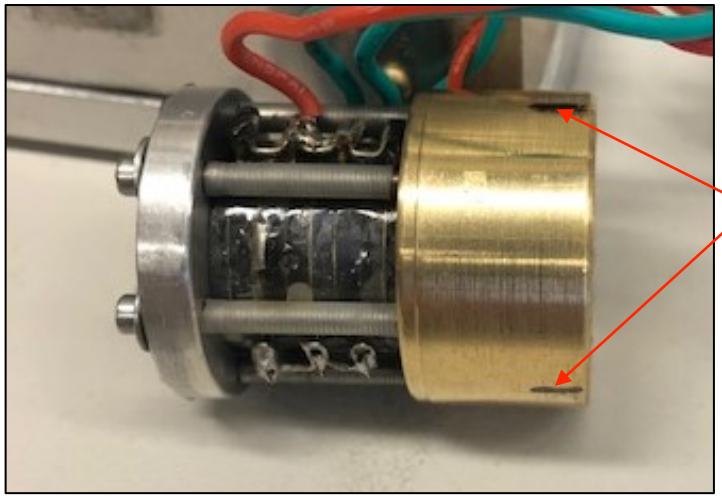

Figure 8.1. The brass mass holes for the mounting screws were marked so the same holes were used for all the mounting brackets tested.

Screw holes are marked with black sharpie pen.

The same procedure was used for all the tests. A Picoscope 5242B was setup to measure the displacement from a Polytec vibrometer. The Picoscope was also set up to measure frequency, peak-to-peak voltage, Vpp and AC RMS voltage. The vibrometer was set using the 100 nm per volt scale and a low pass filter of 100kHz. The velocity was not used but set low at 10mm/sec/Volt so that the smaller displacement setting could be used. See Figure 8.2. The laser was focused on the Faraday cage, see Figure 8.3. The same location was used for all the tests. The laser can be auto focused by holding the AF button (see Figure 8.2) for 2 seconds. Fine tuning is allowed on the laser head itself and can be seen on a close up screen showing the laser spot. The laser was on for 20 minutes prior to each test run. For each bracket thickness the vacuum chamber had to be opened and the mount bracket changed, since we were using the same device for all of the tests. The laser was on the entire time that the vacuum chamber was being pumped down. All measurements were done at a vacuum pressure of 80mTorr or below.

Figure 8.2. Vibrometer settings and laser spot of vibrometer focused on the Faraday cage. The same location was used for all tests. Autofocus and fine tuning were used. Laser spot is seen in the photo on the right.

The Picoscope 5254B was setup as follows: in Figure 8.3, below you can see measurements of Frequency, AC RMS and Vpp. The Picoscope was set to 12-bit 1MSa/sec operation and was storing up to 20 waveforms each run. The displacement on the Polytec sensor had been set to 100nm/volt so the Picoscope scale was set to $\pm 10V$. When using an input signal, it was chosen to be 45 kHz sine wave at an amplitude of 700mV.

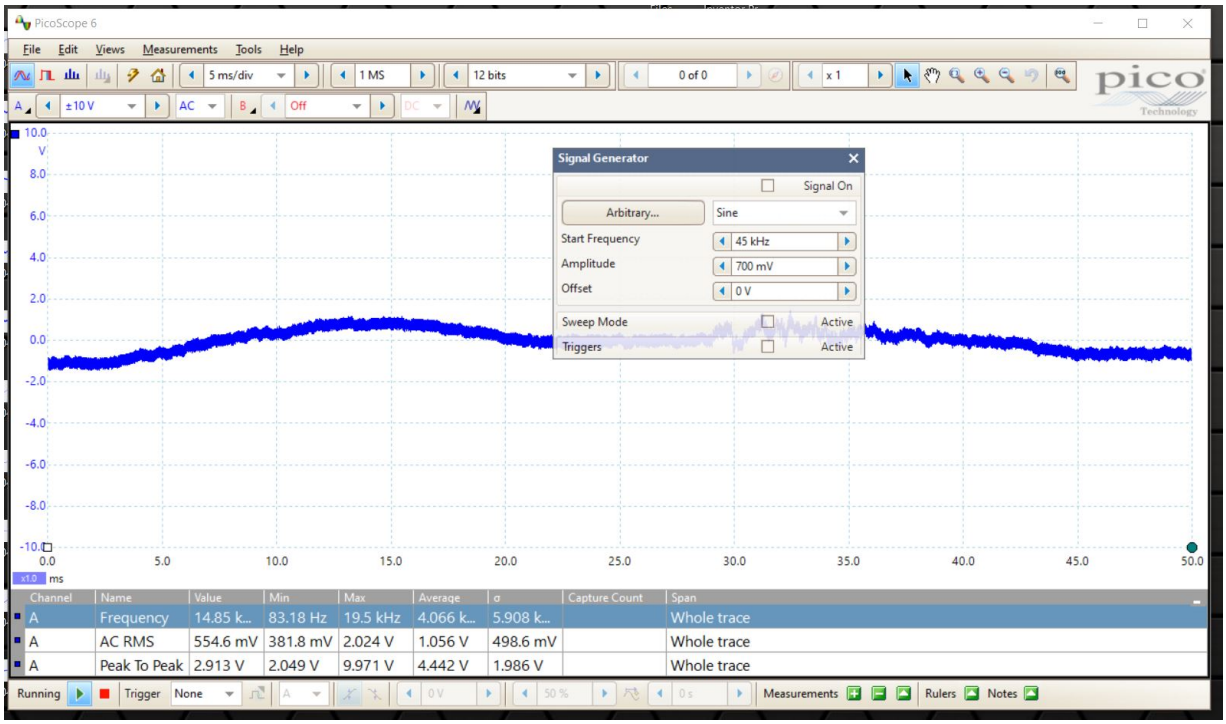

Figure 8.3. Picoscope 5254B setup.

L Bracket Mount 1/8inch thickness

The device setup is shown below in Figure 8.4.

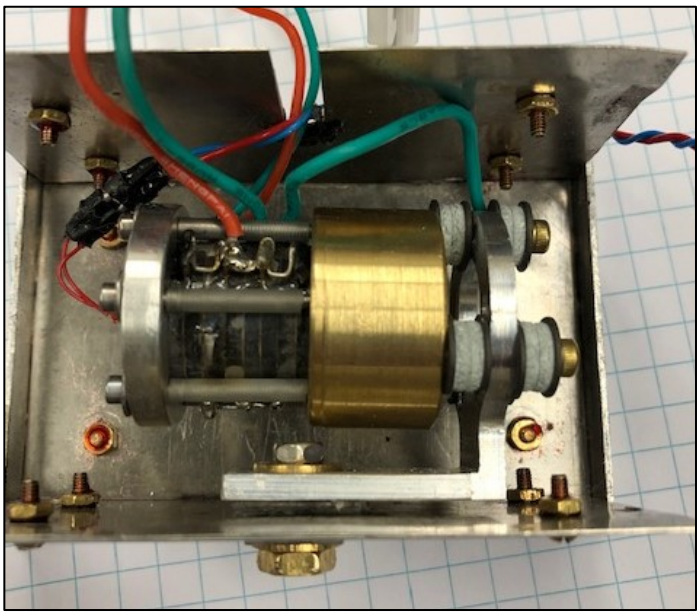

Figure 8.4. Photo of the 0.618 inch brass glued stack on a 1/8 inch thick L bracket. Note the use of fiberglass washers throughout.

First 4 background runs (20 files per run) were recorded using the Picoscope. The arbitrary waveform generator was not turned on at this time. The Vpp was divided by 2 to get the amplitude and then multiplied by 100 to get the displacement in nanometers. To get the displacement in microns simply divide the nm displacement by 1000.

Table 8.1 Background Signal 45 kHz, 700mV.

FREQ (Hz)	AC rms	Vpp
29.49	0.758	2.472
28.53	1.226	4.406
30.45	0.81	2.615
28.31	0.9199	3.241
25.15	0.6235	1.954
27.16	0.5636	2.459
27.26	0.315	1.546
28.35	0.711	3.112
32.37	0.5252	2.002
35.3	0.3646	1.375
30.54	1.017	3.364
29.96	0.5172	2.302
29.47	1.131	3.684

FREQ (KHz)	AC rms	Vpp
2.59	0.4619	2.09
0.819	0.6108	2.383
17.71	0.1971	1.028
2.3	0.4613	2.41
9.037	0.746	2.962
0.8334	0.6056	2.478
3.094	0.4614	2.056
3.774	0.4597	2.206
1.921	0.4658	2.049
1.449	0.5436	2.172
1.064	0.5662	2.185
1.446	0.4779	2.049

33.02	0.8365	2.867	4.846	0.2945	1.3
30.74	0.7104	2.424	4.178	0.4754	2.042
31.51	0.9233	3.023	0.6919	0.4827	2.505
36.99	0.421	1.477	3.467	0.4306	1.77
27.59	0.7223	2.88	0.2249	0.6792	2.56
27.91	1.23	3.881	0.3585	0.6316	3.063
27.38	0.6888	2.438	1.053	0.5147	2.205
30.41	0.8542	2.989	1.23	0.4678	1.953
29.48	1.222	3.901	4.259	0.4154	2.042
27.63	0.5823	1.941	0.1392	0.6952	2.893
32.22	0.546	1.954	f=2.8906478	Vop=	1.052196
31.83	1.012	3.153			
29.71	0.7876	3.118			
31.52	0.9001	2.9			
32.96	0.505	1.825			
35.94	0.6781	2.424			
f=29.306	Vop=	1.29545			

Table 8.1 shows a sample of the data taken. The average background Faraday cage vibration was f= 29.3 Hz, and the average displacement of the Faraday cage was x=0.129 microns.

When the 45 kHz signal (700mV input amplitude) was turned on and applied to the device, the Faraday cage vibration data was as in Table 8.1, right above. (4 data runs with about 20 waveforms per file taken.)

The average frequency of vibration of the Faraday cage was found to be 2.89 kHz. The displacement of the Faraday cage was found to be x=105.219 nm or 0.10522 microns which is less than the background noise but at a higher frequency.

L Bracket Mount 1/16 inch thickness

The device setup is shown in Figure 8.5 below.

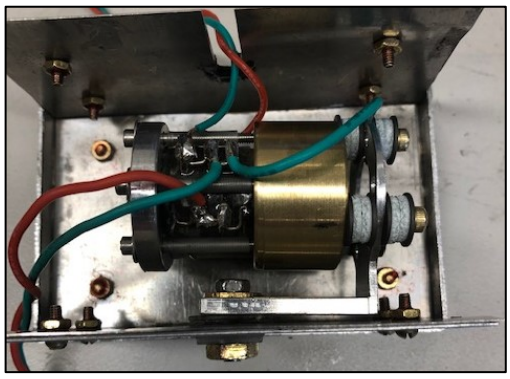

Figure 8.5. The thin 1/16”L bracket mount.

The background table is tabulated below in Table 8.2.

Table 8.2. Background Signal 45 kHz (700mV) applied L bracket 1/16inch.

Freq (Hz)	AC rms	Vpp		Freq (kHz)	AC rms	Vpp
27.37	1.895	6.278		3.612	0.5936	3.118
44.01	1.453	5.706		0.5737	1.11	4.603
34.09	1.374	4.59		0.4336	1.32	5.706
77.28	1.667	6.074		5.042	0.5745	3.254
29.25	1.335	4.603		0.3377	1.05	4.508
69.03	0.796	3.405		0.4095	1.232	4.902
89.55	0.836	3.16		0.9994	0.872	4.385
27.68	1.253	4.386		1.402	2.198	15.03
27.33	1.054	4.031		7.057	0.4315	2.424
30.66	1.325	4.89		0.4023	1.919	8.961
65.48	0.7581	3.364		8.258	0.5172	2.819
107.1	1.222	4.371		0.8741	0.9133	4.154
29.43	1.248	4.726		5.422	0.5865	2.928
92.98	1.509	5.053		3.016	1.156	8.865
23.15	0.6677	2.588		6.935	0.5426	2.518
38.49	1.08	4.44		1.788	0.5394	2.641
28.39	1.952	6.251		0.4022	1.104	4.431
27.01	1.976	6.537		0.4393	1.496	10.45
59.01	1.371	4.985		1.447	0.8797	3.567
42.95	1.237	4.386		5.7	0.7229	3.335
53.62	0.8315	3.718		7.454	0.6762	2.927
28.67	1.41	5.08		1.372	0.5926	4.601
23.15	0.6677	2.588		0.272	1.413	6.378
30.66	1.325	4.89		0.9259	1.098	4.159
27.68	1.253	4.386		0.34464	1.441	5.384
27.33	1.054	4.031		0.4639	1.576	7.303
28.67	1.41	5.08		1.039	0.9926	4.642
29.3	0.6048	2.533		0.7297	1.072	5.01
29.57	1.633	5.216		2.12	0.811	3.369
f=41.62967	Vop=	2.1891		f=2.309065	Vop=	2.439533

Frequency background f=41.6 Hz. Displacement background x=0.2189 microns.

When the signal of 45 kHz was applied (amplitude 700mV) the following data was gathered; the frequency of the Faraday cage vibration was found on average to be 2.3 kHz. The displacement was 0.244 microns.

Sledge Bracket Mount 1/8 inch thickness.

The devices setup is shown below in fig 8.6.

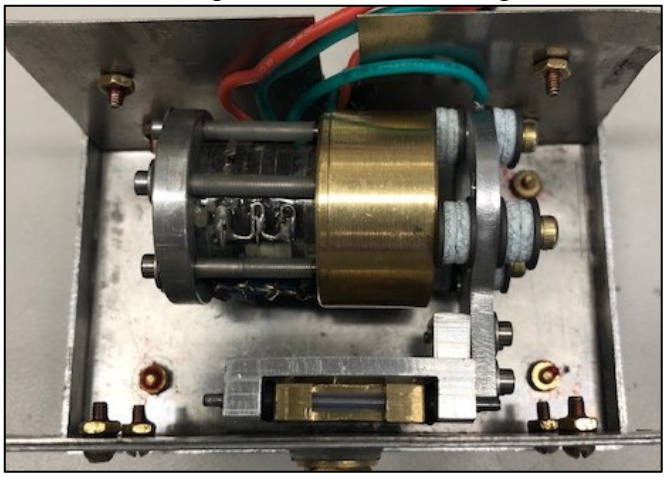

Figure 8.6. The sledge mount 1/8" thick.

The vibration data is follows.

Table 8.3. Background sledge mount 1/8 inch. Signal 45 kHz (700mV)

Freq (Hz)	AC rms	Vpp	Freq (Hz)	AC rms	Vpp
30.08	1.462	4.877	33.21	0.9956	3.309
31.61	0.7362	2.718	30.82	1.31	4.174
34.7	0.9225	3.454	26.72	1.245	4.29
29.47	1.418	4.795	32.82	1.163	4.051
34.16	0.9002	3.154	32.17	1.143	3.942
29.09	1.076	3.808	27.65	1.163	3.691
30.19	1.113	3.597	30.61	1.174	3.772
31.2	1.049	3.597	28.94	0.7842	2.642
35.39	0.9346	3.392	30.67	1.082	3.874
28.93	1.429	5.095	30	1.56	5.223
32.21	1.072	3.638	28.88	1.136	3.874
31.2	1.276	4.394	29.09	0.8957	3.234
30.55	1.161	4.08	32.89	1.32	4.344
27.23	1.264	4.326	28.14	0.5635	2.131
30.43	0.9963	3.501	32.47	0.8357	2.983
42.1	0.5286	2.425	28.21	1.079	3.65
28.73	1.087	4.298	26.95	1.509	4.794
28.43	1.223	4.291	27.98	0.7827	2.969
28.52	0.997	3.964	31.32	1.118	3.963
31.31	1.424	4.863	31.31	1.32	4.453
32.19	1.293	4.597	38.69	0.7175	2.955

25.28	0.893	3.078	29.18	1.588	5.107
31.22	1.075	3.398	25.24	0.8052	2.826
29.75	1.259	4.093	30.88	1.12	3.643
30.88	0.9673	3.262	30.75	1.018	3.541
27.99	1.414	4.604	30.14	0.8371	3.391
31.59	0.7767	2.758	30	0.979	3.799
34.47	1.106	3.718	29.25	0.8762	3.085
27.83	1.141	3.882	30.06	1.42	6.822
f=29.891	Vop=	1.86095	f=29.168	Vop=	1.8422

The background frequency of vibration of the Faraday cage was found to be 29.9 Hz. The displacement of the Faraday cage was 0.186 microns.

When the signal of 45 kHz was applied to the device the following data was recorded. The frequency of vibration of the Faraday cage was found to be on average f=29.2 Hz. The displacement of the Faraday cage was found to be 0.184 microns. This is very similar to the background levels for this sledge. ***Note the difference between the sledge and the L bracket.. the L bracket vibration jumped to 1-2 kHz… here it stays at the background frequency.***

Sledge Bracket Mount 1/16 inch thickness.

The devices setup is shown below in fig.8.7

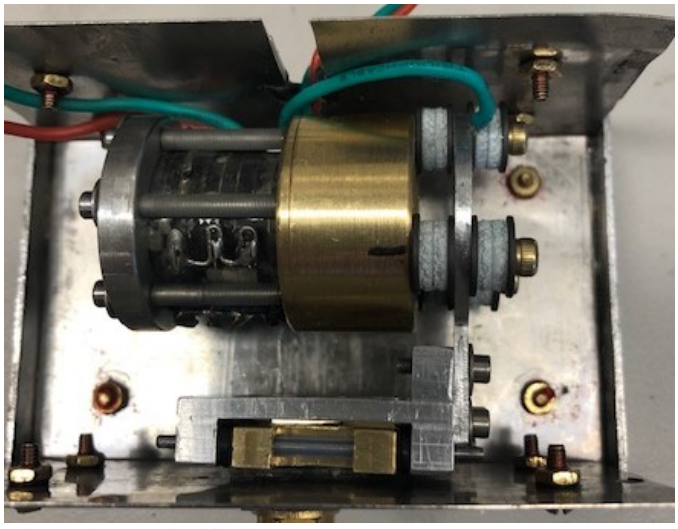

Figure 8.7 Thin 1/16 inch sledge mount bracket setup.

The background table is tabulated below in Table 8.4 below.

Table 8.4. Background for sledge 1/16 inch thickness. Signal 45kHz (700mV) applied

Freq (Hz)	AC rms	Vpp	Freq (Hz)	AC rms	Vpp
33.14	0.7482	2.581	42.94	0.5821	2.389

29.25	0.4126	1.559		25.54	0.537	2.035
29.1	0.7898	2.825		31.58	0.9671	3.355
29.53	1.68	5.338		34.12	0.5722	2.144
37.87	0.9688	3.438		38.6	0.3865	1.511
28.02	0.9326	3.132		34.58	0.7929	2.892
33	0.9088	3.234		30.75	1.184	3.689
29.61	0.4213	1.648		28.26	0.3608	1.531
30.85	0.7854	2.825		30.79	1.51	4.914
30.4	0.6259	2.063		31.06	1.148	3.981
26.74	0.3159	1.457		33.5	0.4396	1.599
31.69	1.473	5.1		28.7	0.6958	2.416
23.63	0.8184	2.559		32.82	1.317	4.029
33.19	0.9249	3.261		31.56	0.904	3.076
27.92	0.6221	2.505		36.14	0.7697	2.709
38	0.4833	1.933		29.22	0.9477	3.083
23.41	1.082	3.635		29.69	1.12	3.668
30.08	1.133	4.037		29.6	0.9793	3.226
28.28	0.6089	2.471		30.24	0.9331	3.171
31.66	1.185	4.248		32.94	1.497	4.342
33.94	0.9119	3.526		31.92	0.8313	2.886
26.88	1.306	4.214		37.85	0.513	2.443
30.38	1.652	5.473		29.41	0.7825	2.777
26.57	0.5433	2.103		27.1	1.235	3.784
27.01	0.9918	3.445		27.49	0.7581	2.498
36.04	0.6263	2.457		24.55	0.6262	2.144
26.19	0.6596	2.212		28.09	0.6571	2.239
33.61	0.7952	2.839		33.62	0.6474	2.423
26.91	0.5341	2.104		34.04	1.042	3.587
f=29.09667	Vop=	1.470367		f=30.55667	Vop=	1.409017

The background vibration frequency of the Faraday cage was found to be f=29.1 Hz. The displacement of the Faraday cage was 0.147 microns.

The frequency of vibration of the Faraday cage was found to be f=30.6 Hz and the displacement of the cage was 0.141 microns which is similar to the background levels.

Summary So Far

The L bracket does isolate the Faraday cage from the high frequency oscillation (45kHz) of the device but tends to allow a 1-2 kHz vibration which is not deemed important. This has nothing to do with the resonant frequency of the device so the resonant motion is NOT transferred to the Faraday cage and hence to the beam arm.

The sledge brackets isolate the Faraday cage from the high frequency oscillations of the device so well the results are indistinguishable from the background measurements. However it should be noted that the beam arm had been balanced for the L brackets not the sledges. For the sledges we should have added an extra 15g to the counterpoise on the left of the beam arm to compensate for the extra mass of the sledge over the L brackets. Also the 1/8 inch mounts had 2 g more mass than the 1/16 inch mounts. We take this into account in the next test on resonance for each mount bracket.

On Resonance Tests For Each Mounting Bracket

The vibrometer tests above were redone but this time we adjusted the counterpoise mass to correctly balance the beam arm for each device mounting and we used an on resonance signal for a few seconds only, so as not to damage the device. The device used was the same as above the 0.618 inch brass glued stack. At this point one of the 2-56 screws had sheared off at the brass end and had been glued into position using red Loctite. This may affect the resonance frequency slightly, so a linear sweep was completed (from 45kHz down to 25 kHz in 20 seconds) before each vibrometer run to test for the resonance frequency.

L Bracket Mount 1/8inch thickness on resonance 35 kHz signal

The linear sweep test was conducted using the L bracket of 1/8 inch thickness to determine the resonant frequency. The Picoscope plot of the run is below.

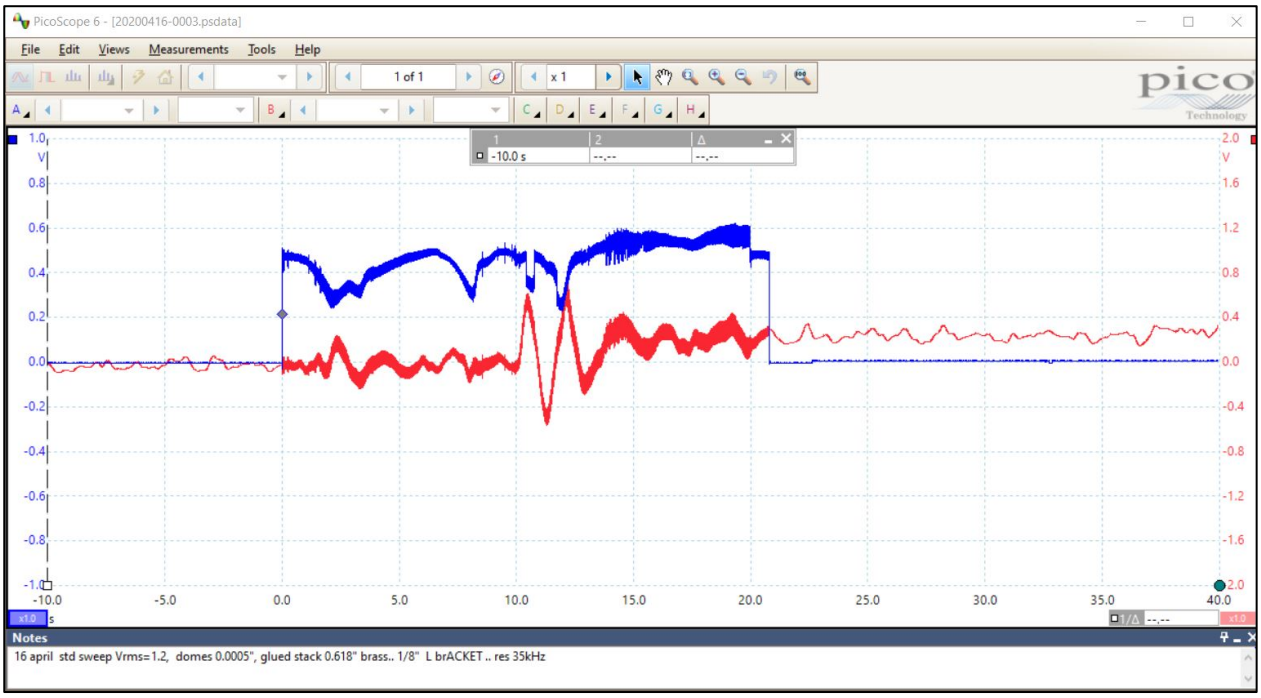

Figure 8.8. Picoscope view of the linear sweep 45-25kHz in 20 seconds which gives 1 kHz per second. The red trace shows the force. The resonance occurs at 10 seconds; this corresponds to 35 kHz.

The vibrometer was set up exactly as before with the laser spot on the Faraday cage.

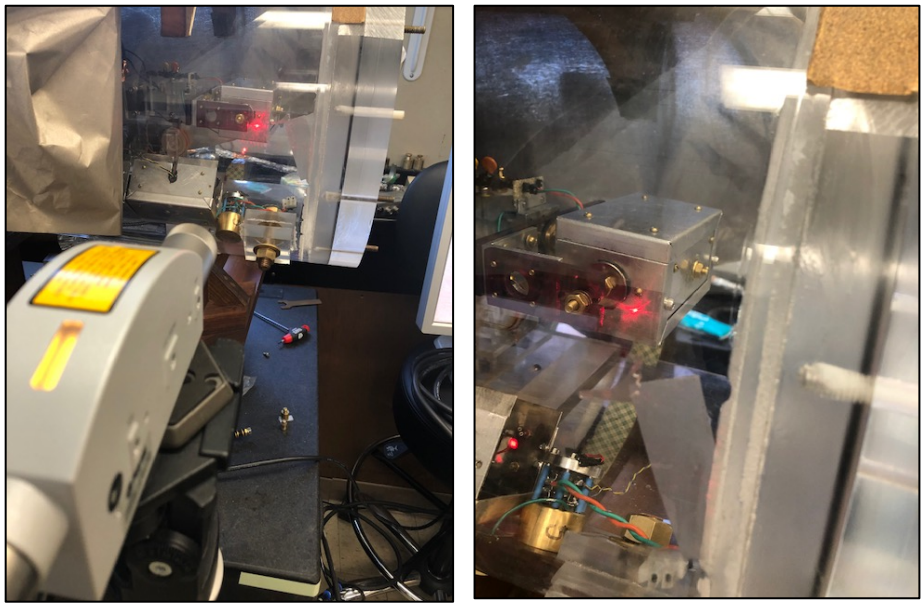

Figure 8.9. Shows a photograph of the vibrometer laser spot on the Faraday cage, as before.

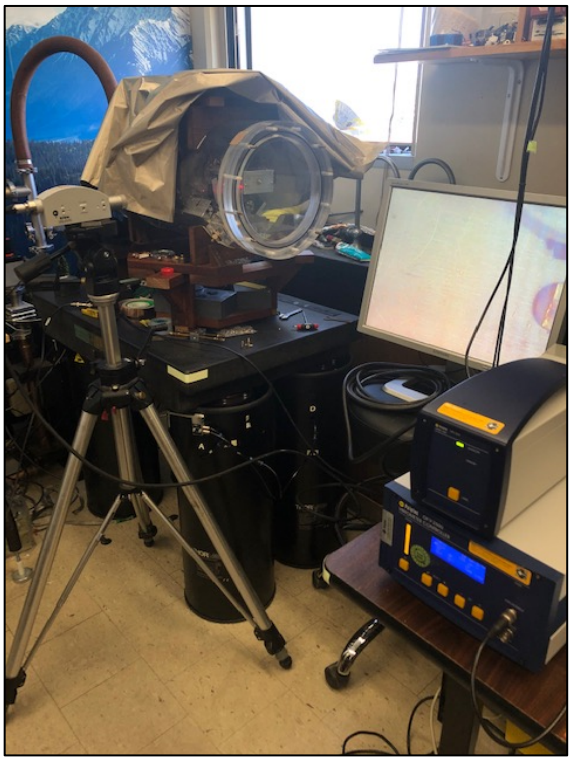

Figure 8.10. Shows a photograph of the complete vibrometer setup, with the tripod holding the laser and the controller on the small desk next to the chamber. The RF shield on the vacuum chamber was being used mainly to shield the vacuum chamber from the heat of the sun from the window. To the right of the controller was a laptop with a Picoscope attached, taking the data from the vibrometer controller displacement sensor. The BNC cable to the Picoscope is visible at the bottom right of the photograph.

The vibrometer was set to have a low pass filter of 100kHz and the displacement measurement was set for 100 nm/volt.

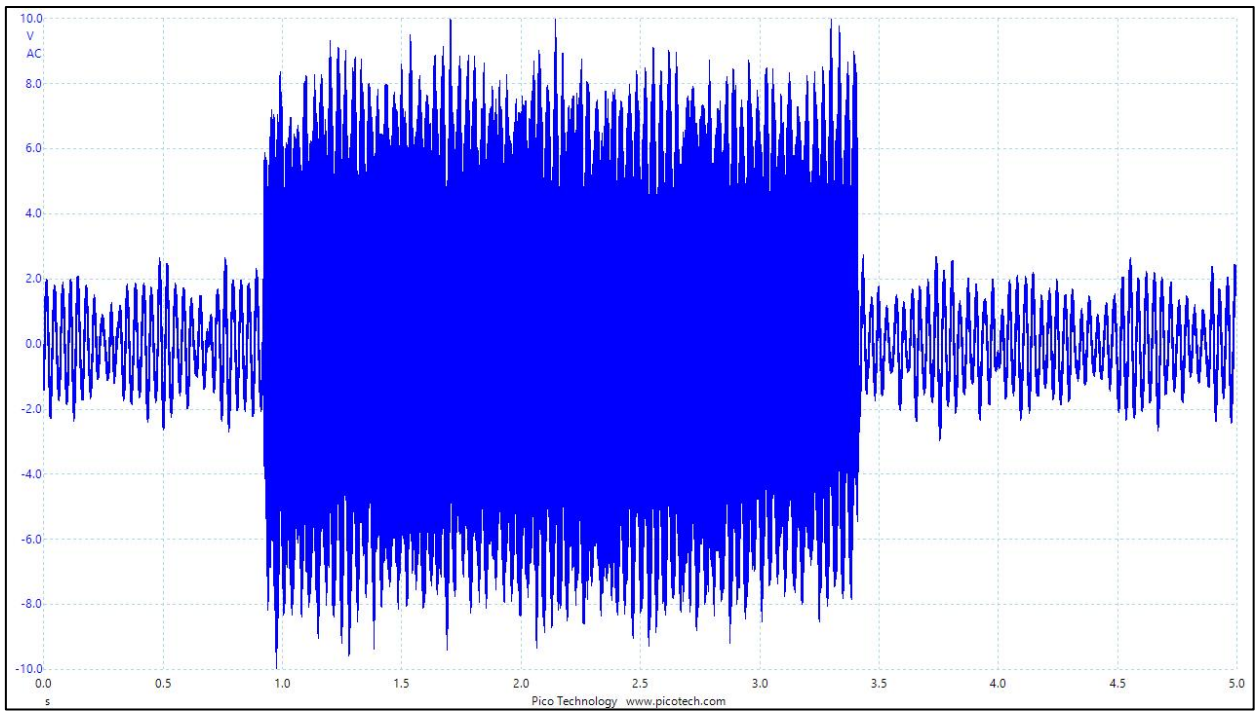

Figure 8.11. Showing the background data and the vibration of the Faraday cage when the resonant signal was sent to the device inside the Faraday cage. Note that the average background vibrational was at 28.24 Hz at an average amplitude displacement of 0.210 microns and the average vibration frequency when the signal was turned on was found to be 15.34 kHz with an average displacement of 0.590 microns.

The displacement is found by taking the average Vop*100 for nm and the nanometer result/1000 for microns. The amplitude zero-peak voltage (Vop) average is given in green in the tables.

Table 8.4. Data for the L bracket 1/8 inch.

Background vibration. Signal 34 kHz applied. (800mV)

Freq (Hz)	Vpp (V)	freq (kHz)	Vpp (V)
29.16	3.382	15.28	11.69
29.88	4.266	16.16	11.83
30.28	3.681	17.34	11.84
25.51	3.722	15.61	11.85
30.04	5.505	19.75	10.95
30.73	4.525	14.47	12.13
27.25	3.735	12.93	12.23
29	4.606	20.25	10.64
29.59	5.069	16.11	11.35
26.75	4.001	16.64	11.87
29.26	4.94	16.07	11.91
30.57	5.151	12.53	12.59

28.98	3.273	16.65	11.03
30.65	4.885	21.35	10.39
29.15	4.198	10.89	12.99
28.68	2.456	14.4	12.49
31.15	4.845	14.81	11.79
30.09	5.001	13.59	13.53
28.4	3.627	15.51	12.53
29.21	4.423	12.77	13.62
29.22	5.042	16.37	12.3
26.94	3.885	19.16	11.64
29.05	4.722	11.8	13.67
29.4	3.735	16	12.59
31.14	5.049	16.64	12.49
28.73	4.042	15.53	12.8
28.88	4.498	17.95	13.6
30.08	5.389	14.03	13.55
29.44	4.573	19.59	12.38
28.24033333	2.103767	15.3393333	5.9045
Av Freq Hz	Vop	Av Freq kHz	Vop

Note that the average background vibrational was at 28.24 Hz at an average amplitude displacement of 0.210 microns. The average vibration frequency when the signal was turned on was found to be 15.34 kHz with an average displacement of 0.590 microns.

L Bracket Mount 1/16 inch thickness on resonance 34 kHz signal.

The linear sweep test was conducted using the L bracket of 1/16 inch thickness to determine the resonant frequency. The Picoscope plot of the run is below.

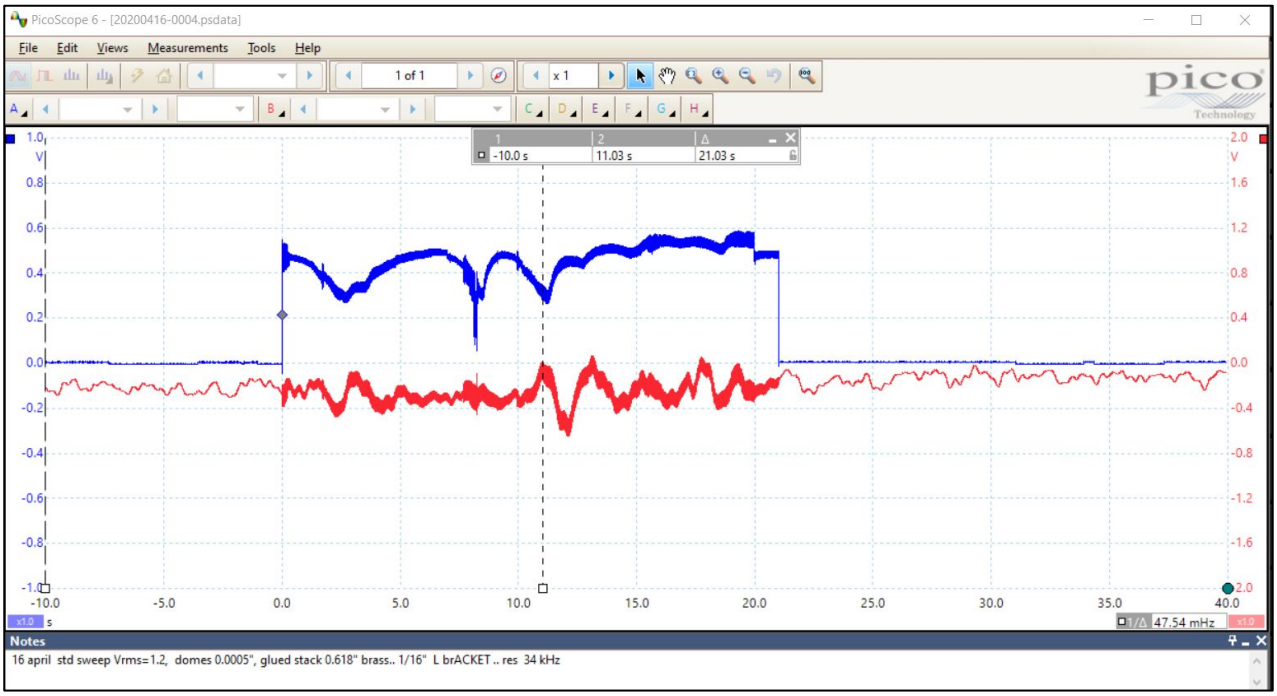

Figure 8.12. Picoscope view of the linear sweep, 45-25kHz in 20 seconds which gives 1 kHz per second. The red trace shows the force. The resonance occurs at 10 seconds which corresponds to 34 kHz.

The vibrometer was set to have a low pass filter of 100kHz and the displacement measurement was set for 100 nm/volt. The Rigol signal generator was used to switch the signal on/off after a few seconds to show both the signal generated vibration noise and the background noise on the same plot as seen below in figure 8.13.

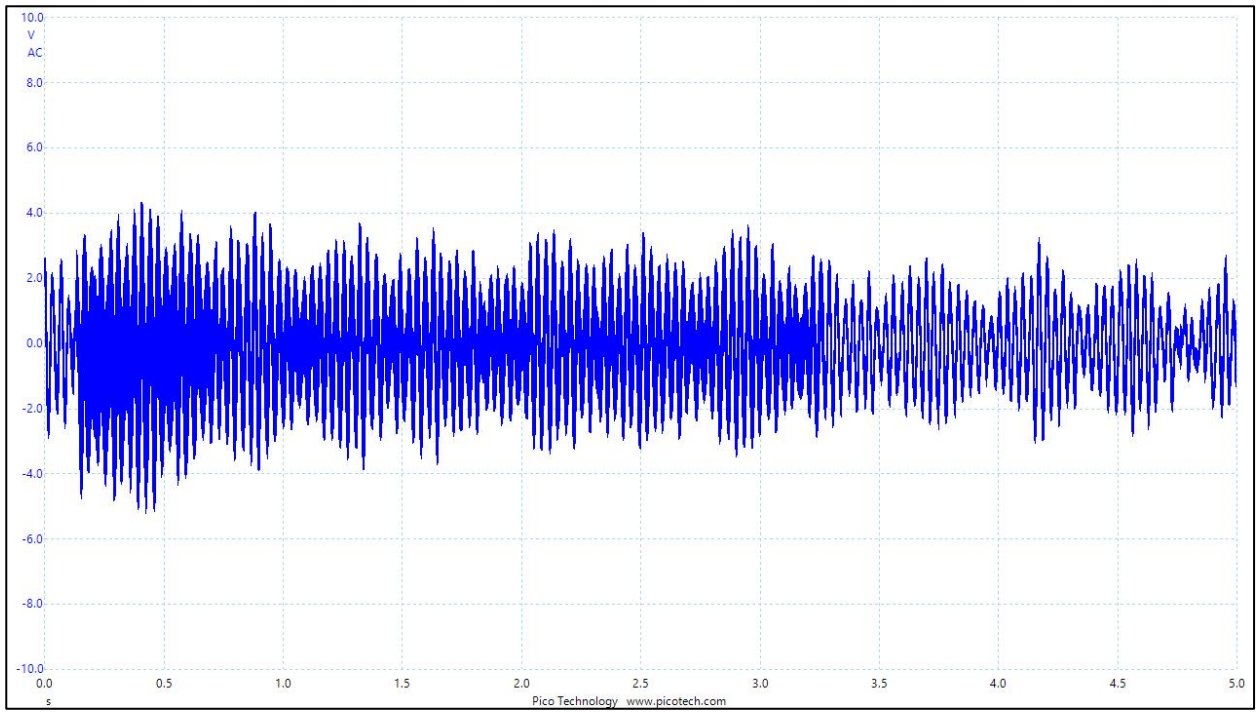

Figure 8.13. Showing the background data and the vibration of the Faraday cage when the resonant signal of 34 kHz was sent to the device inside the Faraday cage. Note that the average background vibrational was at 31.02 Hz at an average amplitude displacement of 0.231 microns and the average vibration frequency when the signal was turned on was found to be 8.25 kHz with an average displacement of 0.303 microns. Note that the average displacement is slightly higher than the background building noise. An average of 30 waveforms was taken.

Table 8.5. Data for the L bracket 1/16 inch. Signal 800mV.

freq (Hz)	Vpp (V)	Freq (kHz)	Vpp (V)
29.58	5.17	3.541	7.259
31.42	4.21	7.046	6.857
35.48	4.674	9.405	6.143
34.54	3.504	5.266	7.048
37.54	4.565	7.183	6.585
42.27	4.524	11.9	6.021
29.13	5.374	8.546	6.109
30.92	5.776	5.246	6.776
29.36	4.177	10.22	5.558
45.06	3.939	3.993	8.007
30.61	5.81	4.813	7.361
29.07	3.912	9.991	5.571
31.56	6.02	4.453	7.197
30.95	4.986	9.922	5.157
28.07	3.912	8.495	5.993
44.22	5.368	5.884	6.762
29.92	4.789	11.25	5.68
31.03	4.51	12.64	5.857

30.28	6.068		5.696	6.674
33.16	5.17		13.91	6.184
29.32	5.136		15.61	4.939
29.99	5.81		5.635	6.64
29.1	3.245		9.803	6.027
30.19	5.197		3.857	7.306
30.66	4.878		10.49	5.49
29.68	3.395		11.05	5.229
28.95	5.98		4.993	7.041
30.98	4.537		11.01	5.612
27.41	4.415		15.8	4.891
31.015	2.317517		8.25493333	3.0329
Av Freq Hz	Vop		Av Freq kHz	Vop

Note that the average background vibrational was at 31.02 Hz at an average amplitude displacement of 0.231 microns and the average vibration frequency when the signal was turned on was found to be 8.25 kHz with an average displacement of 0.303 microns. Note that the average displacement is slightly higher than the background building noise. An average of 30 waveforms was taken.

Sledge Mount 1/8 inch thickness on resonance 36 kHz signal.

The linear sweep test was conducted using the sledge of 1/8 inch thickness to determine the resonant frequency. The Picoscope plot of the run is below. As before, the vibrometer was set to have a low pass filter of 100kHz and the displacement measurement was set for 100 nm/volt. The Rigol signal generator was used to switch the signal on/off after a few seconds to show both the signal generated vibration noise and the background noise on the same plot, as seen below in figure 8.15.

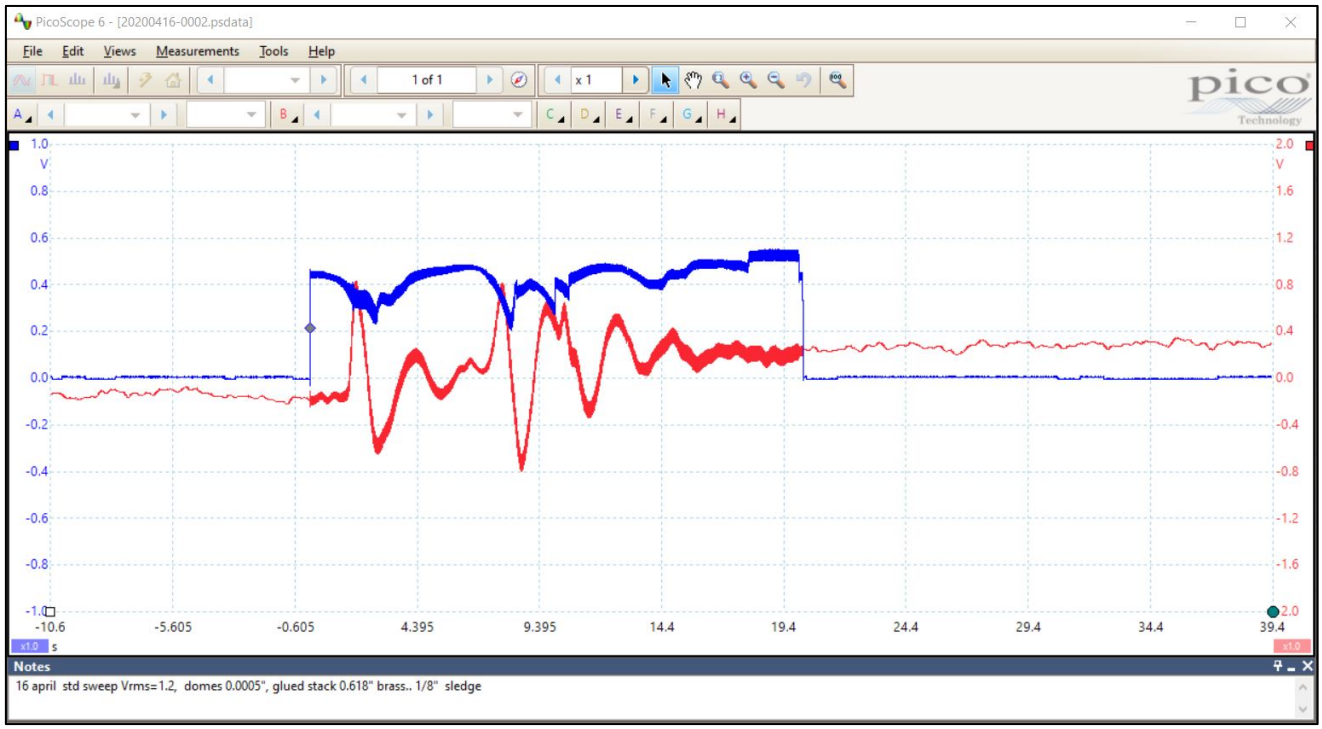

Figure 8.14. Picoscope view of the linear sweep, 45-25kHz in 20 seconds which gives 1 kHz per second. The red trace shows the force. The resonance occurs at 10 seconds which corresponds to 36 kHz.

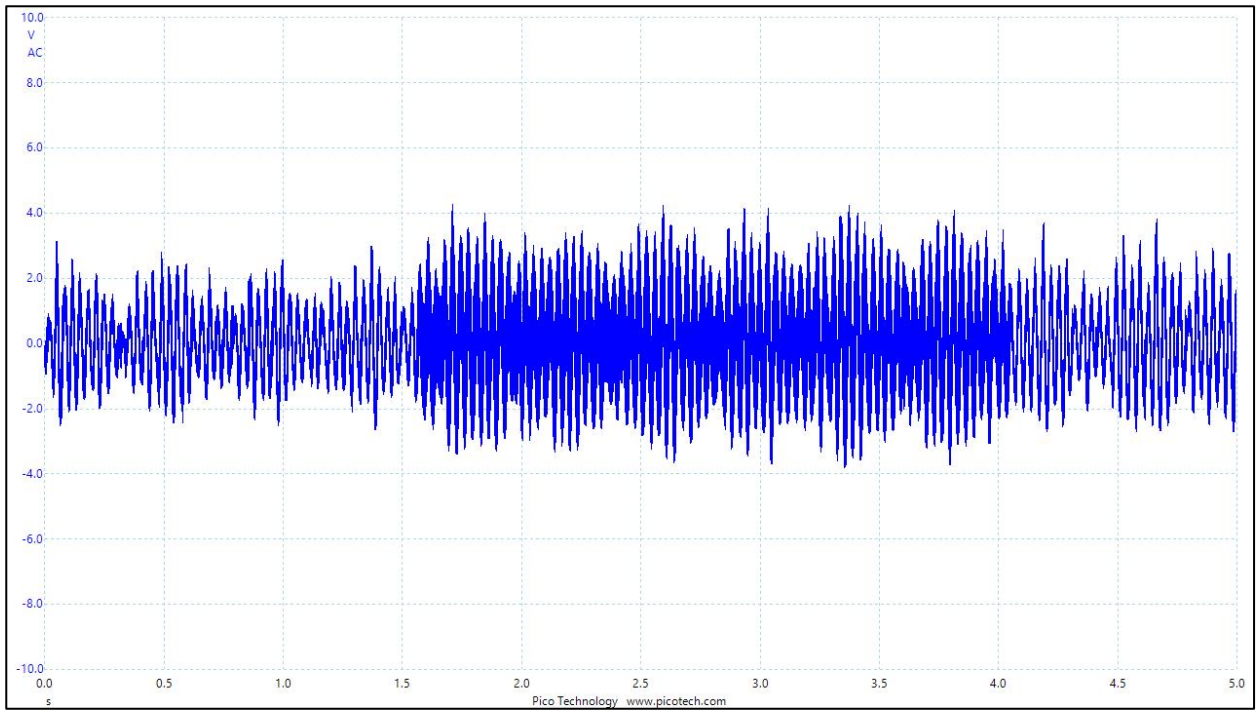

Figure 8.15. Showing the background data and the vibration of the Faraday cage when the resonant signal of 36 kHz was sent to the device inside the Faraday cage. Note that the average background vibrational was at 29.91 Hz at an average amplitude displacement of 0.219 microns. The average vibration frequency when the signal was turned on, was found to be 2.23 kHz with an average displacement of 0.299 microns. Note that the average displacement is slightly higher than the background building noise. An average of 29 waveforms was taken for the background and an average of 23 waveforms was taken for the resonant signal case.

Table 8.6. Background and signal on vibration of Cage. Signal 800mV.

freq (Hz)	Vpp (V)		freq (kHz)	Vpp (V)
30.03	4.876		3.998	5.264
29.46	4.624		1.239	7.082
37.2	5.026		2.562	5.325
29.88	4.427		1.387	6.469
30.23	4.209		3.093	5.597
29.91	5.292		3.032	6.067
28.34	3.576		1.612	6.905
30.14	5.21		1.907	5.515
28.91	3.262		1.423	7.102
32.71	4.025		3.496	5.604
29.6	3.93		1.266	6.973
32.09	5.237		2.718	5.985
29.62	4.188		2.016	6.496
29.83	5.073		3.512	5.713
29.68	4.637		1.802	6.291
29.9	3.718		1.4	7.319

30.13	4.386
49.77	5.543
28.14	3.732
28.98	4.406
29.87	4.515
31.51	5.019
31.45	4.093
32.41	5.931
30.63	5.713
29.41	4.222
28.52	3.745
28.98	4.406
29.907931	2.190017
Av Freq Hz	Vop

3.313	5.399
2.348	6.114
2.933	5.692
1.884	6.42
2.066	6.843
2.389	7.34
2.2346087	2.989457
Av freq kHz	Vop

Note that the average background vibrational was at 29.91 Hz at an average amplitude displacement of 0.219 microns. The average vibration frequency when the signal was turned on, was found to be 2.23 kHz with an average displacement of 0.299 microns. Note that the average displacement is slightly higher than the background building noise. An average of 29 waveforms was taken for the background and an average of 23 waveforms was taken for the resonant signal case.

Sledge Mount 1/16 inch thickness on resonance 37 kHz signal.

The linear sweep test was conducted using the sledge of 1/16 inch thickness to determine the resonant frequency. The Picoscope plot of the run is below.

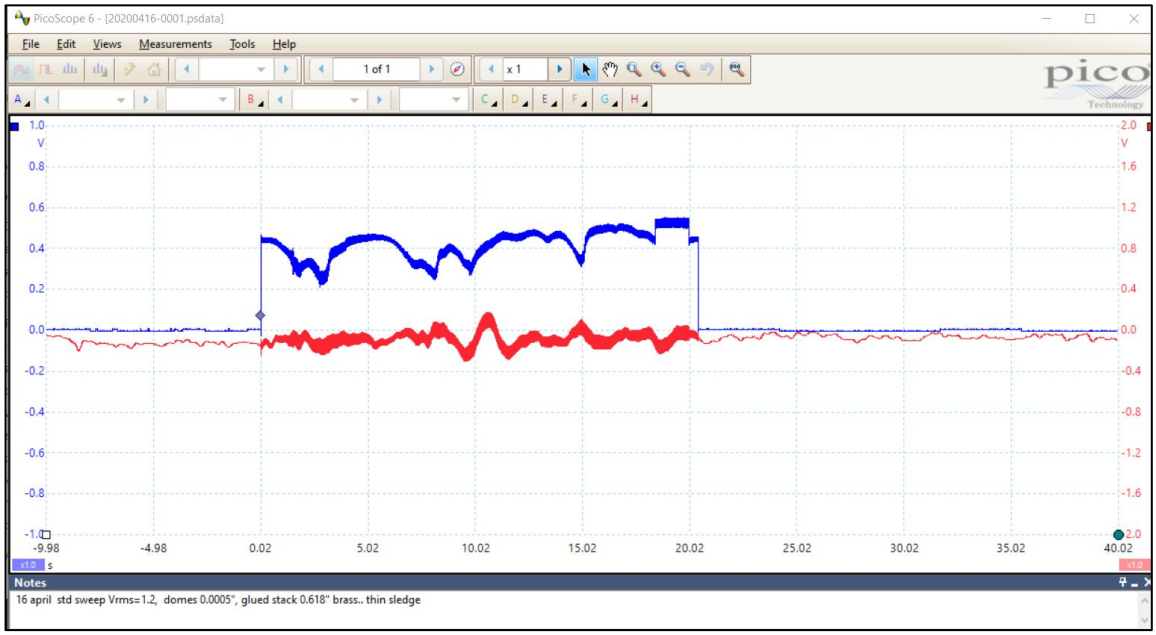

Figure 8.16. Picoscope view of the linear sweep, 45-25kHz in 20 seconds which gives 1 kHz per second. The red trace shows the force. The resonance occurs at 10 seconds which corresponds to 37 kHz.

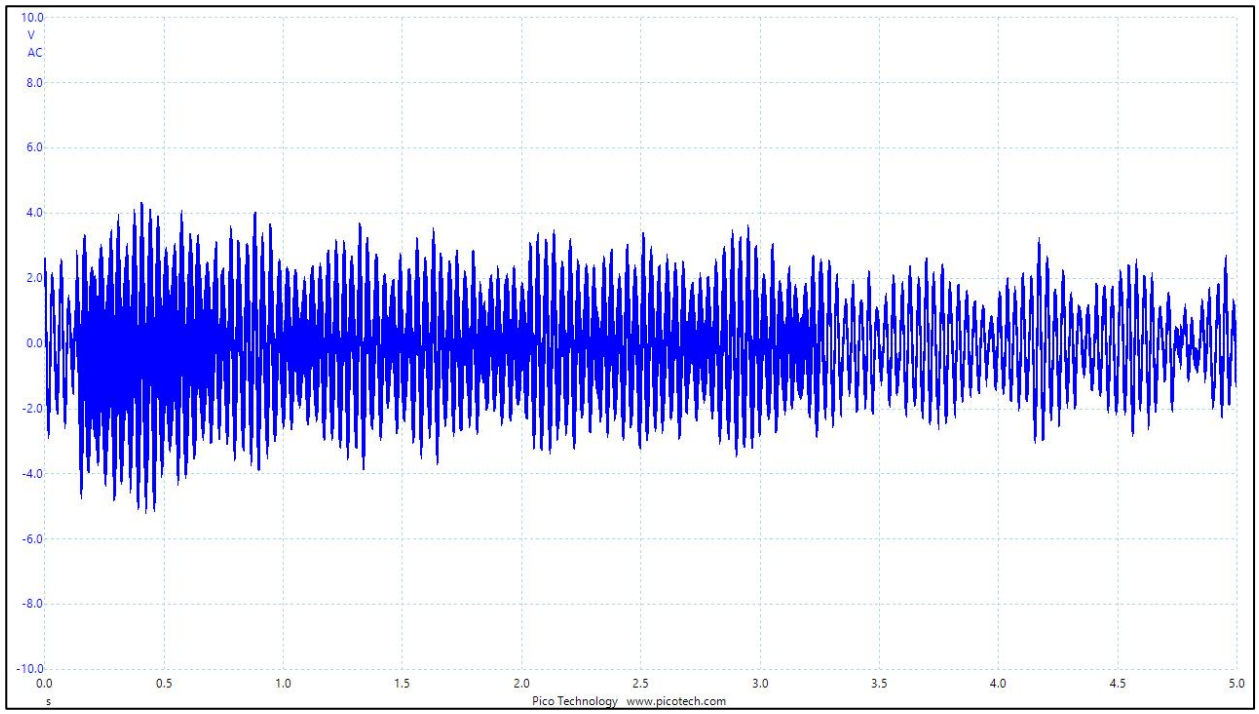

Figure 8.17. Showing the background data and the vibration of the Faraday cage when the resonant signal of 37 kHz was sent to the device inside the Faraday cage. Note that the average background vibrational was at 30.82 Hz at an average amplitude displacement of 0.168 microns. The average vibration frequency when the signal was turned on, was found to be 1.23 kHz with an average displacement of 0.362 microns. Note that the average displacement is slightly higher than the background building noise. An average of 30 waveforms was taken for the background and an average of ONLY 2 waveforms was taken for the resonant signal case due to some picoscope error in saving the waveforms.

The average background vibrational was at 30.82 Hz at an average amplitude displacement of 0.168 microns. The average vibration frequency when the signal was turned on was found to be 1.23 kHz with an average displacement of 0.362 microns. Note that the average displacement is slightly higher than the background building noise. An average of 30 waveforms was taken for the background and an average of ONLY 2 waveforms was taken for the resonant signal case due to some picoscope error in saving the waveforms.

Table 8.12. Background and signal on data. Signal 800mV.

freq (Hz)	Vpp (V)
32.12	4.823
37.23	2.977
28.66	4.509
31.42	3.822
34.54	4.223
35.51	1.587
31.27	3.842
30.7	3.351

freq (kHz)	Vpp
1.8	6.895
0.669	7.603
1.2345	3.6245
Av freq kHz	Vop

	25.39	2.697		
	25.93	3.583		
	30.39	4.264		
	30.83	2.868		
	28.19	2.997		
	46.56	2.425		
	34.97	3.345		
	32.68	3.603		
	33.29	3.495		
	30.56	2.152		
	40.02	2.064		
	30.24	4.488		
	28.82	4.658		
	35.38	3.065		
	30.71	4.113		
	33	4.229		
	30.1	4.059		
	25.87	2.254		
	30.26	3.991		
	31.05	3.46		
	28.8	4.229		
	30.8163333	1.686217		
	Av Freq Hz	Vop		

Conclusions

It is important to balance the beam to get accurate measurement data regardless of whether you are operating at resonance or not. Even a small mass difference of 5-15g can cause errors. It should be noted that the Faraday cage is NEVER oscillating at the resonance frequency of the device, always at much lower frequencies.

The vibration frequency of the background was consistently between 28-31 Hz for all mount brackets. This is building noise.

For the L bracket 1/8th inch thick; the resonance frequency of the device was 35 kHz, the background displacement was 0.2 microns. When the resonant frequency was applied to the device the Faraday cage vibrated at 15.34 kHz, with an amplitude displacement of approximately 0.6 microns.

For the L bracket of 1/16th inch thickness; the resonance frequency of the device was 34 kHz. The background displacement amplitude of the Faraday cage was about 0.2 microns. When the resonance frequency was applied to the device the faraday cage was found to vibrate at 8.25 kHz (half the frequency of the thicker L bracket) with an amplitude displacement of about 0.3 microns. This is half the displacement of the thicker bracket.

For the sledge mount of 1/8th inch thickness; the resonance frequency of the device was found to be 36 kHz, and the background displacement was about 0.2 microns. When the resonance frequency was applied to the device the Faraday cage was seen to oscillate at 2.23 kHz with an amplitude oscillation of about 0.3 microns.

For the sledge mount of 1/16th inch thickness; the resonance frequency of the device was found to be 37 kHz and the background displacement of the Faraday cage was about 0.17 microns. When the resonance signal was applied to the device the Faraday cage was found to vibrate at 1.23 kHz with an average displacement of 0.36 microns, about double the background noise.

The background displacement was consistently 0.2 microns and at a frequency of around 30 Hz. The thinner L brackets appear better at vibration isolation than the thicker bracket. For the sledge the opposite was found to be true, the thicker mounting was better at vibration isolation. The Faraday cage vibrates at a lower frequency when the sledge mounting is in use. The difference between the sledge mount vibration (of the Faraday cage) at 1-2 kHz and the vibration from the L bracket 8-15kHz is significant.

Prior 2019 results

It should be noted that in August 2019 we did only one run using the expensive Polytec vibrometer, which using the nylon washers and an L bracket 1/8” gave a Faraday cage vibration of 24 kHz. In comparison, we have averaged over 30 runs here.

Figure 8.18. Polytec OFV-2500, measuring vibration of Faraday cage
In August 2019. The setting was 1µm/volt as shown.

Results of the vibration test in August 2019 are shown in Figure 8.19.

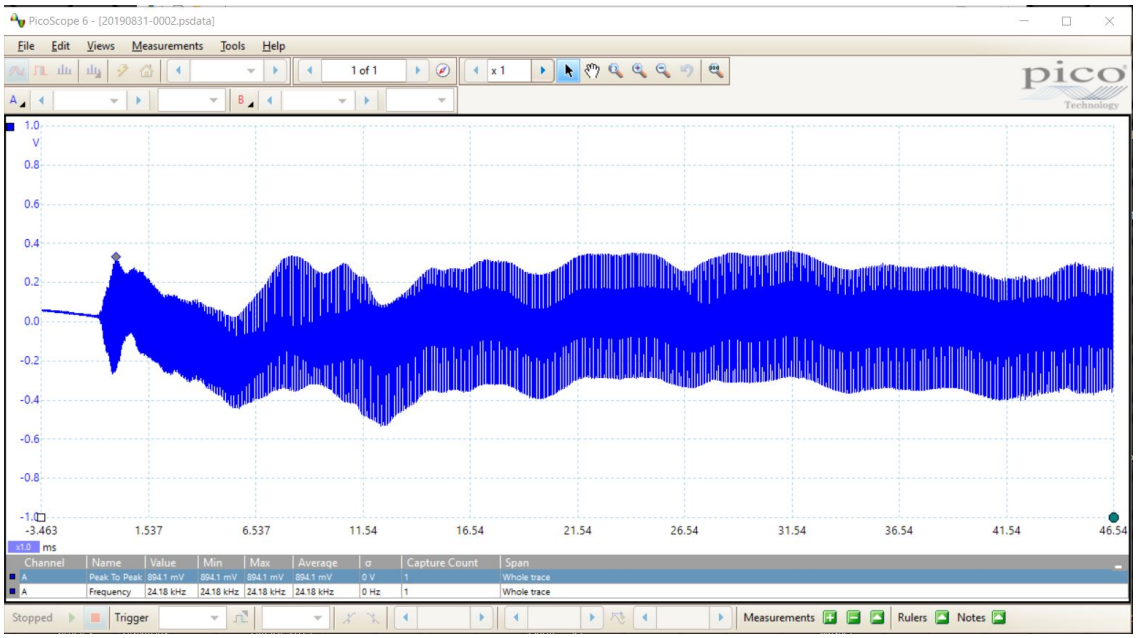

Figure 8.19. The frequency of the Faraday cage was measured at 24 kHz. This was only one run not an average of runs. The device was the DEMO run using a thicker L bracket 1/8" looks like about 0.2-0.3 micron displacement. The setting on the vibrometer was 1µm/volt.

9. Use Of Glued 0.618 Inch Brass Stack With 0.18 Inch Aluminum L Bracket And Different Material Washers

Introduction to the test procedure: The PZT stacks are usually just held in between the brass and aluminum end masses by the 6, 2-56 stainless steel screws. In this test we used 1 new glued stack with the PZT glued directly to the masses and then cured the epoxy in a laboratory oven (Oven OF-02G) for 2 hours at 160°F . The brass mass used was 0.618 inches long, the aluminum end mass used was 0.18 inches long for this test; this was a glued stack. The glued stack has 8 Steiner Martins PZT SM-111 discs that are 2mm thick and 19mm in diameter. The strain gauge in the device was centered.

Test Protocol: A Rigol signal generator DG1032Z with V_{RMS} =1.2 volts input was used to produce a signal to a Carvin DCM2000 amplifier, at level 12. The signal used was a sweep from 45 kHz down to 25 kHz over 20 seconds. We measure the output voltage to the device, the force produced by the device and several other parameters like the strain, FFT and temperature during the run. All the data is collected by Picoscopes and a movie is made using Movavi screen capture software. All runs were made using the basic L bracket mount with 1/8" thickness.

The test above was performed, under the same operating conditions, using the following washer setups:

Phenolic material:

- 1 phenolic washer each side of the L bracket mounting, with titanium flat washers.
- 2 phenolic washers each side of the L bracket mounting, with titanium flat washers.
- 3 phenolic washers each side of the L bracket mounting with titanium flat washers.

E-glass reinforced epoxy (Electric-glass):

- 1 E-glass washer on each side of the L bracket with titanium flat washers.
- 2 E-glass washers on each side of the L bracket with titanium flat washers.
- 3 E-glass washers on each side of the L bracket with titanium flat washers.
- 4 E-glass washers on each side of the L bracket with titanium flat washers.

Vespel (polymide):

- 1 Vespel washer on each side of the L bracket with brass flat washers.
- 2 Vespel washers on each side of the L bracket with brass flat washers.
- 3 Vespel washers on each side of the L bracket with brass flat washers.
- 4 Vespel washers on each side of the L bracket with brass flat washers.

***Carbon reinforced PEEK**:*

- 1 carbon PEEK washer on each side of the L bracket with brass flat washers.
- 2 carbon PEEK washers on each side of the L bracket with brass flat washers.
- 3 carbon PEEK washers on each side of the L bracket with brass flat washers.
- 4 carbon PEEK washers on each side of the L bracket with brass flat washers.

- 5 carbon PEEK washers on each side of the L bracket with brass flat washers

  Rubber*:* 1 rubber inner tube washer with brass flat washers spacers

Phenolic Material Evaluation

10 of the phenolic washers have a mass of 1 gram. It was deemed unnecessary to compensate the counterpoise of the balance for the addition of multiple washers.

One Phenolic Washer

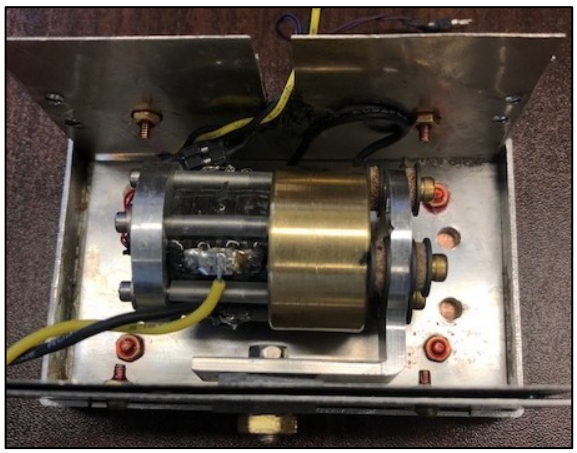

Figure 9.1. New glued stack 0.618 inch brass and 0.18 inch aluminum with 1 phenolic washer each side of the L bracket mount.

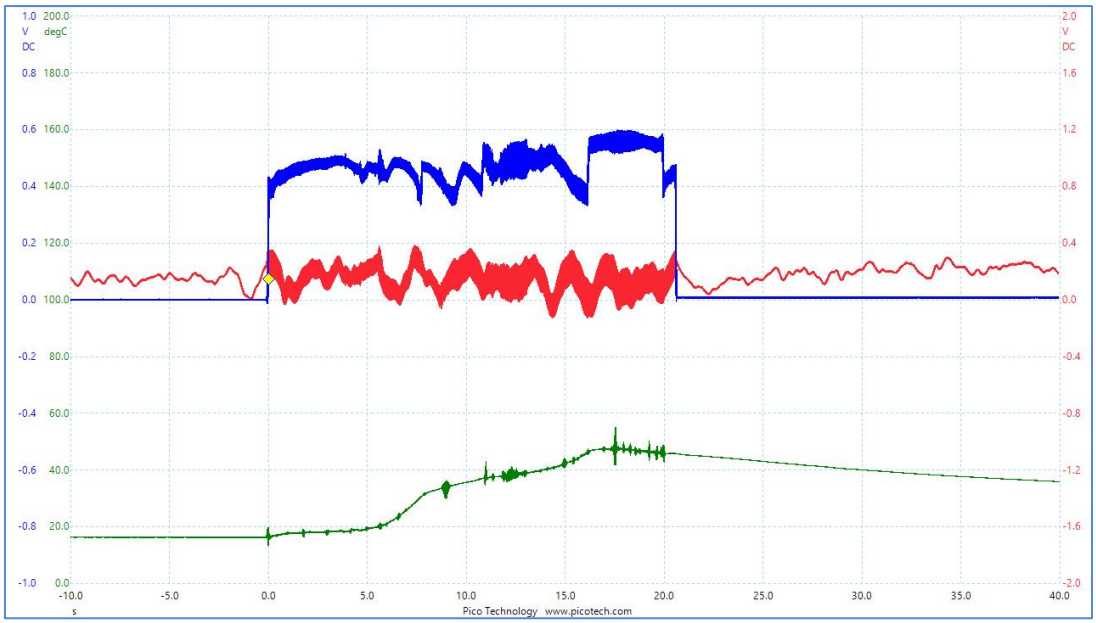

Figure 9.2. Picoscope screenshot of a single forward run, using 0.618" brass and 0.18" aluminum masses on an L bracket with 1 phenolic washer. The force here is about 1 µN. A force of 1 µN corresponds to about 0.11 volts on the red scale. The blue scale is amplitude input voltage and the green scale in Celsius, is temperature measured by a thermistor embedded in the aluminum mass.

Two Phenolic Washers

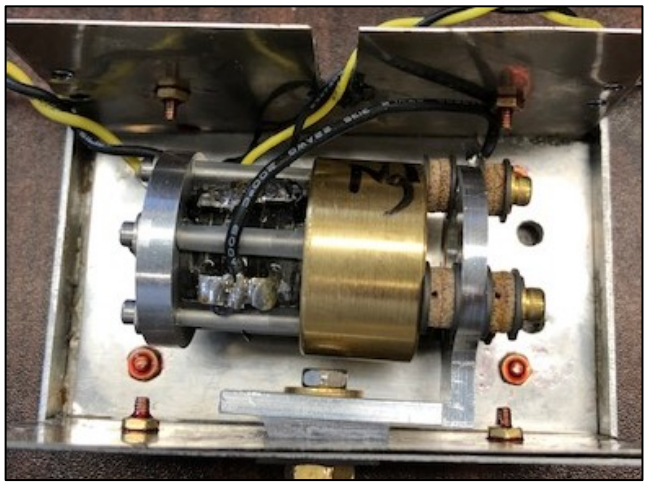

Figure 9.3. New glued brass 0.618" stack with an aluminum 0.18" end mass. The brass mass is labeled "NG" for New Glued stack. Here we show two phenolic washers on each side of the L bracket mounting.

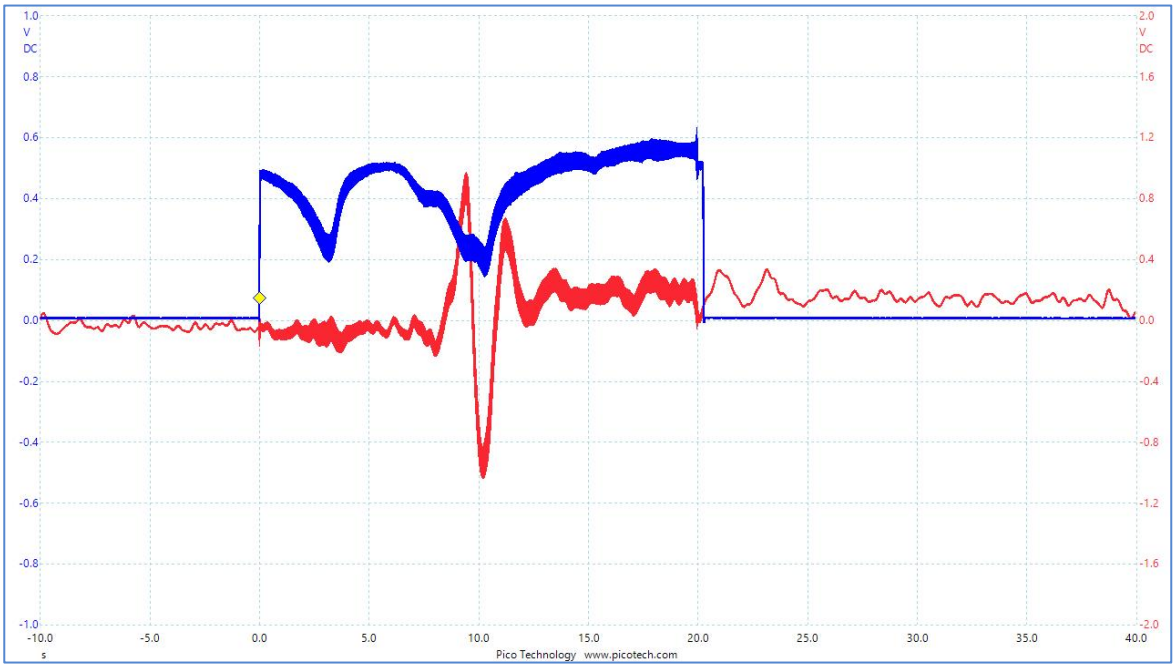

Figure 9.4. Picoscope screenshot of a single forward run, using 0.618" brass and 0.18" aluminum masses on an L bracket with 2 phenolic washers. The force here at 36 kHz is about 9μN.

The phenolic washers appear to be quite sensitive to temperature and can "burn". We noticed a problem with them and decided to run the smaller brass mass only with fiberglass washers which are more temperature resilient. There was quite a variation of resonance with frequency so the average data was a bit noisy.

Three Phenolic Washers

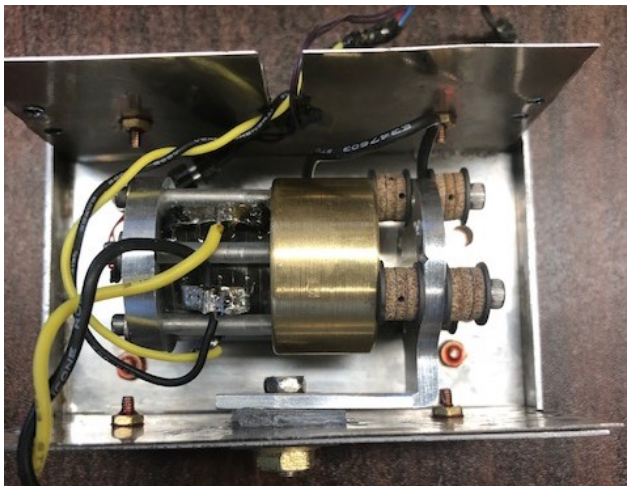

Figure 9.5. New glues stack 0.618 inch brass and 0.18 inch aluminum using 1 phenolic washer each side of the L bracket mount.

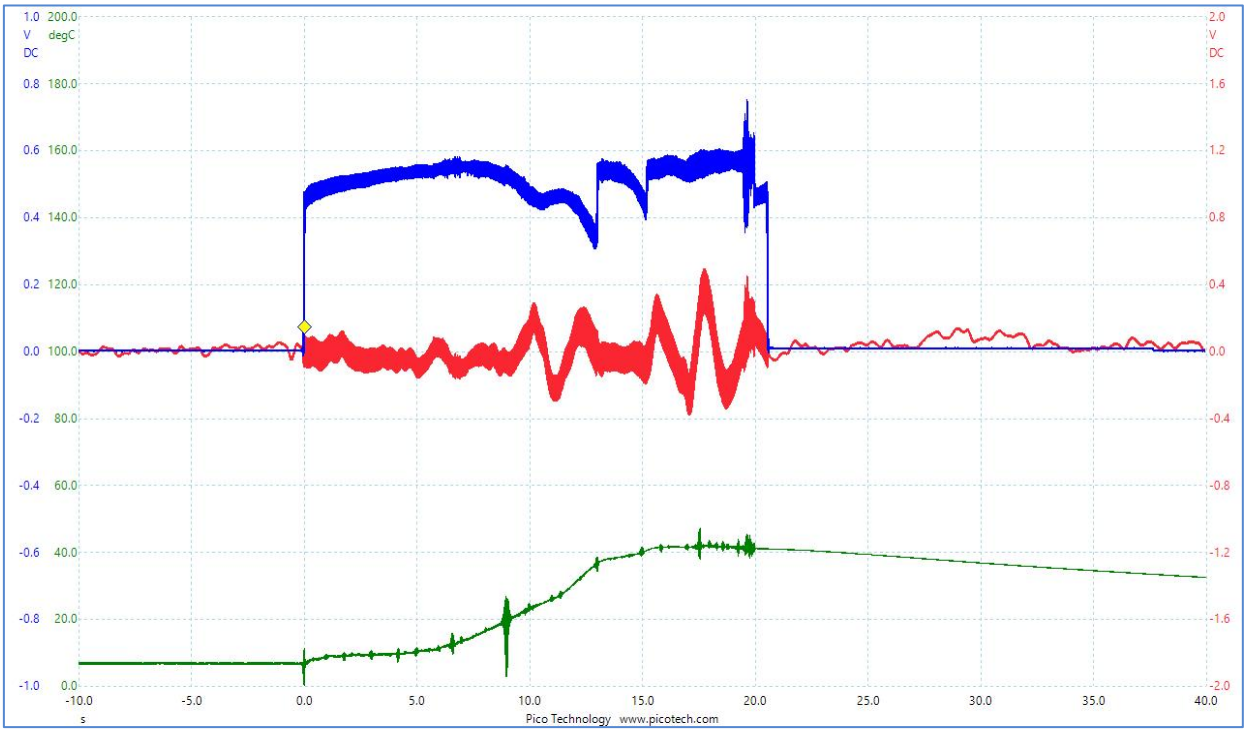

Figure 9.6. Picoscope screenshot of a single forward run, using 0.618" brass and 0.18" aluminum masses on an L bracket with 3 phenolic washers. The force here is at 36 kHz is about 3.5 µN.

E-glass Reinforced Epoxy Washer Material Evaluation

10 of these E-glass reinforced epoxy washers have a mass of 1.3 gram so it was deemed unnecessary to compensate the counterpoise for the addition of washers. Also due to the similar mass of the fiberglass and phenolic washers no compensation was made to the counterpoise of the balance.

One E-glass Washer

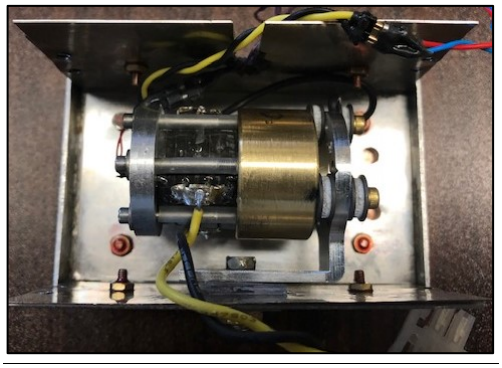

Figure 9.7. New glues stack 0.618 inch brass and 0.18 inch aluminum using one E-glass washer each side of the L bracket mount.

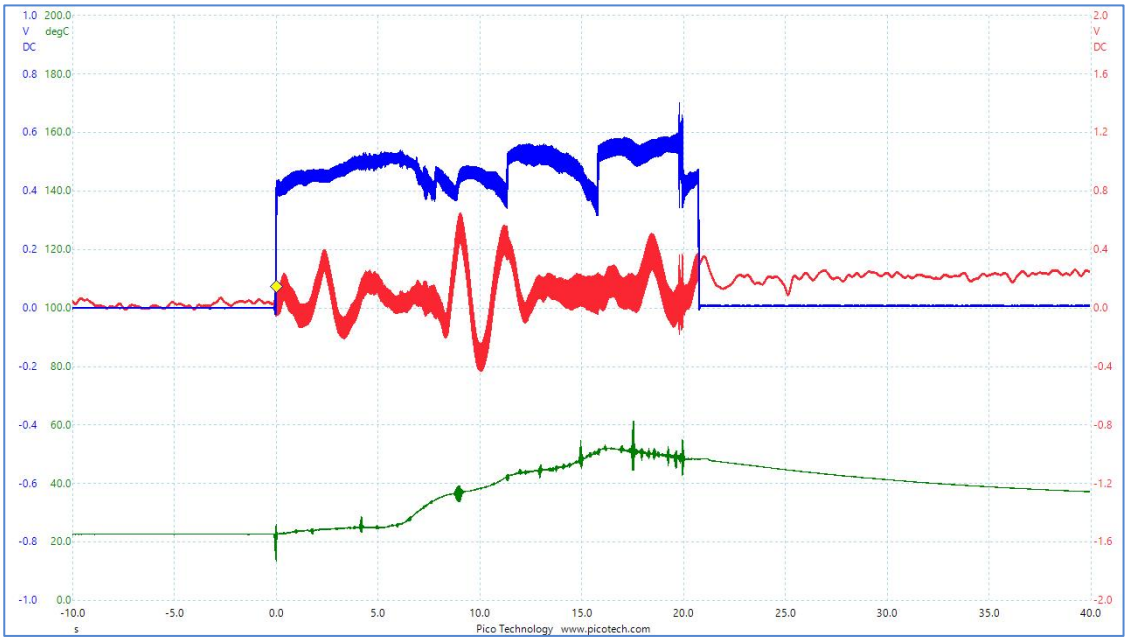

Figure 9.8. Picoscope screenshot of a single forward run, using 0.618" brass and 0.18" aluminum masses on an L bracket with 1 fiberglass washer. A force of 1 µN corresponds to about 0.11 volts on the red scale. The blue scale is amplitude input voltage and the green scale in Celsius, is temperature measured by a thermistor embedded in the aluminum mass. The force here is at 36 kHz is about 7 µN.

Two E-glass Washers

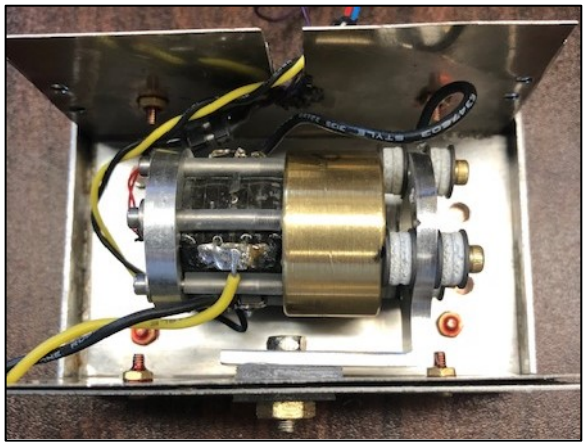

Figure 9.9. New glues stack 0.618 inch brass and 0.18 inch aluminum using two E-glass washers each side of the L bracket mount.

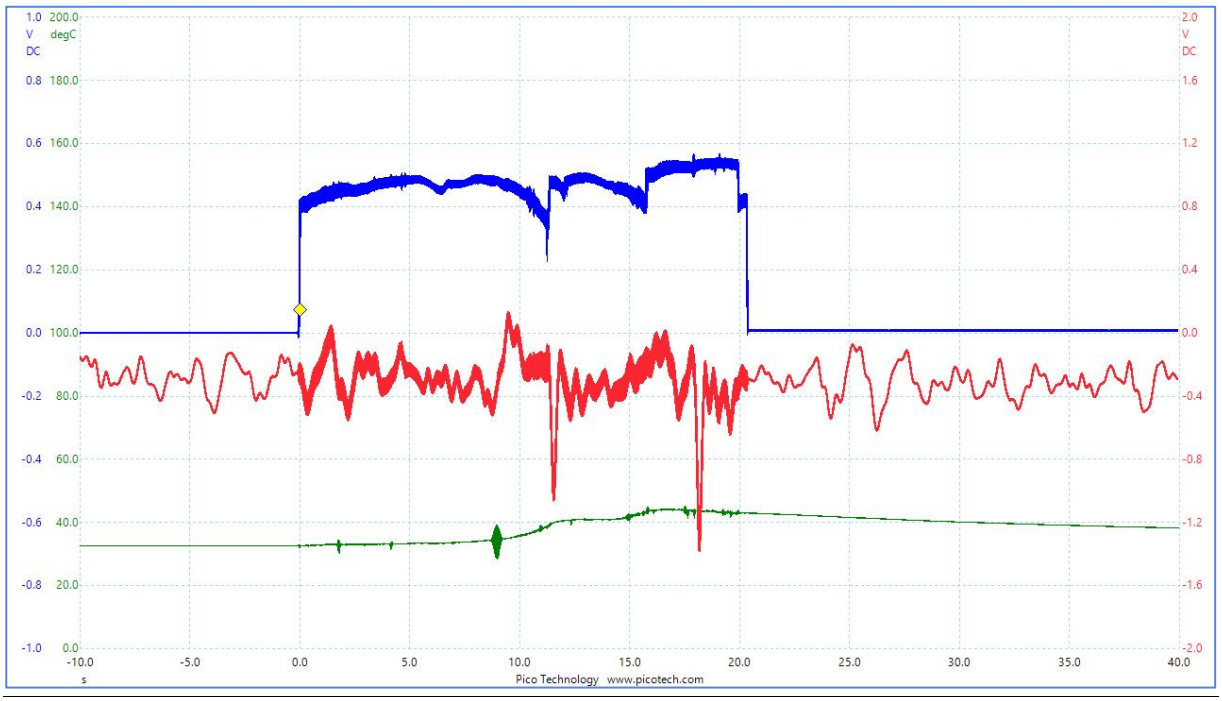

Figure 9.10. Picoscope screenshot of a single forward run, using 0.618" brass and 0.18" aluminum masses on an L bracket with 2 E-glass washers. A force of 1 µN corresponds to about 0.11 volts on the red scale. The blue scale is amplitude input voltage and the green scale in Celsius, is temperature measured by a thermistor embedded in the aluminum mass. The force here is at 36 kHz is about 3µN but there is considerable background noise. *Possible low level earthquake was in progress.* The downward spikes at 34 kHz and 28 kHz appear to be electronic noise.

Three E-glass washers

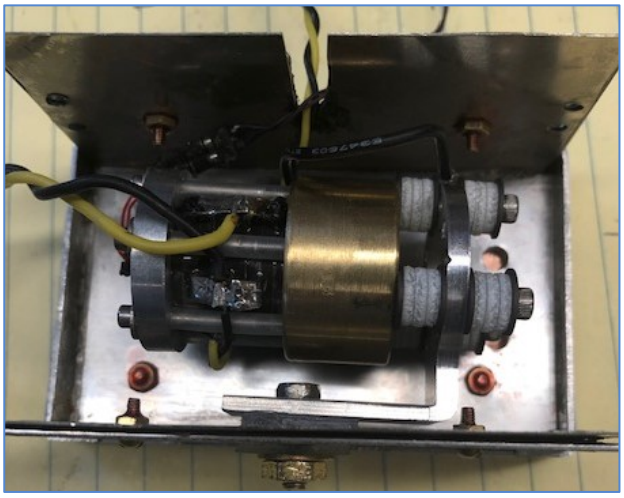

Figure 9.11. New glues stack 0.618 inch brass and 0.18 inch aluminum using three E-glass washers each side of the L bracket mount.

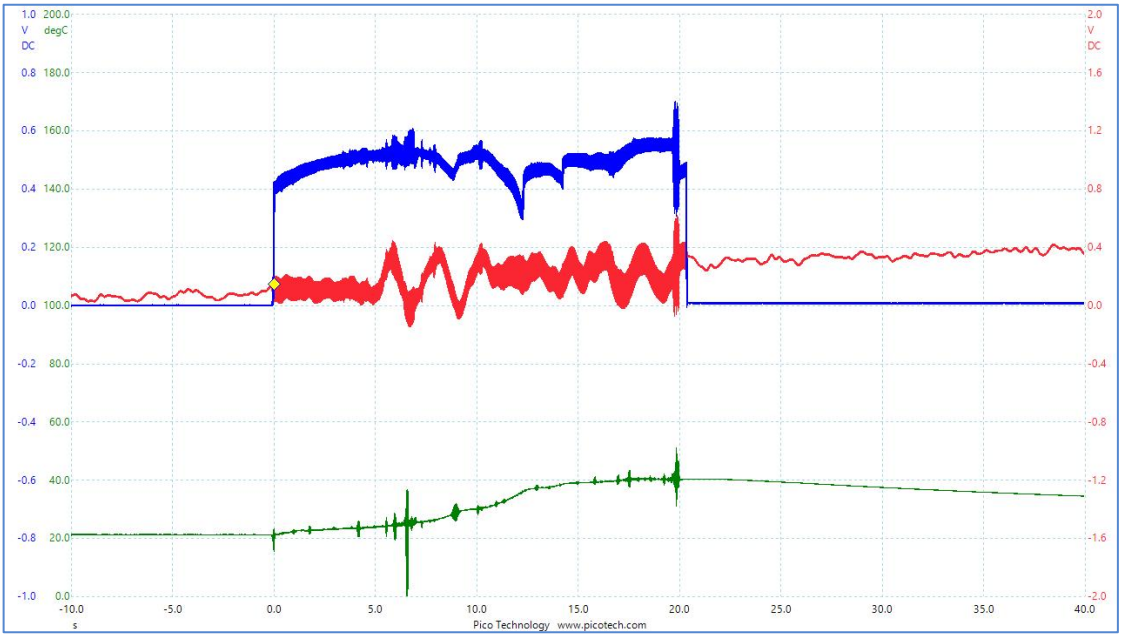

Figure 9.12. Picoscope screenshot of a single forward run, using 0.618" brass and 0.18" aluminum masses on an L bracket with 3 fiberglass washers. A force of 1 µN corresponds to about 0.11 volts on the red scale. The blue scale is amplitude input voltage and the green scale in Celsius, is temperature measured by a thermistor embedded in the aluminum mass. The force here is at 36 kHz is about 1.8 µN.

Four E-glass washers

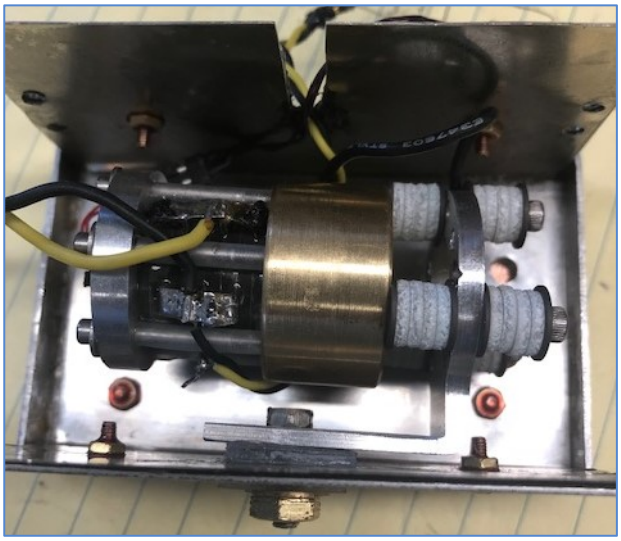

Figure 9.13. New glues stack 0.618 inch brass and 0.18 inch aluminum using four E-glass washers each side of the L bracket mount.

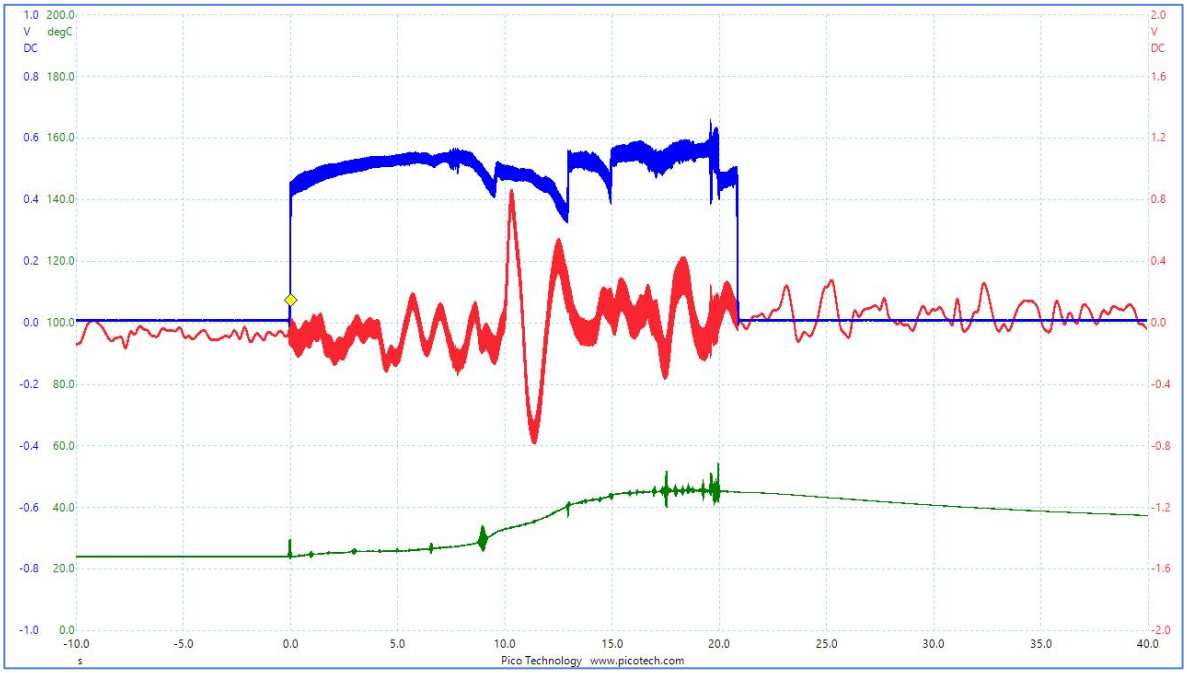

Figure 9.14. Picoscope screenshot of a single forward run, using 0.618" brass and 0.18" aluminum masses on an L bracket with 4 E-glass washers. A force of 1 µN corresponds to about 0.11 volts on the red scale. The blue scale is amplitude input voltage and the green scale in Celsius, is temperature measured by a thermistor embedded in the aluminum mass. The force here is at 36 kHz is about 10.9 µN.

Vespel® (Polymide) Evaluation

The flat washers used here appear silver but they are zinc-coated brass washers.

One Vespel Washer

During these tests we stopped using the thermistor in the aluminum mass and started using a new thermistor embedded in the L bracket to better find the temperature of the washers. The figure captions will indicate which thermistor is being used. For one Vespel washer the thermistor was is the aluminum mass.

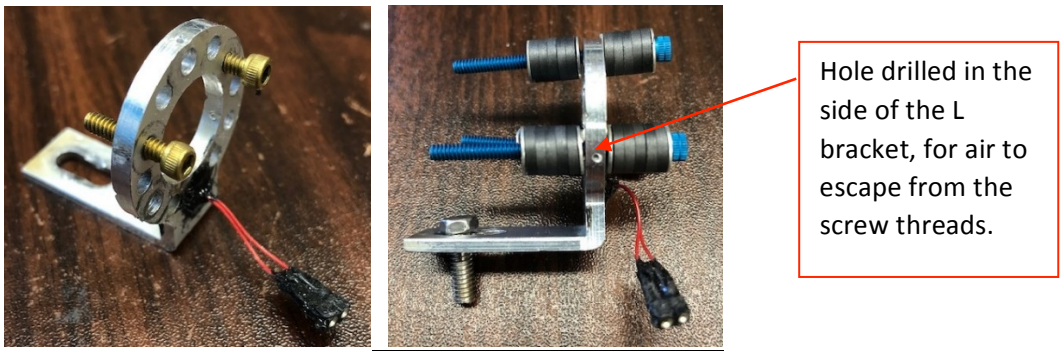

Figure 9.15. New thermistor embedded in the L bracket. Also holes were drilled in the side of the bracket to allow air to escape from screw threads.

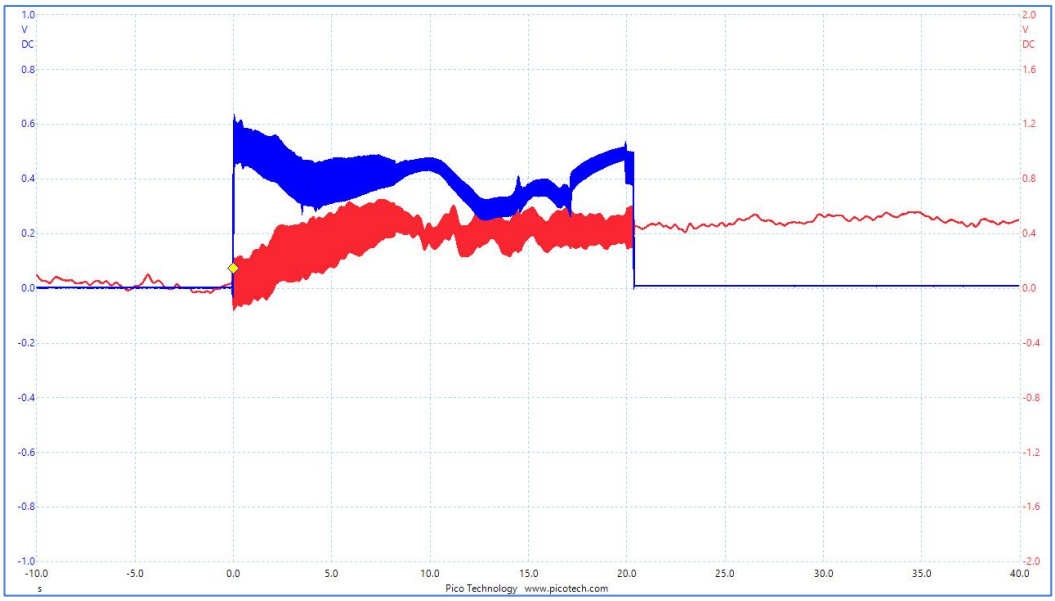

Figure 9.16. Picoscope screenshot of a single forward run, using 0.618" brass and 0.18" aluminum masses on an L bracket with one Vespel washer. The force here is about 1 µN around 31 kHz. A force of 1 µN corresponds to about 0.11 volts on the red scale. The blue scale is amplitude input voltage and the green scale in Celsius, is temperature measured by a thermistor embedded in the aluminum mass.

Two Vespel Washers

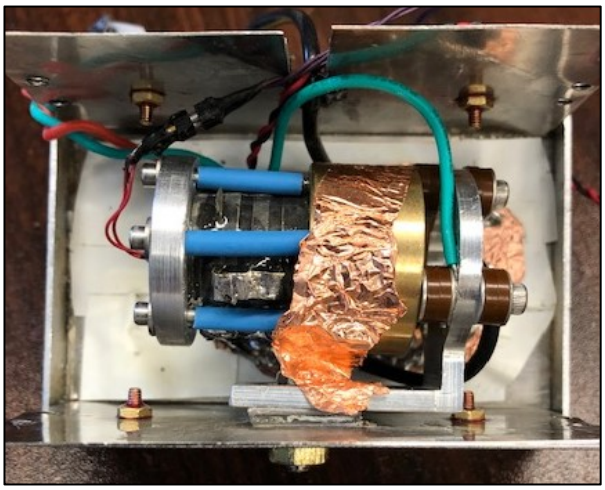

Figure 9.17. Two Vespel washers each side of the L bracket. The copper tape was removed as a failed attempt at cooling. Still using thermistor in the aluminum mass. This is an off-center
Strain gauge glued stack. The central strain gauge stack lost its thermistor.

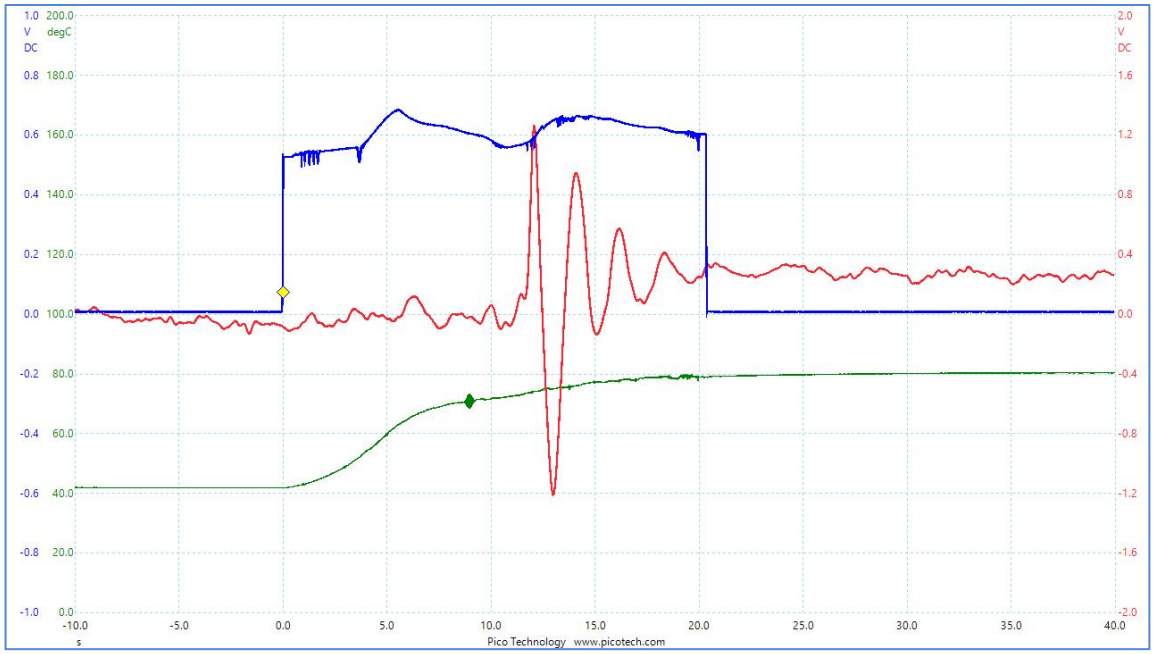

Figure 9.18. Picoscope screenshot of a single forward run, using 0.618" brass and 0.18" aluminum masses on an L bracket with two Vespel washers. The force here is about 11 µN around 32 kHz. A force of 1 µN corresponds to about 0.11 volts on the red scale. The blue scale is amplitude input voltage and the green scale in Celsius, is temperature measured by a thermistor embedded in the aluminum mass. The force was reduced to about 3 µN in later runs.

Three Vespel Washers

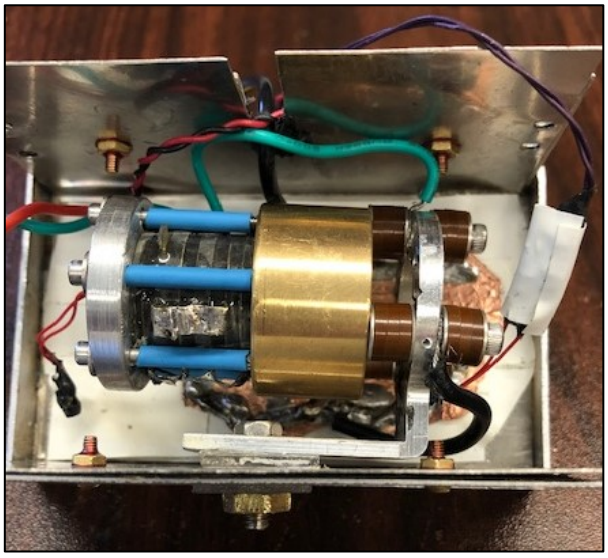

Figure 9.19. Three Vespel washers each side of the L bracket. The thermistor is now in the L bracket.

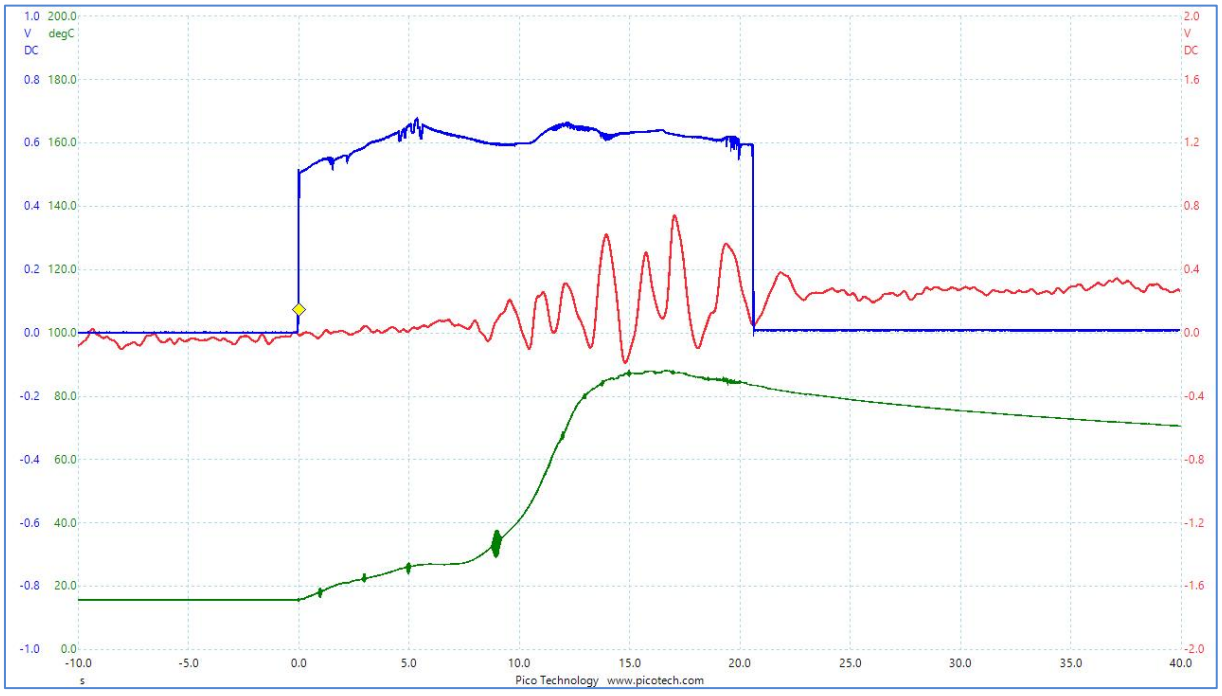

Figure 9.20. Picoscope screenshot of a single forward run, using 0.618" brass and 0.18" aluminum masses on an L bracket with three Vespel washers. The force here is about 4.5 µN around 32 kHz. A force of 1 µN corresponds to about 0.11 volts on the red scale. The blue scale is amplitude input voltage and the green scale in Celsius, is temperature measured by a thermistor embedded in the aluminum mass.

Four Vespel Washers

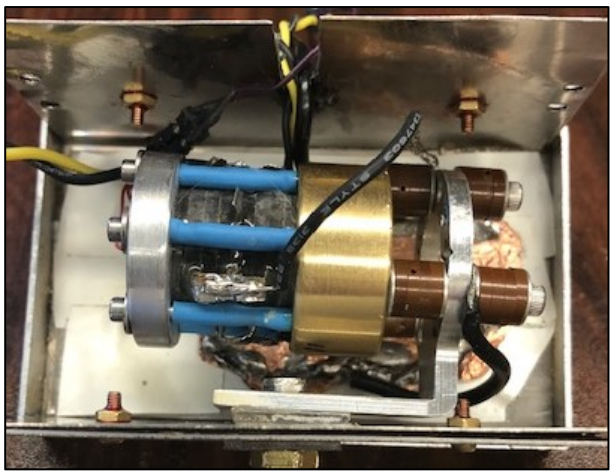

Figure 9.21. Four vespel washers each side of the L bracket. Older data, thermistor in the aluminum mass.

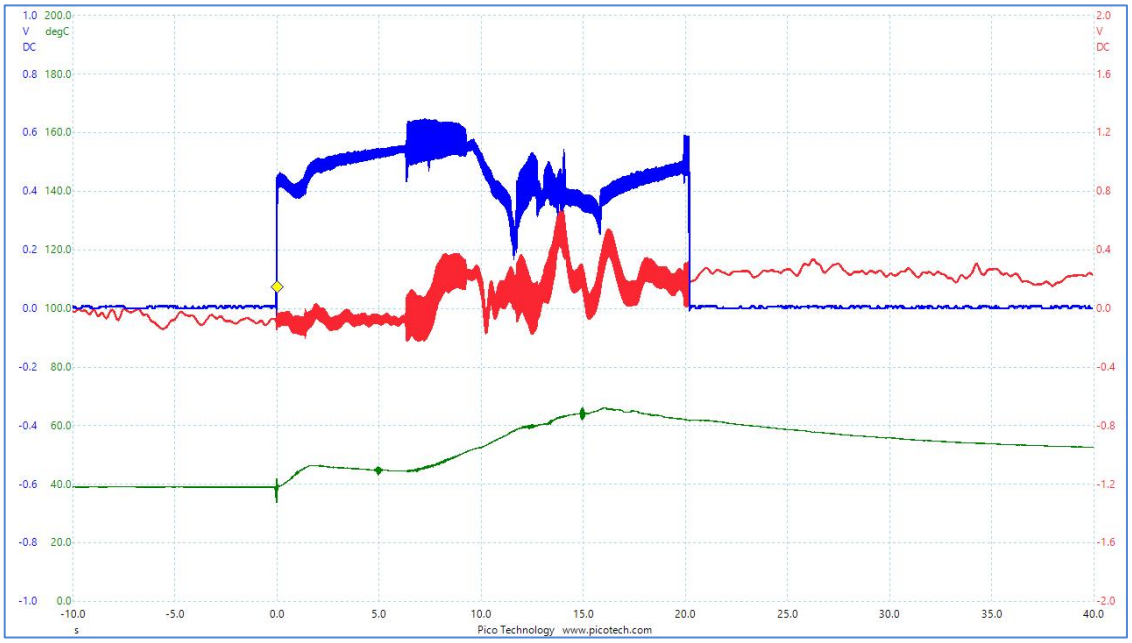

Figure 9.22. Picoscope screenshot of a single forward run, using 0.618" brass and 0.18" aluminum masses on an L bracket with four Vespel washers. The force here is about 4 µN around 31 kHz. A force of 1 µN corresponds to about 0.11 volts on the red scale. The blue scale is amplitude input voltage and the green scale in Celsius, is temperature measured by a thermistor embedded in the aluminum mass.

Carbon Reinforced PEEK Evaluation

One Carbon PEEK Washer

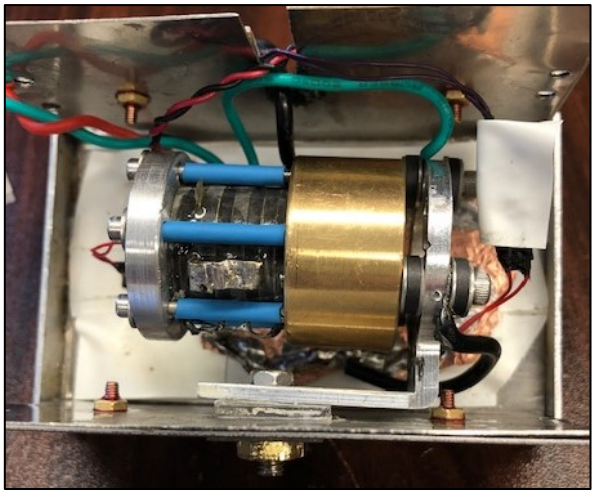

Figure 9.23. One carbon-reinforced PEEK washer each side of the L bracket. This stack has the strain gauge off center.

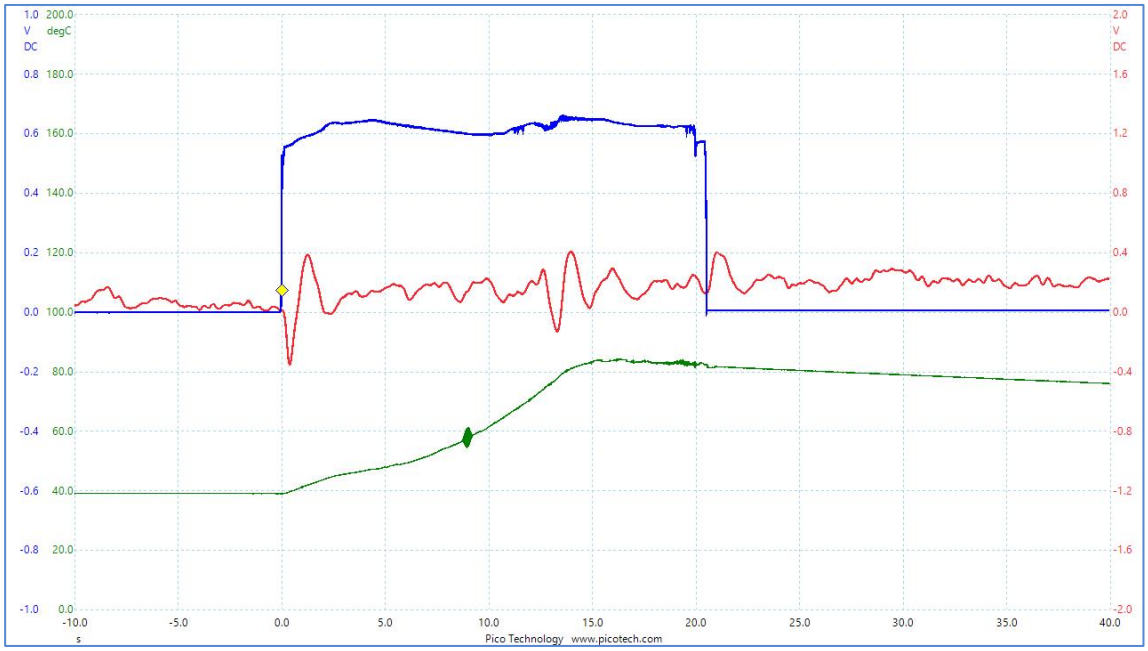

Figure 9.24. Picoscope screenshot of a single forward run, using 0.618" brass and 0.18" aluminum masses on an L bracket with one carbon-reinforced PEEK washer. The force here is about 2 µN around 32 kHz. A force of 1 µN corresponds to about 0.11 volts on the red scale. The blue scale is amplitude input voltage and the green scale in Celsius, is temperature measured by a thermistor embedded in the L bracket.

Two Carbon PEEK Washers

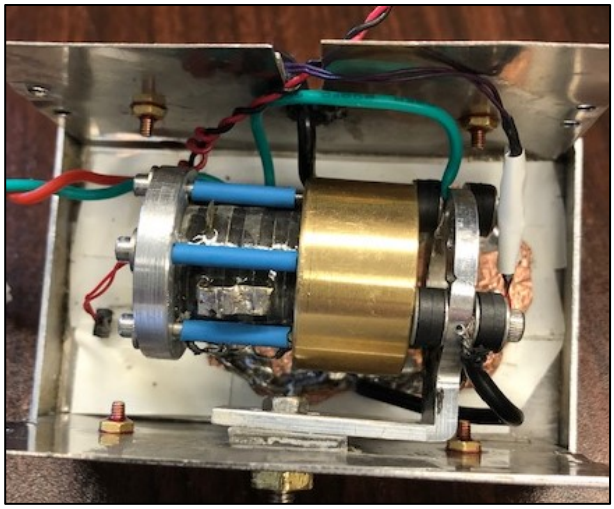

Figure 9.25. Two carbon-reinforced PEEK washers each side of the L bracket.

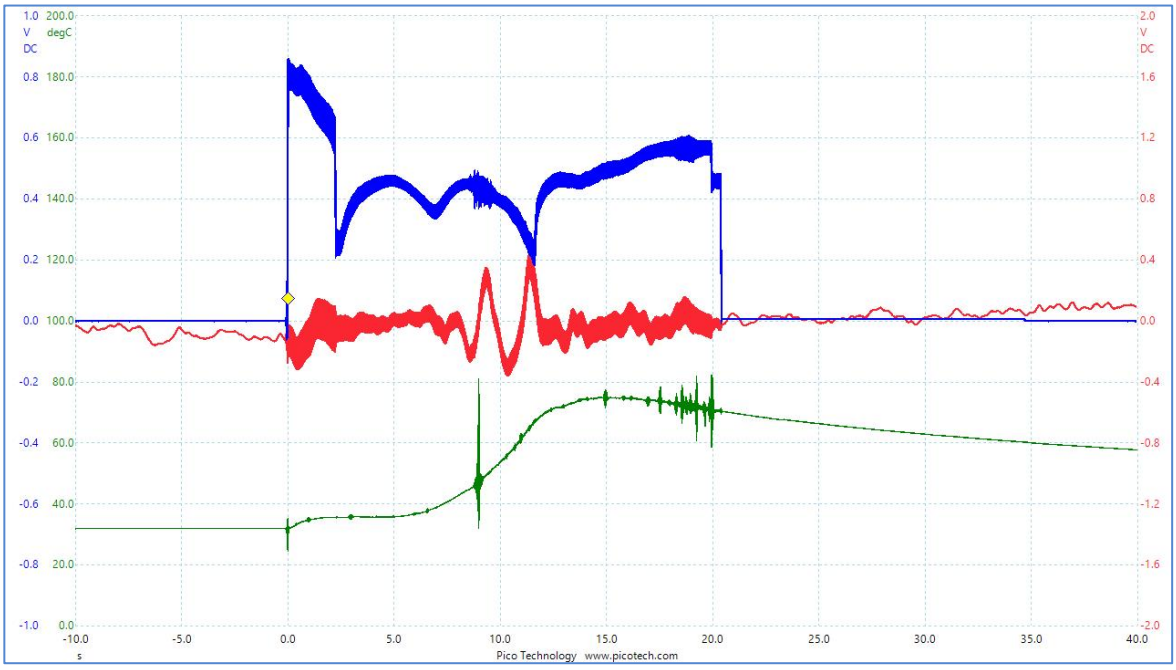

Figure 9.26. Picoscope screenshot of a single forward run, using 0.618" brass and 0.18" aluminum masses on an L bracket with two carbon-reinforced PEEK washers. The force here is about 3.6 µN around 36 kHz. A force of 1 µN corresponds to about 0.11 volts on the red scale. The blue scale is amplitude input voltage and the green scale in Celsius, is temperature measured by a thermistor embedded in the L bracket.

Three Carbon PEEK Washers

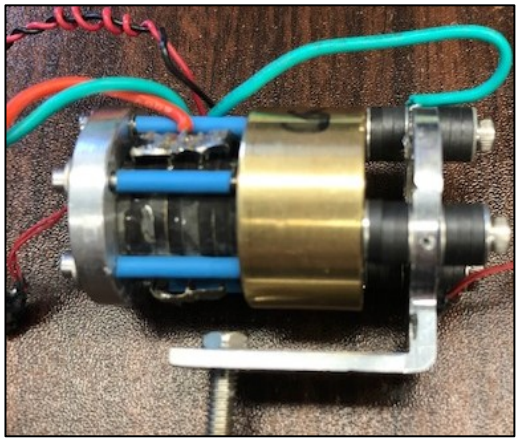

Figure 9.27. Three carbon-reinforced PEEK washers each side of the L bracket.

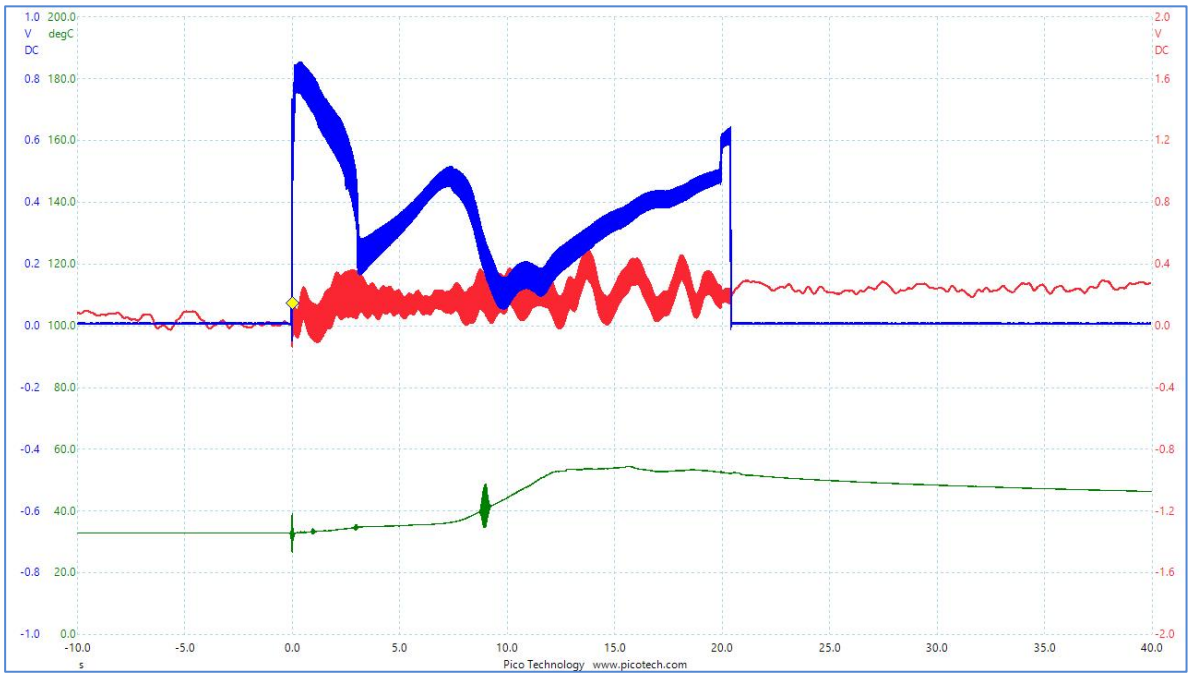

Figure 9.28. Picoscope screenshot of a single forward run, using 0.618" brass and 0.18" aluminum masses on an L bracket with three carbon-reinforced PEEK washers. The force here is about 2 µN around 31 kHz. A force of 1 µN corresponds to about 0.11 volts on the red scale. The blue scale is amplitude input voltage and the green scale in Celsius, is temperature measured by a thermistor embedded in the L bracket.

Four Carbon PEEK Washers

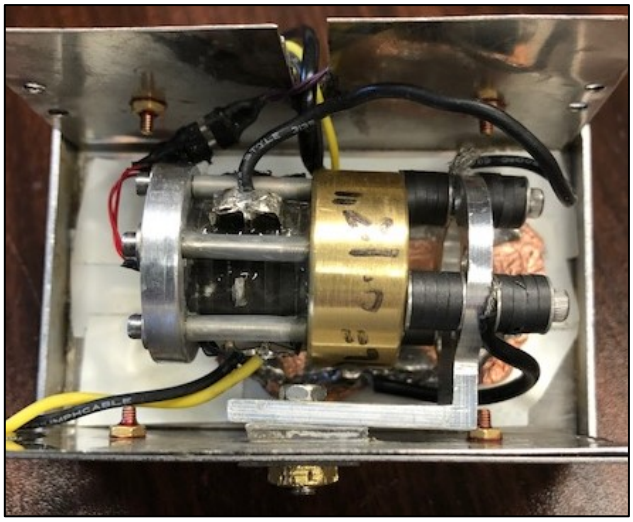

Figure 9.29. Four carbon-reinforced PEEK washers each side of the L bracket.

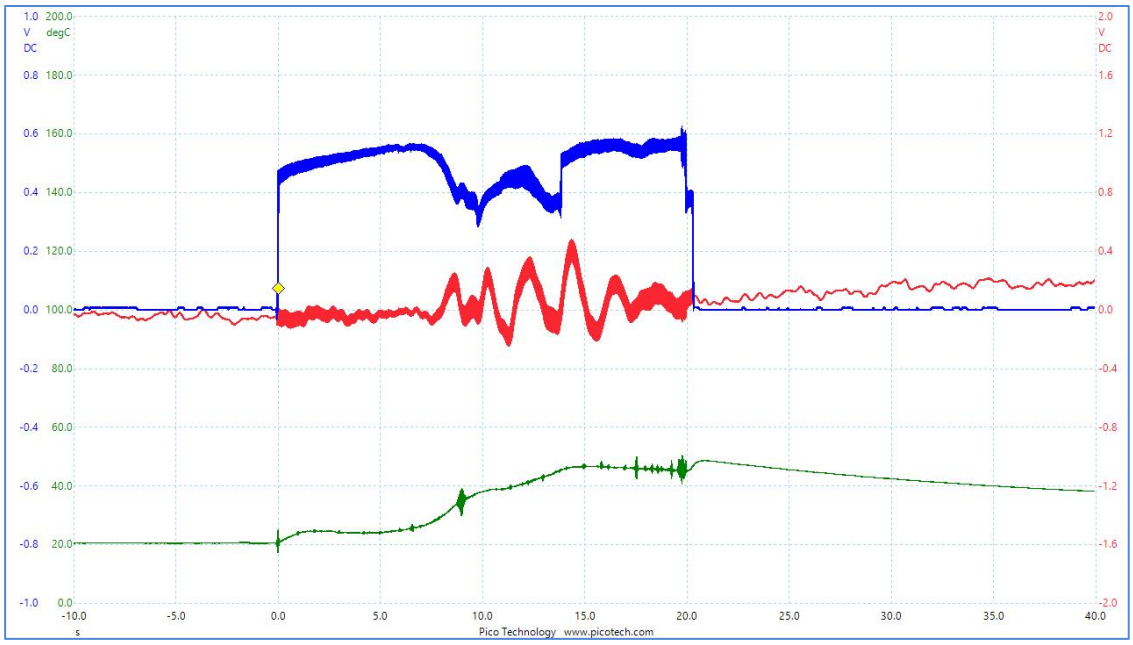

Figure 9.30. Picoscope screenshot of a single forward run, using 0.618" brass and 0.18" aluminum masses on an L bracket with four carbon-reinforced PEEK washers. The force here is about 2 µN around 35 kHz. A force of 1 µN corresponds to about 0.11 volts on the red scale. The blue scale is amplitude input voltage and the green scale in Celsius, is temperature measured by a thermistor embedded in the L bracket.

Five Carbon PEEK Washers

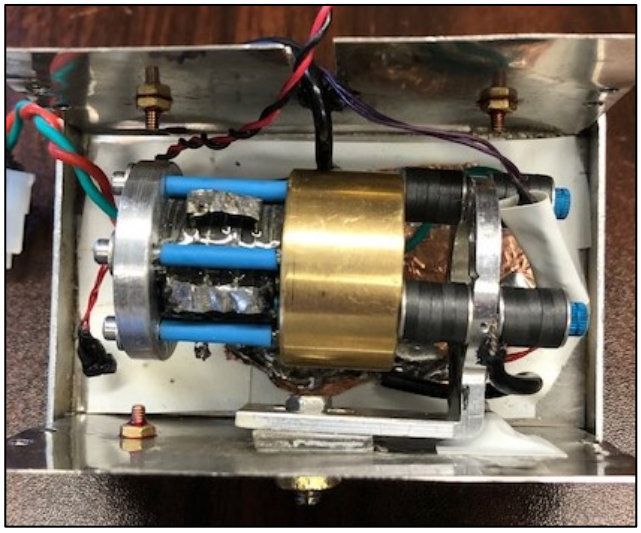

Figure 9.31. Five carbon-reinforced PEEK washers each side of the L bracket.

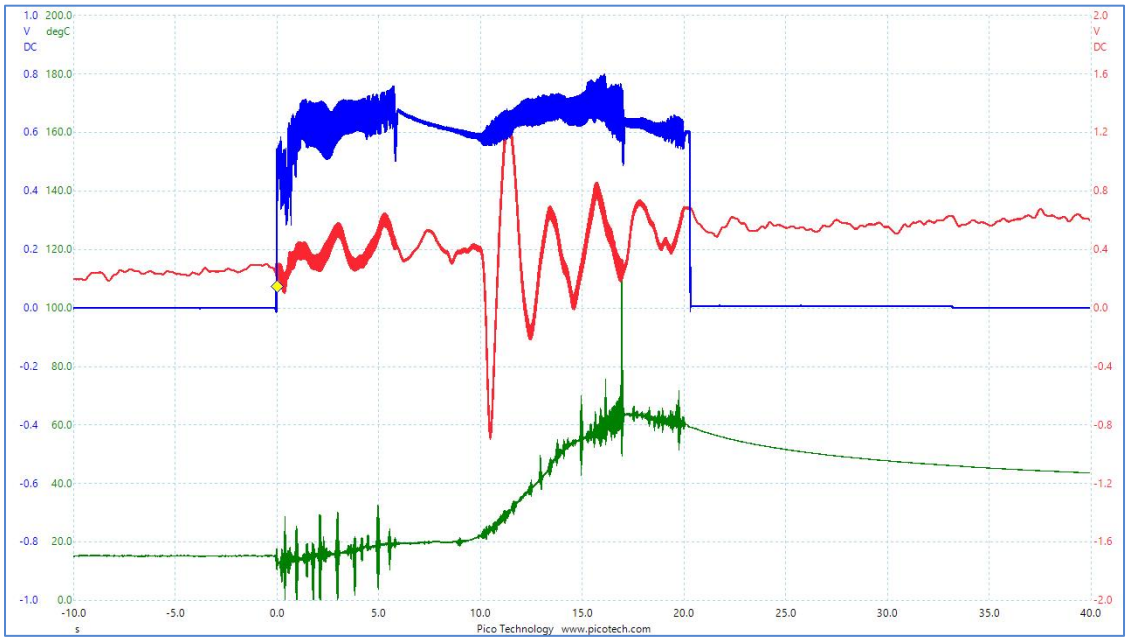

Figure 9.32. Picoscope screenshot of a single forward run, using 0.618" brass and 0.18" aluminum masses on an L bracket with five carbon-reinforced PEEK washers. The force here is about 11 µN around 35 kHz. A force of 1 µN corresponds to about 0.11 volts on the red scale. The blue scale is amplitude input voltage and the green scale in Celsius, is temperature measured by a thermistor embedded in the L bracket.

Rubber Inner-Tube Washer Material Evaluation

One Rubber Washer

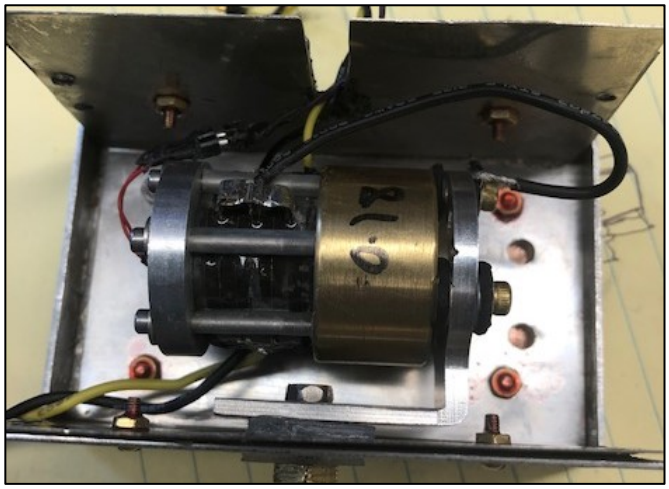

Figure 9.33 New glued stack 0.618 inch brass and 0.18 inch aluminum with 1 rubber washer each side of the L bracket mount.

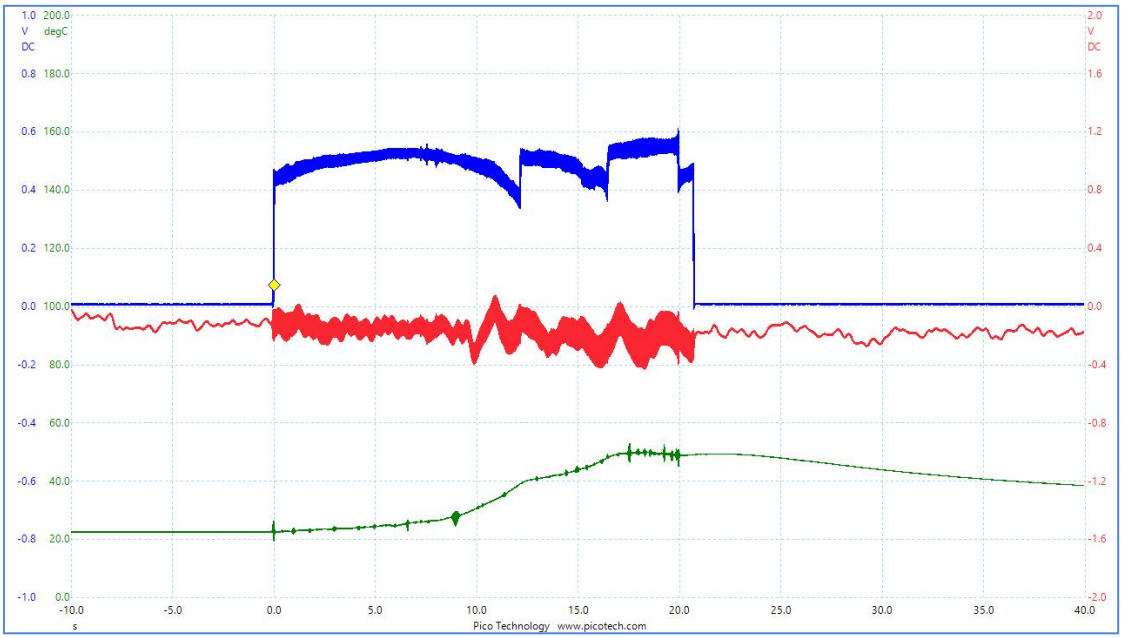

Figure 9.34. Picoscope screenshot of a single forward run, using 0.618" brass and 0.18" aluminum masses on an L bracket with 1 rubber washer. The force here is at 36 kHz is about 1.75 μN. Clearly rubber washers are not the way to go and neither are the old rubber pads previously used.

Conclusions

The phenolic washers produced good force results – 9μN with two washers either side of the mounting "L" bracket. However, the phenolic has a tendency to carbonize at higher temperature and the washers stick together which is not a desirable feature. The E-glass washers (milspec) gave good results for the glued stack with centered strain gauge for four washers either side of the L bracket. The force was 10.9 μN, which is slightly better than the phenolic. The E-glass responded better to temperature and the washers did not stick together but the properties change with temperature and result degrade after the first run. Some of the E-glass washers turn a dull brown color. The Vespel (or polymide) washers showed good results with an off-center strain gauge glued stack.

Two Vespel washers either side of the L bracket produced a force of 11 μN. The carbon reinforced PEEK washers showed no visible degradation at higher temperatures and five washers either side of the L bracket gave a force of 11 μN. Finally to compare with the old rubber (inner tube) washers, one washer either side of the L bracket gave a force of 1.75 μN with a centered strain gauge stack. The newer materials are producing about ten times the original force. It is recommended to use off-center strain gauge stacks rather than centered.

The stack with the blue heat shrink on the screws, and red/green power cord was the off centered strain gauge glued stack. The stack with the clear heat shrink on the screws and yellow/black power cord was the centered strain gauge glued stack. Both stacks use 0.618 inch brass mass and 0.18 inch aluminum masses.

We also tested carbon-reinforced Vepsel (polymide) washers; they were no different to the Vespel washers used here.

10. New Sledge Design #2 And Use Of Wire Springs

Since the old sledge design #1 was successful in isolating high frequency vibration from the faraday cage, and was capable of mimicking a true in-space propulsion system being of the "free-free" mass model, it seemed appropriate to design a better version of the sledge allowing for greater movement of the device.

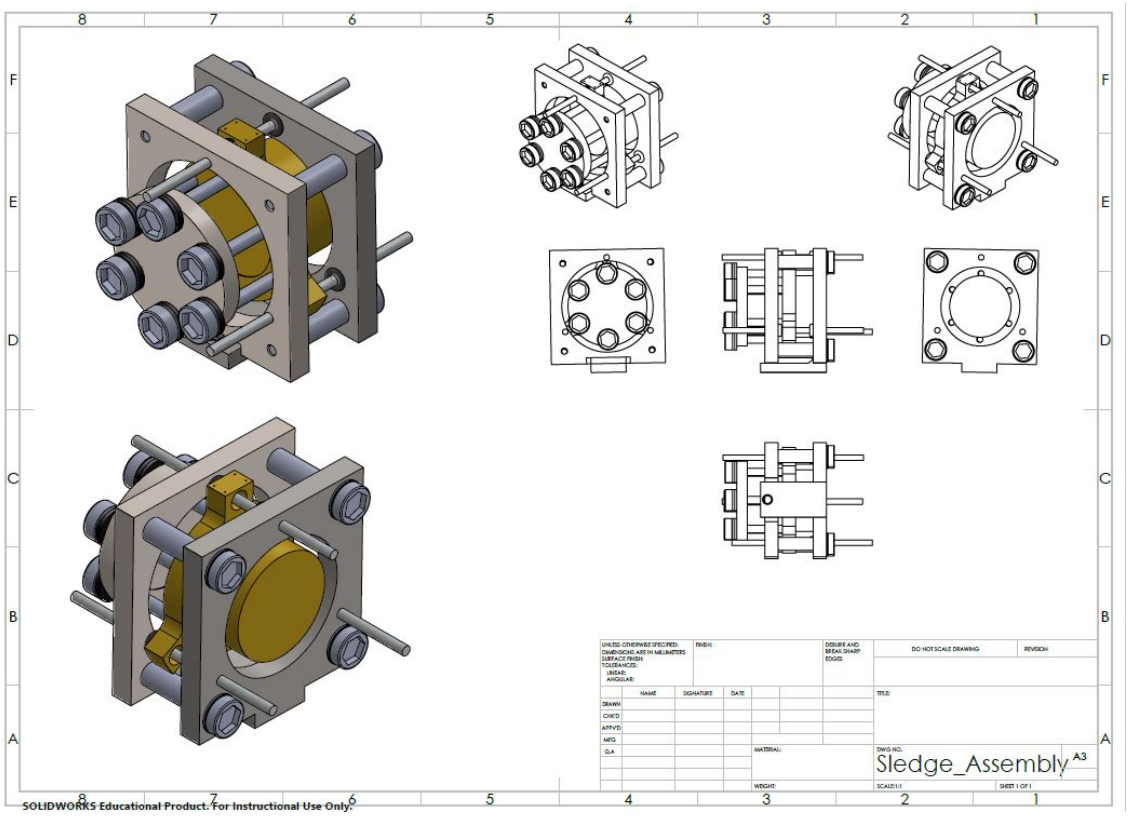

Figure 10.1. Solidworks CAD design by Jon Woodland and David Matalon (grad student). All the parts were CNC machined in the machine shop by Jon Woodland CSUF.

A basic CAD model, see Figure 10.1, of the design without showing the PZT stack which would be between the brass and aluminum masses as usual. There are 3 sliding rods. The brass has 3 "ears", each with a hole that supports a linear ball bearing. The brass mass slides along the rods on these ball bearings. The aluminum bracket with the foot is bolted down to the mounting bracket on the balance arm. Photographs of the assembled device are seen below in Figure 10.2.

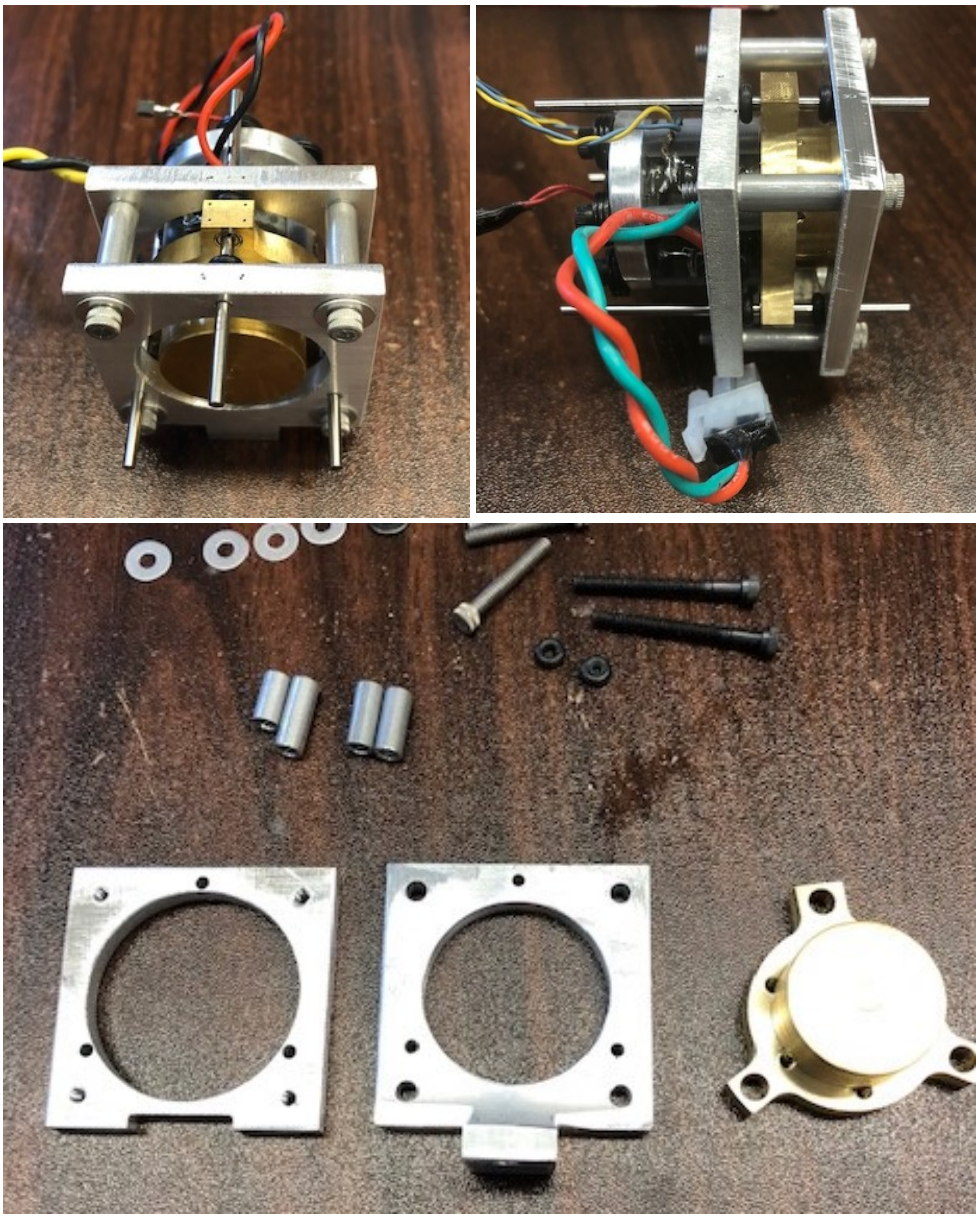

Figure 10.2. Photographs of the device assembly and parts. Note the small holes drilled into the brass "ear" and the square aluminum brackets top left. Linear ball bearings are fitted into the holes in the "ears" in the brass mass.

The device was tested in a slightly larger Faraday cage and also in a new bracket shown below so that the motion of the device could be video recorded. As seen in fig 10.2, top right, rubber O-rings were placed on the rods between the square aluminum brackets and the brass mass "ears" to stop the brass from moving up against the aluminum bracket along the rod. The device was run in this manner only to find that the device could "bounce" off the O-rings and show

multiple oscillations. Different thicknesses of aluminum spacers were also tried. It was then decided to place "springs" between the brass mass ears and the aluminum square brackets.

Figure 10.3. New open bracket for vibrometer testing and video recording the movement of the device inside the plastic vacuum chamber. The hole next to the bolt attachment is for the laser vibrometer to access the device from outside the vacuum chamber.

The springs were made from electric guitar wire, we tried several diameters of wire. We chose optima gold plated strings, 0.008" diameter, 0.011" and 0.014" diameter to evaluate.

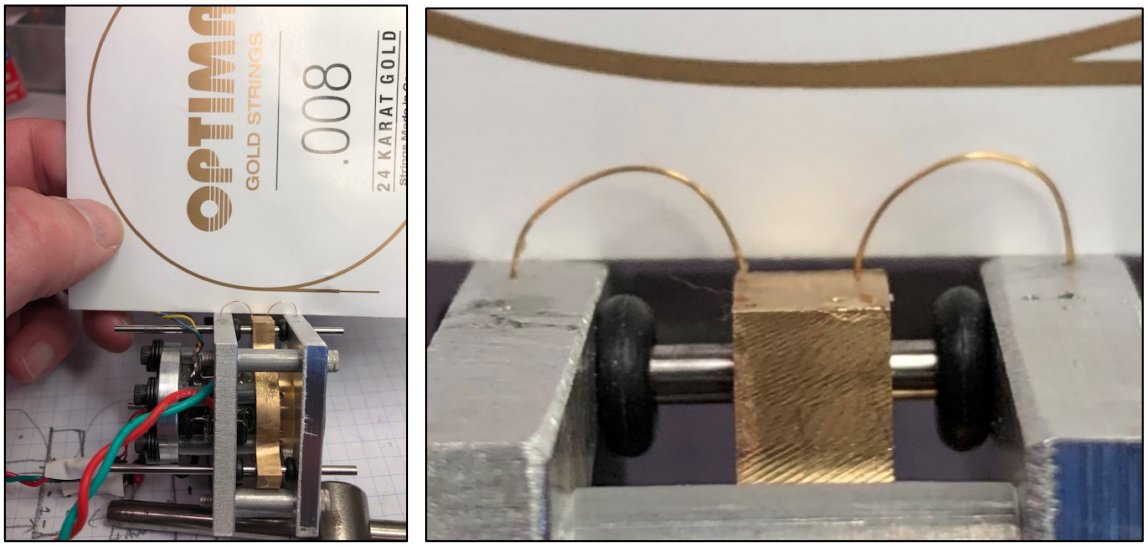

Figure 10.4. The gold plated steel guitar wire attached to the device via the tiny holes drilled in the top brass "ear" and the aluminum square brackets.

The wire was bent by hand in an arch shape. We tried to avoid any sharp bends or 'kinks' in the wire that would be stress points. The base length between the holes is roughly twice the height of the arch. We were trying for a circular cross-section that would give the least stiff arrangement. It was possible to calculate the stiffness of these springs and it was found that:

[Following calculation by José Rodal]

For horizontal distance between holes supporting wire = 0.335 inch, and vertical height of wire = 0.168 inch and Radius of wire arch = 0.1675 inch (almost equal to the height)

Then, using Castigliano's theorem, we get a stiffness of $k = \{0.5\ E\ (r_{wire})^4\}/(R_{arch})^3$ using E = 30 million psi for steel, r_{wire} = 0.004 inch, for the 0.008 inch diameter wire, R_{arch} = 0.1675 inch, the stiffness is k = 0.817 lbf/in or k = 0.143 microNewtons/nanoMeter,
(using the conversion 1 lbf/in = 0.1751268 μN/nm) therefore, 10 μN => 70 nm.

We can relate the stiffness of the 0.008in diameter wire (k_{008}) to the 0.014 inch diameter wire (k_{014}) as follows; $(k_{014} / k_{008}) = (r_{014} / r_{008})^4 = (0.007/0.004)^4 = 9.38$ or ~10.

This is assuming the radius of the arch (R_{arch}) is roughly the same in each case and using the same steel Young's modulus E for the wires. This means that k_{014} is roughly 10 times stiffer than k_{008}. Adding more springs in parallel, either on the same brass ear or different ears, will have the effect of multiplying the stiffness by the number of springs.

Considering 4 "ears" on the brass rather than 3, the more ears on the brass mass: (1) the more friction, the lower the Q and (2) the more springs, the smaller the displacement of the device will be. Another adaptation was the use of a vertical wire glued to a hole in the brass "ear" to allow high frequency vibration of the device to be "seen" by the video camera. See Figure 10.5.

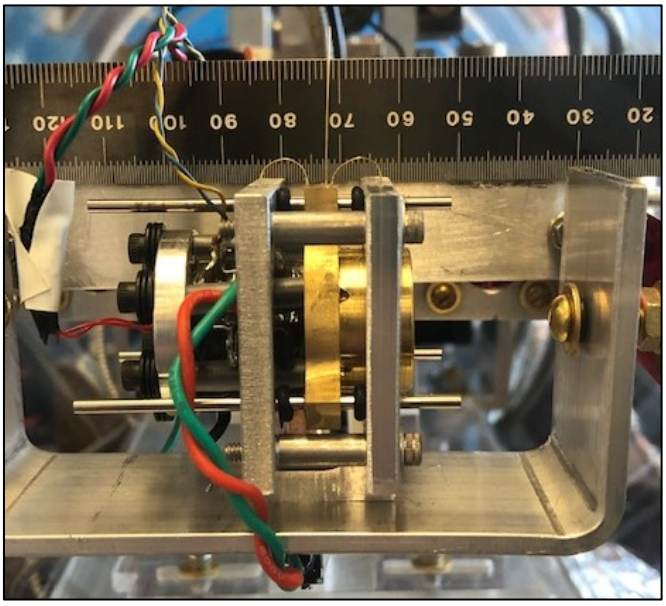

Figure 10.5. Shows a photograph of the new sledge design in an open cage mounting with springs and a vertical wire as a crude 'Fearn vibrometer'. The black lower scale has markings every 0.5mm. The upper scale has marks every 1mm. The vertical wire is 0.011 inch diameter. The springs were made from 0.008 inch diameter wire in this photograph.

Results Section: No springs, ballistic movement (6 Aug 2020)

We ran a standard test of the device using a sweep of 45 to 25 kHz in 20 seconds. The first test was on the device with no springs see fig 10.6. The input voltage was V_{RMS} = 1.0 volts. The Carvin DCM2000 amplifier was on level 12. We were recording the temperature of the aluminum mass, the strain gauge in the PZT stack and the displacement of the optical Philtec sensor, which has been calibrated to measure force. The scale of 0.1 volt is equivalent to 1 μN. The full scale of 10 volts on the Picoscope trace, is equivalent to 100μN.

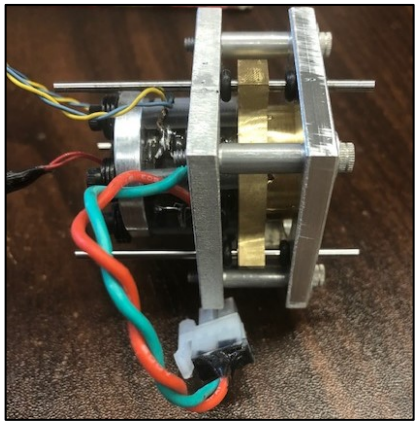

Figure 10.6. No springs attached. Free ballistic type motion of the device.

The force trace in red on the Picoscope image below reads a full scale of 10 volts, again is equivalent to 100 μN. The force here is off the scale greater than 100 μN.

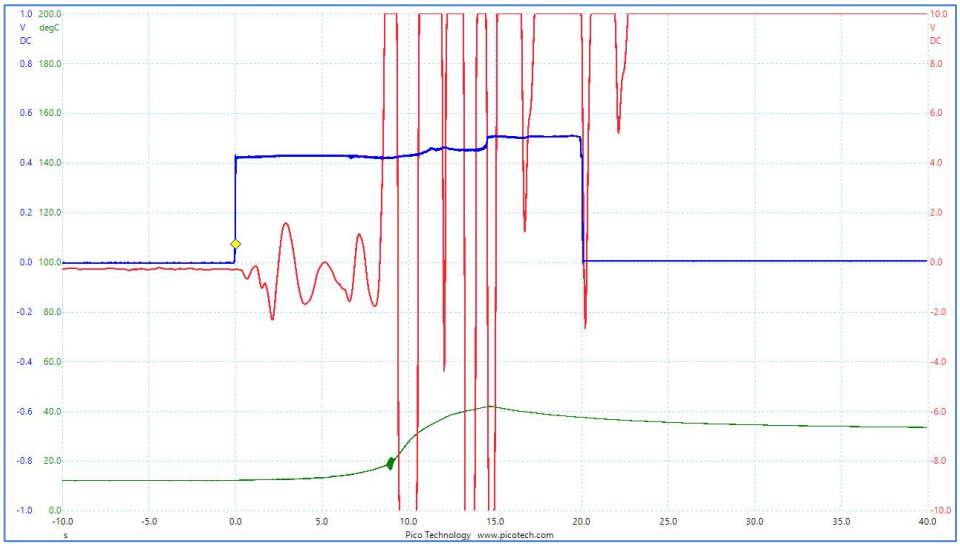

Figure 10.7. Ballistic "free flight" motion of the device with no springs attached. The starting and finishing position of the device is different as seen by the shift in the plot. Blue trace is the applied voltage amplitude, red trace is the force in volts and green is the temperature of the aluminum mass in Celsius. The red trace scale is ± 10 volts, which corresponds to 100μN.

The video tells the story. The starting and finishing position of the device are different due to stick-slip on the rods.

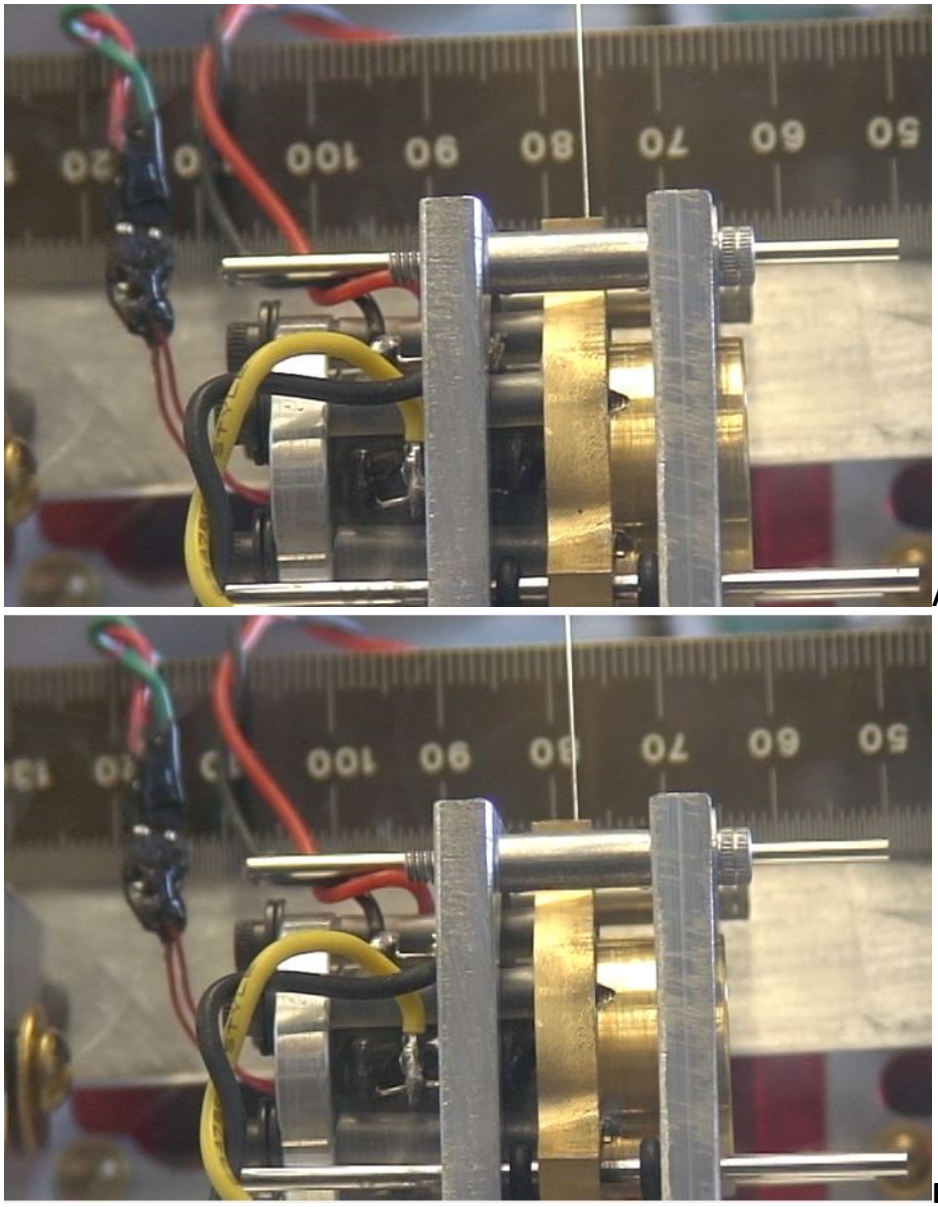

Figure 10.8. Top A, is the starting position of the device. After the run ends the end position is shown in B. There is a shift of approximately 2mm, you can see either by looking at the left edge of the brass "ear" (80-82mm) or the vertical wire moves from 84mm to 82mm. Taken with Sony camcorder.

A 2 mm shift (as we will see later in the moving mass report) gives a beam displacement of 1/30 mm or 33.33 μm. The Philtec sensor gives 0.75 volts per micron. So this is equivalent to about 25 volts (this converts to 250 μN force). This explains why the red trace off-scale at the end of the run. We must be cautious about these offsets.

Results using springs 0.008" diameter (6 Aug 2020)

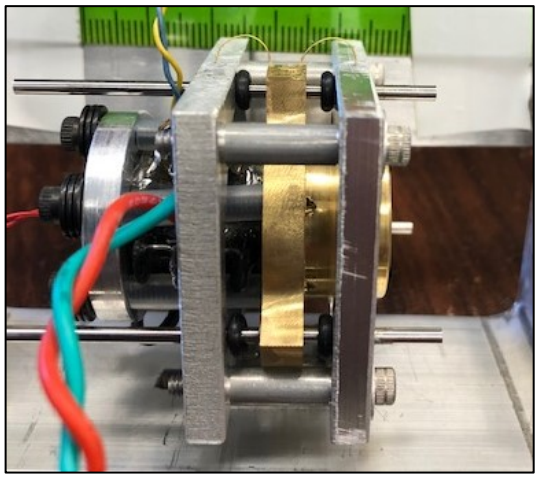

Figure 10.9. This spring is of 0.008 inch diameter.

The same test was run on a device with 0.008 inch diam wire attached as springs. This is a sweep of 45 - 25 kHz over 20 seconds at V_{RMS}=1.0 volt and DCM2000 amplitude level 12.

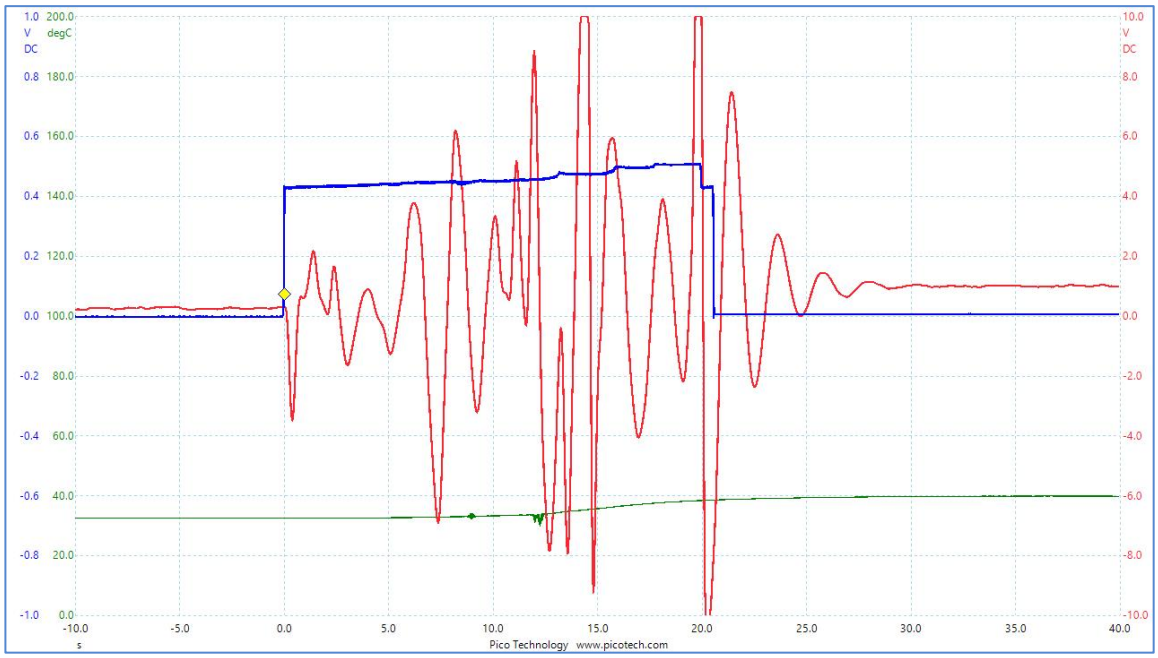

Figure 10.10. Blue trace is the applied voltage amplitude, red trace is the force in volts and green is the temperature of the aluminum mass in Celsius. This run the device had 2 springs made with 0.008 inch diameter guitar wire. Still showing about 100 µN, little displacement from beginning to end.

Results using springs 0.014" diameter with stiffness, k ~ 10 times greater than the 0.008" springs (7 Aug 2020)

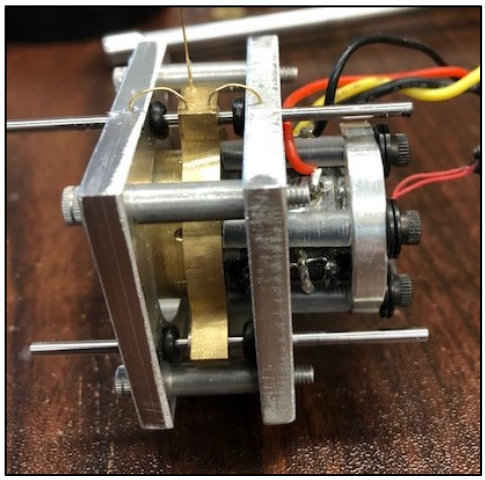

Figure 10.11. Thicker springs attached to the device with previously no springs. These thicker wires were 0.014 inch diameter.

The same test again a sweep 45-25 kHz in 20 seconds. We show two separate runs of the device to show consistency.

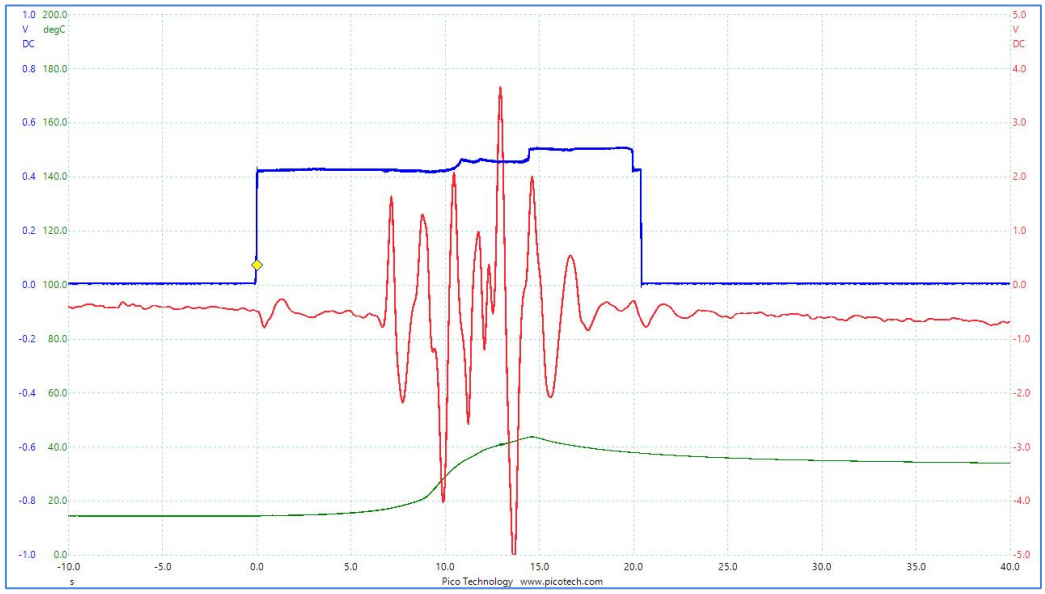

A

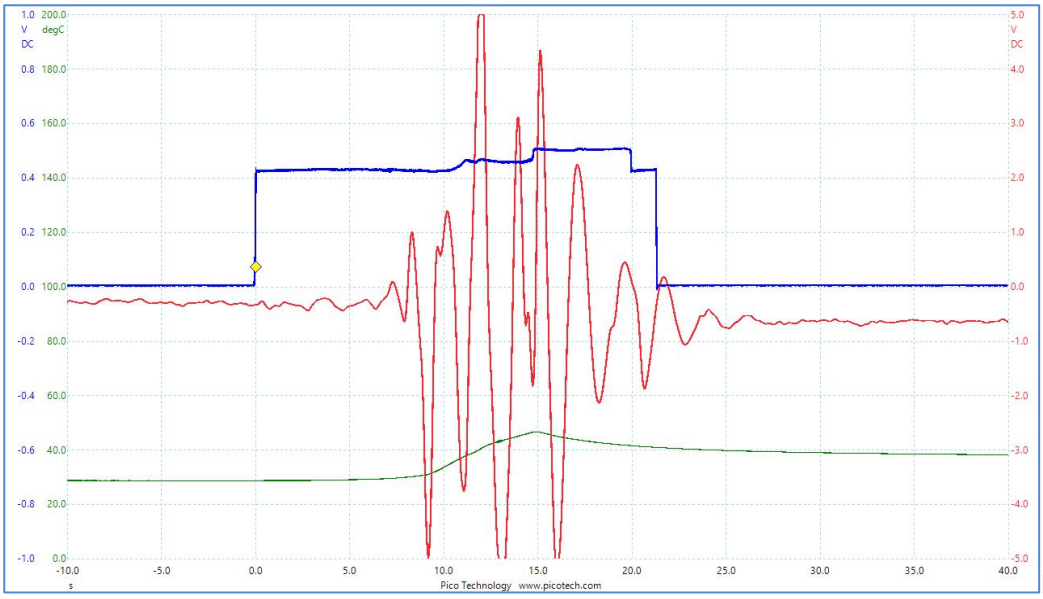

B

Figure 10.12. Blue trace is the applied voltage amplitude, red trace is the force in volts and green is the temperature of the aluminum mass in Celsius. In both these runs A and B, the device had 2 springs made with 0.014 inch diam guitar wire. The stiffness of these springs is roughly 10 times greater than the 0.008 inch diameter wire used previously. Note that the red scale has been changed to $\pm$ 5 volts , which corresponds to 50µN. We may be seeing around 30-40 µN force here.

It appears that increasing the spring constant by a factor of ~10 decreased the output force by a factor or 3. We have gone from 100 µN with the 0.008 inch diameter wire springs to roughly 30µN with the 0.014 inch diameter wire springs. These stiffer springs may be slightly overkill. (It may be harder to overcome the static friction in the bearings with the stiffer springs attached.)

Movies are available of all the runs here and many others. These movies show a ballistic movement of the device toward the aluminum end [1]. A Dropbox link can be made available upon request. Michelle Broyles was kind enough to point out a online software which allows for "enhancement of motion", also a TED talk [2].

Acknowledgements

We would like to thank Michelle Broyles for her suggestion of guitar wire springs and the use of the video link [2].

References

[1] Email communication from José Rodal: **Why is the initial ballistic movement important?** Calculations of both the frictional force (assuming 4 times **less** coefficient of friction than assumed by Jim) and of the bending stiffness showed that for the device, to display the motion displayed in the movie, **implies forces larger than 100 µN**. Such forces were

discounted by people, and instead they were expecting forces like 20 μN or less. The forces involved appear to be larger than what people were expecting. As initially requested by Paul, the ballistic motion of the device is more interesting than the vibratory motion, because it provides information that one should analyze (displacement vs time) to see **whether it reveals acceleration in free flight (or constant velocity in free flight)**
See this movie springs-oscill31july2020.MOV in this link:
https://www.dropbox.com/sh/miyt1v5k3hrx9ym/AACqtDvBRsj8-_52aSqcJiU-a?dl=0

[2] Sped-up video link https://lambda.qrilab.com/site/ see explanatory Ted talk also.

11. Moving Mass Perpendicular To Beam Arm And Re-Zeroing Effect On The Balance

It has been suggested that the torsional balance may be registering a false positive due to the Center of Mass (CoM) of the device moving during the experiment. We want to show exactly how much the new sledge design can move and what effect it will have on the balance arm.

Previously, using an "L" bracket or the two rail sledge, the motion of the CoM of the device was found to deviate only nanometers, (by using a Polytec vibrometer) and this was not sufficient to account for the displacement (and hence the force) registered by the balance. Using the new design, the device can move substantially more, several mm in fact, and now there is a possible problem with re-zeroing of the balance and CoM shift of the device. We need to know, how much can the device move in a given run and what that shift translate to, in terms of beam deflection, or force. The apparatus is shown below in Figure 11.1.

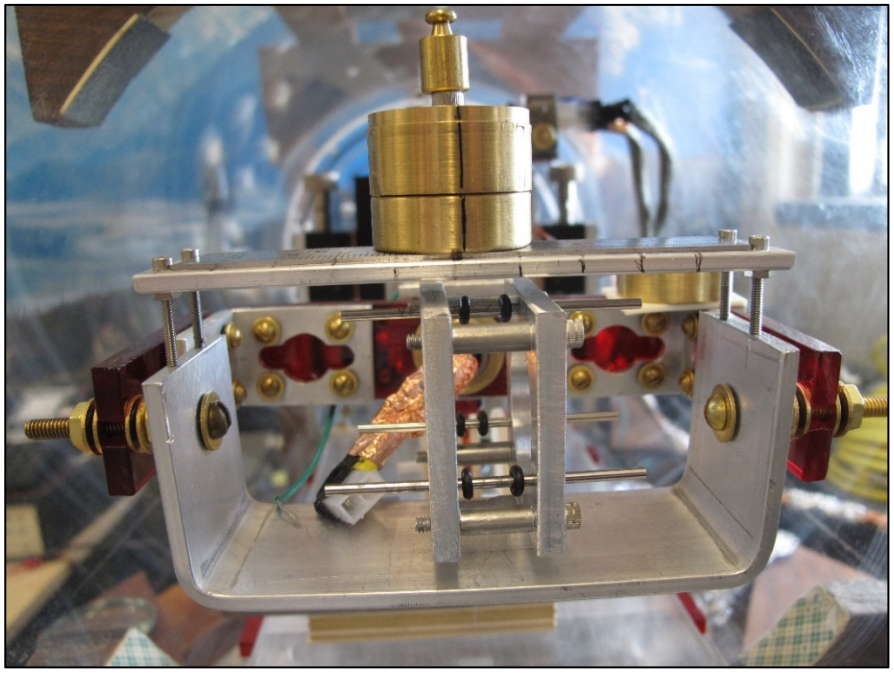

Figure 11.1. Rather than use the Faraday cage, a new mount bracket was designed to hold the sledge mounting and rails. The moving part of the device was weighed and an equivalent mass used in the experiment. The equivalent mass was found to be 125grams. The equivalent mass was given 3 vertical lines in order to align the lines with the ruler scale and central line down the ruler. This was to aid in the accurate placement of the mass. This open mounting was also used for movies of the device, to show the motion during operation. Mass here is shown in the center position; the ruler reads 5cm.

It was important that the top ruler be level for accurate measurements, see Figure 11.2.

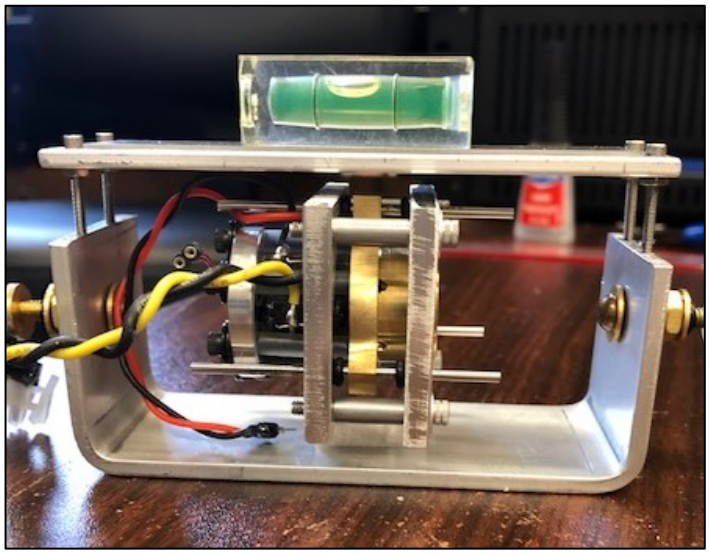

Figure 11.2. Ruler on top of the mount bracket was leveled.

For this test no power was required and the mass was moved without a vacuum. The plastic end plate of the chamber was replaced to reduce the air currents for accurate measurements. The optical Philtec sensor was found to be unstable without the vacuum present, so we introduced another simple measurement scheme. The center coil moves with the balance. A thin wire, of 0.011inch diameter thick guitar string was attached to the center coil with superglue. A ruler with 0.5mm markings was placed under the coil so the position of the wire could easily be read on the ruler. See Figure 11.3 below.

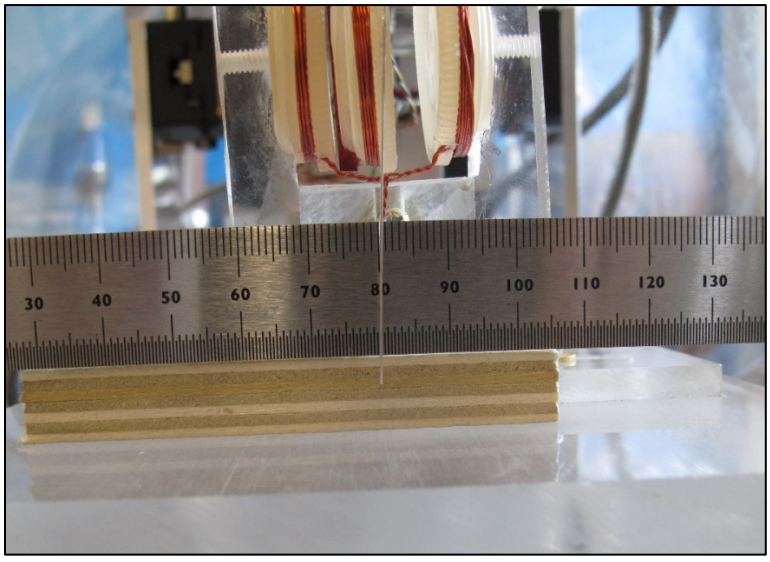

Figure 11.3. Here is the wire indicator when the mass is in the center position. The wire reads 80mm we take that as the zero position.

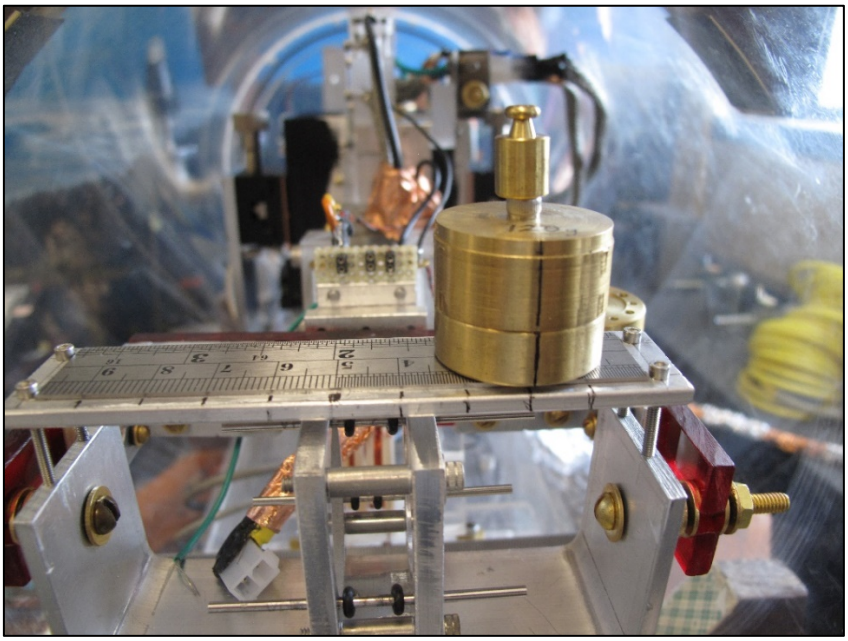

Figure 11.4. The mass is shifted to the right, at position 2cm on the ruler.

If the mass is moved to position 2cm on the top ruler, this is a shift in 30mm to the right, see figure 11.4, then the wire reads 79.5mm or it shifts from the center position a distance 0.5mm to the left. See Figure 11.5.

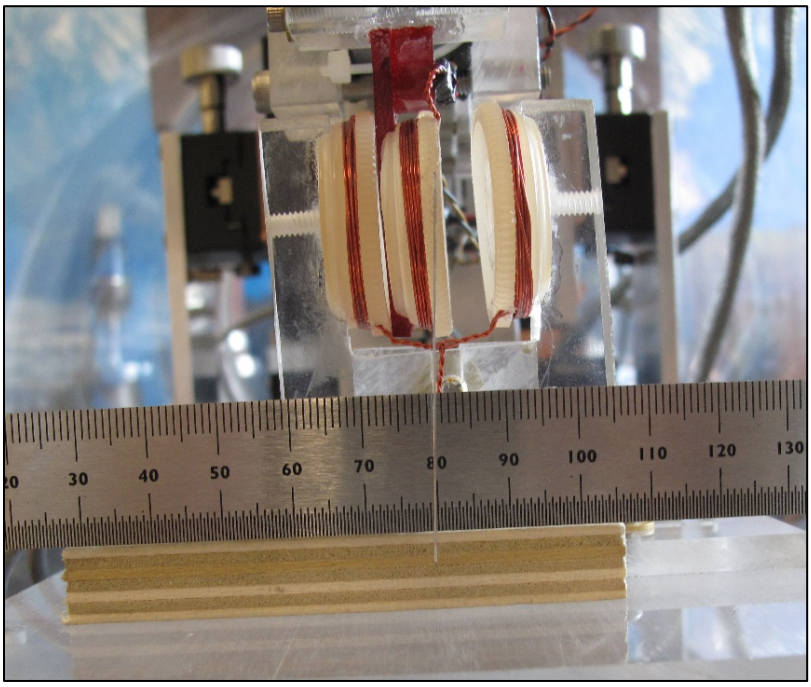

Figure 11.5. The wire reads 79.5mm when the mass is shifted 3cm to the right.

Then we moved the mass 30mm to the left of center, to position 8cm on the ruler. See Figure 11.6.

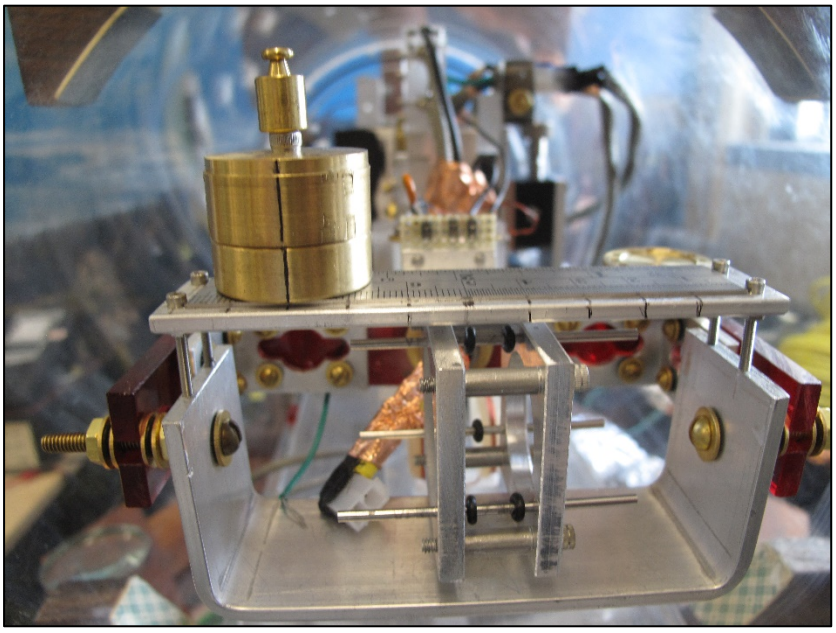

Figure 11.6. The mass is shifted 30mm to the left, at position 8cm on the ruler.

The wire for this case moved to the right 0.5mm as shown in Figure 11.7.

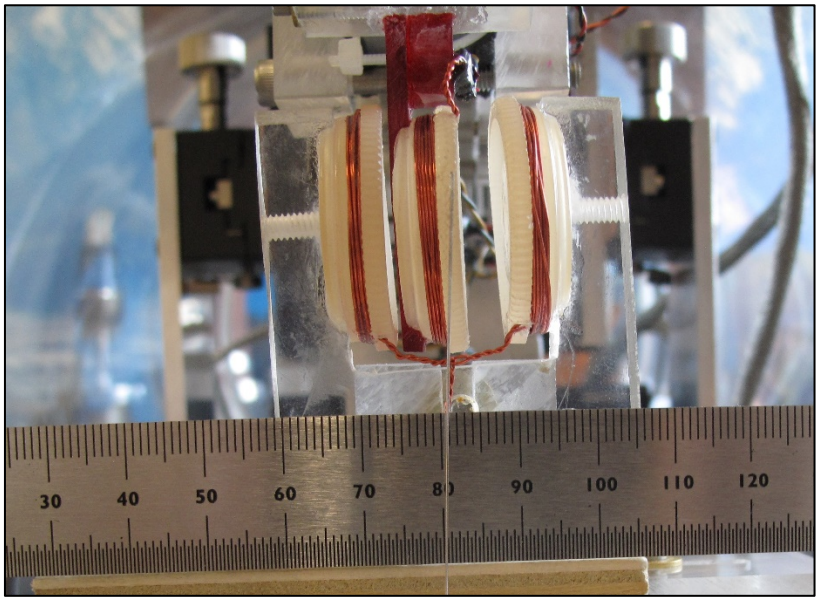

Figure 11.7. The mass is shifted 30mm to the left, the wire moves to the right to position 80.5mm.

The mass was moved to other positions (on the ruler) to confirm the left and right displacements. They were all found to be consistent with the above measurements. We found a linear relationship between the mass movement y and the wire position x.

If y = Ax ; when y=30mm and x=0.5mm then constant A=60.

If the CoM of the mass moves 0.5mm then we would expect the wire to move 0.5mm/60 = 8.33 µm. We found previously, in the Philtec sensor calibration, that a voltage of 0.75 volts gives 1 µm of displacement. So, if we assume 8.33µm displacement due to CoM motion that would register a sensor voltage of 6.2 volts or equivalent to roughly 62 µN. (We find that 0.1 volt is roughly 1µN force of the device). This is very significant and must be taken into account.

It appears that a torsional balance is not the best apparatus for measuring *Mach effect* type forces in the sliding-sledge type arrangement with the almost friction free ball bearing sliders.

Above we assumed that the ball bearings are almost friction free because the PZT device is causing high frequency (30-60 kHz) vibration which will *shake loose* any stick-slip [3], in the bearings, making them practically friction-free [4-6]. This assumes that the rods are parallel. The linear ball bearings were found in Switzerland, with 1.5mm inner diameter (ID), 3.0mm outer diameter (OD) .

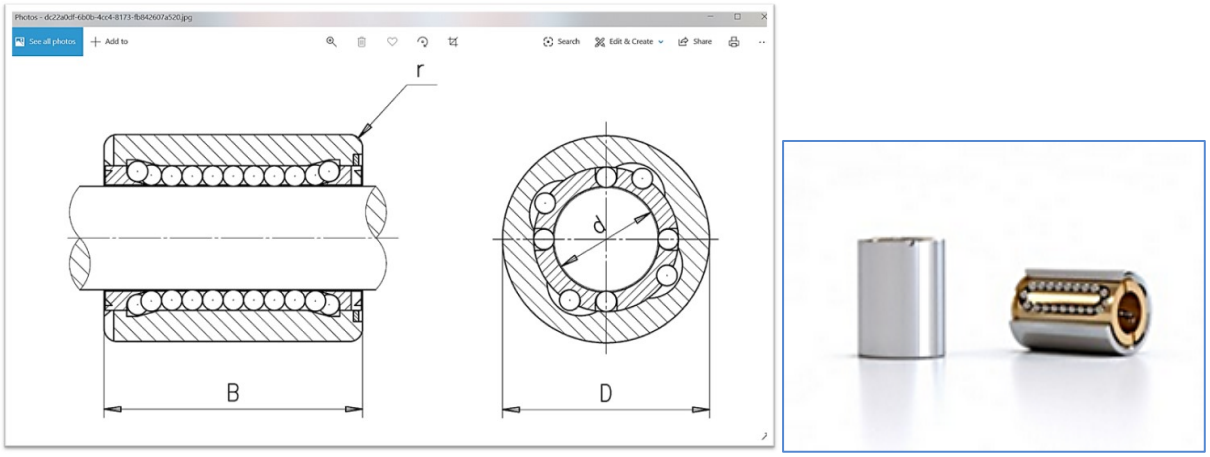

Figure 11.8. Linear ball bearings MPS microsystems, for the slider mount are assumed practically friction free. See ref [1].

Friction of linear ball bearings is given on this webpage reference [2].

Assuming we cannot neglect friction on the linear bearings, then let us assume the smallest possible frictional coefficient which according to [2] is 0.001. To calculate the force needed to move the MEGA drive over the bearings is then calculated as follows:

Calculation of Force required to move a MEGA drive over linear ball bearings:

(1) a weight of the MEGA drive of 125 g
(2) that this weight **is *equally distributed*** on the 3 linear bearings (N = 125 g /3 = 41.67~42 g)
(3) the absolute *lowest* coefficient of friction (μ = 0.001) according [2].

The force required to move the MEGA drive device on the bearings is:

F = μ N
= (0.001) (125 gf /3)
= 42 mgf (milligram force)
= 412 μN (using 1mgf = 9.81 microNewtons.)

If the weight of the device is not equally distributed over the 3 linear bearings then the frictional force could be much larger than that calculated here. Linear plastic bearings where the lubricant is encased in the plastic might be a solution to the stick slip problems [7], if the vibration alone does not cure it, [4-6]. The actual force of the device might actually be larger than what we are recording on the Picoscopes.

Acknowledgements

Thanks to Michelle Broyles for help finding these references on how vibration can alleviate stick-slip in bearings. Also thanks to José Rodal for doing a preliminary calculation of the force required to move the MEGA drive over bearings with friction.

References

[1] https://www.mpsag.com/fileadmin/document/microsystems/MPS-MS_Brochure_SystemeLineaire_EN_001.pdf?1593975451660

[2] https://medias.schaeffler.com/medias/en!hp.tg.cat/tg_wf*ST4_307654667

[3] https://www.linearmotiontips.com/faq-what-is-stick-slip/

[4] https://savkar.math.uconn.edu/wp-content/uploads/sites/574/2014/08/107400.pdf
Mechanics of the Dynamic Release Process for Stiction Failed Micro Cantilever Beams Using Structural Vibrations

[5] https://link.springer.com/referenceworkentry/10.1007%2F978-0-387-92897-5_209.

[6] https://asmedigitalcollection.asme.org/tribology/article-abstract/119/3/391/434824/A-Fractal-Analysis-of-Stiction-in?redirectedFrom=fulltext

[7] https://www.igus.com/contentData/wpck/pdf/US_en/Eliminate_Binding_and_Stick-slip.pdf

12. Summary and Conclusions

The original design of the static mount bracket and use of rubber *inner tubing* as washers, was found to be greatly restricting the force capability of these devices. We were seeing only a microNewton at most. A variety of materials were tested, including Belleville washers, which have not been mentioned in a separate report. The Belleville washers were actually the most promising of the static mount/washer design, in terms of force production, yielding 10's of microNewtons for force. Some of the other material washers, Vespel (polymide) and carbon reinforced PEEK also produced 10's of microNetwons. The most improvements came in the form of different mounting- using rails (steel rods) with first Teflon liners in the brass and then linear ball bearings. See section 10. The brass mass shape changed from a basic cylinder to a flanged cylinder from which protrude 3 "ears". The ears hold the linear ball bearings on which the device can move. The rod (or rails) are glued to one side of the aluminum square frame. Steel guitar springs are used as springs to help control
the oscillations of the device.

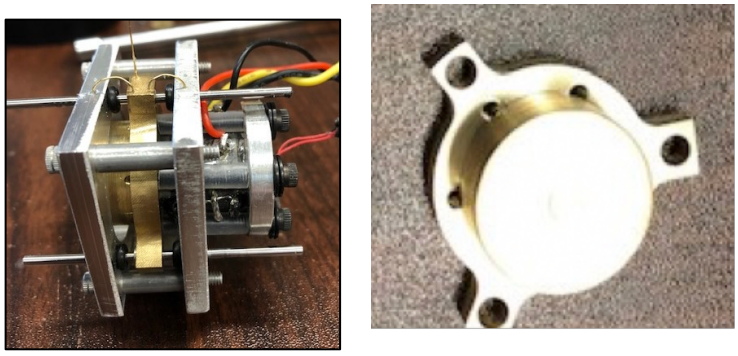

Figure 12.1. The new sledge design left and the new brass mass right. The interface between the brass and the PZT stack is roughly the center of mass (CoM) of the device. Note that we attach the springs close to the CoM.

This new design is responsible for improving the thrust per device by more than two orders of magnitude. This was done by creating the next best thing to an *in-space* demonstration as a way of mounting the devices. HF is still concerned with CoM type movement of the device, since it is now moves much further than in the early devices. However, we must also assume that friction is non- negligible in the linear ball bearings and that some substantial amount of force, generated by the device, is needed to overcome the static friction in the bearings, allowing the device to move suddenly in one direction, as seen in the movies of the device running.

The next logical step is already provided for, to wit, a careful replication by McDonald and Hathaway.

Addendum

Section 13. Report from José Rodal

Section 14. Report from Paul March

Section 15. Report from Michelle Broyles

Section 16. Report from Chip Akins

Section 13

José J. A. Rodal, Ph.D.
jrodal@alum.mit.edu

August 9, 2020

Following are my main contributions to the NIAC Phase II grant in chronological order from Dec. 2018 to Aug. 2020.

---

1. Analysis of the effect of support washers used in the MEGA drive

In December 2018 I authored a comprehensive report (with over 150 equations and over 90 plots) analyzing the vibration isolation of the Mach Effect Gravitational Assist (MEGA) drive. I addressed Jim Woodward's Nov 14, 2018, request for "modeling of devices so that the model correctly replicates the VNA impedance spectra, and then tweaking the model so as to improve its performance." I obtained closed-form exact solutions for the transmissibility of vibration from the MEGA drive to the Faraday cage in the measuring balance. I obtained a new exact solution (not found in the existing literature) for finite strain of rubber washers. I calculated and plotted (using Wolfram *Mathematica*) a large number of cases representing possible MEGA drive experiments. I proved that it is more effective to use compliant washers on both sides of the L-bracket support instead of using them on only the MEGA drive side as was done up to that time (I showed this based on my calculations, one year before Greg Meholic suggested this again to Jim Woodward). I also showed that vibration transmissibility is decreased using longer and thinner L-bracket supports (the lower the bending stiffness of the bracket, the smaller the transmissibility). I also showed that dissipation of energy (using materials with high damping) is unnecessary to reduce vibration transmissibility, and (as shown by MIT Prof. Den Hartog in the 1930's) it is often *counterproductive*. In the case of the MEGA drive, damping (whether by internal or external damping, or worse, by friction) is very detrimental because it reduces the quality of resonance factor (Q).

---

2. Torsional balance calculations / replication of experiments at TU Dresden

I showed the TU Dresden team and Dr. Hal Fearn (who was at Dresden at that time) how to successfully replicate the California State University Fullerton (CSUF) experiments, during two teleconferences in January 2019. TU Dresden operated the device for only 8 seconds, without being able to reproduce the constant force using CSUF electronics. I showed that according to my calculations it takes a minimum of 15 seconds of operation to reproduce the CSUF operation at TU Dresden because of the larger moment of rotational inertia and the lower stiffness of TU Dresden's torsional balance. The experiments at TU Dresden confirmed the accuracy of my prediction. When they tested for 15 seconds duration, the CSUF experimental signature was finally reproduced at TU Dresden (albeit TU Dresden claimed a significantly lower force amplitude than what was claimed by CSUF) .

---

3. Calculations on how to significantly increase the Q of the MEGA drive

I created a computational method of image analysis to determine the quality factor of resonance based on published images of oscilloscope measurements of vibration decay. I analyzed (using Wolfram *Mathematica* image analysis) several images published by Gunma University in Japan and by Mitsubishi Heavy Industries of ultrasonic transducers manufactured with different threading and contact surface technology. Based on this analysis I determined the following:

1) The CSUF stacks (at the time of my report) had very low Q compared to the standards in the ultrasonic transducer industry (Mitsubishi). This confirms Greg Weaver's (Johns Hopkins Applied Physics Laboratory) assessment that CSUF stacks have low Q, upon being told that the CSUF stacks were measured (at TU Dresden with no domes) to have a Q of only 60.

2) This low Q agrees with the data from Japan for stacks with inaccurate machined contact surface (between the stack and the metal ends). I showed that the boundary between the PZT stack and the metal (brass on one end and aluminum on the other) ends is of crucial importance to reduce noise and increase Q.

3) The data from Japan I analyzed showed that the Q could be increased from the present (Q~60 to 80) to Q~360 to 660 (an increase of 6 to 10 times) by improving the accuracy of the machined domes (to eliminate stress concentrations at the edges of the cross-section) and by adhering the ends of the PZT stack to the metal ends. This increase in Q can be achieved while still using threaded screws and machined contact surfaces at the ends of the stack.

4) A Q exceeding 1200 could be achieved by adopting stack fabrication procedures that eliminate threaded screws and machined contact surfaces (such techniques will be necessary if CSUF ever makes micro or nano MEGA drive devices).

---

4. Analysis of vibration data of the MEGA drive/Autocorrelation/Power Spectral Density/Chaotic analysis/Measurement of Q

I also analyzed many computer files (each of them with size of several gigabytes) for the following experimental conditions:

A) steady-state and

B) ring-down decay of voltage (piezo and amplifier).

The examined data was taken at high sampling rates from 20 to 125 megasamples per second. I calculated, analyzed and reported on:

1) Statistical data including histograms, statistical measures of central tendency (mean, median) and spread (standard deviation),

2) Fourier spectra,

3) Power spectra (of the above mentioned variables and of the true power),

4) Autocorrelation,

5) Cross-Power Spectra,

6) Cross-correlation,

7) 2-D and 3-D Phase portraits of nonlinear dynamics,

8) Chaotic analysis including flow analysis of phase portraits, and

9) Measurement of quality of resonance factor Q.

The above were calculated based for the following input data:

a) Strain gauge in the piezoelectric transducer,

b) Voltage in the piezoelectric circuit,

c) Current in the piezoelectric circuit and

d) Current in the amplifier circuit.

I also calculated the

e) Power spectral density for the power and the

f) Magnitude of the impedance and the

g) Angle of impedance vs. frequency.

Data for both Carvin and ENI amplifiers (used at CSUF for the MEGA drive experiments) were analyzed.

Experimental data for 2 exciting frequencies (~35 and ~45 kHz) and 4 separate transformer cases were analyzed (no transformer, and 2-to-1, 3-to-1 and 4-to-1 transformer cases.)

I reported that the MEGA drive experiments show coupling of the piezoelectric transducer with the excitation such that at the voltage used in the MEGA drive experiments the nonlinearity from the amplifier is coupled (due to the transformer) to the piezoelectric drive resulting either in disorganized chaos or in highly organized nonlinear dynamic behavior. This nonlinear dynamic behavior can feature (depending on voltage amplitude) strange attractors and limit cycles that I

plotted using *Mathematica*. This analysis was useful to better understand the behavior of the MEGA drive, which is necessary to optimize the measured force.

The analysis of the data shows that the n*(Exciting Frequency) (with n=2,3,4,5,6,...) harmonics are due to the nonlinear coupling of the MEGA drive with the amplifier/transformer part of the circuit, and are not due to electrostriction. The electrostriction explanation that had been offered by CSUF is falsified by the presence of odd harmonics (with n=3, 5,etc....), and by the fact that electrostriction in the PZT material used in the MEGA drive is known to be orders of magnitude smaller than shown by the experimental amplitude of these harmonics.

My calculations of Q (quality of resonance) showed that the MEGA drive with PolyAmide (PA) (DuPont trade name "Nylon") washers has significantly higher Q than with the rubber pads, and therefore the Nylon washers are preferred to the rubber washers (due to lower tan delta of Nylon compared with the type of rubber used for the MEGA drive). However, Nylon -a trade name for polyamide- should not be used for space applications because it suffers from significant outgassing in a vacuum. Another problem with Nylon is that it has a relatively low melting temperature. Hence I concluded that other engineering polymers that have low outgassing, and higher melting temperatures should be tested as a replacement for Nylon. The analysis in my December 2018 report had previously shown that vibration transmissibility is reduced by correct selection of stiffnesses and masses, and that energy dissipation in the washers is not needed to reduce transmissibility and it is counterproductive, because it reduces the Q.

The brass washers showed even higher Q than the Nylon washers(as expected due to the much lower tan delta of brass compared to Nylon), but the results exhibited complex nonlinear behavior that makes them difficult to use. CSUF stopped testing helical brass springs because of lack of reproducibility.

The analysis of the experimental data shows that the experimentally measured reactance for the 35 kHz, 2-to-1 transformer case is close to zero. The 35 kHz, no transformer case has a power factor of 0.725. This showed how important is the 2-to-1 transformer in the circuit as it provides inductance that enables to run with practically zero reactance (power factor=1).

At my request, Hal Fearn performed further tests with a delay of several seconds (~4 seconds) to explore whether the cases that had practically zero reactance, (power factor~1) were due to a transient turn-on. These experiments were conducted with 2 excitation frequencies using the "Demo" piezoelectric returned from TU Dresden, with the rubber washers replaced by Nylon washers, and using the ENI amplifier with a 2-to-1 transformer. The excitation was a fundamental excitation at 35.8 kHz and a second harmonic excitation, at about the same amplitude at twice that frequency.

This experimental data (conducted with a delay of ~4 seconds) confirms CSUF's previous assertions that the power (after a few seconds) is mostly reactive. The phase angle between voltage and current for the 35.8 kHz exciting frequency is close to 90 degrees**.**

Actually, it is the 45 kHz, 2-to-1 transformer case that has high reactance (power factor=0.211 for the entire run of 83 ms duration, and power factor=0.1 for the 2nd stage: between 17 ms and 83 ms).

The analysis of the experimental data falsifies previous claims that the only amplifier variable that matters is the voltage. My analysis of the data shows that current, correlates better with measured force: the 2-to-1 transformer cases are the leader, showing much higher current. Considering the actual power dissipated, it becomes clear why the "no transformer" case has the worst experimental results: the actual power is 10 times less than the actual power for the 2-to-1 transformer at 45 kHz and 27 times less than the power for the 2-to-1 transformer at 35 kHz.

The voltage (98 V RMS) for the 2-to-1 transformer case at 45 kHz is only 14% higher than the voltage (86 V RMS) for the no transformer case at 45 kHz. The main difference is not the voltage, but the current that is able to go through the piezo transducer. The current (4.09 A RMS) for the 2-to-1 transformer case at 45 kHz is 858% higher than the current (0.43 V RMS) for the no transformer case at 45 kHz.

---

5. Published paper on the Mach Effect on prestigious, peer-reviewed journal General Relativity and Gravitation

During May 2019 my article: "A Machian wave effect in conformal, scalar–tensor gravitational theory" was published in the prestigious, peer-reviewed journal *General Relativity and Gravitation*, 51:64, pp.1-23 (2019), https://doi.org/10.1007/s10714-019-2547-9, Online ISN: 1572-9532, Print ISN: 0001-7701.

I acknowledged that this work was supported by NASA Innovative Advanced Concepts (NIAC) Grant NNX17AJ78G “Mach Effects for In Space Propulsion: Interstellar Mission,” and listed my involvement with the Space Studies Institute.

---

6. Correct calculation of magnetic force between coils used to calibrate measured force of MEGA drive in CSUF experiments

In July 2019 Matthias Koesling (Technische Universität Dresden) wrote a report pointing out that the CSUF's MEGA drive force calibration equations, as detailed in the paper submitted by Fearn and Woodward to the Journal of the British Interplanetary Society, appeared to be incorrectly overestimating the actual force by a factor larger than 5 times. I investigated this issue and I authored the following detailed technical report:

> Rodal, J., Report, "The Magnetic Force Calibration Method used at CSUF," August 14, 2019, 28 pages, including executive summary, conclusions, 4 tables, 12 figures, 12 references.

I found two significant errors in CSUF's calibration method: 1) incorrect calculation of different elliptic integrals (due to incorrect naming of the integrals switching their role in the equations) and 2) incorrect elliptic argument used as input for the elliptic integrals.

CSUF presented two formulas in NASA's midterm Phase II report that gave significantly different values for the measured coil-force, without distinguishing their range of applicability, and hence their validity to model the force. In my August 2019 report I showed that only one of these formulas is applicable to the MEGA drive experiments. I proved that the other formula is inapplicable.

The formulas presented by CSUF to model the measurement of the force in the MEGA drive experiments assumed that the coil thickness is zero. I presented a very accurate formula that takes into consideration the coil thickness without much effort (this is important when the coil thickness is significant compared to the inter-coil thickness).

I concluded in my report that it is advisable to perform a calibration using a force that can be traced to a known standard instead of solely relying on theoretical calculations of the magnetic force between coils, because the theoretical calculations rely on assumptions (i.e. no field interaction between the outside coils) that are not exactly fulfilled in practice, and because the formulas depend on imprecisely known geometrical variables (i.e. the actual midpoint of each coil's winding depends on the winding accuracy).

After my report was distributed, I was asked by George Hathaway (Hathaway Research International, Canada), "to calculate the force expected on the movable coil of the Woodward design using the Babic et al filament method at 2.2cm coil separation."

I used Wolfram's *Mathematica* to perform these calculations and plot them, as documented by Hathaway in the following report:

G. Hathaway. P.E., Summary Measurement Report, "Calibrating Woodward's Calibrator," August 21, 2019

---

7. Comprehensive analytical and numerical formulation of the coupled electroelasticity problem of the MEGA drive

I undertook a comprehensive analytical formulation of the coupled electroelasticity problem of the MEGA drive to analyze its amplitude vs. frequency response with the aim of maximizing the measured force. I advised the NIAC team that the approach taken by John Brandenburg (using COMSOL software to solve the eigenvalue mechanical problem) is fruitless to maximize the force of a piezoelectric stack because Brandenburg's approach a) ignores the electrical-

mechanical coupling which plays a fundamental role in the response (Brandenburg's calculations completely ignore the piezoelectric effect) and b) it is not a modal response analysis and hence unable to identify the actual spectral response (Brandenburg's calculations completely ignore damping, and hence ignore the finite Q).

My analysis starts with Hamilton's principle to obtain the equations of motion. The aim is to consider the electric circuit as well as the mechanical components in order to maximize the dynamic force and the voltage amplification. In order to maximize the force it is imperative to take into account the electrical coupling due to piezoelectricity. The goal is to tune the electrical circuit (with added inductors, for example, precisely selected to provide an electrical resonance tuned to the mechanical resonance) to work with the mechanical components (the piezoelectric stack and the brass and aluminum masses) in order to maximize the dynamic force and the voltage amplification. Experiments were conducted at CSUF with and without a transformer and with and without added inductors to verify my equations. Also Paul March conducted numerical calculations with the program CircuitMaker to verify my predictions. I predicted that shorter stacks (using less than the MEGA drive standard 8 discs, each disc 2 mm thick) provide lower force and that the best way to increase the force is to use longer stacks (longer than 16 mm) with much thinner discs (much thinner than 2 mm).

I incorporated the following electric circuit components in my analytical model:

a) the voltage divider

b) realistic model of the transformer, including non-ideal mutual coupling between the primary and secondary windings

c) additional complex impedance (resistive, inductive and capacitive components) between the secondary of the transformer and the voltage divider

d) additional complex impedance (resistive, inductive and capacitive components) between the voltage divider and the piezoelectric device (MEGA drive

e) additional complex impedance (resistive, inductive and capacitive components) between the primary of the transformer and the amplifier.

I thoroughly analyzed the impedance (resistive, inductive and capacitive components) of the amplifiers used at CSUF for the MEGA drive experiments.

I suggested experiments to be conducted at CSUF to measure the output impedance of the Carvin DCM2000 amplifier. These experiments were conducted by Hal Fearn under carefully controlled conditions. The experimental results show that the output impedance of the Carvin DCM2000 amplifier (at the MEGA drive operating frequency) is about 500 times greater than what is specified in the Carvin DCM2000 amplifier specifications because the Carvin specifications are (implicitly) written for the much lower frequency range of the audio bass

range, which is the main market for the Carvin amplifier. CSUF is operating the Carvin DCM2000 amplifier (for the MEGA drive experiments) at much higher frequencies than what the bass frequency range it is designed for.

The output impedance of the amplifier is of paramount importance for the amplitude of the MEGA drive response because the amplitude of response is limited by this impedance (the lower the impedance, the greater the response amplitude).

Therefore, decreasing the output-impedance of the amplifier is one of several options available to increase MEGA drive response amplitude.

I suggested experiments to be conducted at TU Dresden to measure the output impedance of the Carvin DCM1000 amplifier that was loaned to TU Dresden by CSUF. These experiments were conducted by Prof. Hal Fearn under carefully controlled conditions upon her visit to Dresden during January 2020. The experimental results showed that the output impedance of the Carvin DCM1000 amplifier (at the MEGA drive operating frequency) is > 50 times greater than the output impedance of the Carvin DCM2000 amplifier presently used at CSUF. TU Dresden admitted that their DCM1000 amplifier "has a problem."

The experiments show that the output impedance of the Carvin DCM1000 at TU Dresden peaks in the frequency range of operation of the MEGA drive, and this constitutes a severe hindrance in achieving MEGA drive response amplitude.

---

8. Design of contact interface between PZT stack and metal ends

I analyzed the contact stresses between the PZT stack and the metal ends, when mating with flat contact surfaces I showed that due to the difference in (Dundurs parameter) elastic properties between PZT and brass there are non-uniform contact stresses (including an elastic stress singularity) at the interface between the PZT stack and the metal ends when the contact surface is initially flat. To verify my calculations, I showed Hal Fearn the experimental technique to measure contact stresses using Fuji "prescale" film. Tests with Fuji "prescale" film at CSUF verified my stress calculations. The calculated a profile to minimize the contact stresses, has the shape of a shallow dome. It is a nonlinear profile in the radial direction, flat at the center and increasing its curvature as it approaches the free external cylindrical surface of the PZT stack. The maximum deviation from flatness is less than 0.001 inches. CSUF verified (using Fuji "prescale" film) that using these dome ends the contact stress is much more uniform than when using initially flat contact surfaces. Using this profile is important in order to prevent cracking (due to contact stress) of the PZT stack, and to be able to successfully operate the MEGA drive at a maximum voltage and to maximize fatigue life.

I also calculated that it is better to adhere (with epoxy) the domed ends interface between the PZT stack and the brass mass, in order to prevent contact sliding at this interface. Sliding lowers the Q, due to frictional dissipation of energy. Frictional sliding leads to frictional heating. Adhering (with epoxy) the PZT to brass interface also prevents impact stresses during piezoelectric vibration due to dynamic micro-separation of the PZT to brass interface under high tensile contact stress.

---

9. Optimal location of strain gauge in the PZT stack

My calculations showed that the location of the strain gauge in the PZT stack has a marked effect on the measured displacement (and measured force) of the MEGA drive, and therefore I asked CSUF to perform experiments with the strain gauge placed at different locations. CSUF verified that the measured force was quite higher when the strain gauge was placed asymmetrically (with respect to the ends of the MEGA drive) than when placed at the middle of the PZT stack. I also pointed out that another advantage of using thinner (than 2 mm) PZT discs (besides higher capacitance) is that thinner discs allow better fine-tuning the optimal location of the strain gauge in the PZT stack.

---

10. Analytical design of end springs ("washers") at supported end

In my December 2018 I calculated the effect of the polymer washers at the supported end of the MEGA drive and I showed how using a washer on each side of the support, with the L-bracket being able to freely move to either side would be much more effective than having washer(s) between the brass mass and the L-bracket. The arrangement that CSUF had been using nullified the effect of the polymer washer particularly when the MEGA drive force is in the direction of the aluminum cap end, since in that direction the much higher stiffness of the screws overwhelms the lower stiffness of the polymer washer.

I analyzed several alternatives to replace the PolyAmide (PA) (DuPont trade name "Nylon") washers used at CSUF (at the beginning of the midterm of NIAC Phase II) for fastening the MEGA drive to the L-bracket support. I showed that (high-melting temperature engineering thermoplastic) PolyeEtherEtherKetone (PEEK) washers should behave considerably better than the Nylon washers because PEEK has a much higher melting and heat-deflection temperature and hence is less susceptible to the bottoming/viscoelastic-flow-compression problem suffered by the Nylon washers. Also, the Nylon washers are unacceptable for use in Space applications because Nylon is known to have significant outgassing problems in vacuum, while PEEK has been successfully used in Space applications that demonstrated its insignificant outgassing.

Experimental results at CSUF confirmed my suggestions, as the reported measured force (with the correct calibration procedure) is 0.5 microNewtons when using rubber washers, 1.5 microNewtons when using Nylon washers, and 10 to 15 microNewtons when using PEEK washers. This is a very significant improvement in measured force by a factor of 20 to 30 times when compared to the force measured with rubber washers (used during the NIAC Phase I grant), and 7 to 10 times when compared to the force obtained with Nylon washers.

The improvement of the measured force constitutes one of the deliverables agreed for the Phase II NIAC grant.

Initial experimental results by Prof. Fearn showed up to 35 microNewtons measured force, but reversing to only 4 microNewtons. Since there is an asymmetry due to the number of holes upon reversing the stack, the experiments were repeated with a completely symmetric setup with three supporting screws instead of 6. They showed a significant improvement in measured force by a factor of about 100 times compared to the force obtained with the rubber washers.

Experimental results by Prof. Fearn confirmed more than 20 microNewtons measured force, in both forward and reverse, when using wood-fiber-reinforced phenolic a very significant improvement in measured force by a factor of about 100 times compared to the force obtained with the rubber washers (using the proper calibration of force). However, the phenolic washers turn black after a few runs, indicating that the temperature rises (due to hysteretic heating) to a level high enough for the small amount of oxygen in the vacuum chamber to react with the polymer (leaving black carbon as a residue).

I also worked with Paul March to design and select vendors of other polymer washers, including high-temperature engineering-thermoplastics such as PEEK, (trade name "Vespel") polyimide, and (trade name "Torlon") Polyamide-imide, reinforced with carbon fiber and/or carbon spheres, as well as thermosets such as high glass-transition temperature epoxy with the same reinforcement. The purpose of carbon fillers is to address the hysteretic heating of these washers that results in decomposition of the phenol-formaldehyde resin of reinforced phenolic washers into carbon, with the OH and H groups becoming volatile in the vacuum chamber. This heating is also responsible for the unreinforced PEEK washers becoming "mush" due to high temperature viscoelastic flow under compression exceeding 3000 psi at operating frequencies (35 to 40 kHz).

I showed that the "Torlon" Polyamide-imide (highly recommended to Woodward by another colleague) is not acceptable for Space applications because of Torlon's severe outgassing problems (due to its polyamide content), as determined by NASA. A better choice is to use pure polyimide (trade name "Vespel" from DuPont), which has higher temperature properties and very low outgassing, since (unlike Torlon), it is not contaminated by polyamide (trade name "Nylon). Vespel (unlike Torlon) has been successfully used by NASA in Space applications.

11. Design of Belleville washers

My analysis (later verified by experiments) showed that washers on both sides of the bracket support significantly increase the displacement of the MEGA drive, due to increased compliance (lower stiffness) of the supported end. Given a material with a modulus of elasticity E, the thicker the washer with thickness t (or the greater the number n of washers with thickness t), the lower the total stiffness k= E A/(n t) (where A is the cross-sectional area of the washer), and hence the greater the displacement of the MEGA driven for a given screw force.

Most importantly, it is critical to have a quality of resonance (Q) as high as possible, and hence to use materials with lower tan delta (for example, Vespel is better than Nylon, which is better than rubber, because since rubber has the highest tan delta among these materials, and Vespel the lowest).

I also analyzed Belleville metal washers. Metal has much higher thermal conductivity than polymers, and when used below its yield stress, metal has a well defined elastic behavior with no viscoelasticity. Metal also has a tan delta orders of magnitude lower than polymers. However, Belleville washers can exhibit significant damping (and hence low Q) because they exhibit frictional sliding at the metal contact interface when assembled in series in order to match a given load and prevent bottoming of the Belleville washer. I calculated an exact solution for the effective stiffness of Belleville washers and worked with Paul March to design and select appropriate Belleville washers for the MEGA drive. We submitted several designs to CSUF based on matching the preload on the PZT stacks with a small safety factor to prevent bottoming.

Experiments at CSUF revealed some advantages using Belleville washer instead of polymer washers: the Belleville washers enabled a harmonic oscillation with better defined regular sinusoidal waves, and they did not experience degradation due to heating or fatigue (that prevents long-term use of polymer washers). However, they proved to be difficult to optimize because they are only available commercially in certain sizes that are not optimal for the MEGA drive application. Another disadvantage is that using more than one Belleville washer in series rapidly degrades the Q (and hence lowers the measured force) due to frictional heating at the sliding contact interface between the Belleville washers.

Wave washers were also explored but they exhibit similar problems (available only in certain sizes, have much lower stiffness for the same size than Belleville washers which presents a bottoming problem, and have higher damping than helical springs).

---

12. Precision Linear Bearings

The ideal support design is one that allows the MEGA drive to move longitudinally while transmitting its force to the balance as perfectly- elastically as possible, *with the highest Q (lowest damping) possible*.

CSUF changed the support design from the L-shaped bracket to a sledge (a vehicle on runners, conveying loads over a sliding surface) with flat surface contact interfaces between sliding steel and brass. This design presented a relatively high friction between the steel and brass surfaces, even when lubricated. Not surprisingly, the measured force (about 5 microNewtons) using this sledge was significantly lower than when using phenolic washers (15 to 20 microNewtons) with the L-shaped support bracket instead. However, the sledge design appeared promising because the vibration transmissibility to the balance was lower than with the L-shaped support bracket. To lower the friction, the sledge design was changed to a steel to (trade name "Teflon") PTFE flat surface contact interface. This resulted in a marginal improvement.

I showed CSUF that it is much better to use precision linear bearings for the sledge design because linear bearings use ball bearings that *roll* rather than slide at the contact interface. Since rolling friction is much lower than sliding friction, the friction of linear bearings using rolling ball bearings can be 40 (or more) times lower than the flat contact sliding friction between steel and Teflon. This was verified experimentally at CSUF. Video showed that the MEGA drive (undergoing piezoelectric vibration at ~30 kHz) can displace 2 mm on the linear bearings. However, when the force is only transmitted through friction, the response is not harmonic, as expected when there is no support stiffness in the equation of motion. In order for the MEGA drive to engage in harmonic motion with the sledge foundation, one needs to connect its ends to the foundation with a soft elastic spring, with a sufficiently low stiffness and with high Q. My calculations showed that the best way to do this is to use a steel guitar string with a constant radius of curvature, with a diameter between 0.008 inches and 0.014 inches. I showed that the stiffness of the spring is proportional to the modulus of elasticity, and to (r^4) the 4th power of the string diameter, and inversely proportional to (R^3) the 3rd power of the radius of curvature of the arch of the spring. The ideal shape of the spring is an arch with height equal to the radius of curvature R of the arch, and a chord length equal to (2 R) twice the radius of curvature of the arch R, with the string supported perpendicular at both of its end-support surfaces. Video of the experiments at CSUF showed that the MEGA drive (undergoing piezoelectric vibration at ~30 kHz) displaces 0.5 mm on the linear bearings when supported at its two ends by a guitar steel string of (2 r =) 0.008 inch diameter, and that the displacement when using a guitar steel string of (2 r =) 0.014 inch diameter was about ten times smaller, confirming my analytical prediction (since $(0.014/0.08)^4 = 9.38$). The experimentally measured force at CSUF (with the MEGA drive oriented in only one direction, undergoing a frequency sweep) has peaks exceeding 50 microNewtons whether unrestrained by the strings, or whether restrained by 0.008 inch or the 0.014 inch diameter guitar steel strings.

Section 14

Date: 08-07-2020

Consultant: Paul March, Friendswood, TX 77546

Duration of consulting support: May 2018 to August 2020

Services Rendered: Consulting & supporting Lab work for Dr. Woodward and Dr. Fearn who were the Principle Investigators (**PI**) for their 2-year long NASA/NIAC-Phase-II Mach Effect Gravity Assist (**MEGA**)-drive development project located at the California State University – Fullerton (**CSUF**) Campus. Basic goal of the contract was to increase the consistent thrust output of the MEGA-drive from the 1-to-2 micro-Newton (**uN**) thrust levels observed up to early 2018 in most the of the MEGA-drives by one-to-two orders of magnitude, i.e., 20-to-200 uN.

1. Provided engineering, design, procurement and supporting historical data searches in my 22 year long (1999-to-2020), Mach-Effect data base that supported the design and fabrication of various MEGA-drive test articles built by Dr. Woodward & Dr. Fearn during this phase-II contract. This included the design and vendor search and procurement of the MEGA-drive's PZT-stack's brass and bronze mesh brass and bronze electrodes used in the fabrications of the MEGA-drive's PZT stacks.

2. Provided the PIs at CSUF lab equipment and subsystem upgrade recommendations during the initial portion of the phase-II contract. This included finding the vendor for the required resonant frequency tracking amplifiers, drive software and supporting equipment needed to track the time varying resonant frequency of the operating MEGA-drive PZT-stack.

3. Attended weekly Zoom internet conferences every Friday or more often as needed by the PIs.

Section 15

A Summary Report of the Last 3 Months of Involvement With the NIAC Phase II Grant Team & The MAGA Mach Effect Device

Michelle Broyles

I became involved with the research team by and PI Dr. J. Woodward and PI Dr. H. Fearn in June 2020. I was honored to be able to offer my services even when a short time remained on the NASA NIAC Phase II grant.

This will be a short summary finalizing the last 90 days ending 9 August 2020. Other NIAC phase II team members have detailed a longer period. I'll highlight device issues that needed to be addressed and the questions that have arisen from the optimization of the drive.

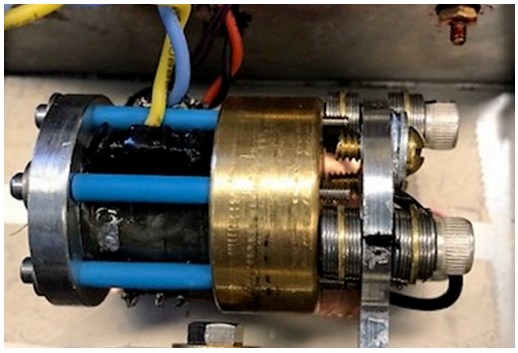

The device as of June 2020. Consisting of the Aluminum mass on the right secured to the PZT stack with screws and into the brass mass that was coupled to the L-bracket on the right with washers and screws. The bottom of the L-bracket was attached to the torsion arm.

Over the last 90 days the device went through major revisions, in the way the device is built and coupled into the torsion arm, while still keeping the PZT and masses intact as they have been for years. When I started it was attached to the torsion arm through a series of screws and various washers to a L bracket which was then attached to the end of the Torsion Arm. This was deemed unworkable for several reasons.

1. The actual L-Bracket being coupled to the end brass piece needed to dampen high frequency vibrations >30kHz while still allowing an increased mechanical Q with the second order harmonics. This wasn't feasible because of the materials utilized for the washers. Composite washers break down and Belleville springs due to the number of stacked washers needed dampened the device through surface friction. (Plus alignment of the stacks of the washers was quite difficult).

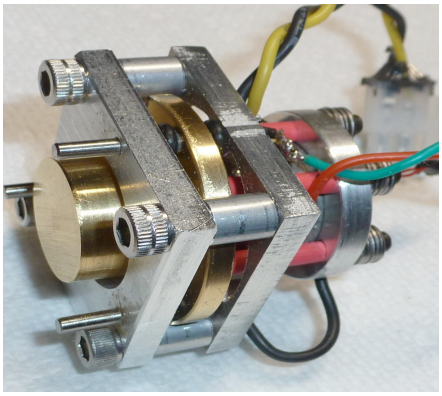

Gone is the brass end coupling and the device is now "floating" within the 2 endplates that are coupled to the torsion arm. This isolates the high frequency from the torsion arm and allows the device to increase the second order harmonics without restrictions imposed by the L-Bracket assembly.

2. The L-Bracket acted as a one-arm tuning fork introducing chaotic harmonics into the torsion arm during frequency sweeps.

Through emails, zoom teleconferencing and testing in the lab (mainly by Dr. H. Fearn who had to do the testing alone as pandemic restrictions were imposed). We were still able to do revisions and produce a device that was more stable.

One of the issues was the coupling used in the device. The L-bracket's issues were a headache. It was agreed that device's center of mass instead of the end of the brass mass design was to be pursued and to provide vibration isolation of the high frequencies to float the device in the center of its mass and provide coupling at that point.

Dr. J. Woodward presented his idea in a July 3rd 2020 Zoom Teleconference. The design was innovative in it not only ran the devise floating within the center of mass it also provided a friction-less vibration isolation platform to work with.

We proceeded to secure the linear bearings and stainless steel rods

to incorporate into this new design. Dr. Woodward also had changed the brass reaction mass by the addition of a central ring around the brass mass centering on the device's center of mass. O-Rings were added on the stainless steel rods hoping to couple the device to the endplates and to the torsion arm.

A revision was needed. It was decided to attach springs to the center of the now 3 “eared” brass mass and to the 2 endplates. This would allow the actions of the device to not be dampened while still coupled to the endplates and torsion arm.

One of the issues noted was the device shouldn't be able to overcome the slip-stick and coefficient of friction introduced by the linear ball bearings on the stainless steel slides. In a Zoom meeting I cited work I'd done in linear slides using bearings where due to requirements of movement of a arm within ½ micron we were able to move it. It was found that vibrations of another device negated the slip-stick and reduced the coefficient of friction.

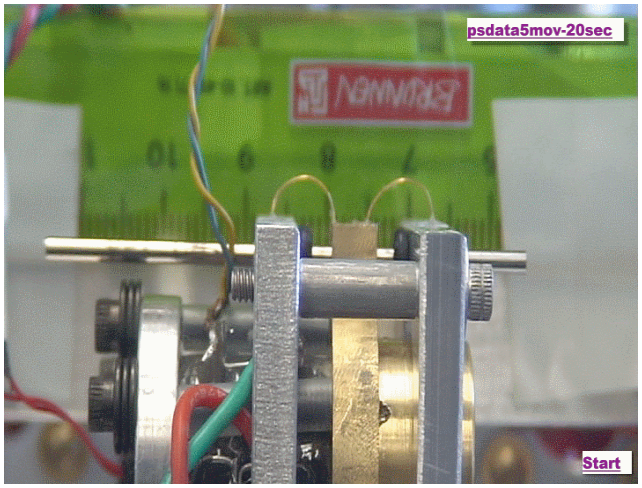

Redesigned running with new springs

Reaping the rewards of our redesign.

In a teleconference meeting 7 August 2020 in which results we had observed over the last week were discussed, from no springs in the device with just O-ring bumpers with a tiny gap to a large gap to running with .009” springs. I was wondering if the CoM was a large driving factor in the deviations of the torsion arm per H. Fearns tests with a static torsion and sliding weight which showed displacements of .5mm on the device would equate to ~60 microNewton measurements on the beam. (Note: We were also seeing 80 microNewton and upwards of +100micronNewtons during some runs). H. Fearn might be right that the device's movement on the stainless steel rods were contributing to the thrust signal. I could see only one way to address this issue by constriction the device's movements even further. J. Woodward and H. Fearn agreed to replace the smaller springs .009” running on the brass ears of the device to the supporting endplates with the larger ones .014" with a ~10x greater calculated stiffness. Which would mean that the movement was restricted to <.05mm or around 6 microNewtons.

I was able to see with the magnified video and the new mm scale that indeed the beam was deviating less than <.05mm. This would calculate out to (using H. Fearn's linear calculation weights on the beam) to 6 micro Newtons.

Dr. H. Fearn's calculations as referenced from a current report 9 August 2020

If y = Ax ; when y=30mm and x=0.5mm then constant A=60.

If the CoM of the mass moves 0.5mm then we would expect the wire to move 0.5mm/60 = 8.33 μm. We found previously, in the Philtec sensor calibration, that a voltage of 0.75 volts gives 1 μm of displacement. So, if we assume 8.33μm displacement due to CoM motion that would register a sensor voltage of 6.2 volts or equivalent to roughly 62 μN. (We find that 0.1volt is roughly 1μN force of the device). This is very significant and must be taken into account.

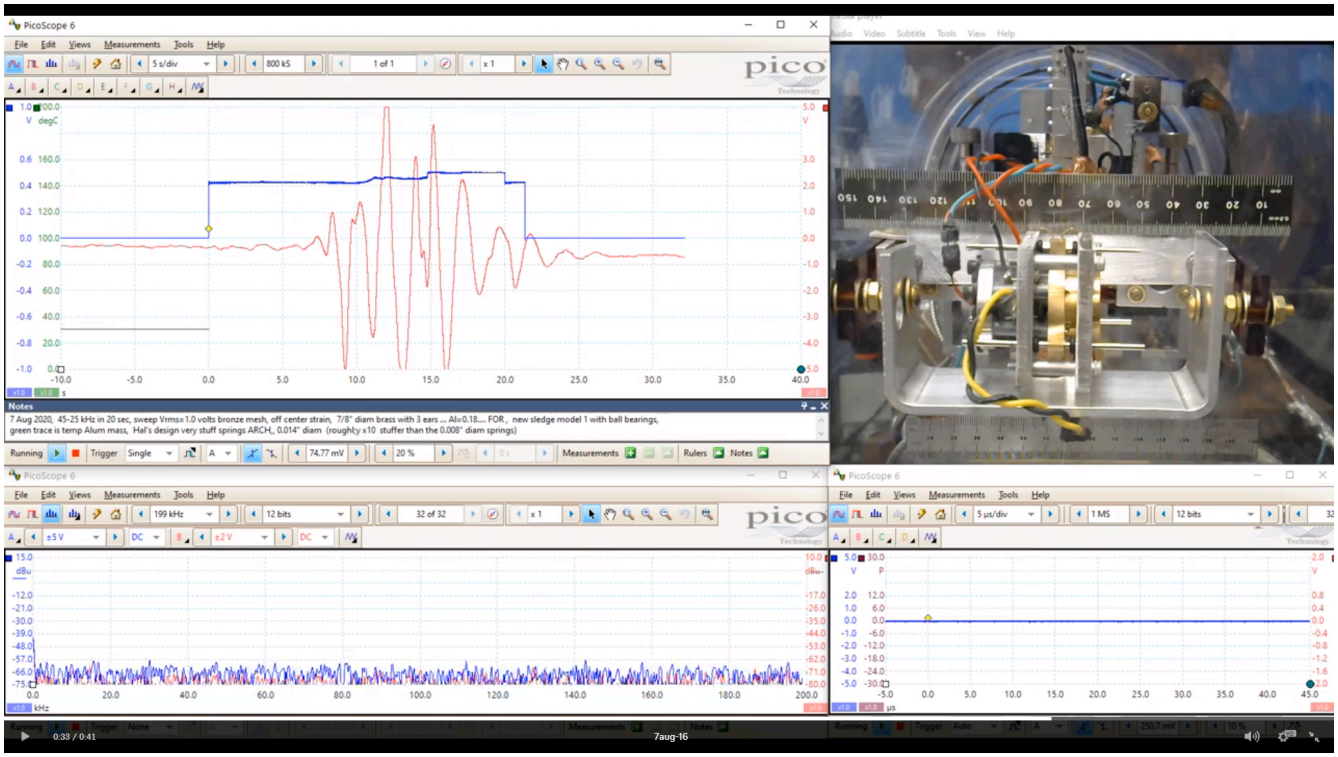

7 August 2020 .013" diameter larger springs run

That is not what is seen from the PICO data taken with the heavier springs .013” diameter on 7 August 2002. We are still seeing a torsion arm deviation measurement of 50-60 microNewtons. Which lowers the Conservation of Mass movement of the device argument with the beam deflection via shifting of the device on the slide. As best as I can tell the device is moving under .05mm or according H. Fearn's calculations ~6 microNewtons.

These latest test runs raise the question, are we seeing Mach Effects because we have effectively limited the device's movements to under .05mm which relates to only 6 microNewtons deviation on the torsion arm while measuring 60 microNewtons?

To expand on this question and potential ways to address them

One is to limit the frequency sweeps to 2kHz and 10 seconds for each sweep picking a harmonic high Q point. Expanding that would be to do 10 pulsed sweeps of 2kHz 10 seconds each. Then ascertain if a unidirectional direction of force was maintained in the accumulative pulsed streams.

The next would be pulsed thrust locked single frequency operations for an extended time. Fullerton doesn't have that equipment in house as of yet.

Adding 2 more sets of secured symmetrically spaced springs on the devices outer ears this would keep CoM device shifts objections using a calculated and real movement under 10 microNewtons.

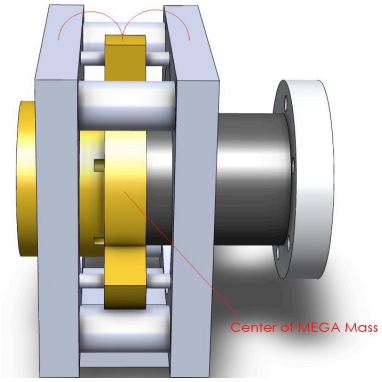

Concept drawing of new MEGA Device

Because of these tests run these last few weeks with the redesigned device we've been able to bring out thrust effects by dampening and restricting device movement on the torsion arm. This also reduced the chaotic coupling with a pendulum that results in motion that cycles chaotically between normal modes and will lead to more repeatable thrust signatures at even higher power. The Mach Effect may be there to take advantage of, to make it so we need to provide definitive and repeatable proof with a stable device in other labs. Finally because of the last few month's activities (even through the pandemic restrictions) we'll be to be able to optimize the device with passive cooling, increased drive power, and frequency locking hardware with higher Q designs.

Progress Report -- METDrive

Chip Akins 12/15/2019

The METDrive system we are developing is designed specifically as a laboratory instrument for optimizing thrust in MET devices. MET in this context refers to the Mach Effect Thruster.

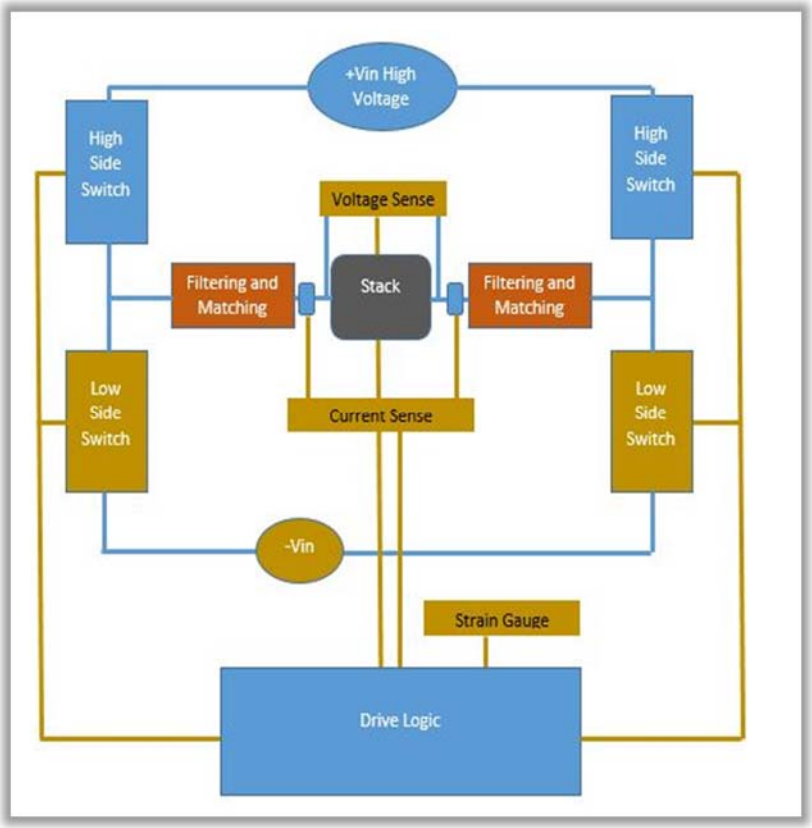

A simplified block diagram is shown here. The waveform is created using Pulse Width Modulation (PWM), and then filtered through a 1MHz low-pass filter. Voltage and current are sensed at the terminals for the Device Under Test (DUT -- "Stack" in the drawing).

Since the system uses ***feedback from the device*** to generate the desired waveform, we can be far less concerned with inductive and capacitive reactance. We can test specific waveforms and frequencies to find the optimum drive signal.

The system can also monitor 2 additional inputs, like strain gauge and temperature, for intelligent control of the MET device.

In software we are able to create waveforms consisting of the fundamental and any of its harmonics we wish. The amplitude and phase of the harmonics are also adjustable. In addition, we are able to sweep the frequency of the waveform we have created and capture the frequency which creates highest thrust.

The hardware is assembled for the first drive channel, and FPGA logic and MCU firmware have been created. We are able now to load the logic to the FPGA for testing, and we are able to program and run the MCU. We have USB communications from the PC to the MCU, and the MCU is the supervisory control for the FPGA logic and waveform generation.

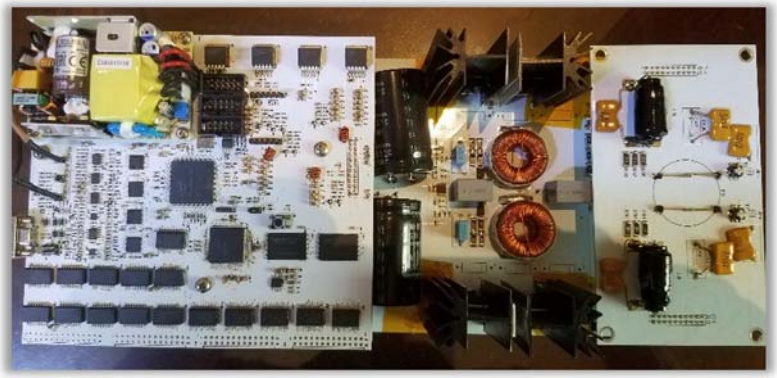

Right now we are working on getting the serial RAM configuration device to automatically configure the FPGA on power up. Once that task is complete, we will begin driving PZT elements and testing the apparatus.

Concept

The concept which inspired this METDrive system is the idea that we can create an instrument for electrically testing this sort of device which makes it much easier than conventional methods. We can more accurately and more quickly discover the requirements for optimizing thrust in these types of experiments, by developing an instrument with the capabilities of the METDrive. Arbitrary waveform generation, with feedback from the DUT, insures that we actually get the waveform requested, regardless of the capacitive or inductive reactances we encounter. Conventional methods require that we design an interface, and tune the circuit again, every time we need to test at a different frequency. But with the METDrive, all we have to design is the waveform itself. The software for the METDrive can create custom waveforms as we want them designed. Alternately we can create a waveform using data analysis and computations of the physical system in other scientific software, or Excel, and import those waveforms into the METDrive for testing.

Another advantage we encounter using the METDrive approach is the ability later to employ artifical neural networks (machine learning) to help us enhance and optimize the system for more thrust.

In the block diagram above, the blue box labeled “Drive Logic” is actually and FPGA running at 200MHz coupled with an MCU which is USB connected to a PC running control and data acquistion software for the METDrive.

Most of the electrical systems have been through initial testing. First drafts of the FPGA logic, and MCU firmware have been developed. Once automatic FPGA configuration on power up is working, we will be able to finish testing and deliver the first channel of the drive system. The system is designed to be expandable to 8 channels.

Note: Due to the nature of the driver design, and the feedback, the driver presents a low impedance to the device under test which is a significant advantage in providing the desired signal to the device.

In general terms the METDrive as currently configured should be able to drive 300 VRMS and at least 1 Amp continuous per channel arbitrary waveforms. The channels are isolated so they may be connected in series or parallel for higher voltages or currents respectively. The maximum rated breakdown voltage is about 1500V per channel.